Investigating the Ubiquitin-proteasome System during Poxvirus Infection

by

Jianing Dong

A thesis submitted in partial fulfillment of the requirements for the degree of

Doctor of Philosophy

in

Virology

Department of Medical Microbiology and Immunology

University of Alberta

Abstract

Ubiquitylation is a post-translated modification that is important for the host immune response to virus infection. Concurrently, it is also exploited by poxviruses for viral replication and evasion of the host immune response. Thus, this project focused on further elucidating how the ubiquitin (Ub) system is engaged during poxvirus infection.

p28, a poxvirus encoded E3 Ub-ligase, is a virulence factor of ectromelia virus (ECTV) in susceptible strain A mice. To further investigate p28 function, we completely deleted the p28 gene from ECTV (ECTV-Δp28). The ECTV-Δp28 virus exhibited severely impaired virus production and genome replication in a mouse strain, cell type, and multiplicity of infection-dependent manner. Moreover, a FLAG-tagged p28 protein with a fusion Ub moiety was expressed and developed as a tool to capture p28 potential substrate proteins. To determine the DNA binding properties of p28, I purified recombinant His-tagged p28 and examined the interaction between p28 and poxvirus hairpin DNA.

To get a more comprehensive understanding of how proteins are ubiquitylated early after vaccinia virus (VACV) infection, a proteomics approach was used to identify and quantify ubiquitylated peptides in cells with or without VACV infection. These included peptides associated with TRIM25, a cellular E3 Ub/ ISG15-ligase, whose ubiquitylation is induced by a gene(s) in either arm of the VACV genome. Taken together, this thesis has revealed novel information about how poxviruses manipulate ubiquitylation.

Preface

A version of Chapter 3 was published as "Jianing Dong, Patrick Paszkowski, Dana Kocincova, Robert J. Ingham. Complete deletion of Ectromelia virus p28 impairs virus genome replication in a mouse strain, cell type, and multiplicity of infection-dependent manner. *Virus Research.* 323 (2023) 198968, doi: 10.1016/j.virusres.2022.198968."

A version of Chapter 5 was in "Jianing Dong, Shu Luo, Summer Smyth, Grace Melvie, Olivier Julien, Robert J. Ingham. Characterizing changes in protein ubiquitylation during vaccinia virus infection." (Under review, manuscript # JVI00430-24)

Acknowledgements

I would like to thank my supervisor, Dr. Rob Ingham, for the opportunity to continue my virus research and for his support during my PhD studies. I am very grateful for the skills I have learned from him, particularly in enhancing my critical thinking and academic presentations. I would also like to thank the past and present members of the Ingham laboratory, especially Patrick Paszkowski for his technical support, which helped me adapt to a new research environment and become familiar with many poxvirus-related experimental methods. I thank Dana Kocincova for her technical support. I would like to thank Summer Smyth and Grace Melvie for their contributions to my research.

To my committee members, Dr. David Evans and Dr. Maya Shmulevitz, thank you for your valuable advice and continued support. Every time we talked, I gained new ideas for my research, including different directions and new methods to try. Their thoughtful commentary and suggestions encouraged me to improve my work.

Thank you to the students and faculty of the MMI department for being such a great group. Special thanks to Dr. Baldwin's laboratory for providing C57/BL6 mice and assistance in purifying mouse macrophages. Special thanks to Drs. Matthias Götte and Egor Tchesnokov for helping me establish the baculovirus expression system. Special thanks to Drs. James Lin and David Evans for providing Mpox-infected HeLa cell lysates. Special thanks to Dr. Olivier Julien and Shu Luo for their collaboration in the mass

spectrometry analysis of diglycine peptides in cells uninfected or infected with poxviruses. Their expertise greatly enriched my research work and contributed to this thesis. I thank Drs. Evans, Shmulevitz, Marchant, Hobman, Yanow, Lemieux and the members of their labs for sharing reagents, facilities, and helpful advice. I thank Dr. David Evans, Dr. Mary Hitt, Dr. Maya Shmulevitz, and Dr. Troy Baldwin and their laboratories for helpful discussions during joint laboratory meetings. I thank cell imaging core, flow cytometry facility, and animal facility in University of Alberta for their support.

I am thankful to CIHR, NSERC, and the LKSIoV for providing financial support in my academic research. I am also grateful for the scholarships that allowed me to undertake my PhD studies. This includes Alberta Innovates Graduate Student Scholarship, Faculty of Medicine & Dentistry/Alberta Health Services Graduate Student Recruitment Studentship, and University of Alberta Doctoral Recruitment Scholarship.

I have been lucky to make great friends in this department. Joyce, Cathy, Patrick, Wan Kong, and Kang helped me both with my research and life here in Canada. Thanks to my classmates for their support. I would especially like to thank my good friend Fran, whose friendship has been with me throughout my PhD studies.

To my family, I want to thank them for their encouragement and for believing in me to succeed. I would like to thank my husband Xiyu for his support and companionship. Your support and confidence in me have given me the strength to accomplish more than I thought possible.

Table of Contents

List of Tables

List of Figures

Abbreviations

Ab	antibody
ANKR	ankyrin repeat
ANOVA	analysis of variance
Ara-C	cytosine arabinoside
ATCC	American type culture collection
BEVS	baculovirus expression vector system
BMDM	bone marrow-derived macrophage
BR	Brighton Red
BTB	Broad complex, Tramtrack, Bric-a-brac
CMC	carboxymethyl cellulose
Cop	Copenhagen
CPXV	cowpox virus
CRL	cullin-RING Ub ligase
Cul	cullin
CVA	chorioallantois vaccinia Ankara
DAPI	4',6-diamidino-2-phenylindole
DCAF	DDB1 and Cul4-associated factor
DDB1	DNA damage-binding protein 1
diGly	diglycine
DMEM	Dulbecco's modified eagle medium
dsDNA	double-stranded DNA
DTT	dithiothreitol
ECTV	Ectromelia virus
EDTA	Ethylenediaminetetraacetic acid
EEV	extracellular enveloped virus
EFC	entry-fusion complex
ER	endoplasmic reticulum
FBS	fetal bovine serum
FBXW8	F-box and WD repeat domain containing protein 8
FPXV	fowlpox virus
gpt	xanthine-guanine phosphoribosyltransferase
HECT	homologous to the E6-AP carboxy terminus
HFFF-TERT	telomerase reverse transcriptase (TERT)-immortalized primary human fetal foreskin fibroblast
hiGlpG	rhomboid protease from haemophilus influenzae
hpi	hour-post infection

Hsp70	heat shock protein 70
IF	Immunofluorescence microscopy
IFIT	IFN-induced proteins with tetratricopeptide repeat
IFN	interferon
IHD-W	International Health Department-White
IP	immunoprecipitation
IPTG	isopropyl β-D-1-thiogalactopyranoside
ISG	interferon stimulated gene
IV	immature virion
LD_{50}	median lethal dose
M-CSF	macrophage colony-stimulating factor
MEM	minimum essential medium eagle
MOI	multiplicity of infection
Mos	Moscow
MPXV	Mpox virus
MV	mature virus
MVA	modified vaccinia Ankara
NEM	N-ethylmaleimide
NYCBH	New York City Board of Health
OPG	*Orthopoxvirus* gene
OPV	*Orthopoxvirus*
ORF	open reading frame
PBS	phosphate-buffered saline
PCR	polymerase chain reaction
PFA	paraformaldehyde
PFU	plaque forming unit
PM	peritoneal macrophage
PMSF	phenylmethylsulphonyl fluoride
qPCR	quantitative polymerase chain reaction
RBR	RING-between-RING
RIG-I	retinoic acid-inducible gene I
RING	really interesting new gene
RPMI 1640	Roswell Park Memorial Institute 1640
SDS-PAGE	sodium dodecyl sulfate polyacrylamide gel electrophoresis
SFV	Shope fibroma virus
Skp1	S-phase kinase-associated protein 1
SOCS	Suppressors of cytokine signaling
ssDNA	single-stranded DNA
SUMO	small Ub-like modifier

TEVp	tobacco etch virus protease
TFA	trifluoroacetic acid
TIR	terminal inverted repeat
TLR	Toll-like receptor
TRIM25	Tripartite motif-containing protein 25
Ub	ubiquitin
UBAIT	ubiquitin-activated interaction trap
UPS	ubiquitin-proteasome system
VACV	vaccinia virus
VARV	variola virus
VHL	von Hippel-Lindau protein
vIRD	viral inducer of RIPK3 degradation
WHO	world health organization
WR	Western Reserve
WV	wrapped virion
YFP	yellow fluorescent protein

Chapter 1: Introduction

1.1 Poxviruses

Poxviruses are large, double-stranded DNA (dsDNA) viruses that infect a variety of vertebrate and invertebrate species (1). Unlike other DNA viruses, poxviruses replicate exclusively in the cytoplasm. The large genomes of poxviruses range from 130 to 360 kbp (2). In addition to encoding viral structure proteins, poxvirus genomes also encode virulence factors, host range factors, and proteins that modulate the host immune responses (3-6). Given the characteristics that poxviruses can stimulate strong immune responses, have the capacity to insert and express large foreign genes, and replicate in the cytoplasm with low risk of DNA recombination with host genes, poxvirus-based vectors are strong candidates for vaccine development (7). For example, fowlpox virus-based vectors are now used in chickens as vaccines against infections caused by Newcastle disease virus (8, 9), infectious laryngotracheitis (10), and avian encephalomyelitis virus (11). Many human clinical trials have been conducted using VACV attenuated poxvirus vector against diseases including HIV/AIDS (12, 13), influenza A (14), Hepatitis B (15), or malaria (16, 17).

The *Poxviridae* family contains 83 species which are divided into two subfamilies: the *Entomopoxvirinae* and the *Chordopoxvirinae* (18). The *Entomopoxvirinae* subfamily infects insects, and the *Chordopoxvirinae* infects vertebrates **(Table 1.1)**. Most identified poxviruses belong to the *Chordopoxvirinae* subfamily and can be further separated into 18 genera (18). Of those genera, the *Orthopoxvirus* (OPV), *Molluscipoxvirus*, *Parapoxvirus*, and *Yatapoxvirus* have been reported to infect in humans (19). In my thesis work, I focus

on studying OPVs.

1.1.1 OPVs

The OPVs consist of many well-known poxvirus species with different host ranges and can infect a variety of mammals, including humans, rodents, and livestock (**Table 1.1)**. Among these viruses, variola virus (VARV) is the most infamous member of the *Poxviridae* family (2, 20). VARV has a narrow host range, infecting only humans and causing smallpox disease in humans (21, 22). This disease was responsible for around 400 million deaths in the twentieth century (23). Fortunately, global eradication of smallpox was declared by the World Health Organization (WHO) in 1980 because of worldwide vaccination programs using VACV (7, 20). After the eradication of smallpox, the potential use of stored VARV as bioweapons, as well as zoonotic poxviruses in the wild, still poses continuing threats to humans (20, 24-27). For example, Mpox virus (MPXV), identified in 1958, has become a human health concern, causing more than 91,000 cases from 2022 to 2023 (28-31). In addition, the abolition of VARV vaccination programs results in an increase in the proportion of the population unprotected against poxviruses, raising the potential threat of poxviruses to human health (20, 32-34). Thus, VACV is still widely studied in research related to developing poxvirus vaccines and viral pathogenesis.

Genus	Virus	Major hosts
Orthopoxvirus	Variola virus	Humans
	Vaccinia virus	Humans, cattle, buffalo, swine, rabbits
	Ectromelia virus	Rodents
	Monkeypox virus	Squirrels, anteaters, great apes, monkeys, humans
	Cowpox virus	Rodents, cattle, humans
	Camelpox virus	Camels
	Taterapox virus	Gerbils
Leporipoxvirus	Myxomavirus	Tapeti, brush rabbits
	Hare fibroma virus	Cottontail rabbits
Avipoxvirus	Fowlpox virus	Birds
	Sparrowpox virus	
	Canarypox virus	
Capripoxvirus	Goatpoxvirus	Goats
	Sheeppox virus	Sheep
	Lumpy skin disease virus	Cape buffalo, cattle
Cervidpoxvirus	Deerpoxvirus	Deer
Molluscipoxvirus	Molluscum contagiosum virus	Humans, primates, birds, dogs

Parapoxvirus	Bovine papular stomatitis virus	Cattle, humans
	Orf virus	Sheep, goats, humans
Suipox virus	Swinepox virus	Swine
Yatapoxvirus	Tanapox virus	Monkeys, humans
	Yaba-like disease virus	Monkeys, humans
	Yaba monkey tumour virus	Primates

Table 1.1 Poxvirus taxonomy and their major hosts

The table shows representative viruses from the *Chordopoxvirinae* and their major hosts. The table is adapted from figures in Maclachlan, N.J. *et al.*, 2010 and Barrett, J.W. *et al.*, 2008 (19, 35)

1.1.1.1 VACV

In 1798, Edward Jenner used material from cowpox lesions to immunize, protecting humans against smallpox (36). Over time, VACV became the virus used during the smallpox eradication program (37). *"Vacca"* in Latin means "cow", which suggests that VACV is the virus inducing cowpox (38). However, the genome of VACV is distinct from cowpox virus (CPXV) and is more closely related to horsepox virus (39). From 1950 to 1980, many VACV strains were used to eradicate smallpox. The names of some virus strains are related to the geographic regions where the vaccine was used. For example, the Tian Tan strain was used in China, and the Ikeda strain was used in Japan (40). The New York City Board of Health (NYCBH) strain was widely used in the United States. Many different strains of VACV were used in Europe, including the Paris strain used in France and the Copenhagen (Cop) strain used in Denmark. Many of these vaccines were made from lymph collections from the skin of VACV-infected calves or sheep (41). To improve the safety of smallpox vaccines, new-generation smallpox vaccines, such as ACAM2000™ which can be produced in tissue culture cell lines instead of animals, are licensed for use in the twenty-first century (7, 41). Furthermore, attenuated VACV strains have been generated and used in studies for developing vaccines and understanding the host-pathogen relationship. For instance, modified vaccinia Ankara (MVA) is generated by passaging chorioallantois vaccinia Ankara (CVA) for over 570 times in chicken embryo fibroblast cells causing the virus to lose about 15% of its genome and rendering it unable to replicate

in many mammalian cells (42, 43).

1.1.1.2 Ectromelia virus (ECTV)

ECTV, the causative agent of mousepox, is another member of the OPV genus (44). Unlike CPXV and VACV, ECTV has a narrow host range and only infects rodents in nature **(Table 1.1)** (21, 45). Thus, the mouse, as a natural host of ECTV, is a model for the study of the pathogenesis of poxvirus *in vivo*. The Moscow strain of ECTV (ECTV-Mos) was described as a highly infectious and virulent ECTV strain for mice compared to the Hampstead strain and NIH79 strain (46). In the natural environment, ECTV can infect mice through skin abrasions (47), but the severity of the disease depends on the mouse strain (48). In susceptible mouse strains, such as the strain A and BALB/c, infection with ECTV causes severe illness and mortality (48). However, other mouse strains like C57BL/6 and AKR strains are resistant to severe disease and recover from ECTV infection (49). The resistance of mice to ECTV infection requires both a functional innate immune response, especially activation of type I interferons, and the host adaptive immune response (45).

1.2 Poxvirus structure

1.2.1 Poxvirus genome structure

The central region of the poxviral genome consists of genes that are highly conserved within the *Chordopoxvirinae*. These genes encode viral proteins and enzymes that are essential for viral entry into cells, genome replication, transcription, and structural proteins for virion assembly (2, 50). The two arm regions are variable in different poxviruses and

contain genes that are important for virus virulence, host range, and immune evasion (46, 51). The right and left terminal regions of the viral genome are called terminal inverted repeats (TIRs) (50). The two strands of the viral genome are connected at their termini by AT-rich hairpin loops, structures essential for virion maturation (52, 53). **(Figure 1.1A)**

The genome of the VACV-Cop can be divided into fragments after *Hind*III restriction endonuclease digestion, and these DNA fragments are named from A to P based on size (51) **(Figure 1.1B)**. The VACV genes are named by letters that represent which fragment the gene is located in, Arabic numbers that represent the position of the gene in the fragment (the number from left to right), and L (represents left) or R (represents right) that indicates the direction the open reading frame (ORF) is transcribed (51). In 2021, Senkevich *et al.* proposed a new nomenclature, OPV genes (OPGs), based on the analysis of OPV gene evolution (54). This nomenclature unifies the names of the genes of OPV and is valuable to indicate homologues.

1.2.2 Structure of the poxvirus virion

The poxvirus virion is a brick-shaped structure with dimensions of 360×270×250 nm (55). It contains a core with a single lipid membrane, two lateral bodies, and an outer membrane(s) **(Figure 1.2)**. There are two infectious forms of poxviruses based on the study of VACV: mature virus (MV) and extracellular enveloped virus (EEV). MV is surrounded by a single lipid bilayer membrane with about 20 surface proteins (56, 57), including D8, A26, and A27, which can bind to chondroitin, laminin, or heparan on the cell

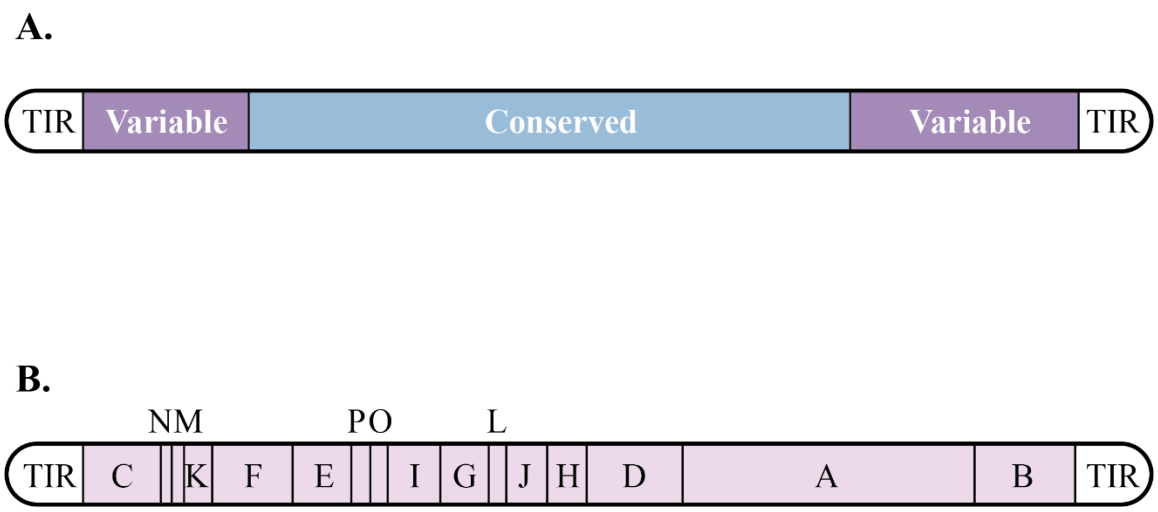

Figure 1.1 Poxvirus genome

A, Poxviruses DNA genome. The center region of the genome contains genes that are conserved and encodes essential viral proteins for replication. The two arms of the genome contain genes that are variable including viral proteins related to the host range and virulence. The TIRs are at the ends of the genome. **B,** The VACV genome fragments labeled by letters. The VACV-Cop genome fragments are digested by *Hind*III and named A to P from the longest to the shortest. The figure is adapted from (51).

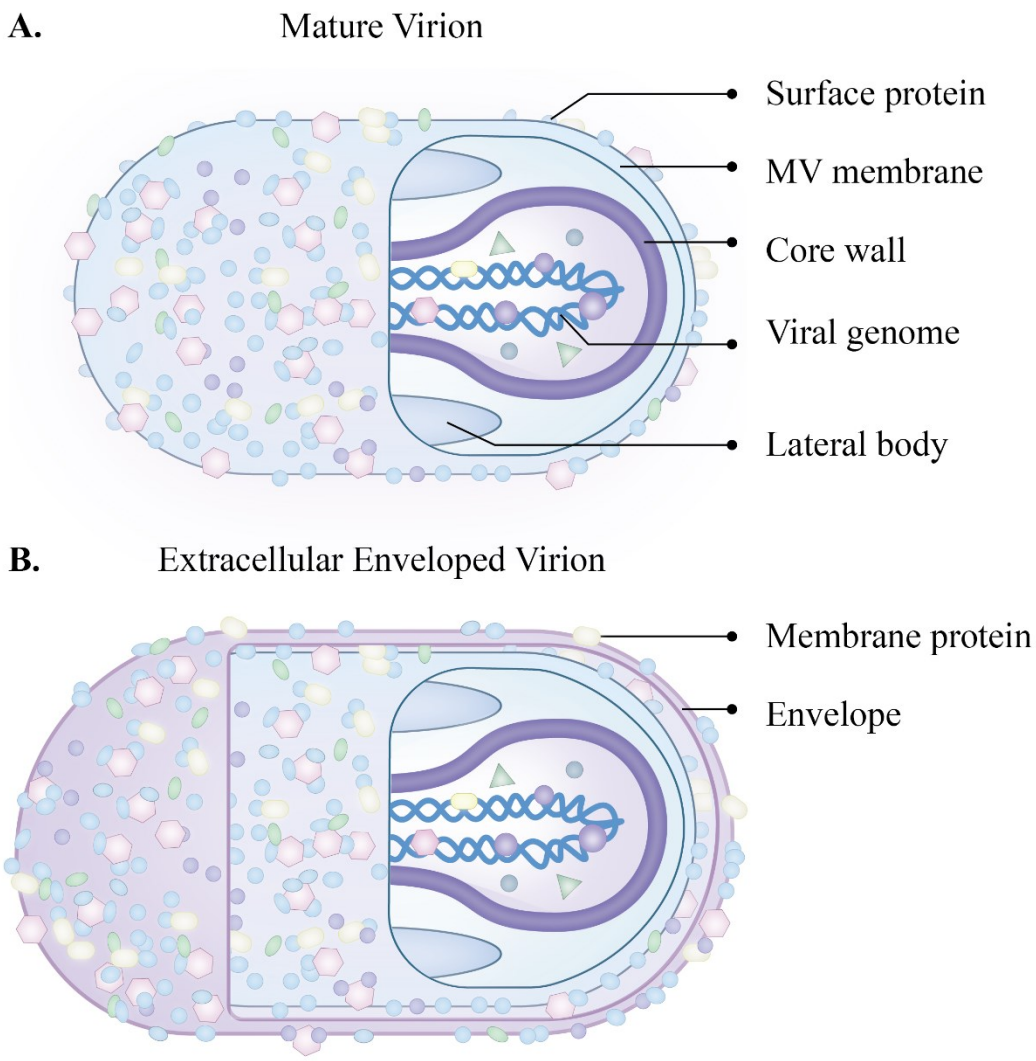

Figure 1.2 Structure of poxvirus virion

A, Mature virion. The virion is covered by single membrane with surface proteins. The core of poxvirus contains viral genome which is dsDNA enclosed in a protein formed core wall. Two lateral bodies are located on either side of the core. **B,** Extracellular enveloped virion. MV is covered by an extra membrane with specific viral proteins. The figure is adapted from (19).

membrane (58-60). Alternatively, EEV has an additional lipid membrane with at least six unique membrane proteins suggesting that EEV may bind different receptors on the cell membrane (61-63). The extra membrane protects virions against antibody (Ab) neutralization and makes EEV more infectious than MV (64, 65). However, MVs are the predominant poxvirus infectious particles (19). Most of the MVs remain in the cytoplasm and are released from the infected cell upon cell lysis, whereas EEVs remain on the surface of the cell or are liberated from the infected cells through exocytosis (19, 66).

1.3 Poxvirus replication cycle

Poxvirus replication occurs exclusively in the cytoplasm of infected cells **(Figure 1.3)**. First, a virion attaches to molecules on the cell surface, then fuses with cell membrane and releases the virus core into the cytoplasm, which occurs together with viral early protein expression. After uncoating, the viral genome is released from the virus core, and a virus factory is formed, acting as the location of viral genome replication, protein synthesis, and virion assembly. EEVs and MVs are released by exocytosis or cell lysis, respectively. In the following sections, I will discuss in detail each step of poxvirus replication in cells.

1.3.1 Attachment and entry

The efficient binding between poxvirus and the cell surface is supported by the viral proteins on the virion surface as mentioned before. EEV enters the infected cell by macropinocytosis (67) **(Figure 1.3 ①)**. The low pH in macropinosomes contributes to the rupture of the outer membrane of EEV (67). The released MV-like virion exposes its entry-

fusion complex (EFC) for membrane fusion in the next step (68). The EFC is a complex formed by eleven viral proteins (A16, A21, A28, F9, G3, G9, H2, J5, L1, L5, and O3) and is required for virus entry and viral membrane fusion (69) **(Figure 1.3 ②)**. Virion entry can be inhibited using neutralizing Abs against the components of EFC, A28 or L1 (70, 71). The genome of poxviruses also encodes some viral proteins, such as A56 and K2, which are localized on the surface of infected cells and act as suppressors of viral attachment, impairing membrane fusion by binding to EFC on the new virion, thereby avoiding secondary infections of cells by the same virus (72, 73).

1.3.2 Uncoating

Following the fusion of the MV membrane with the cell membrane, the viral core and other viral components, such as the viral proteins in the lateral bodies, are released into the cytoplasm **(Figure 1.3 ③)**. F17 and H1 are proteins in the lateral bodies that inhibit immune responses by downregulating the cGAS and STING pathway, respectively (74, 75). Before the viral core breaks down, the viral early protein mRNAs can be synthesized with the help of cellular ribonucleotide triphosphates **(Figure 1.3④)** (76). The translation of these mRNAs is critical for virus uncoating **(Figure 1.3⑤)**, genome replication **(Figure 1.3⑥)**, and intermediate gene expression **(Figure 1.3⑦)** (64, 77-79). For example, the AAA+ ATPase D5 is a viral early protein detected by an siRNA screen as required for poxvirus uncoating (79). In addition to D5, other viral proteins (68k-ank or B18, C5, and M2) with mutually redundant functions related to virus uncoating were identified (80). Of

note, B18 and C5 are viral adaptor proteins associated with cellular E3 Ub-ligase complexes (79, 81). Furthermore, the inhibition of proteasomal activity abolished the virus uncoating (79-84). These results reveal the essential role of the Ub-proteasome system (UPS) in VACV replication, which I will discuss in more detail later.

1.3.3 Poxvirus replication in virus factories

Viral genome replication **(Figure 1.3 ⑥)** and late protein synthesis **(Figure 1.3 ⑧)** occur in a membrane-associated structure, called a "virus factory" (77, 85). The membrane of the virus factory is wrapped from endoplasmic reticulum (ER) membranes which can be detected as early as 2 hours post-infection (hpi) (86). At early time points, each infectious particle generates one factory (86). These virus factories expand in size and merge with other factories formed by other virions, which is important for recombination of the viral genome with other replicating poxviruses (87, 88). The formation of virus factories protects viral components from detection and degradation by the host DNA sensors, RNA sensors, and enzymes involved in the host immune responses (86). The replication of the viral genome is essential for viral intermediate **(Figure 1.3⑦)** and late gene expression **(Figure 1.3⑧)** (89). Many proteins encoded by these genes, such as viral structural proteins and transcription factors, are packed into the progeny virions **(Figure 1.3⑨)** (90).

1.3.4 Assembly and release

Progeny genomes and viral proteins are packed into an oval lipid structure called the immature virion (IV) **(Figure 1.3⑨)**, which then forms a dense, brick-shaped infectious

virus particle, MV **(Figure 1.3⑩)** (90). The maturation of virions requires the help of many viral late proteins, such as D13 and A5 (91-93). MVs constitute the majority of infectious viral particles, and their release is achieved by cell lysis **(Figure 1.3⑰)** (90). Some MVs are wrapped in trans-Golgi or endosomal membrane to become wrapped virions (WVs), which have triple membranes on the surface of the viral particles (94-97). WVs are then transported along microtubules to the cell surface (98-102). The outer membrane of WV fuses with the cell membrane, followed by the release of an EEV from the infected cell (61).

Overall, the replication cycle of poxviruses is complex. It includes multiple steps and requires different virus-host interactions. Many steps of poxvirus replication, like uncoating and virus factory formation, require the host Ub system.

1.4 Ubiquitylation

Ubiquitylation changes the properties of the target protein, including the abundance, localization, activity, or interactions with other proteins (103). This post-translational modification is also critical in the regulation of numerous cellular processes during poxvirus infection (82, 104-106).

1.4.1 The ubiquitylation reaction

Ubiquitylation is a process of attaching Ub to a specific target protein. Ub is a 76-amino acid small protein that is highly conserved in eukaryotic cells (104). The modification of a protein by Ub occurs by forming an isopeptide bond between the Ub C-

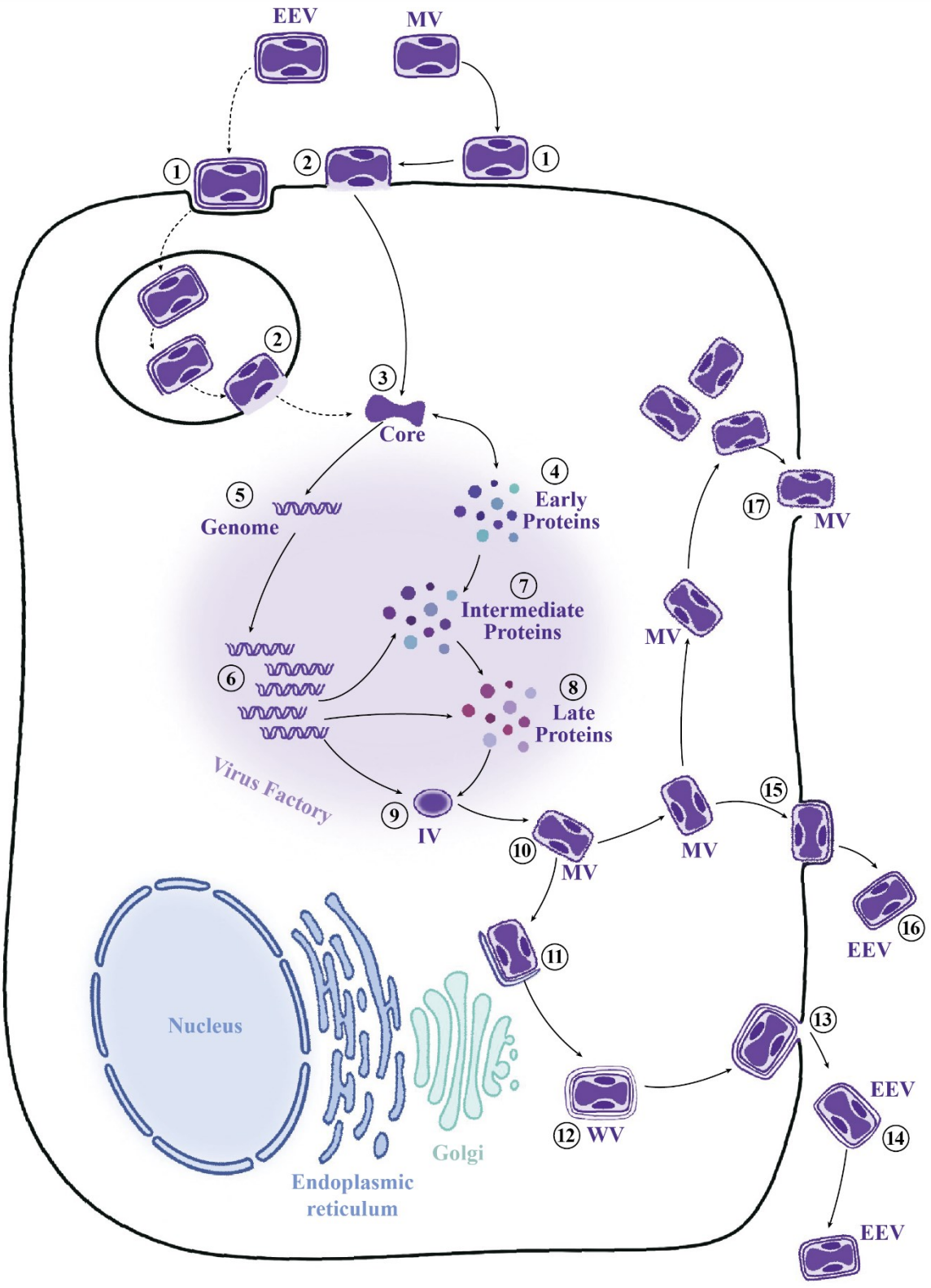
EEV
MV
1
2
1
2
3
Core
4
Early
Proteins
5
Genome
6
7
Intermediate
Proteins
8
Late
Proteins
Virus Factory
9
IV
10
MV
11
12
WV
13
EEV
14
EEV
15
MV
16
EEV
17
MV
MV
Nucleus
Endoplasmic
reticulum
Golgi

Figure 1.3 Poxvirus replication cycle

The schematic shows the VACV replication cycle. EEV or MV attaches ① and fuses ② with the cell membrane. ③ Virus core and other components, like lateral bodies, are released into the cytoplasm. ④ Expression of viral early proteins initiates the virus core uncoating and ⑤ viral genome liberation. The genome of poxvirus replicates in the virus factory ⑥ and then the intermediate ⑦ and late proteins ⑧ begin to be expressed. ⑨ IVs are assembled in the virus factory and consist of lipid, viral genome, and viral proteins. ⑩ Mature virions are released from the virus factory, and ⑪ a small portion traffick upon microtubules to get an extra double-membrane derived from trans-Golgi or endosome. ⑫ WVs traffick to the cell surface and ⑬ the outer membrane fuse with the plasma membrane to release the ⑭ EEVs from cell. ⑮ Some MVs get an additional membrane from the plasma membrane forming EEV which are released from the cell ⑯. ⑰ Most of the MVs in the infected cells are released by cell lysis.

terminal glycine residue and the ε-amino group of the lysine residue in the target protein **(Figure 1.4 A)**. The process utilizes three enzymes: E1 Ub-activating enzyme, E2 Ub-conjugating enzyme, and E3 Ub-ligase enzyme **(Figure 1.4B)** (107, 108). First, Ub is activated by the E1 Ub-activating enzyme in an ATP-dependent manner. Then the activated Ub is transferred from E1 to an E2 Ub-conjugating enzyme. The E2 enzyme then facilitates, directly or indirectly, the ligation of Ub to the target protein specifically recognized by an E3 Ub-ligase.

The eukaryotic E3 Ub-ligases can be separated into three families: really interesting new gene (RING) domain, homologues to the E6-AP carboxy terminus (HECT) domain, and RING-between-RING (RBR) domain **(Figure 1.5)** (109). E3 Ub-ligases with a RING domain bind to E2, allowing Ub transfer from E2 to target proteins **(Figure 1.5A)**. Alternatively, E3 Ub-ligases with a HECT domain or a RBR domain bind to E2, then the activated Ub is transferred from the cysteine on the E2 to the E3, forming a thioester bond between the cysteine on the E3 and the Ub **(Figure 1.5B and C)**. Then, the Ub is transferred from E3 to the target protein **(Figure 1.5B and C)**.

To specifically recognize target proteins for ubiquitylation, E3 Ub-ligases have not only a catalytic domain but also a domain responsible for binding target proteins. The catalytic domain and substrate binding domain may exist within an individual protein or in separate proteins that combine to form a multi-subunit E3 Ub-ligase complex **(Figure 1.6A)**. Cullin-RING Ub ligases (CRL) are a large subfamily of multi-subunit E3 Ub-ligases

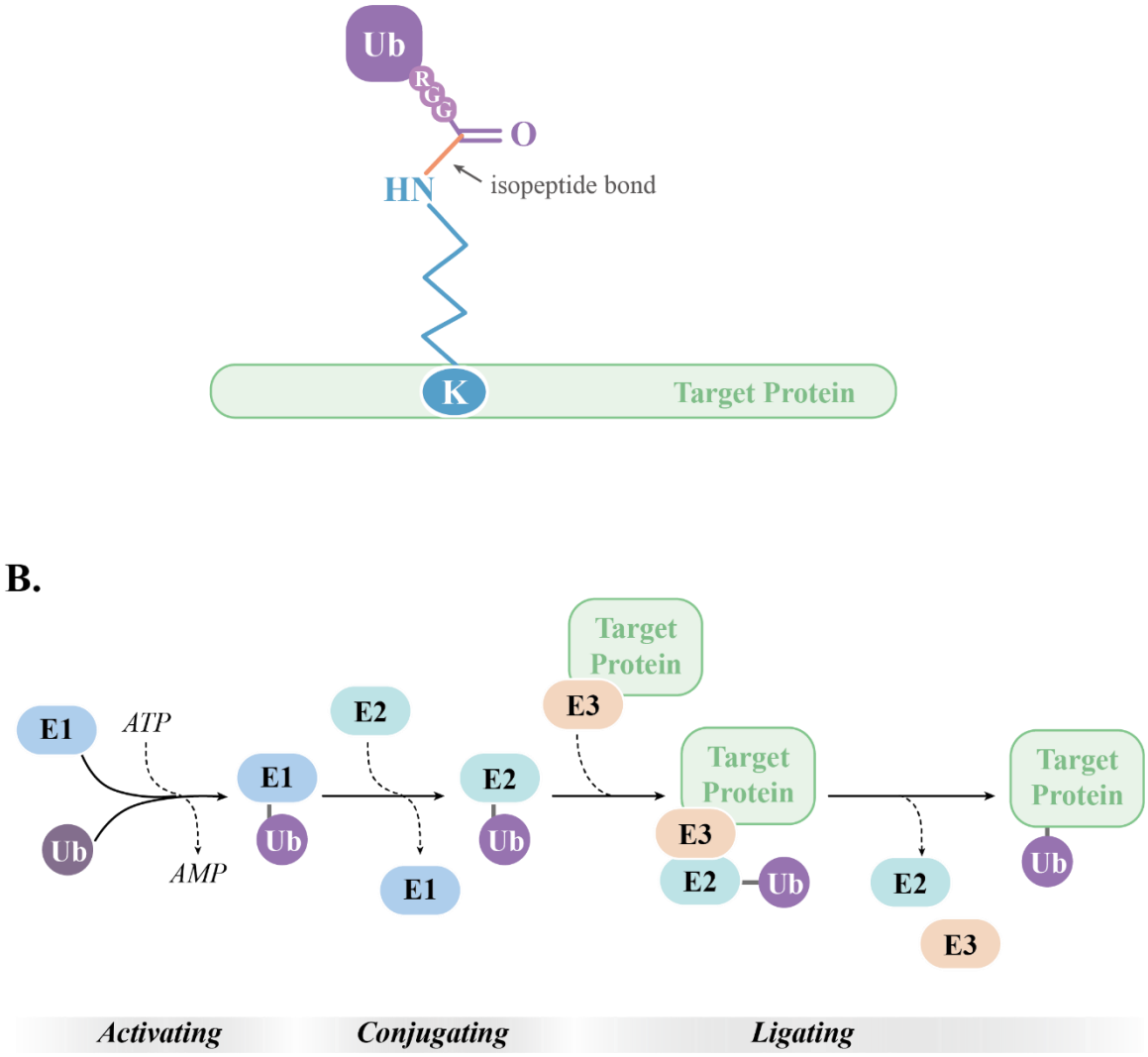

Figure 1.4 The ubiquitylation reaction

A, Modification of Ub on a target protein. Ub is covalently attached to lysine residues of target proteins. An isopeptide bond (orange) links ε-amino group of K (blue) of target protein and the C-terminal glycine (G) residue of Ub. **B,** Ubiquitylation process. Ub is activated by E1 Ub-activating enzymes in an ATP-dependent manner. Activated Ub is transferred to E2 Ub-conjugating enzymes. E3 recruits target protein(s) to E2 followed by ubiquitylation of the target protein(s).

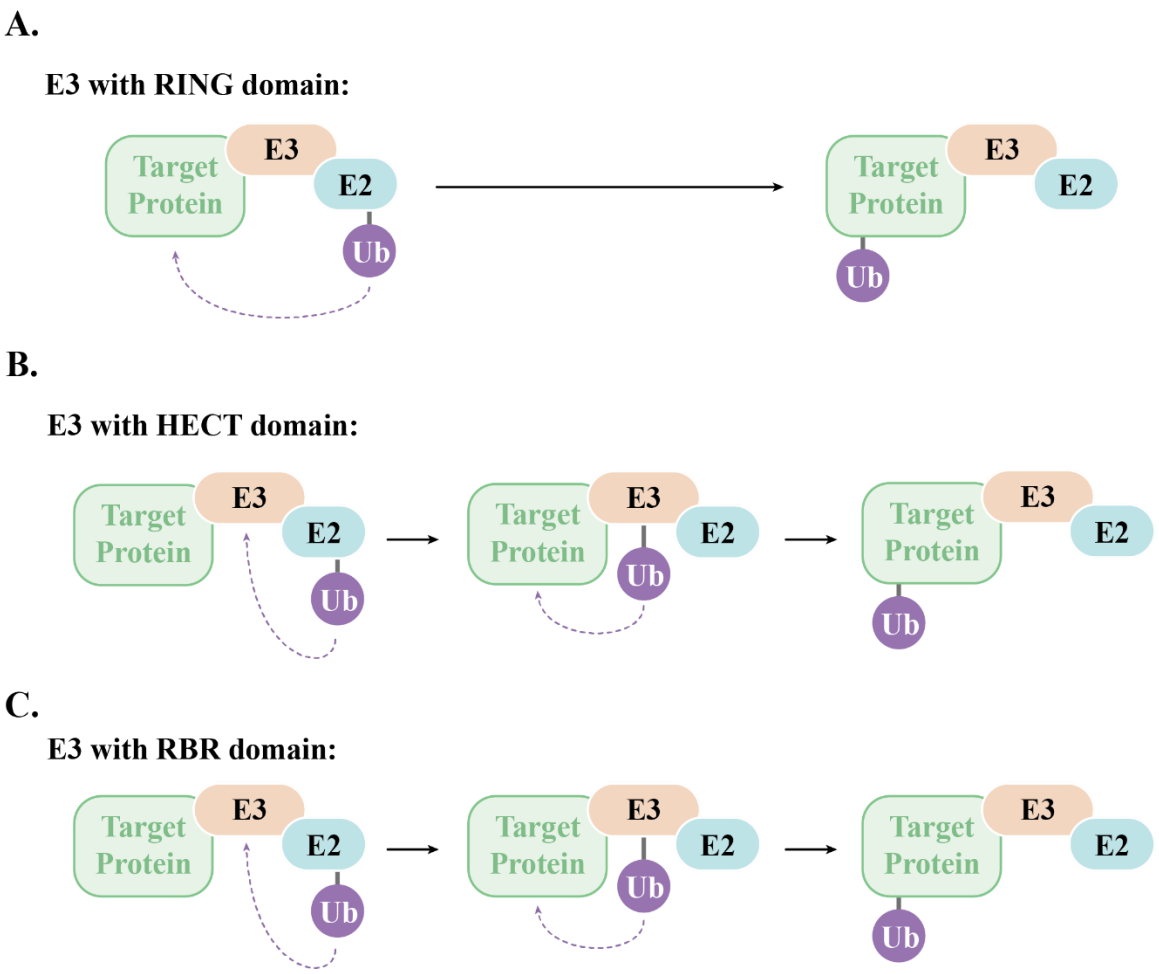

Figure 1.5 Classification of E3 Ub-ligase proteins

A, E3 Ub-ligase proteins with RING domain bind to E2. The complex allows Ub transfer directly from E2 to the target protein. E3 Ub-ligase proteins with HECT domains **(B)** or RBR domains **(C)** bind to E2 and then transfer activated Ub from E2 to E3. The Ub on E3 is then transferred onto the target protein. The figure is adapted from (110).

(110). They comprise a central scaffold protein, a cullin (Cul) protein, which binds to an adaptor protein(s) at the N-terminus and a RING domain containing protein at the C-terminus **(Figure 1.6A)** (111).The RING domain-containing protein is crucial for CRL binding with E2-Ub. Eight mammalian Cul proteins (Cul1, 2, 3, 4A, 4B, 5, 7, and 9) have been identified, each recruiting its own adaptor protein(s) **(Figure 1.6B)** (111, 112). For instance, the adaptor protein of Cul1 is S-phase kinase-associated protein 1 (Skp1), which interacts with substrate receptors, F-box proteins, to recruit target proteins for ubiquitylation (113). The activation of Cul1 E3 Ub-ligases is stimulated by the modification of Cul1 with a Ub-like protein, Nedd8 (114-116). Cul1 without covalently attached of Nedd8 binds its inhibitor CAND1, which suppresses the function of Cul1 Ub-ligases (116, 117). Furthermore, Broad complex, Tramtrack, Bric-a-brac (BTB) protein serves as an adaptor that binds to Cul3 (118). Instead of recognizing target proteins by associating with substrate receptors, BTB proteins are capable of recruiting substrate proteins via their substrate binding motif, often kelch repeats (118).

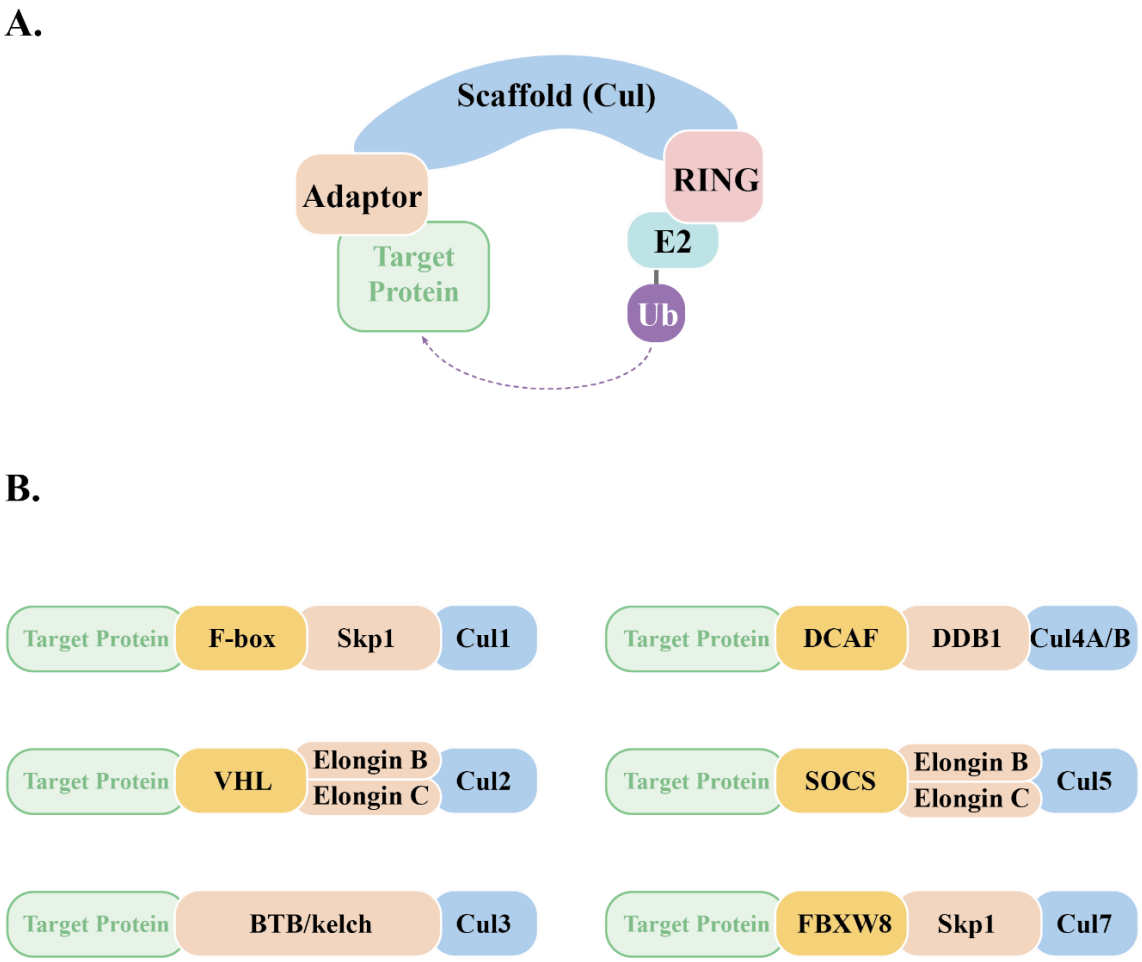

Figure 1.6 Model of CRL E3 Ub-ligases and their distinctive adaptor proteins

A, CRL E3 Ub-ligases. Multiple subunits form a complex that catalyzes the transfer of Ub from E2 to the target protein. A scaffold or Cul protein (blue) connects a RING domain containing protein (pink) and an adaptor protein (orange), which respectively binds to E2 and recognizes specific target protein. RING domain containing proteins recruit E2 with Ub to CRL E3 Ub-ligase. Target proteins (green) are recognized by adaptor proteins. **B,** The distinctive adaptor protein(s) of the CRLs. The adaptor proteins (orange) bind to the N terminus of Cul protein and recruit target proteins by their own substrate recognizing motif or the substrate receptors (yellow) interacting with it. Skp1, S-phase kinase-associated protein 1; VHL, von Hippel-Lindau protein; BTB, broad-complex, tramtrack and bric à brac domain; DCAF, DDB1 and Cul4-associated factor; DDB1, DNA damage-binding protein 1; SOCS, Suppressors of cytokine signalling; FBXW8, F-box and WD repeat domain containing protein 8. The figure is adapted from (111).

1.4.2 Types of Ub chains

The Ub modification regulates protein abundance and functions by attaching different types of Ub chains (119). A single Ub molecule can be added to one or more lysine residues in a target protein. These single-Ub modifications on the target proteins are associated with the regulation of DNA replication and repair, gene transcription, endocytosis, protein localization, and activity (120). Alternatively, target proteins can be modified by conjugating Ub chains (104). Ub contains seven lysine residues (K6, K11, K27, K29, K33, K48, and K63) and an N-terminal methionine residue (M1), which allow adding additional Ub molecules and forming different types of poly-ubiquitylation chains **(Figure 1.7)**. Ub added to different residues in Ub produces chains with different topologies and functions. Chains generated through the addition of Ub to lysine 48 of Ub (K48-linked chains) are the most abundant homotypic polyubiquitin linkage in cells (about 29% of all lysine-residue-based linkages in yeast cells) (121). All polyubiquitin chains have been shown to be involved in protein degradation by the 26S proteasome (121, 122). However, K48-linked chains primarily serve as a signal for targeting substrates to the 26S proteasome for degradation (123). In contrast, chains generated through the addition of Ub molecules to lysine 63 (K63-linked chains) can alter protein function and mediate protein-protein interactions (124).

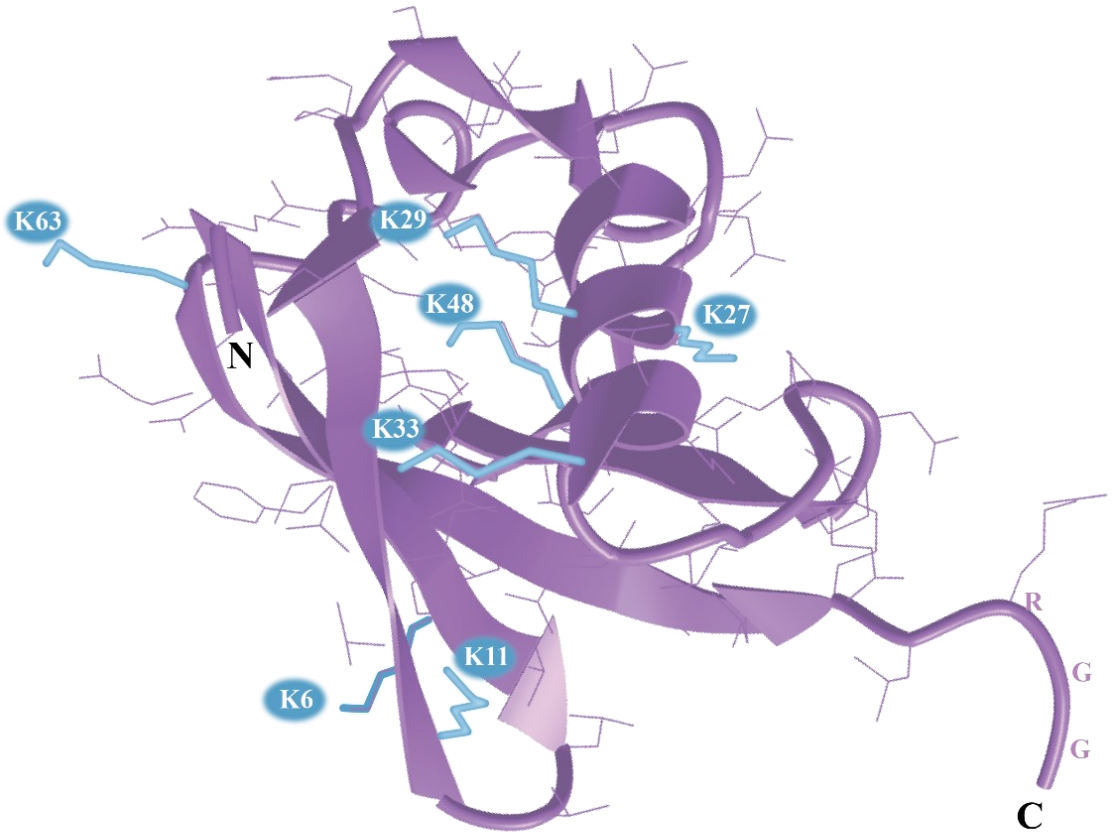

Figure 1.7 The structure of Ub

The 3D view of the structure of Ub (Homo sapiens) with side chains of the amino acids shown in purple. The side chains of the 7 lysine residues (K6, K11, K27, K29, K33, K48, and K63) in Ub are highlighted in blue. The highly conserved C-terminal RGG residues are labeled by purple letters. The image of Ub structure was downloaded (November 2023) from MMDB, updated in October 2007. PDB ID: 1UBQ, MMDB ID: 57540.

It is worth noting that, in addition to homotypic polyubiquitylation, heterotypic polyubiquitin chains are also found (103). Furthermore, other Ub-like proteins, such as small Ub-like modifier (SUMO), can participate in the formation of "mixed" Ub chains (125, 126). Some post-translational modifications, like phosphorylation and acetylation, on Ub in polyubiquitin chains alter their structure and function (127-129). Thus, ubiquitylation plays multiple roles and regulates numerous processes by attaching various types of polyubiquitin chains to target proteins. During poxvirus infection, the Ub system is also involved in activating immune responses (105). It is not surprising that poxviruses utilize the Ub system during their infection (82, 106).

1.5 Poxvirus manipulation of the Ub system

1.5.1 The necessity of the UPS for poxvirus replication

The UPS of the host not only plays a crucial role in regulating protein levels (121), but is also required for poxvirus replication **(Figure 1.8)** (82). Many proteins in poxvirus particles have been shown to be ubiquitylated (83, 84). Inhibition of the UPS by the proteasome inhibitor, MG132, impaired poxvirus DNA replication and late gene expression (81, 82). Further studies demonstrated that both proteasome activity and early gene expression were required for poxvirus uncoating during infection (79, 80, 84) **(Figure 1.8 ①)**. However, treatment with the E1 inhibitor, UBE1-41, had no effect on virus uncoating, suggesting that proteasome-mediated degradation rather than de novo protein ubiquitylation was necessary for poxvirus uncoating (84). Nonetheless, using UBE1-41 to

treat poxvirus-infected cells impaired the formation of virus factories, indicating that ubiquitylation was required for poxvirus replication after viral core breakdown (84) **(Figure 1.8 ②)**.

1.5.2 The genomes of poxviruses encode viral E3 ligases and adaptor proteins

To hijack the host Ub system and suppress host immune responses, The genomes of OPVs encode four groups of viral E3 Ub-ligases and adaptor proteins associated with cellular E3 Ub-ligase complexes **(Figure 1.9)** (106).

1.5.2.1 Viral adaptor proteins

Poxvirus genomes encode three families of adaptor proteins, ankyrin repeat/F-box (ANKR/F-box), ANKR/BC-box, and BTB/kelch proteins (130). These viral proteins interact with distinct cellular E3 Cul proteins and serve as adaptor proteins for the Cul E3 Ub-ligase complexes (131) **(Figure 1.9 A, B, and C)**. The genes encoding these viral proteins are located in the variable regions of the genome and are sometimes duplicated in both arms of the genome (54). CPXV encodes all families of OPV adaptor proteins, while some genes of these adaptor proteins can be lost or truncated in VACV and ECTV (132, 133). These adaptor proteins from selected OPVs and their functions are summarized in **Table 1.2** (46, 54).

Poxviral ANKR/F-box proteins play multiple roles in evading host immune responses. For instance, VACV C9L (OPG25) encodes a protein that mediates interferon (IFN)-induced proteins with tetratricopeptide repeats (IFITs) ubiquitylation and proteasomal

degradation (134, 135). IFITs bind directly to RNAs without eukaryotic caps to inhibit translation of these non-self RNAs (136). Apart from synthesizing viral RNAs with IFIT-resistant cap 1 (137), poxvirus genomes encode C9 to degrade IFITs in infected cells, which is essential for poxvirus genome uncoating and DNA replication (134, 135). An ANKR/F-box protein of cowpox virus, CPXV006 (OPG3), recognizes NF-κB1 p105 and inhibits the NF-κB signaling pathway (138, 139). In addition, CPXV006 is known as viral inducer of RIPK3 degradation (vIRD) (140). RIPK3 is a necroptosis adaptor that induces death of infected cells to control poxvirus replication (141). To inhibit necroptosis in infected cells, CPXV006 targets RIPK3 for ubiquitylation and degradation via the proteasome (140). Some viral E3 adaptor proteins have redundant functions with other viral genes. For example, CPXV025 (OPG23), also known as CP77, rescues the host range defects induced by deletion of K1L gene which is required for viral replication on rabbit kidney (RK13) cells (142).

Poxviruses also encode another group of ANKR proteins containing a C-terminal BC box that interact with Cul2 (143). ANKR/BC proteins of ECTV (EVM010) and CPXV (CPXV016) (OPG14) inhibit innate immune signalling, including DNA sensing, RNA sensing, and Toll-like receptor (TLR) signalling pathways (143). Another ANKR/BC protein encoded by CPXV, CPXV019 (OPG17), also blocks the TLR signalling pathway. The effect of EVM010 on the inhibition of innate immunity was suppressed without association with Cul2 (143). This indicates that the ability of viral ANKR/BC proteins is

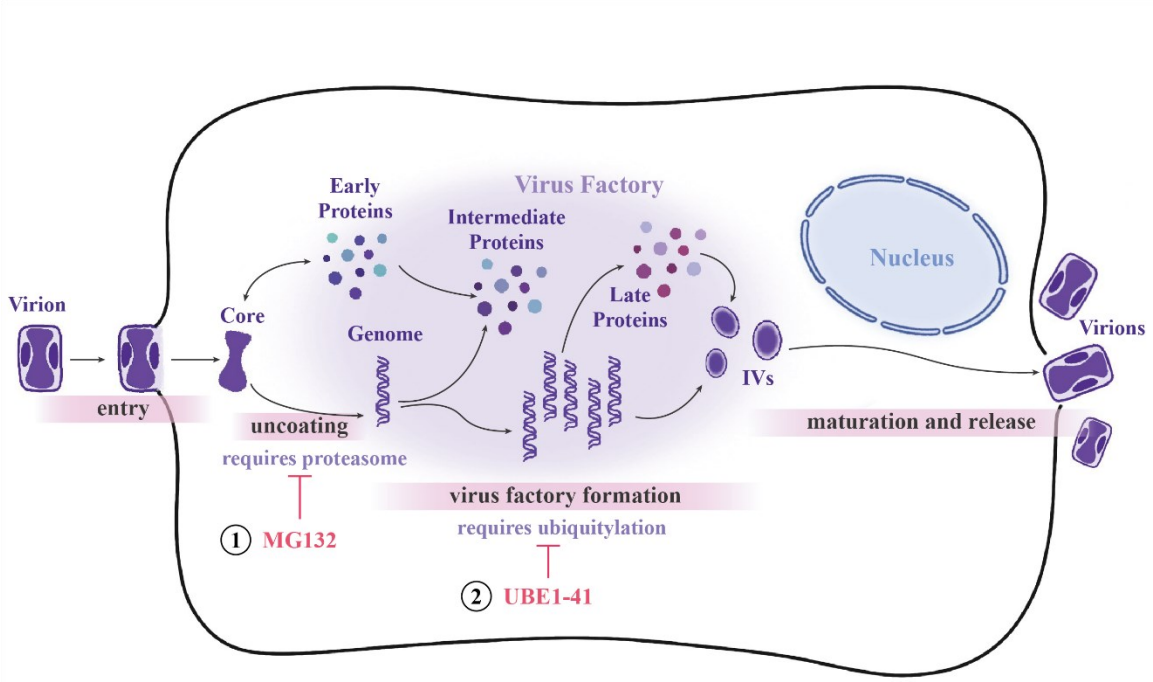

Figure 1.8 The Ub system is required by poxvirus replication

The schematic shows the steps of poxvirus replication that require a functional host Ub system. ①MG132 inhibits proteasome activity and impairs virus uncoating. ② UBE1-41 is an E1 enzyme inhibitor and inhibits the Ub system of the host. Inhibiting the ubiquitylation of the infected cells using UBE1-41 impairs virus factory formation.

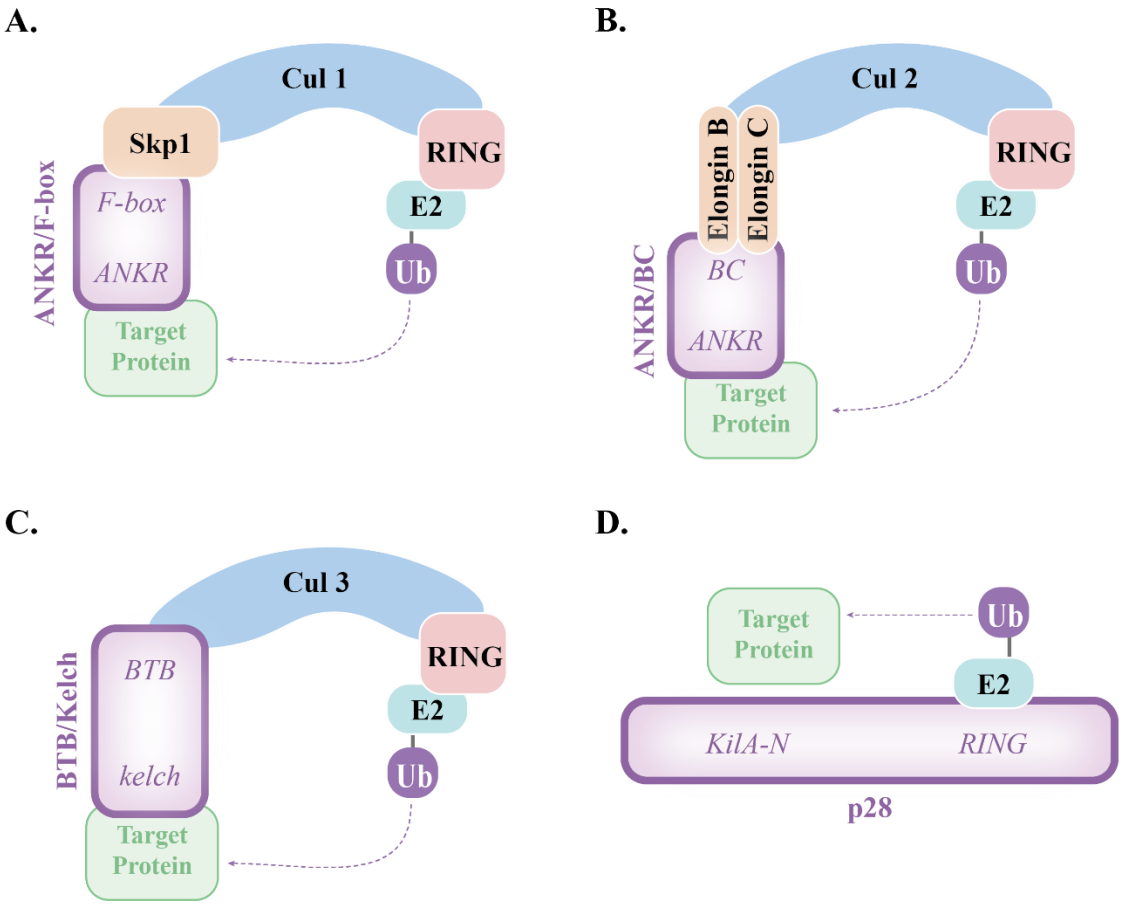

Figure 1.9 E3 Ub-ligases and adaptor proteins encoded by OPV genomes

OPV genomes encode four groups of proteins involved in the Ub system: ANKR/F-box **(A)**, ANKR/BC **(B)**, and BTB/kelch **(C)** are viral adaptor proteins associated with Cul1-, Cul2- and Cul3-based multi-subunit E3 Ub-ligases, respectively. Viral proteins have purple borders. **D,** p28 contains an N-terminal KilA-N domain and a C-terminal RING domain. It functions as a single subunit E3 Ub-ligase. The figure is adapted from (106).

dependent on participation in a Cul2 E3 Ub-ligase complex.

Viral BTB/kelch proteins are associated with immunopathology and influence host innate immune responses. The loss of VACV C2L (OPG33) was related to smaller plaque size *in vitro.* (144) Furthermore, C2L appears to play a role in promoting increased cell infiltration into infected ears in an intradermal mouse model (144). The deletion of VACV F3L (OPG47) did not affect virus replication in tissue culture cells, but resulted in smaller lesion and increased numbers of NK cells in virus-infected ears of mice (145). The NF-κB signalling pathway was also inhibited by a BTB/kelch protein encoded by VACV A55R (OPG184) (146). Interestingly, the inhibition was not dependent on the interaction of A55 with cellular Cul3, and the kelch domain alone was sufficient to impair NF-κB signalling (146). This suggests that the function of the viral adaptor proteins does not necessarily require their association with cellular E3 Ub-ligase components or their ubiquitylation activity.

Both viral ANKR/F-box and BTB/kelch proteins are important for poxvirus infection. VACV B18R (OPG203) encoding an ANKR/F-box protein, and VACV C5L (OPG30), a gene encoding for a BTB/kelch protein, were identified as poxvirus uncoating and DNA replication factors with mutually redundant functions (80). B4, an ANKR/F-box protein encoded by the VACV B4R gene (OPG189), is suggested to play a role in virion release and spread (147). Taken together, poxviral adaptor proteins interact with cellular Cul proteins, inhibit host immune responses, and contribute to virus infection.

Structure	OPG	CPXV-BR	VACV-Cop	ECTV-Mos	Role during infection
ANKR/ F-box	3	006/225[a]	C19L	002/171[a]	induce RIPK3 proteasomal degradation and prevent necroptosis (140) inhibit NF-κB pathway (138, 139)
	4	008/223[a]	C17L		
	9	11		5	
	15	17			
	23	25			host range (142)
	25	27	C9L		induce IFIT ubiquitylation and degradation, thereby enabling viral genome uncoating (134, 135)
	189	198	B4R	154	virus spread (147)
	203	211	B18R	165	virus uncoating (80)
	205	213			
	211	220			
ANKR/BC	14	16		10	inhibit innate immunity (143)
	17	19			inhibit TLR signalling pathway (143)

BTB/kelch	11	13			
	30	32[b]	C5L		Uncoating (80)
	33	35	C2L	18	inhibit inflammation (144)
	47	50	F3L	27	small lesion size (145)
	184	193	A55R	150/167	impair NF-κB pathway (146)
	196	204	B10R[c]		
	206	215			

Table 1.2 E3 adaptor protein genes of OPVs

The table shows the poxviral genes encoding for E3 adaptor proteins in CPXV (Brighton Red strain, CPXV-BR), VACV-Cop, and ECTV-Mos. The table includes the OPG names of the genes in OPVs, as well as gene names in CPXV-BR, VACV-Cop, and ECTV-Mos. Also shown in the table are the roles of these poxviral adaptor proteins during poxvirus infection. [a] The genes presented on both arms of the viral genome. [b] CPXV32 only has BTB domain. [c] B10R only has a kelch domain. The data is adapted from Chen, N. *et al.* 2003 and Senkevich, G.T. *et al.* 2021 (46, 54).

1.5.2.2 p28 and its homologues

p28 (OPG21) is a ~28-kDa E3 Ub-ligase **(Figure 1.9D)**. Its homologues are found throughout the *Chordopoxviruses* **(Figure 1.10)** (106, 148, 149), except for VACV-Cop, which has completely lost the p28 gene, and VACV strain Western Reserve (VACV-WR), which expresses a truncated p28 (150). The amino acid identity between p28 and its homologues is shown in **Table 1.3**. The Fowlpox virus (FPXV) genome encodes two p28 proteins (151), while most other strains, like ECTV and VARV, encode one p28 (46). p28 is expressed at both early and late stages of poxvirus replication and localizes to virus factories (150-155). There are two functional domains of p28: the N-terminal KilA-N domain and a C-terminal RING domain **(Figure 1.9D)**. The KilA-N domain was previously found in bacteriophages and large DNA viruses, and suggested to be homologous to the APSES fungal DNA-binding domain (156). The predicted structure of the KilA-N domain has two 2-β-strand-α-helix units, which is identical to the APSES domains (156). The p28 encoded by Shope fibroma virus (SFV-N1R), a poxvirus that infects rabbits, binds to both single-stranded DNA (ssDNA) and dsDNA columns (155). In addition, a truncated p28 encoded by VACV-WR was identified in the complex of nascent DNA and proteins during poxvirus infection (157). p28 without a RING domain (p28 KilA-N alone) is sufficient for virus factory localization (152). The deletion of a highly conserved seven amino acid residues (44-50; YINITKI) in the KilA-N domain disrupted p28 virus factory localization (153). The RING domain of p28 is a RING-finger domain with highly conserved cysteine

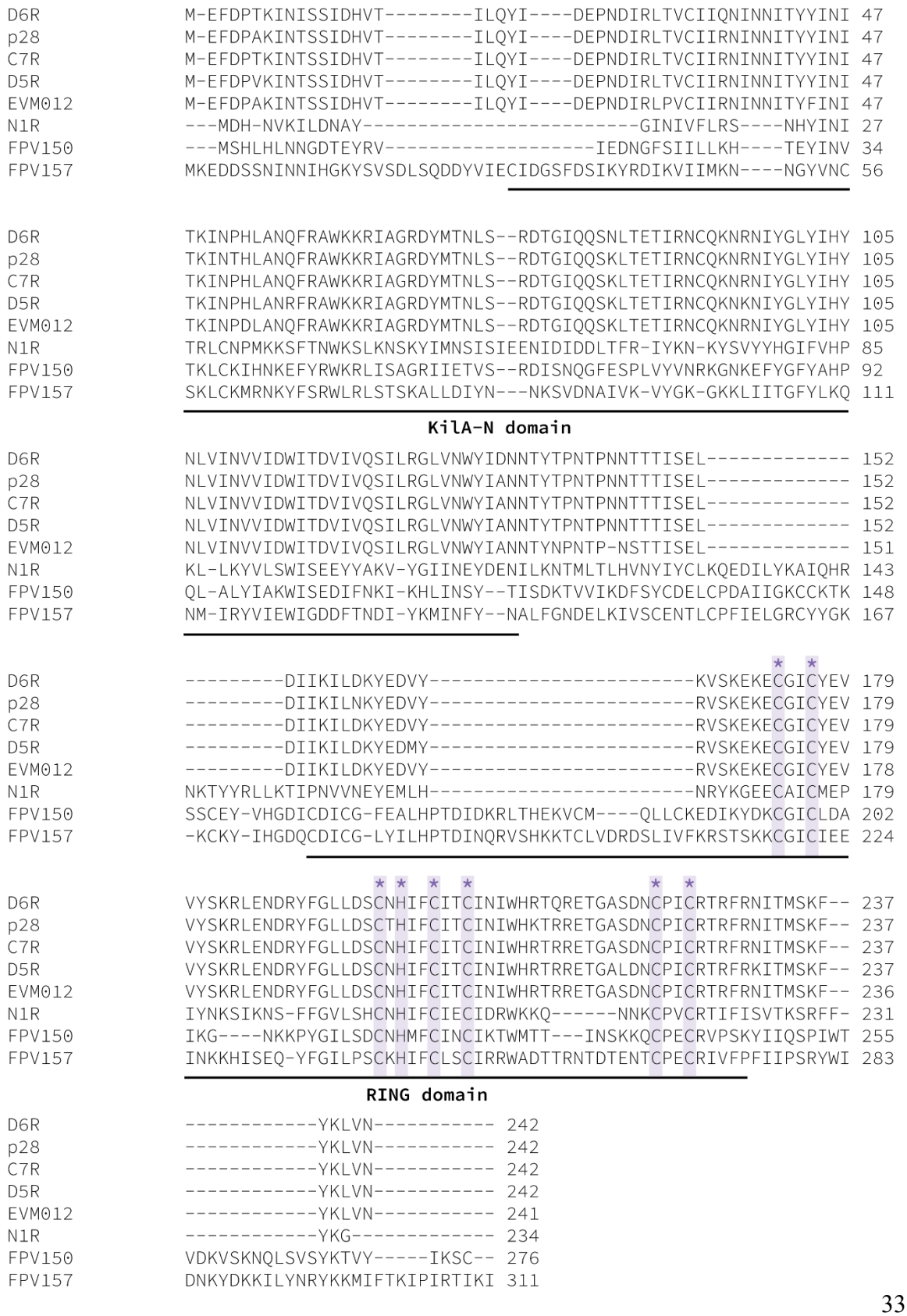
D6R M-EFDPTKINISSIDHVT--------ILQYI----DEPNDIRLTVCIIQNINNITYYINI 47
p28 M-EFDPAKINTSSIDHVT--------ILQYI----DEPNDIRLTVCIIRNINNITYYINI 47
C7R M-EFDPTKINTSSIDHVT--------ILQYI----DEPNDIRLTVCIIRNINNITYYINI 47
D5R M-EFDPVKINTSSIDHVT--------ILQYI----DEPNDIRLTVCIIRNINNITYYINI 47
EVM012 M-EFDPAKINTSSIDHVT--------ILQYI----DEPNDIRLPVCIIRNINNITYFINI 47
N1R ---MDH-NVKILDNAY-----------------------GINIVFLRS----NHYINI 27
FPV150 ---MSHLHLNNGDTEYRV-------------------IEDNGFSIILLKH----TEYINV 34
FPV157 MKEDDSSNINNIHGKYSVSDLSQDDYVIECIDGSFDSIKYRDIKVIIMKN----NGYVNC 56
D6R TKINPHLANQFRAWKKRIAGRDYMTNLS--RDTGIQQSNLTETIRNCQKNRNIYGLYIHY 105
p28 TKINTHLANQFRAWKKRIAGRDYMTNLS--RDTGIQQSKLTETIRNCQKNRNIYGLYIHY 105
C7R TKINPHLANQFRAWKKRIAGRDYMTNLS--RDTGIQQSKLTETIRNCQKNRNIYGLYIHY 105
D5R TKINPHLANRFRAWKKRIAGRDYMTNLS--RDTGIQQSKLTETIRNCQKNKNIYGLYIHY 105
EVM012 TKINPDLANQFRAWKKRIAGRDYMTNLS--RDTGIQQSKLTETIRNCQKNRNIYGLYIHY 105
N1R TRLCNPMKKSFTNWKSLKNSKYIMNSISIEENIDIDDLTFR-IYKN-KYSVYYHGIFVHP 85
FPV150 TKLCKIHNKEFYRWKRLISAGRIIETVS--RDISNQGFESPLVYVNRKGNKEFYGFYAHP 92
FPV157 SKLCKMRNKYFSRWLRLSTSKALLDIYN---NKSVDNAIVK-VYGK-GKKLIITGFYLKQ 111
KilA-N domain
D6R NLVINVVIDWITDVIVQSILRGLVNWYIDNNTYTPNTPNNTTTISEL------------ 152
p28 NLVINVVIDWITDVIVQSILRGLVNWYIANNTYTPNTPNNTTTISEL------------ 152
C7R NLVINVVIDWITDVIVQSILRGLVNWYIANNTYTPNTPNNTTTISEL------------ 152
D5R NLVINVVIDWITDVIVQSILRGLVNWYIANNTYTPNTPNNTTTISEL------------ 152
EVM012 NLVINVVIDWITDVIVQSILRGLVNWYIANNTYNPNTP-NSTTISEL------------ 151
N1R KL-LKYVLSWISEEYYAKV-YGIINEYDENILKNTMLTLHVNYIYCLKQEDILYKAIQHR 143
FPV150 QL-ALYIAKWISEDIFNKI-KHLINSY--TISDKTVVIKDFSYCDELCPDAIIGKCCKTK 148
FPV157 NM-IRYVIEWIGDDFTNDI-YKMINFY--NALFGNDELKIVSCENTLCPFIELGRCYYGK 167
D6R ---------DIIKILDKYEDVY----------KVSKEKECGICYEV 179
p28 ---------DIIKILNKYEDVY----------RVSKEKECGICYEV 179
C7R ---------DIIKILDKYEDVY----------RVSKEKECGICYEV 179
D5R ---------DIIKILDKYEDMY----------RVSKEKECGICYEV 179
EVM012 ---------DIIKILDKYEDVY----------RVSKEKECGICYEV 178
N1R NKTYYRLLKTIPNVVNEYEMLH----------NRYKGEECAICMEP 179
FPV150 SSCEY-VHGDICDICG-FEALHPTDIDKRLTHEKVCM----QLLCKEDIKYDKCGICLDA 202
FPV157 -KCKY-IHGDQCDICG-LYILHPTDINQRVSHKKTCLVDRDSLIVFKRSTSKKCGICIEE 224
D6R VYSKRLENDRYFGLLDSCNHIFCITCINIWHRTQRETGASDNCPICRTRFRNITMSKF-- 237
p28 VYSKRLENDRYFGLLDSCTHIFCITCINIWHKTRRETGASDNCPICRTRFRNITMSKF-- 237
C7R VYSKRLENDRYFGLLDSCNHIFCITCINIWHRTRRETGASDNCPICRTRFRNITMSKF-- 237
D5R VYSKRLENDRYFGLLDSCNHIFCITCINIWHRTRRETGALDNCPICRTRFRKITMSKF-- 237
EVM012 VYSKRLENDRYFGLLDSCNHIFCITCINIWHRTRRETGASDNCPICRTRFRNITMSKF-- 236
N1R IYNKSIKNS-FFGVLSHCNHIFCIECIDRWKKQ------NNKCPVCRTIFISVTKSRFF- 231
FPV150 IKG----NKKPYGILSDCNHMFCINCIKTWMTT---INSKKQCPECRVPSKYIIQSPIWT 255
FPV157 INKKHISEQ-YFGILPSCKHIFCLSCIRRWADTTRNTDTENTCPECRIVFPFIIPSRYWI 283
RING domain
D6R ----------YKLVN---------- 242
p28 ----------YKLVN---------- 242
C7R ----------YKLVN---------- 242
D5R ----------YKLVN---------- 242
EVM012 ----------YKLVN---------- 241
N1R ----------YKG---------- 234
FPV150 VDKVSKNQLSVSYKTVY-----IKSC-- 276
FPV157 DNKYDKKILYNRYKKMIFTKIPIRTIKI 311

Figure 1.10 p28 proteins encoded by poxvirus genomes

Alignment of p28 proteins from selected *Chordopoxviruses*. The indicated p28 protein sequences were aligned by CLUSTAL format alignment, MAFFT FFT-NS-i (v7.487). The relative location of the KilA-N and RING domains (153) are underlined. Amino acids which conserved in RING domain are highlighted in purple and indicated by asterisk. D6R; VARV (Somalia-1977); AAA69414, p28; VACV (International Health Department-White, IHD-W); AIX98929, EVM012; ECTV (Mos); AAM92318, C7R; CPXV (BR); CAA64092, D5R; MPXV (Zaire-96-I-16); AAL40466, N1R; Rabbit fibroma virus (Kasza); NP_052029, FPV150; FPXV (Iowa); NP_039113.1, FPV157; FPXV (Iowa); NP_039120.1

	D6R	p28	C7R	D5R	EVM012	N1R	FPV150	FPV157
D6R	-	95.45	97.52	95.04	95.02	29.67	29.03	29.26
p28		-	97.93	95.87	96.27	30.14	28.57	28.82
C7R			-	97.52	97.51	29.67	29.03	28.82
D5R				-	95.44	29.67	29.49	28.82
EVM012					-	29.81	28.7	28.51
N1R						-	32.59	29.2
FPV150							-	35.42
FPV157								-

Table 1.3 The identities between p28 and its homologues

The overall percent amino acid identities between the p28 and its homologues are indicated. D6R; VARV (Somalia-1977); AAA69414, p28; VACV (IHD-W); AIX98929, EVM012; ECTV (Mos); AAM92318, C7R; CPXV (BR); CAA64092, D5R; MPXV (Zaire-96-I-16); AAL40466, N1R; Rabbit fibroma virus (Kasza); NP_052029, FPV150; FPXV (Iowa); NP_039113.1, FPV157; FPXV (Iowa); NP_039120.1. The identities were created by Clustal2.1 and determined using the EMBOSS Needle alignment tool.

and histidine residues (C_3HC_4) **(Figure 1.10)**, which has the ability to bind zinc (150, 158). The first two conserved cysteines of the p28 RING domain, C173 and C176, are essential for the auto-ubiquitylation activity of p28 (151, 152).

p28 is a critical virulence factor of ECTV in susceptible mice. Senkevich *et al.* generated a p28 deletion mutant virus (ECTV-$p28^{RING\text{-}gpt}$) by exchanging the RING domain of p28 with a xanthine-guanine phosphoribosyltransferase (*gpt*) selection cassette in an orientation opposite to the p28 gene (158). When strain A susceptible mice were infected with ECTV-$p28^{RING\text{-}gpt}$, the median lethal dose (LD_{50}) of ECTV was increased by 6 logs compared with wild-type ECTV (158). The titers of the ECTV-$p28^{RING\text{-}gpt}$ in livers and spleens of footpad infected strain A mice were significantly lower than the wild-type ECTV (158). A follow-up study showed that virus replication and factory formation of ECTV-$p28^{RING\text{-}gpt}$ were severely inhibited in resident peritoneal macrophages (PMs) from susceptible strain A mice (154). Macrophages are vectors that transport ECTV in mice from the skin (footpad infection site) to the organs where the virus primarily replicates, such as the liver and spleen (47, 154). The inhibition of ECTV-$p28^{RING\text{-}gpt}$ replication in macrophages may be the reason for the reduced virus titer in the liver and spleen in the infected strain A mice. Furthermore, expressing p28 allowed ECTV to replicate in cells pre-treated with UV irradiation (159). Overexpressing N1R reduced apoptosis-associated fragmentation of nuclear DNA induced by VACV infection (155). These results indicate p28 may inhibit the apoptosis of infected cells. p28 was also demonstrated as a host range

factor of CPXV in macrophage cell lines (RAW 264.7 and J774A.1), rat primary PMs, and human PBMC-derived macrophages (160). The RING domain of p28 was critical for the productive replication of CPXV in the cell types mentioned above (160). In addition, overexpression of p28 localized conjugated Ub to virus factories (151, 153). Ubiquitylation assays indicated that both the p28 of ECTV and VARV cooperate with the E2s that catalyzed K48-linked polyubiquitin chains (Ubc4 and UbcH5c) and with Ubc13/Uev1A, a heterodimeric E2 that promoted K63-linked chains formation (149). These results suggest that p28 may function as a poxviral E3 Ub-ligase. However, how p28 recognizes its substrates and what the substrates of p28 are remain unknown.

1.6 Thesis objectives

Poxviruses manipulate the Ub system of infected cells to facilitate viral replication, evade innate immune responses, and prevent programmed cell death of infected cells. On the other hand, the Ub system is also involved in host immune responses against virus infection. I was interested in further elucidating the impact of poxvirus infection on the host Ub system, including how poxviruses exploit the host Ub system through viral E3 Ub-ligases and what changes occur in host protein ubiquitylations during poxvirus infection.

p28 is a critical virulence factor in specific mouse strains (154, 158). To further address the function of p28, **in Chapter 3**, we completely deleted the gene of p28 from ECTV (ECTV-Δp28). As an initial characterization of this virus, I examined how the complete deletion of p28 impacted virus production in different cell types, including cell lines and

murine PMs from susceptible and resistant mice. **In Chapter 4,** I used several methods to establish the p28 substrates and the function of the KilA-N domain of p28 *in vitro*. Small-scale experiments demonstrated the feasibility of using Ub-activated interaction traps (UBAITs) to capture proteins in close proximity to p28. Furthermore, I purified p28 via the baculovirus expression system, which will be valuable for our future studies to identify the substrates and the functions of p28 *in vitro.* To understand the global impacts of poxvirus infection on Ub modification in infected cells, **in Chapter 5**, we enriched ubiquitylated peptides, in this case, peptides with a diglycine (diGly) motif, from VACV-infected and uninfected cells. Quantitative changes of these diGly peptides after VACV infection were detected by mass spectrometry. This provided further information about the diverse roles of the Ub system and ubiquitylated proteins during poxvirus infections. I further studied the effect of virus infection on one of these ubiquitylated proteins, tripartite motif-containing protein 25 (TRIM25), in which several diGly peptides were either exclusively found or enriched in VACV-infected cells. I proceeded to reveal TRIM25 as a novel protein potentially involved in the host-virus tug-of-war in the Ub system. This research further enhances our understanding of the interaction between poxvirus infection and the Ub system of the host cell.

Chapter 2: Materials and Methods

Parts of this chapter of the thesis have been published in:

"Jianing Dong, Patrick Paszkowski, Dana Kocincova, Robert J. Ingham. Complete deletion of Ectromelia virus p28 impairs virus genome replication in a mouse strain, cell type, and multiplicity of infection-dependent manner. *Virus Research.* 323 (2023) 198968, doi: 10.1016/j.virusres.2022.198968."

And the manuscript:

"Jianing Dong, Shu Luo, Summer Smyth, Grace Melvie, Olivier Julien, Robert J. Ingham. Characterizing changes in protein ubiquitylation during vaccinia virus infection." (Under review, manuscript # JVI00430-24)

The schematic representations of the experiment were created with BioRender.com.

2.1 Materials

The materials used in this thesis were listed below.

Table 2.1 Commercial Kits

Kit	Source
Aurum™ Total RNA Mini Kit	Bio-Rad
QIAprep Spin Miniprep Kit	QIAGEN
QIAquick Gel Extraction Kit	QIAGEN
QIAquick PCR Purification Kit	QIAGEN
Superscript II Reverse Transcriptase System	Invitrogen

Table 2.2 Buffers

Buffer	Composition
1% NP-40 Lysis Buffer	50 mM Tris-HCl pH 7.4, 150 mM NaCl, 2 mM Ethylenediaminetetraacetic acid (EDTA), 1% NP-40, 10% glycerol
5× Protein Loading Buffer	312.5 mM Tris-HCl pH 6.8, 500 mM dithiothreitol (DTT), 10% glycerol, 11.5% sodium dodecyl sulfate (SDS), 0.1% Bromphenol Blue
EMSA Reaction Buffer	10 mM Tris-HCl pH 7.5, 100 mM KCl, 0.2 mM EDTA, 0.5 mM DTT, 10% w/v glycerol, 200 μg/mL BSA, 100 μg/mL poly-d(IC)
FACS Buffer	phosphate-buffered saline (PBS) containing 1% fetal bovine serum (FBS)
Mowiol Mounting Medium	0.1 mg/mL Mowiol, 0.1 M PBS pH 7.4, 25% glycerol, 2.4% triethylenediamine
Ubiquitination Reaction Buffer	50 mM Tris-HCl pH 7.5, 200 mM NaCl, 1 mM DTT

Table 2.3 Oligonucleotides

Name	Restriction sites	Usage	Sequence
SmaI-p28-rev	SmaI	PCR	5’-CTAGCTGACCCGGGTTAGTTAACTAGCTTATAGAAC-3’
SmaI-Ub-rev	SmaI	PCR	5’-CCCGGGTTAACCACCTCTTAGTC-3’
5'-FLAG-fwd	N/A	PCR	5’-CGATCACTGACTACAAAGACGATGACGACAAG-3’
BamHI-KilA-N-fwd	BamHI	PCR	5’-CGATCACTGGATCCCAATACATAGATGAACCAAATGATATAAGACTAC-3’
BamHI-p7.5-fwd	BamHI	PCR	5’-CGATCACTGGATCCTCGACATATACTATATAG-3’
BamHI-RING-fwd	BamHI	PCR	5’-CGATCACTGGATCCCTGGATAAATACGAGGACGTGTATAGAGTAAG-3’
BglII-EVM013-fwd	BglII	PCR	5’-AGATCTGAACGGATGTCCTCCAAC-3’
EVM049 (VACV E9L) standard curve template	N/A	qPCR	5’-GGATTGGCAAACCGTAACATACCGTTAGATAACTCTGCTCCATTTAGTACCGATTCTAG ATACAAGATCATTCTACGTCCTATGGATGTGCAACTCTTAGCCGAAGCGTATGAGTATAGA GCACTATTTCTAAATCCCATCAGACCATAT-3’

EVM049 (VACV E9L)-fwd	N/A	qPCR	5’ - CTCTGCTCCATTTAGTACC GATTC - 3’
EVM049 (VACV E9L)-rev	N/A	qPCR	5’- TACTCATACGCTTCGGCTA AGA–3’
EVM011-fwd	N/A	RT-PCR	5’- GTCTAATTGGGCACCCTTA ACT-3’
EVM011-rev	N/A	RT-PCR	5’- CCGACGTTATATTTCCTGTA GGG-3’
EVM013-fwd	N/A	RT-PCR	5’- AACCGTTCGTACCACAGAT G-3’
EVM013-rev	N/A	RT-PCR	5’- CGTAGTGAGGACACAAGT GAA-3’
EVM056-fwd	N/A	RT-PCR	5’- CAACTGGCCAAGGCAATT ATC-3’
EVM056-rev	N/A	RT-PCR	5’- CGTTAGCCACCACTTCTCT ATC-3’
Hairpin DNA	N/A		5’- ACATTTTTTTCTAGACACT AAATAAAATATTTAAAATAT AATATTAATGTACTAAAAC TTATATATTATTAATTTATCT AACTAAAGTTAGTAAATTA TATATATAATTTTATAATTAA TTTAATTTTACTAATTTTAT TTAGTGTCTAGAAAAAAA- 3’
KpnI-Linker-Ub-fwd	KpnI	PCR	5’- GGTACCGGTGGTTCTGGTG GTG-3’

NotI-EVM013-rev	NotI	PCR	5’-GCGGCCGCCTTCAGTATTGGATGAATCTC-3’
p28(int)-fwd	N/A	PCR	5’-AGAGGGTTGGTAAATTGGTACAT-3’
p28(int)-rev	N/A	PCR	5’-CAACTTCATAGCAAATTCCACATTC-3’
pGEX 3' Sequencing Primer	N/A	PCR	5’-CCGGGAGCTGCATGTGTCAGAGG-3’
pGEX 5' Sequencing Primer	N/A	PCR	5’-GGGCTGGCAAGCCACGTTTGGTG-3’
qPCR probe	N/A	qPCR	5’ /56FAM/AGATCATTC/ZEN/TACGTCCTATGGATGTGCAAC/3IABKFQ/ 3’
SalI-EVM011-fwd	SalI	PCR	5’-CGATCACTGTCGACGTCGTTACATCATACCTTATA-3’
SalI-p28-fwd	SalI	PCR RT-PCR	5’-GTCGACGAATTCGATCCTGCCAAAATC-3’
SmaI-KilA-N-rev	SmaI	PCR	5’-CGATCACTCCCGGGTTAATTAGCTATGTACCAATTTACCAACCCTC-3’
SmaI-p28-rev	SmaI	RT-PCR	5’-CCCGGGTTAGTTAACTAGCTTATAGAAC-3’
SmaI-RING-rev	SmaI	PCR	5’-CGATCACTCCCGGGTTATCTAAAACGGGTACGGCATATAGGAC-3’
SpeI-EVM011-rev	SpeI	PCR	5’-ACTAGTCTCTACCTCTAGATATGATAC-3’

TK fwd	N/A	PCR	5’-TATTCAGTTGATAATCGGCCCCATGTTT-3’
TK rev	N/A	PCR	5’-GAGTCGATGTAACACTTTCTACACACCG-3’
XhoI-EVM011-rev	XhoI	PCR	5’-CGATCACTCTCGAGCTCTACCTCTAGATATGATAC-3’
yellow fluorescent protein (YFP)/gpt qPCR-fwd	N/A	PCR	5’-GATGCCTTCTGAACAATGGAAAG-3’
YFP/gpt qPCR-rev	N/A	PCR	5’-GTCGTGATCGTAGCTGGAAATA-3’
β-actin-fwd	N/A	RT-PCR	5’-CCTGGCACCCAGCACAAT-3’
β-actin-rev	N/A	RT-PCR	5’-GCCGATCCACACGGAGTACT-3’

Table 2.4 Plasmids

Plasmid	Characteristics	Source
pDGloxP	Vector for exchange a poxviral gene with YFP/gpt cassette	Dr. David Evans (University of Alberta)
pDGloxP-EVM013-EVM011	The target plasmid which was used to generate p28 knock-out ECTV	Constructed by Patrick Paszkowski
pFastBac-1-ECTV-p28	Donor plasmid for baculovirus generation. Contain the gene of full length ECTV p28	Purchased from GenScript
pFastBac-1-ECTV-p28-KilA-N	Donor plasmid for baculovirus generation. Contain the gene of the KilA-N domain of ECTV p28	Purchased from GenScript
pFastBac-1-ECTV-p28-RING	Donor plasmid for baculovirus generation. Contain the gene of the RING domain of ECTV p28	Purchased from GenScript

pGEX-4T-1	GST gene fusion vector, express GST under the control of an isopropyl β-D-1-thiogalactopyranoside (IPTG) inducible promoter	Purchased from Amersham Biosciences
pGEX-4T-1-KilA-N	GST gene fusion vector with the gene of the KilA-N domain of ECTV p28	Constructed in this study
pGEX-4T-1-p28	GST gene fusion vector with the gene of full length ECTV p28	Constructed in this study
pGEX-4T-1-RING	GST gene fusion vector with the gene of the RING domain of ECTV p28	Constructed in this study
pSC66	Vector with poxviral early/late promoter. Express proteins in poxvirus-infected cells	Dr. David H. Evans (University of Alberta)
pSC66-FLAG-p28	poxvirus early/late promoter (pE/L), followed by a gene encoded full length ECTV p28 with a FLAG tag at the N terminus	Constructed in this study
pSC66-FLAG-p28-Ub	pE/L, followed by a gene encoded full length ECTV p28 with a FLAG tag at the N terminus and a linker with Ub motif at the C terminus	Constructed in this study

Table 2.5 Antibodies (Abs)

Ab	Application	Origin	Source	Dilution
6×His, His-tag	WB/IP	Mouse	#66005-1-Ig, Proteintech	1:1,000/2 μg
A34	WB/IF	Rabbit	Dr. Bernard Moss (National Institute of Allergy and Infectious Disease)	1:1,000/1:1,000
B5	WB	Mouse	Dr. Stuart Isaacs (University of Pennsylvania)	1:1,000

CDK2	WB	Mouse	#MA5-17052, Invitrogen	1:1,000
FLAG	WB/IF	Rabbit	#F7425, Sigma-Aldrich	1:1,000/1:500
FLAG (M2)	WB/IF/IP	Mouse	#F3165, Sigma-Aldrich	1:1,000/1:500/1 µg
HJURP	IP	Rabbit	#703460, Invitrogen	1-5µg
Heat shock protein 70 (Hsp70)	WB	Mouse	#sc-66948, Santa Cruz	1:500
I3	WB/IF	Mouse	Dr. David Evans (University of Alberta)	1:5,000/1:1,000
mouse Alexa 488	IF	Goat	#A11001, Invitrogen	1:1,000
mouse CD11b (M1/70) PE-Cyanine7	Flow	Rat	#25-0112-82, Invitrogen	1:2,000
mouse F4/80 eFluor 450 (BM8)	Flow	Rat	#48-4801-80, eBioscence	1:1000
mouse IRDye 800	WB	Goat	#92632210, LI-COR Biosciences	1:20,000
p28	WB	Rabbit	Buller and Brien labs (St. Louis University)	1:1,000
rabbit Alexa Fluor 647	IF	Goat	#111-605-144, Jackson ImmunoResearch	1:1,000
rabbit IRDye 680	WB	Goat	#92668071, LI-COR Biosciences	1:20,000
TRIM25	WB/IP	Rabbit	#ab167154, Abcam	1:1,000/1-5 µg
Ub (FK2)	WB/IF/IP	Mouse	#BML-PW8810, Enzo Life Sciences	1:1,000/1:500/2 µg
Ub (P4D1)	WB	Mouse	#39741, Active Motif	1:1,000
β-actin	WB	Mouse	#A5441, Millipore Sigma	1:5,000
β-tubulin	WB	Mouse	#TM1541, ECM Biosciences	1:1,000

2.2 Methods

2.2.1 Cells

2.2.1.1 Cell lines

Table 2.6 Cell lines

Cell line	Source
293T	American Type Culture Collection (ATCC)
BSC-40	Dr. David Evans (University of Alberta)
HeLa	Dr. Jim Smiley (University of Alberta)
Neuro-2a	Dr. Roslyn Godbout (University of Alberta)
Sf9	Dr. Matthias Götte (University of Alberta)
YAC-1	Dr. Hanne Ostergaard (University of Alberta)

BSC-40 cells were cultured in Minimum Essential Medium Eagle (MEM; Sigma) supplemented with 5% FBS (Sigma-Aldrich), 1% non-essential amino acids (Gibco), 2 mM L-glutamine (Gibco), 1 mM sodium pyruvate (Gibco), and 1% antibiotic-antimycotic solution (Gibco). HeLa and 293T cells were grown in Dulbecco's Modified Eagle's Medium – high glucose (DMEM; Sigma) supplemented with 10% FBS, 2 mM L-glutamine, and 1% antibiotic-antimycotic solution (Gibco). YAC-1 cells were cultured in Roswell Park Memorial Institute 1640 (RPMI 1640; Gibco) media containing 10% FBS and 1% antibiotic-antimycotic solution. Neuro-2a cells were grown in DMEM containing 10% FBS and 1% antibiotic-antimycotic solution. All mammalian cells were incubated at 37°C and 5% CO_2. Sf9 insect cells were grown in Sf-900^{TM} II SFM (Gibco) and incubated at 30°C.

2.2.1.2 Purification of resident peritoneal macrophages (PMs)

Strain A (also known as A/J or A/JCr) and BALB/c mice were purchased from Charles River (Saint-Constant, QC, Canada) or Jackson Laboratory (Bar Harbor, ME). C57BL/6 mice were obtained from the breeding colony of Dr. Troy Baldwin (University of Alberta). Mice were maintained in accordance with protocols approved by the University of Alberta Animal Care and Use Committee (AUP00002579). Resident PMs were isolated as previously described **(Figure 2.1A)** (161). Briefly, cells were flushed from the peritoneal cavity with ice cold, sterile PBS, enriched by centrifugation at 400×*g* for 10 min at 4°C, and then plated on 12-well tissue culture treated plates at a density of 1×10^6 cells/mL. Cells were incubated in macrophage media (DMEM with 10% FBS, 100 U/mL penicillin, and 100 μg/mL streptomycin) at 37°C and 5% CO_2 for 2 h. To remove non-macrophages, the isolated cells were washed with warm PBS three times and incubated in fresh macrophage media at 37°C overnight. The isolated macrophages were stained with anti-F4/80 and anti-CD11b which are two surface antigens of macrophages (162), and the percentage of cells with both these macrophage antigens were tested by flow cytometry (BD Biosciences) **(Figure 2.1B)**. Data was analyzed using FlowJo software (Ashland, OR) and results showed that greater than 80% of the cells were CD11b and F4/80 double positive **(Figure 2.1B)**. I routinely isolated ~1 million cells per mouse.

A.

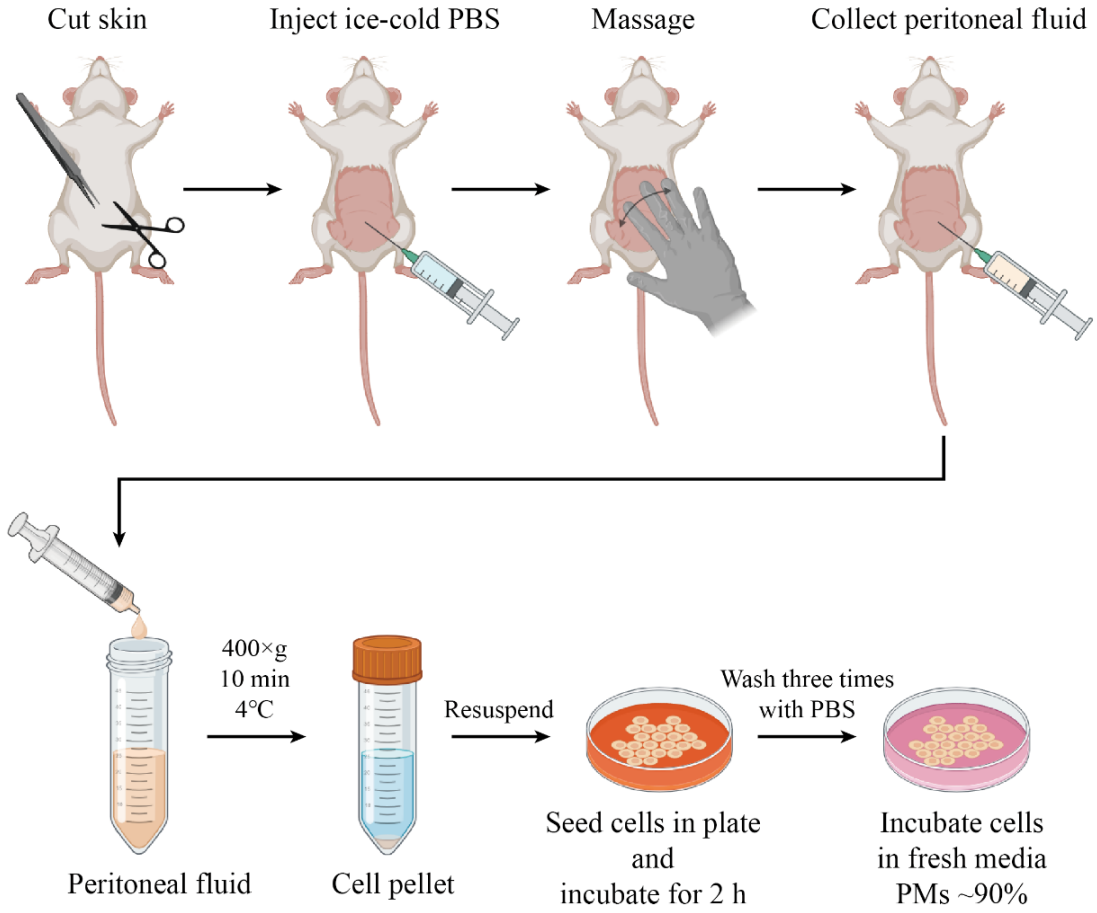
Cut skin
Inject ice-cold PBS
Massage
Collect peritoneal fluid
400×g
10 min
4°C
Resuspend
Wash three times
with PBS
Peritoneal fluid
Cell pellet
Seed cells in plate
and
incubate for 2 h
Incubate cells
in fresh media
PMs ~90%

B.

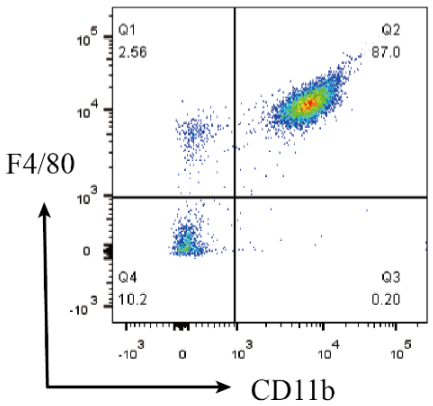
Q1
2.56
Q2
87.0
Q4
10.2
Q3
0.20
F4/80
CD11b

Figure 2.1 PM isolation from mice

A, Diagram of PM isolation. PMs were isolated from mice using previously described methods (161). Total cells in the peritoneal fluid were collected in ice-cold PBS. These cells were centrifuged and resuspended in macrophage media. Then, cells were seeded into tissue culture-treated plates and incubated at 37℃ for 2 h. The non-adherent cells were washed away with PBS. **B,** Flow cytometry examining the macrophage surface antigens on the isolated cells. Cells were fixed and stained with anti-F4/80 and anti-CD11b Abs and then analyzed by flow cytometry. Routinely, more than 80% cells were CD11b and F4/80 double positive.

2.2.1.3 Generation of bone marrow-derived macrophages (BMDMs)

Bone marrow cells were isolated from strain A mice as previously described **(Figure 2.2A)** (163). The femur and tibia were washed with ice cold, sterile PBS and cut at the joint. Ice-cold, sterile PBS was used to flush the bone marrow cells into a 50 mL conical tube through a 70 μm cell strainer which was used to filter the solid fragments. Bone marrow cells were centrifuged down and resuspended in bone marrow differentiation medium (RPMI-1640 supplemented with 20% FBS, 100 U/mL penicillin, 100 μg/mL streptomycin, 2 mM L-Glutamine and 20 ng/mL macrophage colony-stimulating factor (M-CSF, ≥1 unit/ng) (PeproTech)). Cells were seeded in non-tissue culture treated plates and incubated at 37°C and 5% CO_2 for 4 days. Fresh media was added to cells on day 4, and cells were then incubated for another 3 days. Non-macrophages were washed away with sterile PBS. Flow cytometry (BD Biosciences) revealed that approximately 90% of the cells were CD11b and F4/80 double positive **(Figure 2.2B)**.

A.

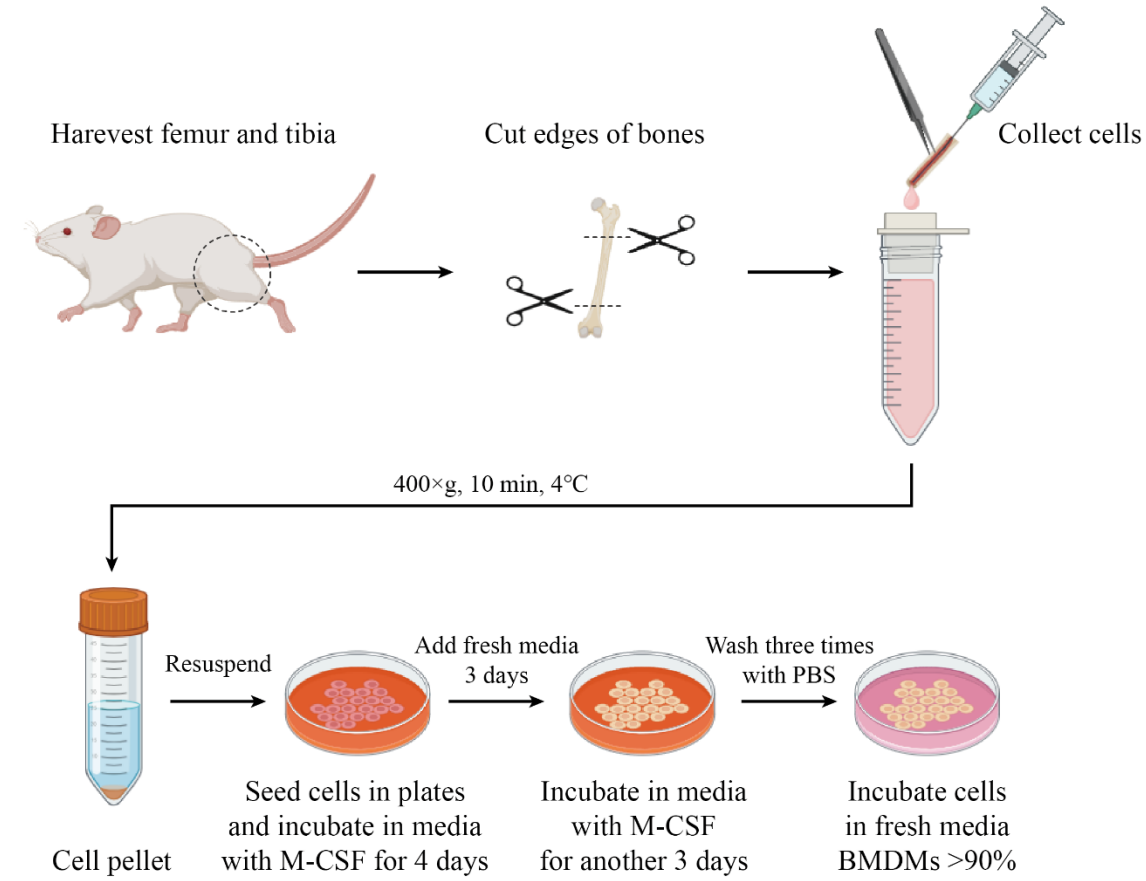
Harevest femur and tibia
Cut edges of bones
Collect cells
400×g, 10 min, 4°C
Resuspend
Add fresh media
3 days
Wash three times
with PBS
Cell pellet
Seed cells in plates
and incubate in media
with M-CSF for 4 days
Incubate in media
with M-CSF
for another 3 days
Incubate cells
in fresh media
BMDMs >90%

B.

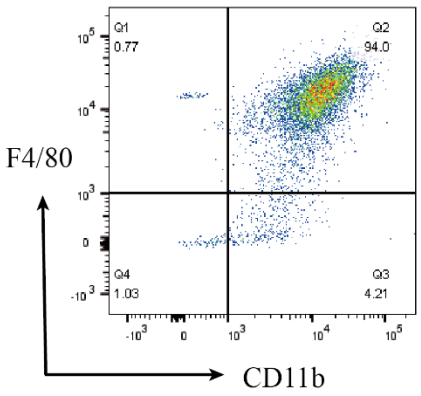
Q1
0.77
Q2
94.0
Q4
1.03
Q3
4.21
F4/80
CD11b

Figure 2.2 BMDM isolation from mice

A, Diagram of BMDM isolation. BMDMs were isolated from mice using previously described methods (163). Bone marrow cells were collected in PBS. These cells were seeded into non-tissue culture-treated plates and incubated in culture media with M-CSF at 37℃ for 4 days. Add fresh media with M-CSF and incubate cells for another 3 days. Non-adherent cells were washed away with PBS. **B,** Isolated cells were fixed and stained with anti-F4/80 and anti-CD11b Abs and then analyzed by flow cytometry. Routinely, more than 90% cells were CD11b and F4/80 double positive.

2.2.2 Viruses

Table 2.7 Viruses

Virus	strain	Characteristics	Source
ECTV-Mos	Moscow		Dr. Michele Barry (University of Alberta)
ECTV-Δp28	Moscow	Knock-out p28	Generated by Patrick Paszkowski
ECTV-Δp28-Rev	Moscow	Generated from p28 knock-out ECTV; expresses p28	Generated in this study
VACV-Cop	Copenhagen		Dr. Michele Barry (University of Alberta)
VACV-IHD-W	International Health Department-White		Dr. Michele Barry (University of Alberta)
VACV-WR	Western Reserve		Dr. David Evans (University of Alberta)
VACV-TianTan	Tian Tan		Dr. David Evans (University of Alberta)
ACAM2000™			Dr. David Evans (University of Alberta)
CPXV-BR	Brighton Red		Dr. David Evans (University of Alberta)
vP811		Deletion viruses derived from VACV-Cop (ΔC23L-F4L; ΔB13R-B29R)	Generated by Dr. Enzo Paoletti group (164). Obtained from Dr. Michele Barry (University of Alberta)
vP759		Deletion viruses derived from VACV-Cop (ΔB13R-B29R)	Generated by Dr. Enzo Paoletti group (164). Obtained from Dr. Michele Barry (University of Alberta)

vP798		Deletion viruses derived from VACV-Cop (ΔC23L-F4L)	Generated by Dr. Enzo Paoletti group (164). Obtained from Dr. Michele Barry (University of Alberta)

Deletion viruses derived from VACV-Cop (vP811, vP759, and vP798) were originally generated by the Poaletti group (164), and were also provided by Dr. Michelle Barry. Lysates of MPXV (Clade IIb)-infected HeLa cells were generously provided by Dr. David Evans.

2.2.2.1 Production of poxviruses

Virus stocks were generated by infecting five or ten 150 mm plates of BSC-40 cells at a multiplicity of infection (MOI) of 0.05 for 48 h. The infected cells were harvested by scraping into the media and collecting in 50 mL conical tubes. The cells were pelleted by centrifugation at 2,000×*g* for 10 mins, washed with PBS once, and then resuspended in 6 mL of 10 mM Tris (pH 8.0). The virus was released from cells by Dounce homogenizations. Cell fragments were removed by centrifugation at 2000×*g* for 10 mins and supernatants were transferred to a new centrifuge tube. The pellet was again resuspended in 6 mL of 10 mM Tris (pH 8.0) followed by Dounce homogenization. The supernatants from the two Dounce homogenization were adjusted to 19 mL using 10 mM Tris (pH 8.0). 19 mL of 36% sucrose in 10 mM Tris (pH 8.0) was layered under the supernatant. The extracted viruses in the supernatant were pelleted by centrifugation at 4℃ for 90 mins at 26,500×*g*. The supernatant was aspirated, and the virus pellet was resuspended in 1 mL of 10 mM Tris

(pH 8.0). 200 μL of resuspended viruses was placed into each aliquot tube. Viruses were stored at -80°C.

2.2.2.2 Determination of virus titer

To determine the titer of poxviruses, samples with virus were 10-fold serially diluted with MEM to an appropriate range. Then, BSC-40 cells were infected with diluted samples in triplicate in 12-well plates. After 1 h of inoculation, the diluted samples were aspirated. VACV-infected cells were incubated in fresh complete media for 24 h. ECTV-infected or deletion viruses derived from VACV-Cop (vP811, vP759, and vP798) infected cells were incubated in fresh media containing 1% carboxymethyl cellulose (CMC) for 72 h. Then, crystal violet solution (1.3% crystal violet, 5% ethanol, and 10% formaldehyde in H_2O) was directly added to the media for 2 h at room temperature to fix and stain for viral plaques. The plates were washed with water and the plaques were counted for virus titer calculation.

$$Virus\ titer = \frac{Average\ count\ of\ plaques\ per\ well}{Volume\ of\ inoculation\ per\ well} \times Dilution\ fold$$

2.2.2.3 Generation of recombinant virus

ECTV-Mos genomic DNA was used to generate a targeting vector where the gene encoding for p28, EVM012, was replaced by a YFP/*gpt* cassette flanked by loxP sites. The generation of recombinant viruses has been previously described (165). Briefly, BSC-40 cells were infected with ECTV-Mos and transfected with the linearized targeting vector.

Recombinant YFP-positive viruses were selected for in the presence of media containing 25 µg/mL mycophenolic acid, 15 µg/mL hypoxanthine, and 250 µg/mL xanthine (Millipore Sigma). YFP-positive plaques were plaque purified for three rounds. To remove the selection marker, cells were infected with YFP-positive virus and transfected with a plasmid expressing the Cre recombinase and YFP-negative plaques were selected under a fluorescence microscope. YFP-negative plaques were plaque purified for three rounds. The resulting virus was validated by Polymerase Chain Reaction (PCR) screening and whole genome sequencing. The revertant virus was generated by replacing the YFP/*gpt* cassette with EVM012. YFP-negative plaques were selected under a fluorescence microscope. YFP-negative plaques were plaque purified for three rounds. PCR and whole genome sequencing were used to validate the virus.

2.2.2.4 Virus growth curve experiments

Growth curves were performed by infecting the indicated cell lines with viruses at a MOI of 3 (single-step growth curve) or a MOI of 0.03 (multi-step growth curve). Infected cells were harvested by scraping cells into 1 mL of culture medium at the indicated times post-infection. Virus was released from cells by three rounds of freeze-thawing and titers were determined on BSC-40 cells as previously described in 2.2.2.2. The input virus titer was shown as the 0 h time point titer in the curve.

2.2.2.5 Virus DNA isolation

Total cellular and viral DNA was isolated by phenol extraction for PCR or quantitative

PCR. Virus-infected cells were harvested by centrifuge and the pellets were lysed in lysis buffer (1.2% SDS, 50 mM Tris pH 8, 4 mM EDTA, and 4 mM $CaCl_2$, fresh proteinase K was added to 0.5 μg/μL before use) for 4 h at 37℃. The cell lysate was mixed with buffer-saturated phenol and centrifuged in a phase lock gel light 2 mL tube (#2302820, Quantabio). The upper layer (aqueous layer) was collected in a new centrifuge tube. 2.5×volume of 95% ethanol and 0.1×volume of 3 M sodium acetate was added and mixed with the aqueous layer. The mixture was placed at -80℃ overnight. The DNA was pelleted from the sample by centrifuging at 20,000×*g* for 30 min at 4℃, then washed once with 70% ice-cold ethanol. The ethanol in the tube was dried and then the DNA pellet was resuspended in ddH_2O.

To prepare viral DNA for sequencing, 200 μL of purified virus was incubated with 100 μL virion lysis buffer (50 mM TrisHCl pH 9.5, 0.7 M NaCl, 10 mM EDTA, and 1% SDS) and incubated with freshly added proteinase K (0.5 μg/μL) at 37℃ overnight. The viral DNA was mixed with 350 μL ultrapure phenol-chloroform-isoamyl alcohol solution (25:24:1) and centrifuged. The upper layer was collected in a new centrifuge tube and mixed with phenol-chloroform-isoamyl alcohol solution again. After centrifugation, the aqueous layer was mixed with chloroform: isoamyl alcohol (24:1) and centrifuged. The DNA was precipitated in ethanol and pelleted from the sample by centrifuging. The ethanol in the tube was dried and then the DNA pellet was resuspended in ddH_2O.

2.2.2.6 Quantification of viral genome replication

PMs were infected with viruses for the indicated times. The cellular and viral DNA

were isolated as described above. For the cytosine arabinoside (Ara-C) experiments, cells were pretreated with complete media with or without Ara-C (40 μg/mL) for 2 h, then infected at a MOI of 0.03 for 1 h. The infected cells were incubated in fresh media with or without Ara-C for the indicated times before total cellular and viral DNA purification by phenol extraction.

Virus genomic copy number was detected by quantitative polymerase chain reaction (qPCR) using a 5' 6-FAM (6-carboxyfluorescein) probe (IDT) as previously described (53, 166). The region amplified is an 89 bp conserved region from the EVM049 gene.

- The primers used in this experiment were:

  EVM049 (VACV E9L)-fwd: 5'-CTCTGCTCCATTTAGTACCGATTC-3'

  EVM049 (VACV E9L)-rev: 5'-TACTCATACGCTTCGGCTAAGA-3'

- A standard curve was generated by using a gene block with the following sequence:

  5'-GGATTGGCAAACCGTAACATACCGTTAGATAACTCTGCTCCATTTAG
TACCGATTCTAGATACAAGATCATTCTACGTCCTATGGATGTGCAACTCTTA
GCCGAAGCGTATGAGTATAGAGCACTATTTCTAAATCCCATCAGACCATAT-3'

- The probe was labeled with 5' FAM dye, an internal ZEN quencher, and a 3' quencher Iowa Black FQ:

  5'-/56FAM/AGATCATTC/ZEN/TACGTCCTATGGATGTGCAAC/3IABkFQ/-3'

The qPCR master mix was prepared at 4× concentration with 2 μM of each primer and 1 μM probe. To protect the light-sensitive probe, the master mix was aliquoted in black

tubes and stored at -20°C. To prepare the standard curve, nine-fold dilutions of the gene block were made starting from 1.52×10^6 copies/reaction to 2.87×10^1 copies/reaction. In each experiment, the 4× qPCR master mix and 2× qPCR master mix (PerfeCTa Fastmix II, Quantabio) were mixed in a 1:2 ratio and then 15 µL of this mixture was added to each reaction tube. Then, 5 µL of DNA was added, making the final volume 20 µL. The assay was programmed to run on a CFX96™ Real-Time PCR (Bio-Rad) at 95°C for 2 min, and then 40 cycles of 15 sec at 95°C, and 30 sec at 60°C followed by fluorescence reading at the end of each cycle. The standard curve was used to calculate the copy numbers of samples based on their cycle quantification (Cq) values (53, 166).

2.2.2.7 Reverse transcription-PCR (RT-PCR)

Total RNA was isolated from BSC-40 cells left uninfected or infected with indicated viruses using the Aurum total RNA mini kit (Bio-Rad), and the RT reaction was performed using the Superscript II Reverse Transcriptase System (Invitrogen). cDNA was amplified by PCR with the following oligonucleotide pairs: EVM012 forward primer (SalI-p28-fwd) and reverse primer (SmaI-p28-rev); EVM056 forward primer (EVM056-fwd) and reverse primer (EVM056-rev); EVM011 forward primer (EVM011-fwd) and reverse primer (EVM011-rev); EVM013 forward primer (EVM013-fwd) and reverse primer (EVM013-rev).

2.2.2.8 Whole genome sequencing of the p28 knock-out and revertant viruses

Viral genomic DNA was extracted from sucrose-purified virus preparations as

previously described with the help from Dr. Ryan Noyce (167). DNA sequencing libraries were generated using the Nextera XT sample prep kit (Illumina) and paired end sequencing (2×300 bp) was performed using an Illumina MiSeq platform. Raw sequence reads were de novo assembled into contigs and mapped to their appropriate recombinant ECTV reference sequences using CLC Genomics Workbench 20 software (QIAGEN) to confirm their identity. The sequence reads for the viruses used in this study were submitted to the National Center for Biotechnology Information BioSample database (BioProject ID: PRJNA882034).

2.2.3 Molecular biology

2.2.3.1 Polymerase Chain Reaction (PCR)

A typical 50 µL PCR contained 0.2 mM of each primer, 200 µM of dNTPs (Thermo Scientific), 1 U of Phusion high-fidelity DNA Polymerase (Thermo Scientific), and 100 ng of DNA template. All primers used in this study are listed in **Table 2.3**.

2.2.3.2 Restriction endonuclease digestion

Restriction endonuclease digestion was performed according to the manufacturer's instructions. In general, plasmids or PCR products were digested in a total volume of 10-50 µL for 1-4 h at 37°C. The DNA fragments were isolated or purified by agarose gel electrophoresis or using the QIAquick PCR purification kit (QIAGEN).

2.2.3.3 Agarose gel electrophoresis

Samples were mixed with DNA loading buffer (Thermo Fisher Scientific), and DNA fragments in the samples were separated by gel electrophoresis in gels made of 1% (w/v) UltraPure Agarose (Invitrogen) and 0.01% SYBR safe DNA gel stain (Invitrogen) in TAE buffer. Gels were run at 100 V in TAE running buffer in an Owl Separation System (Thermo Scientific). DNA bands were visualized using a Molecular Imager Gel Doc XR+ Imaging System (Bio-Rad).

2.2.3.4 DNA purification and Gel extraction

DNA fragments were cleaned up using the QIAquick PCR purification kit (QIAGEN) or QIAquick gel extraction kit (QIAGEN) following the manufacturer's instructions. In brief, DNA was mixed with the buffers in the kit and then run through a QIAquick DNA column. The DNA on the column was washed with wash buffer containing ethanol before being eluted in 30-50 μL of ddH_2O.

2.2.3.5 DNA ligation

All ligation reactions were performed according to the manufacturer's protocol using T4 DNA ligase (Invitrogen). The molar ratio of vector to insert DNA was 1:3. All ligations were incubated at 16℃ for 18 h.

2.2.3.6 Transformation of *E. coli*

Competent *E. coli* cells were transformed with ligation reactions or plasmids using a heat shock method. DNA and competent cells were incubated on ice for 30 min and then

heated at 42℃ for 90 sec followed by a 2 min recovery on ice. Transformed bacteria were incubated in Luria-Bertani (LB) media in a shaker for 45 min at 37℃ before plating on LB agar plates containing appropriate antibiotics for selection.

2.2.3.7 Plasmid purification

E. coli cells containing the desired plasmid were incubated in LB media with appropriate antibiotics in a shaker overnight at 37℃. Plasmid DNA was prepared using a QIAprep Spin Miniprep Kit (QIAGEN) according to the manufacturer's protocol. The concentration of DNA was examined using a Nanodrop spectrophotometer (Thermo Scientific).

2.2.4 Protein Methodology

2.2.4.1 SDS polyacrylamide gel electrophoresis (SDS-PAGE)

Cells were washed once with PBS and lysed in 1% NP-40 lysis buffer (50 mM Tris-HCl pH 7.4, 150 mM NaCl, 2 mM EDTA, 1% NP-40, 10% Glycerol) containing protease inhibitor cocktail (1 tablet in 10 mL of lysis buffer) (Roche), 1 mM phenylmethylsulphonyl fluoride (PMSF, Bioshop), 5 mM N-ethylmaleimide (NEM, MilliporeSigma), and 1 mM Na_3VO_4 for 30 min on ice. Detergent-insoluble material was removed by centrifugation at 20,000×*g* for 10 min at 4℃. The Bradford assay (BioRad) was used to determine the protein concentration of lysates. Protein samples were boiled with 5× sample buffer for 5 min and then centrifuged for 2 min at 14,000 rpm in a microfuge at room temperature. Samples were separated by SDS-PAGE before being stained with Coomassie blue or

transferred to nitrocellulose membranes (Bio-Rad) using a semi-dry transfer apparatus (Bio-Rad).

2.2.4.2 Western blotting experiments

Proteins separated by SDS-PAGE were transferred to nitrocellulose membranes (Bio-Rad) using a semi-dry transfer apparatus (Bio-Rad). Membranes were then blocked in 5% milk in PBS for 1 h before being incubated with the indicated primary Abs. Membranes were then incubated with secondary Abs (goat-anti-rabbit 680 and goat-anti-mouse 800; LI-COR Biosciences) for 45 min at room temperature and imaged using an Odyssey scanner (LI-COR Biosciences).

2.2.4.3 Immunoprecipitation (IP) experiments

Protein lysates were incubated with 5 μg anti-TRIM25 or control Ab at 4°C overnight before being incubated with 10 μL packed Protein A-Sepharose beads (Millipore Sigma) for 2 h at room temperature. Beads were washed with 1 mL of 1% NP-40 lysis buffer twice and boiled in 30 μL of SDS-PAGE sample buffer to elute bound proteins. For the anti-conjugated Ub IP, 2 μg FK2 Ab was incubated with 10 μL packed Protein G-Agarose beads for 2 h at room temperature. Beads were washed once with 1 mL of 1% NP-40 lysis buffer and then incubated with protein lysates at 4°C overnight. Beads were then washed 3 times with 1 mL of 1% NP-40 lysis buffer and bound proteins were eluted with 30 μL of SDS-PAGE sample buffer.

2.2.4.4 Quantification of protein levels in western blotting experiments

The levels of the immunoreactive bands in western blotting experiments were determined using Image Studio 5.5.4. The protein levels in each sample were normalized to the level of β-actin detected by western blotting. Protein quantification was made relative to either uninfected cells or infected cells without any drug treatment.

2.2.4.5 Transfection

Cells were transiently transfected with lipofectamine 2000 (Invitrogen) as described by the manufacturer's specifications. Cells were grown to approximately 80% confluence in 6-well plates. The media was changed to Opti-MEM (Gibco) before transfection. Plasmid DNA (2 μg) and 5 μL of lipofectamine were mixed in Opti-MEM for 20 min. The mixture was added to cells drop by drop and incubated for 4 h at 37℃ and 5% CO_2. For protein expression, cells were then incubated with fresh complete media for 24 or 48 h. For transfection and infection, the Opti-MEM media was aspirated and then cells were inoculated with virus for 1 h following incubation in complete media at 37℃ and 5% CO_2.

2.2.4.6 GST fusion protein expression using *E. coli*

E. coli (BL21) were transformed with pGEX-4T-1 containing the gene of p28 or p28 the isolated domain of p28. Cells were grown in LB media with ampicillin until reaching an OD_{600} of 0.6. Then, 1 mM IPTG was added to induce the expression of the GST fusion proteins. Cells were incubated at 18℃ for another 18 hours. The lower incubation temperature (18℃ instead of the optimal 37℃) was used to reduce the expression rate of

GST fusion proteins, thereby enhancing the expression of soluble proteins rather than forming inclusion bodies (168). Bacteria were harvested by centrifugation at 1,000 rpm for 40 min at 4℃ in a JLA-16.250 rotor. Cells were resuspended in 1% NP-40 lysis buffer containing protease inhibitors and 1 mM PMSF. Sonication was performed with a tip sonicator at 50% power, 5 sec ON/5 sec OFF for 5 min on ice. For subsequent examination of proteins by SDS-PAGE gel, 200 µL of lysate was removed in a 1.5 mL centrifuge tube. To separate the soluble proteins for purification, lysates were centrifuged at 12,000 rpm for 30 min at 4℃ in a JLA-16.250 rotor. Proteins in cells before and after IPTG induction, soluble proteins (in the supernatant after centrifuge), and insoluble proteins (in the pellet after centrifuge) were analyzed by SDS-PAGE gels followed by Coomassie blue staining.

2.2.4.7 His-tagged protein expression and purification using baculovirus expression vector system (BEVS)

The code-optimized His-tagged ECTV p28 and its isolated domains were synthesized (GenScript) and cloned into the pFastBac-1 vector (Invitrogen). Baculovirus production, protein expression, and purification were performed according to previously described protocols (169). In brief, donor plasmids (pFastBac-1 with the gene of His-tagged p28 or His-tagged p28 domains) were transformed into competent DH 10 Bac cells. Bacteria with recombinant bacmid DNA were selected by antibiotics (50 µg/mL kanamycin, 10 µg /mL tetracycline, 7 µg /mL gentamycin). To generate baculovirus, bacmid DNA was extracted from these bacteria and transfected into Sf9 cells (insect cells, derived from the pupal

ovarian tissue of the fall army worm, *Spodoptera frugiperda*. Invitrogen, provided by Dr. Matthias Götte (University of Alberta)). Baculovirus in the media were collected and amplified in Sf9 cells and then utilized to infect a large number of Sf9 cells for His-tagged protein expression. The Sf9 cells were harvested by centrifuge (1000×*g*, 5 min, 4℃). Cell pellets were then resuspended in 10 mL of Tris buffer pH 8.0 (100 mM Tris, 150 mM NaCl, 10% glycerol, 0.1% Tween-20, 1 tablet protease inhibitor cocktail [Roche] per 10 mL lysis buffer) and lysed by sonicating (5 sec ON/5 sec OFF, 5 min). Cell lysates were centrifuged for 30 min at 30,000×*g* at 4℃. 0.5 mL of Ni-NTA agarose was used to purify His-p28 from the supernatant. A stepwise gradient of increasing concentrations of imidazole (from 20 mM to 500 mM) was used to elute proteins bound to the beads. Protein samples were fractionated by SDS-PAGE gel. Coomassie stain and anti-His western blotting were used to visualize the His-tagged protein in samples from protein purification. Purified protein was then concentrated and stored in 50% glycerol Tris buffer at -20℃.

2.2.5 Analysis of diGly peptides

2.2.5.1 DiGly peptide enrichment

HeLa cells (2×10^7) were pretreated with 10 μM MG132 (#BMLPI1020005, Enzo, Life Science) for 1 h. Cells were then inoculated with VACV-Cop viruses at a MOI of 3 for 1 h and incubated for a further 4 h with 10 μM MG132 in an incubator at 37℃ and 5% CO_2. Cells were lysed in freshly made 9 M urea lysis buffer (9 M urea, 20 mM HEPES pH 8.0, 1 mM sodium orthovanadate, 2.5 mM sodium pyrophosphate, 1 mM β-glycerophosphate),

gentle probe sonicated, and clarified by spin centrifugation at 13,000 rpm for 10 min at 4°C. Proteins were reduced with 10 mM DTT for 45 min at 37°C, alkylated with 30 mM iodoacetamide for 45 min at room temperature, followed by addition of 20 mM DTT. Proteins were then digested with trypsin in 1:100 enzyme:substrate ratio overnight at 37°C, and trypsin was precipitated in 2% trifluoroacetic acid (TFA). Peptides were desalted using SOLA HRP SPE cartridge (#60109-001, Thermo Fisher). Desalted and dried peptides were subjected to automated diGly enrichment using the PTMScan Ub remnant motif kit (#59322, Cell Signaling) on a KingFisher Duo Prime. Briefly, 1 mg of peptide was resuspended in 1 mL HS bind buffer #1 (Cell Signaling) and incubated with 20 µL of the Ab-bead slurry at room temperature for 2 h. The beads were washed four times with 1 mL HS IAP (Cell Signaling) wash buffer and twice with 1 mL H_2O. Peptides were eluted 2 times with 50 µL 0.15% TFA at room temperature.

2.2.5.2 Mass spectrometry analysis

This work was done by Luo Shu in Dr. Olivier Julien lab. Peptides were desalted with C18 ziptips (#ZTC18S960, Millipore) and recovered in buffer A (0.1% formic acid) prior to mass spectrometry analysis. The samples were analyzed using a nanoflow-HPLC (Thermo Scientific EASY-nLC 1200 System) coupled to an Orbitrap Fusion Lumos Tribrid Mass Spectrometer (Thermo Fisher Scientific). Reverse phase separation of the peptides was done with an Aurora Ultimate analytical column (25 cm x 75 µm ID with 1.7 µm media, IonOpticks). Peptides were eluted with a solvent B gradient (80% ACN, 0.1% FA)

for 120 min. The gradient was run at 400 nL/min with analytical column temperature set at 45°C. Data were analyzed using Proteome Discoverer (v2.4.1.15) against the concatenated database of the human proteome (UP000005640) and VACV-Cop proteome (UP000008269), with relaxed false discovery rate set at 5% and restricted at 1%. Search parameters included a maximum of two missed trypsin cleavages, a precursor mass tolerance of 15 ppm, a fragment mass tolerance of 0.8 Da, with the constant modification carbamidomethylation (C), and variable modifications of acetyl (protein N-term), deamidated (N/Q), oxidation (M), and GlyGly (uncleaved K). The maximum number of variable modifications was set to 4. Statistical analysis was performed by Proteome Discoverer using background-based t-test and protein abundance ratios were calculated using pairwise peptide ratios. Mass spectrometry data files are available through MassIVE Repository (MSV000094020). This method is described in Dong, J *et al.* 2023 (under review).

2.2.5.3 Pathway Enrichment Analysis

diGly peptides enriched in either uninfected or infected cells were analyzed by Metascape (v3.5.20230501) using express analysis and the human species setting (170). Categories with a significant adjusted p value ($q<0.05$) are shown.

2.2.5.4 Examination of levels of protein associated with enriched diGly peptides in VACV-infected cells

The data of Soday *et al.* was analyzed to examine whether levels of host proteins with

enriched diGly peptides changed over the course of infection (171). In this study, the MG132 rescue ratio was included.

$$MG132\ rescue\ ratio = \frac{Protein\ abundance(VACV\ infected;\ +MG132)/Protein\ abundance(VACV\ infected;\ -MG132)}{Protein\ abundance\ (uninfected\ +MG132)/Protein\ abundance\ (uninfected;\ -MG132)}$$

2.2.6 Immunofluorescence microscopy (IF)

Isolated PMs were seeded on coverslips and incubated in 12-well plates at 37°C and 5% CO_2 overnight before infection. Cells were infected at a MOI of 0.03 or 3 for 1 h and then incubated in fresh media for the indicated times. Cells were fixed with 4% paraformaldehyde (PFA) for 2 h at room temperature. After permeabilization with PBS containing 0.1% Tween-20 (PBS-T), cells were stained with primary Abs for 1 h at room temperature followed by staining with goat-anti-mouse Alexa 488 (Invitrogen) and goat-anti-rabbit Alexa 649 ReadyProbes reagents (Life Technologies) for 1 h. After washing with PBS-T three times, coverslips were incubated with PBS-T containing 50 ng/mL 4',6-diamidino-2-phenylindole (DAPI, Invitrogen) to visualize nuclear and viral DNA. Finally, cells were mounted using Mowiol mounting medium and visualized using an Olympus IX-81 spinning-disc confocal microscope equipped with 60×/1.42 NA oil objective lenses. For these experiments, 2.5×10^5 to 5×10^5 PMs were used in each well.

2.2.7 Flow cytometry analysis of cells

Cells (1 x 10^6 cells/well) were harvested into a 1.5 mL centrifuge tube and washed

with 1 mL PBS once. Then 500 µL of 2% PFA was used to fix cells for 30 min. Fixed cells were then washed and resuspended in 100 µL FACS buffer (PBS containing 1% FBS) and incubated with the indicated Abs for 2 h on ice, in the dark. Cells were then washed once with 1 mL FACS buffer and resuspended in 1 mL FACS buffer. Samples were analyzed via flow cytometry using a Fortessa X-20 flow cytometer (BD Biosciences).

2.2.8 Auto-ubiquitylation assay

His-p28 protein was incubated with 50 nM E1 (UBE1, human, Boston Biochem), 0.5 µM E2 (recombinant human GST-UbcH5a/UBE2D1 protein, Boston Biochem), 10 mM ATP (Pharmacia Biotech), and 28 µM purified Ub (Sigma). The reaction was performed in ubiquitination reaction buffer (50 mM Tris-HCl pH 7.5, 200 mM NaCl, 1 mM DTT) at 30°C for 90 min, and stopped by adding 5× protein loading buffer. Samples were run out using SDS-PAGE and ubiquitylation was visualized by western blotting with anti-His or anti-conjugated Ub Abs.

2.2.9 Electrophoretic mobility shift assay (EMSA)

EMSA was used in this study to detect the interaction between purified protein and VACV hairpin DNA interactions as described previously (53). The VACV hairpin oligonucleotides labelled with Alexa Fluor 647 were obtained from Dr. David Evans (University of Alberta). Purified protein was incubated with 100 ng of labelled DNA in EMSA reaction buffer in a 10 µL reaction. The reactions were incubated at 37°C for 30 min and then loaded onto a 6% non-denaturing polyacrylamide gel. The gel was run at 50

V, 100 mA for 2.5 h and the tank was kept in ice to maintain low temperature during the run. The gel was imaged using a Typhoon imager (General Electric).

2.2.10 Proteasome inhibition experiments

HeLa cells were pretreated with 10 μM MG132 in complete medium for 1 h at 37°C and 5% CO_2. Cells were then inoculated with VACV-Cop viruses at a MOI of 10 for 1 h and incubated at 37°C and 5% CO_2 in the presence of MG132 for 4 or 8 h before lysis.

2.2.11 Neddylation inhibitor and cycloheximide (CHX) treatments

HeLa cells were pretreated with the indicated concentrations of MLN4924 (172.05477.0001, EMD Millipore Corp) in complete media for 20 h at 37°C and 5% CO_2. Cells were then inoculated with VACV-Cop at a MOI of 10 for 1 h and incubated a further 3 h in the presence of the indicated concentrations of MLN4924 before being lysed. Cells were treated with 50 μg/mL CHX (#01810-1g, Fluka Analytical) in complete medium for 1 h at 37°C and 5% CO_2 before being infected and processed as described for the cells treated with MLN4924.

2.2.12 UV inactivation of virus

VACV-Cop was diluted in 1 mL MEM (~2×10^7 plaque forming unit (PFU)/mL) and placed in a 6-well plate before being irradiated with the indicated UV energies using CL-1000 Ultraviolet Crosslinker (UVP). HeLa cells were then inoculated with VACV-Cop or UV-inactivated virus at a MOI of 10 for 1 h at 37°C, after which the virus was removed from the culture and replaced with fresh media. HeLa cells were harvested at 4 hpi and

then analyzed by western blotting using the indicated Abs. In parallel, I tested the titer of VACV-Cop and the UV-inactivated viruses in BSC-40 cells as previously described (173).

2.2.13 Statistical Analyses

When comparing two samples, one-tailed, paired student *t*-tests were performed. One-way analysis of variance (ANOVA) was performed when comparing more than two samples. Two-way ANOVA followed by Bonferroni's multiple comparisons test was performed to test for statistical significance of virus growth. A p value of ≤ 0.05 was considered significant. * $p<0.05$, ** $p<0.01$ and *** $p<0.001$.

Chapter 3: Investigating the role of p28 during ECTV replication

The data presented in this chapter has been published in:

"Jianing Dong, Patrick Paszkowski, Dana Kocincova, Robert J. Ingham. Complete deletion of Ectromelia virus p28 impairs virus genome replication in a mouse strain, cell type, and multiplicity of infection-dependent manner. *Virus Research.* 323 (2023) 198968, doi: 10.1016/j.virusres.2022.198968."

Contributions to this chapter:

All experiments presented in this chapter were performed by me, except for the generation of recombinant ECTV-Δp28, which was done by Patrick Paszkowski, and determination of virus growth curves in Neuro-2a and YAC-1 cells **(Figure 3.9)**, which were performed by Dr. Dana Kocincova. The writing of this chapter is adapted from Dong *et al.* 2023, which was written by Dr. Ingham and me.

3.1 Introduction

p28, a poxviral E3 Ub-ligase, acts as an important virulence factor in ECTV-infected susceptible strain A mice. Senkevich *et al.* disrupted the function of p28 in ECTV by replacing its RING domain of p28 with a *gpt* selection cassette (158). The p28 mutant form of ECTV has a 6-log increase in the LD_{50} in susceptible strain A mice compared to wild-type ECTV (158). Further investigation demonstrated that p28 is required for ECTV replication in resident PMs from susceptible strain A mice, but not in those from the resistant C57BL/6 mice strain (154). Since macrophages are the carriers of ECTV from the infection site (skin) to mouse organs, this might explain the reason for the lower virus titer of the p28 mutant virus compared to the wild-type virus in their target organ, the liver, in susceptible mice infected by footpad inoculation (47, 154). Instead of examining the effect of the p28 RING domain-mutant virus during ECTV infection (158), a complete p28-deleted ECTV (ECTV-Δp28) was generated to explore how p28 functions as a virulence factor. In this chapter, the characteristics of the ECTV-Δp28 virus were analyzed in different cell types, including cell lines from susceptible strain A mice, BMDMs, and resident PMs from susceptible and resistant mouse strains. The study revealed that the effect of p28 on ECTV virus production depends on the MOI, cell type, and mouse strain.

3.2 Results

3.2.1 Generation of ECTV-Δp28

The gene encoding p28 (EVM012) was deleted from the genome of ECTV-Mos **(Figure 3.1)**. We generated a targeting vector containing DNA which include from EVM011 to EVM013 of ECTV but replaced the EVM012 gene with a YFP/*gpt* cassette flanked by loxP sites **(Figure 3.1)**. Cre recombinase was used to completely remove the YFP/*gpt* cassette and generate the complete p28 knock-out virus, ECTV-Δp28.

To determine whether deletion of the p28 gene impairs transcription of genes flanking p28, we isolated total RNA from uninfected BSC-40 cells or BSC-40 cells infected with ECTV or ECTV-Δp28 at 4 hpi. Reverse transcription-PCR (RT-PCR) analysis of the total RNA showed that p28 RNA can be detected in wild-type ECTV-infected cells, which is consistent with previous reports demonstrating that p28 is an early gene **(Figure 3.2)** (150, 151, 154). p28 RNA was absent in cells infected with ECTV-Δp28, while the transcription of EVM011 and EVM013 was not significantly impaired in ECTV-Δp28. The transcription and translation of VACV I3 begin early after poxviral infection (174, 175). Therefore, the ECTV homologue of I3, EVM056, was used here as an indicator of virus infection.

3.2.2 Characterization of ECTV-Δp28

As an initial characterization of ECTV-Δp28, I infected BSC-40 cells with wild-type ECTV or ECTV-Δp28 at a MOI of 3 for 1 h, 4 h, or 24 h. to analyze viral protein expression.

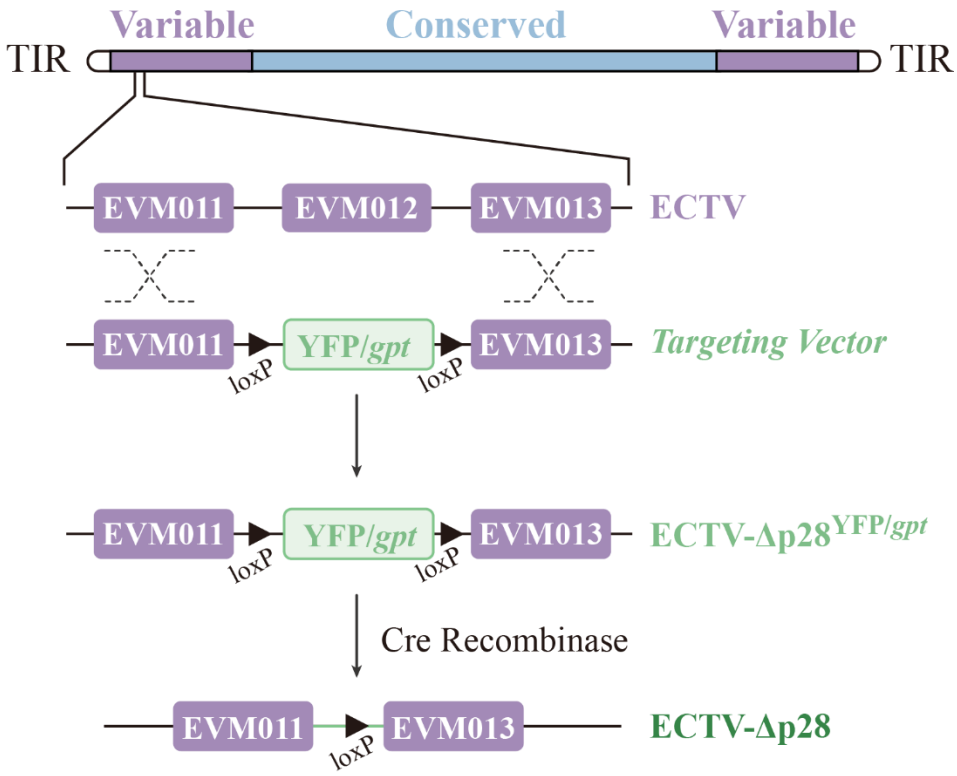

Figure 3.1 Generation of ECTV-Δp28

Schematic representation of the strategy used to delete p28 (EVM012) from ECTV-Mos. BSC-40 cells were transfected with the targeting plasmid and infected with wild-type ECTV-Mos. ECTV-Δp28$^{YFP/gpt}$ recombinant virus was selected for in the presence of mycophenolic acid, hypoxanthine, and xanthine. YFP-positive plaques were purified. Cre recombinase was used to completely remove the YFP/*gpt* cassette through cleavage of loxP sites and generate the complete p28 knock-out virus, ECTV-Δp28. YFP, yellow fluorescent protein; *gpt*, xanthine-guanine phosphoribosyl transferase. This method was described in (165).This figure was adapted and modified from Dong, J *et al*., 2022 (173).

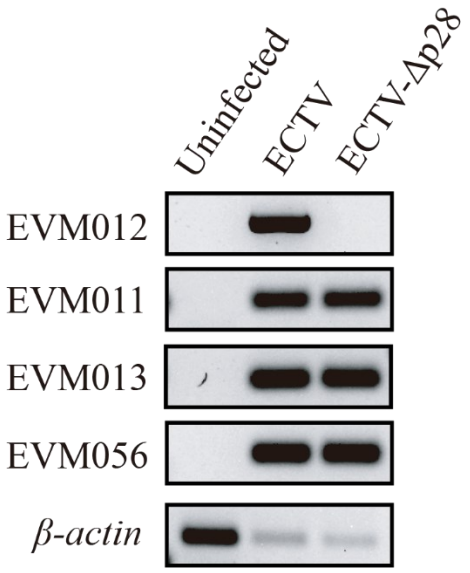

Figure 3.2 Transcription of the genes on both sides of EVM012 are not significantly impaired in ECTV-Δp28-infected BSC-40 cells

RT-PCR examination of the indicated genes in BSC-40 cells infected for 24 h with ECTV or ECTV-Δp28 at a MOI of 3. EVM011 and EVM013 flank EVM012 (p28), and EVM056 is used here to indicate virus infection. The RT-PCR was performed by Patrick Paszkowski and I repeated this experiment. The results presented in the figure were replicated in 3 independent experiments, and the figure displays one of the 3 replicates. This figure was adapted from Dong, J *et al*., 2022 (173).

Western blots showed no p28 protein was observed in cells infected with the ECTV-Δp28 virus at any of the time points **(Figure 3.3; top panel)**. The expression of the viral protein, EVM056 (VACV I3), was detected as early as 1 hpi, and the amount of EVM056 increased at later time points **(Figure 3.3; second panel from top)**. Viral late protein, EVM136 (VACV A34), was observed at 4 and 24 hpi **(Figure 3.3; third panel from top)**. No significant differences were found in the expression of these viral proteins in ECTV-Δp28-infected BSC-40 cells compared with wild-type ECTV.

The virus production of ECTV-Δp28 was examined and compared with the production of ECTV in BSC-40 cells. The growth curves of ECTV and ECTV-Δp28 in BSC-40 cells did not show a significant difference in either single-step **(Figure 3.4A)** or multi-step **(Figure 3.4B)** growth curves. Overall, our results show that deletion of p28 does not impair virus replication in BSC-40 cells.

3.2.3 p28 deletion compromised ECTV production in PMs from strain A mice, especially at low MOI infection

Senkevich *et al.* showed that a functional p28 is essential for the replication of ECTV in resident PMs from susceptible strain A mice (154). To determine whether completely knocking out p28 from ECTV also impaired virus production in this cell type, I isolated PMs from strain A mice (162). These isolated PMs were infected with ECTV or ECTV-Δp28 at high (MOI 3) or low MOI (0.03). A modest, but not statistically significant

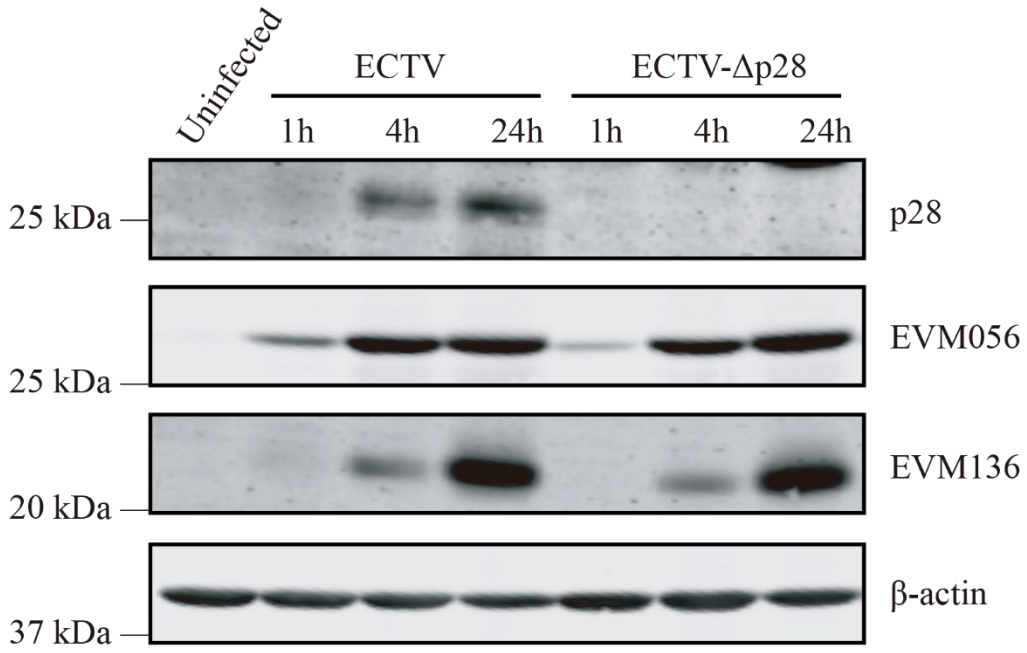

Figure 3.3 Viral protein expression is not inhibited in ECTV-Δp28-infected cells

Western blotting experiments were performed on the whole cell lysates from BSC-40 cells infected with ECTV or ECTV-Δp28 at a MOI of 3 for 1, 4, or 24 h. EVM056 (recognized by anti-I3 Ab) and EVM136 (recognized by anti-A34 Ab) are poxviral proteins, indicating viral infection and late protein expression, respectively. The anti-β-actin blot was included to show protein loading. Molecular mass markers are indicated to the left of blots. The results presented in the figure were replicated in 3 independent experiments, and the figure displays one of the 3 replicates. This figure was adapted from Dong, J *et al*., 2022 (173).

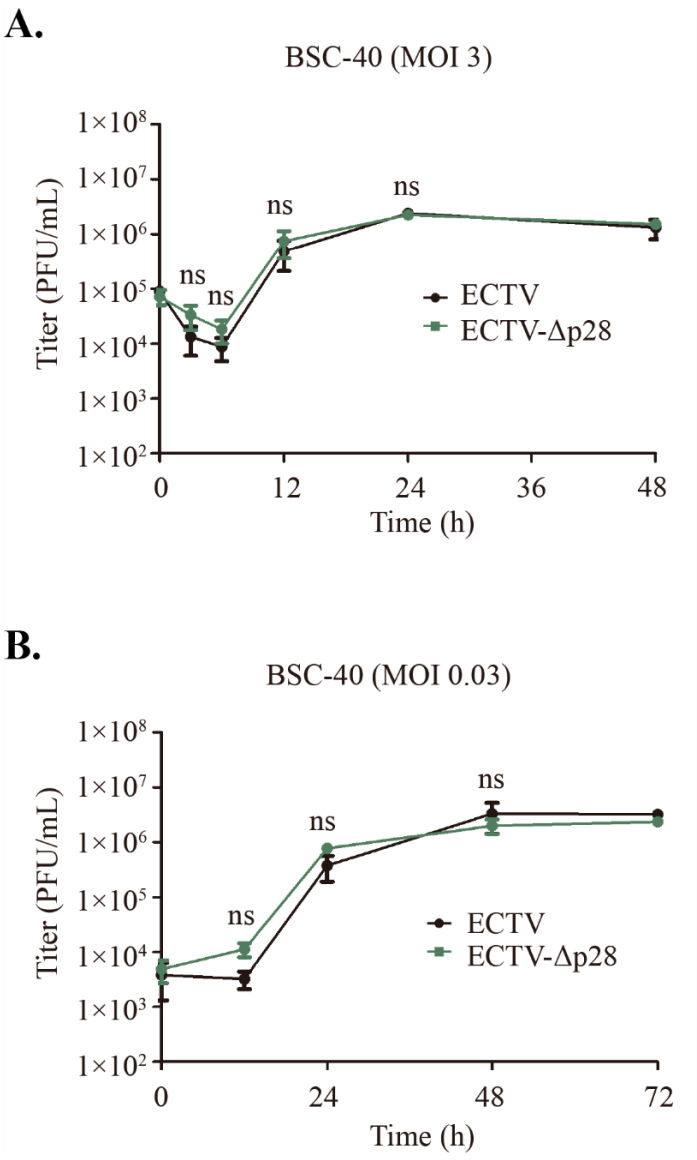

Figure 3.4 The production of ECTV and ECTV-Δp28 is not significantly different in BSC-40 cells

BSC-40 cells were infected with ECTV or ECTV-Δp28 at high MOI (MOI 3) **(A)** or low MOI (0.03) **(B)**. Infected cell samples were harvested at the indicated time points and tested for titer to plot single- or multi-step growth curves. Viral titers are presented as PFU/mL. Results presented for the growth curves represent the mean and standard deviation of 3 independent experiments. A two-way ANOVA was used to calculate statistical significance between the titer of ECTV and ECTV-Δp28 at the indicated time points post-infection. ns; not significant. This figure was adapted from Dong, J *et al*., 2022 (173).

decrease in ECTV-Δp28 production was observed at 12 and 24 hpi when PMs were infected at high MOI compared with the wild-type ECTV **(Figure 3.5A)**. However, ECTV-Δp28 virus production was significantly inhibited compared to ECTV in low MOI-infected PMs **(Figure 3.5B)**. To test whether this reduction in ECTV-Δp28 virus production was sex-dependent, I isolated PMs from male and female strain A mice separately. The inhibition of ECTV-Δp28 production was observed in the PMs from both female and male mice, suggesting no sex differences existed **(Figure 3.6)**.

To confirm that this decrease in virus production was due to p28 deletion, I generated a revertant virus (ECTV-Δp28-Rev) **(Figure 3.7A)**. Using the wild-type ECTV genome as a template, DNA fragments containing the EVM011, EVM012, and EVM013 genes were obtained by PCR. The PCR product was transfected into BSC-40 cells, and the cells were also infected with ECTV-Δp28$^{YFP/gpt}$, which is the virus we used to generate ECTV-Δp28. The p28 revertant virus was selected for the YFP-negative plaques. The p28 knock-out and revertant viruses used in this chapter were sequenced with the help from Dr. Ryan Noyce. The sequence reads for these viruses have been submitted to the National Center for Biotechnology Information BioSample database (BioProject ID: PRJNA882034).

Next, I examined the expression of p28 and other viral proteins in cells infected with ECTV-Δp28-Rev. Western blots showed p28 protein was expressed in BSC-40 cells infected with the p28 revertant virus at levels similar to wild-type ECTV **(Figure 3.7B; top panel)**. No significant differences were found in the expression of viral protein in

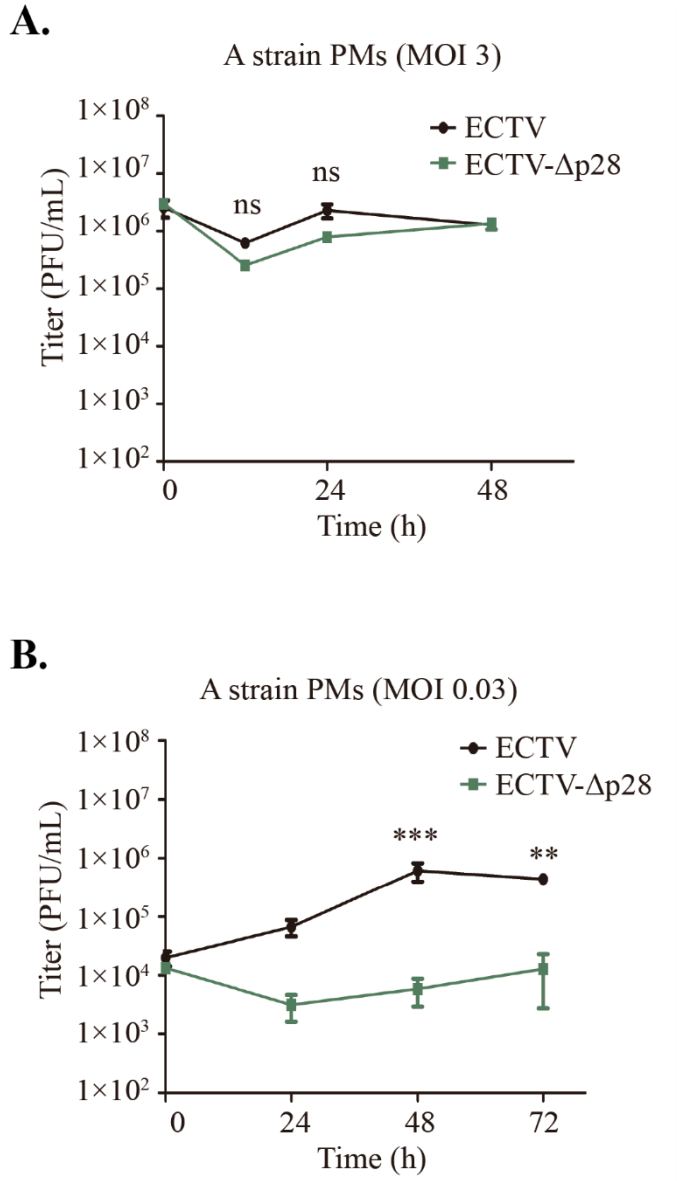

Figure 3.5 Deletion of p28 inhibits virus production in PMs from strain A mice infected at low MOI infection

Single- **(A)** and multi-step **(B)** growth curves in PMs were performed. PMs isolated from strain A mice were infected with ECTV or ECTV-Δp28 at high (MOI 3) **(A)** or low MOI (0.03) **(B)** for the indicated times. Viral titers are presented as PFU/mL. Results presented represent the mean and standard deviation of 3 independent experiments. A two-way ANOVA was used to calculate statistical significance between the titer of ECTV or ECTV-Δp28 at the indicated time points post-infection. ns; not significant, **; $p \leq 0.01$, ***; $p \leq 0.001$. This figure was adapted from Dong, J *et al*., 2022 (173).

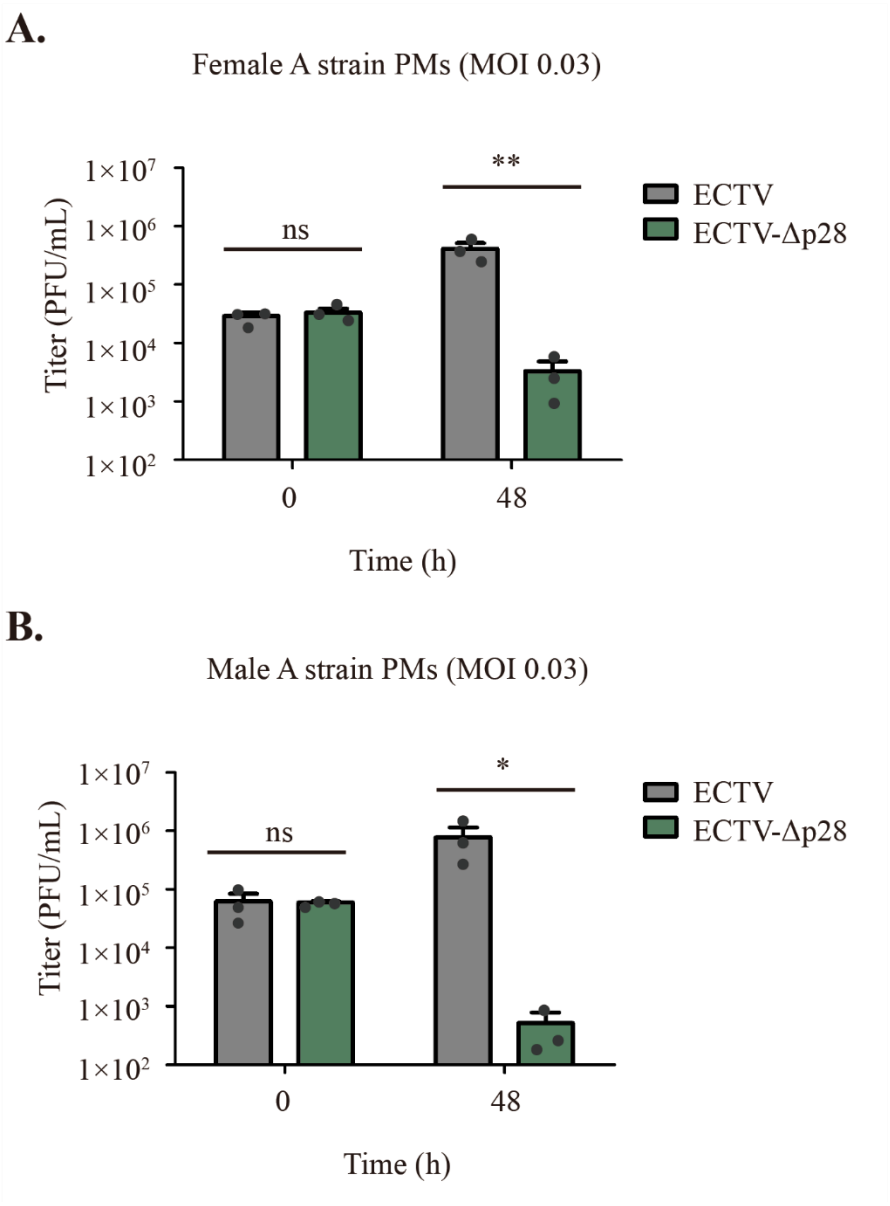

Figure 3.6 Virus production in PMs from female and male strain A mice

ECTV-Δp28 production in PMs isolated from female **(A)** and male **(B)** strain A mice. Isolated PMs were infected with ECTV or ECTV-Δp28 at low MOI (0.03) for the 48 h. Viral titers are presented as PFU/mL. Results presented represent the mean and standard deviation of 3 independent experiments. A two-way ANOVA was used to calculate statistical significance between the titer of ECTV or ECTV-Δp28 at the indicated time points post-infection. ns; not significant, *; $p \leq 0.05$, **; $p \leq 0.01$. This figure was adapted from Dong, J *et al*., 2022 (173).

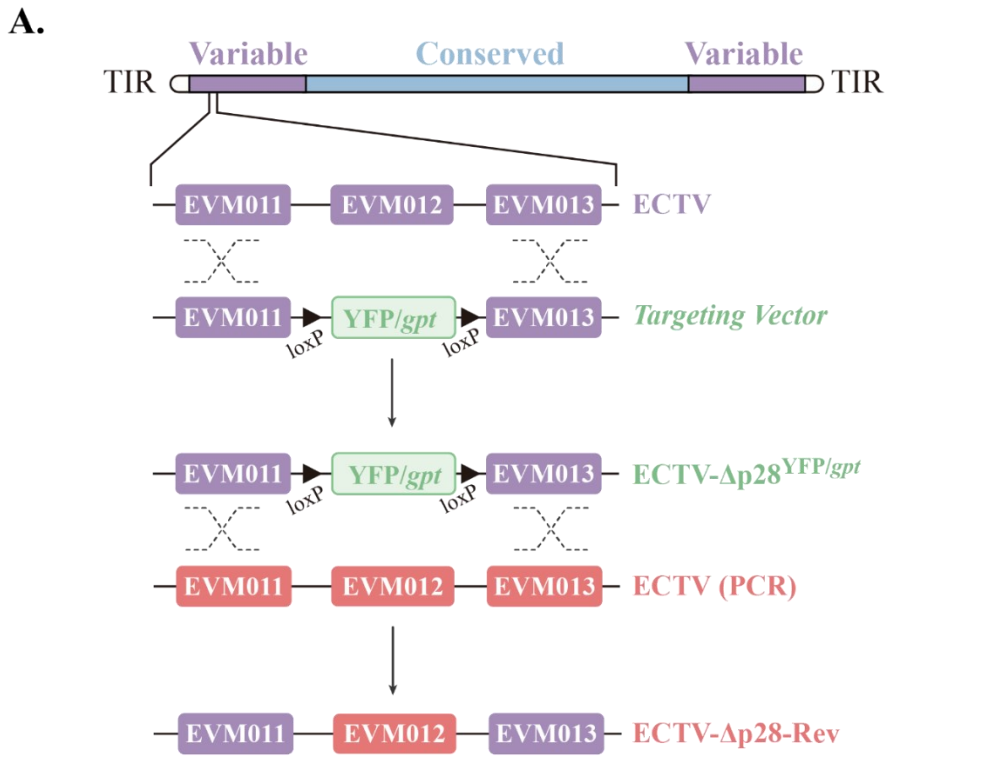
A.
Variable
Conserved
Variable
TIR
TIR
EVM011
EVM012
EVM013
ECTV
EVM011
YFP/gpt
EVM013
Targeting Vector
loxP
loxP
EVM011
YFP/gpt
EVM013
ECTV-Δp28YFP/gpt
loxP
loxP
EVM011
EVM012
EVM013
ECTV (PCR)
EVM011
EVM012
EVM013
ECTV-Δp28-Rev

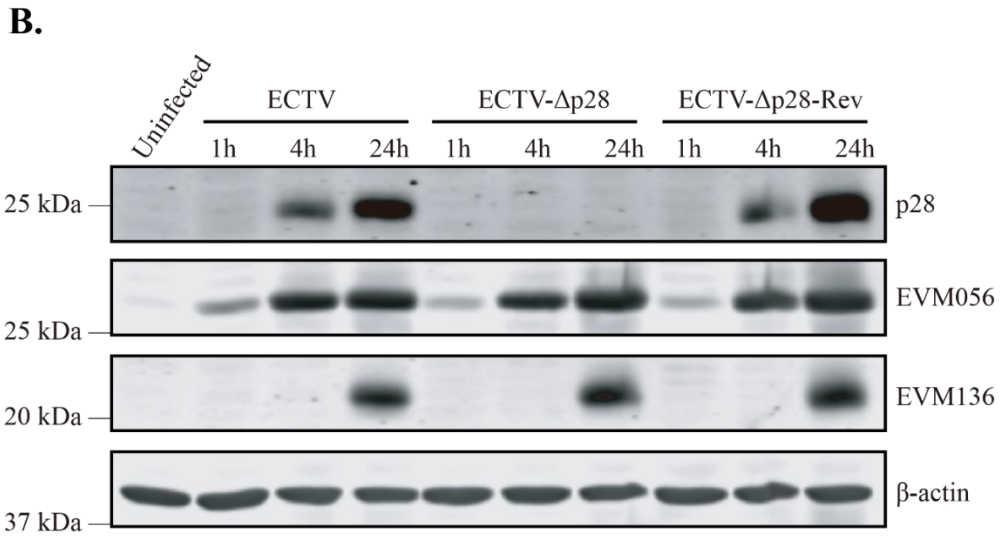
B.
Uninfected
ECTV
ECTV-Δp28
ECTV-Δp28-Rev
1h
4h
24h
1h
4h
24h
1h
4h
24h
25 kDa
p28
25 kDa
EVM056
20 kDa
EVM136
37 kDa
β-actin

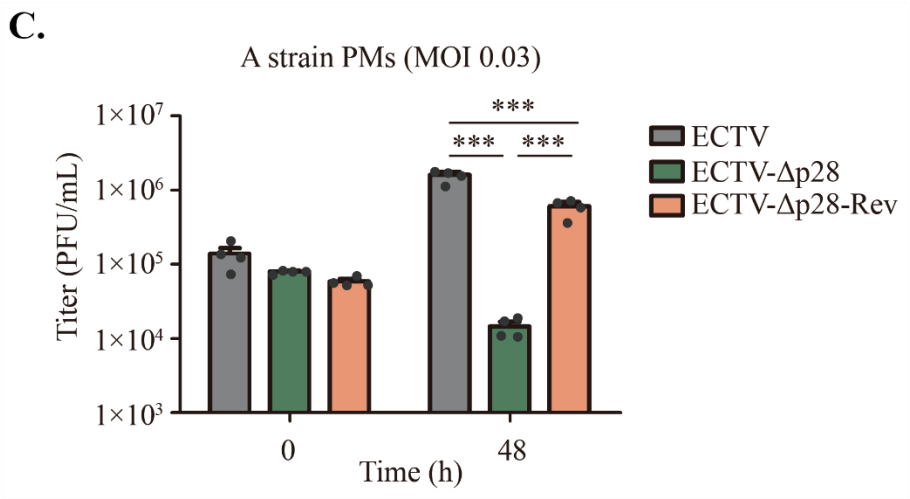

Figure 3.7 Reduced ECTV-Δp28 production in PMs of strain A mice can be rescued by insertion of the p28 gene

A, Schematic representation of the strategy used to generate ECTV-Δp28-Rev. **B,** Western blotting experiments of BSC-40 cells infected for the indicated times with ECTV, ECTV-Δp28, or ECTV-Δp28-Rev at a MOI of 3 for 1, 4, or 24 h. EVM056 (VACV I3) and EVM136 (VACV A34) are poxviral proteins, indicating viral infection and late protein expression, respectively. The anti-β-actin blot was included to show protein loading. Molecular mass markers are indicated to the left of blots. The results presented in the figure were replicated in 2 independent experiments, and the figure displays one of the 2 replicates. **C,** Resident PMs isolated from strain A mice were infected for 48 h with ECTV, ECTV-Δp28, or ECTV-Δp28-Rev at a MOI of 0.03. Viral titers are presented as PFU/mL. Results presented represent the mean and standard deviation of 4 independent experiments with results from individual experiments indicated as points. A two-way ANOVA was used to calculate statistical significance between the titer of ECTV, ECTV-Δp28, and ECTV-Δp28-Rev at 48 hpi. ***; $p \leq 0.001$. This figure was adapted and modified from Dong, J *et al.*, 2022 (173).

ECTV, ECTV-Δp28, or ECTV-Δp28-Rev-infected cells **(Figure 3.7B; second and third top panel)**. The decreased virus production of ECTV-Δp28 at 48 hpi was largely rescued in PMs infected with ECTV-Δp28-Rev **(Figure 3.7C)**. Taken together, these results suggest that p28 is required for efficient production of ECTV in resident strain A PMs, especially at low MOI.

3.2.4 p28 deletion did not significantly impair ECTV production in cell lines and BMDMs derived from strain A mice

The previous study on the replication of p28 RING domain-disrupted ECTV showed that defects in replication were not observed in other cell types and cell lines derived from strain A mice (154). We investigated whether this was true of the p28 deletion virus. This included cell lines derived from strain A mice, YAC-1 (lymphoma cell line) and Neuro-2a (neuroblastoma cell line) cells. We also used macrophage colony-stimulating factor (M-CSF) to induce macrophages from the bone marrow of strain A mice and determined the effect of p28 deletion on ECTV production in these BMDMs. These cells were infected with ECTV or ECTV-Δp28 at low MOI for 48 h and then virus titers were tested. No difference in virus production was observed in YAC-1 cells 48 hpi **(Figure 3.8A)**, but a modest decrease in titer was observed in Neuro-2a cells **(Figure 3.8B)**. In BMDMs, a trend towards a reduction in virus production was observed in ECTV-Δp28-infected cells, but this was not statistically significant **(Figure 3.8C)**. Thus, our data supports that the impairment of ECTV replication caused by complete p28 deletion is cell-type specific.

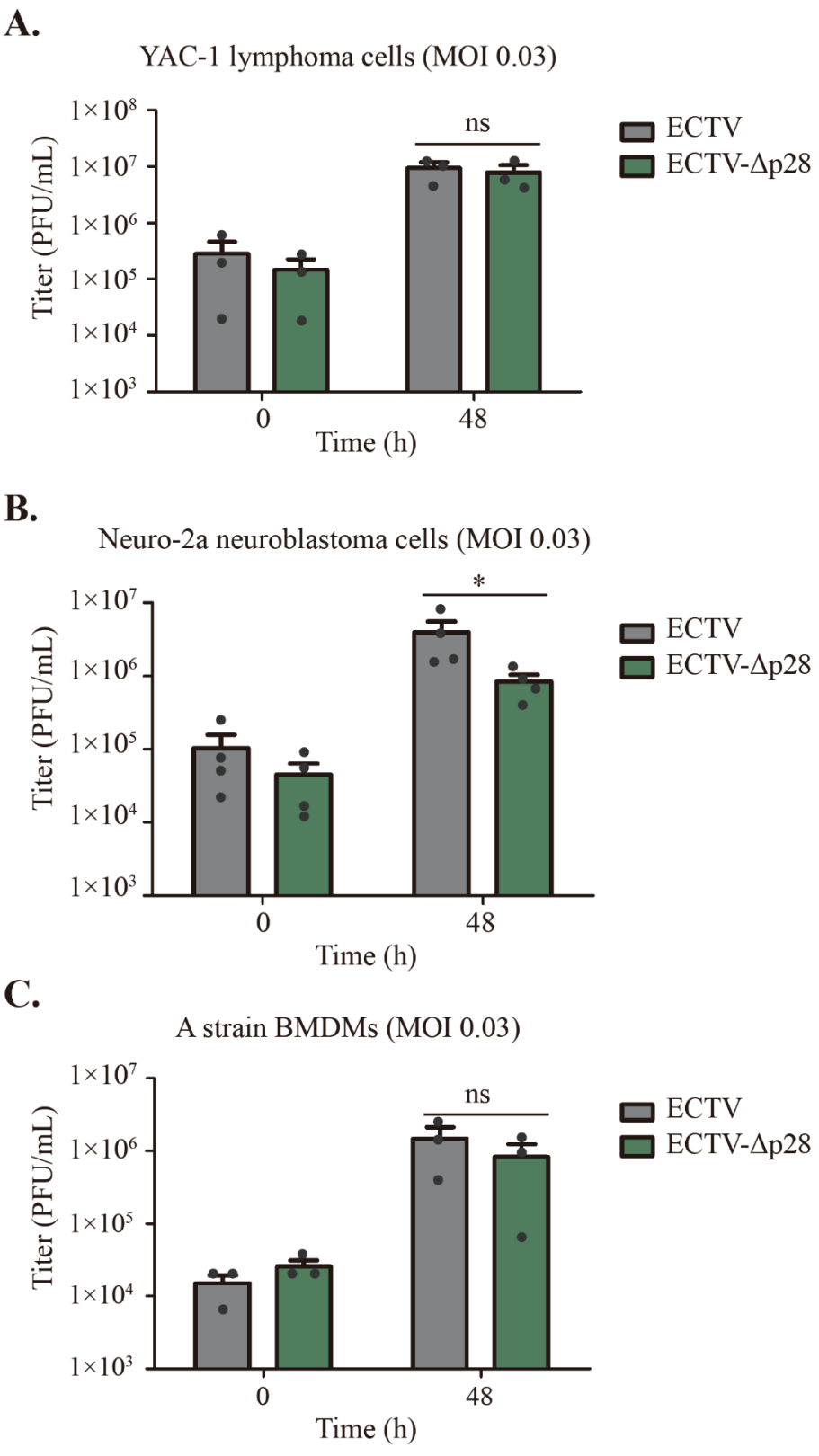
A.
YAC-1 lymphoma cells (MOI 0.03)
Titer (PFU/mL)
1×10^8
1×10^7
1×10^6
1×10^5
1×10^4
1×10^3
ns
0
48
Time (h)
ECTV
ECTV-Δp28
B.
Neuro-2a neuroblastoma cells (MOI 0.03)
Titer (PFU/mL)
1×10^7
1×10^6
1×10^5
1×10^4
1×10^3
*
0
48
Time (h)
ECTV
ECTV-Δp28
C.
A strain BMDMs (MOI 0.03)
Titer (PFU/mL)
1×10^7
1×10^6
1×10^5
1×10^4
1×10^3
ns
0
48
Time (h)
ECTV
ECTV-Δp28

Figure 3.8 ECTV production in cells or cell lines derived from strain A mice was not significantly inhibited by deleting p28

Virus production of ECTV or ECTV- Δp28 was examined in infected YAC-1 **(A)**, Neuro-2a **(B)**, and BMDMs **(C)** at a MOI of 0.03 for 48 hpi. Viral titers are presented as PFU/mL. Results presented represent the mean and standard deviation of 3 **(A** and **C)** or 4 **(B)** independent experiments with results from individual experiments indicated as points. A two-way ANOVA was used to calculate statistical significance. ns; not significant, *; $p \leq 0.05$. Virus growth data in YAC-1 and Neuro-2a was acquired by Dana Kocincova. This figure was adapted from Dong, J *et al*., 2022 (173).

3.2.5 Deletion of p28 decreased ECTV production in PMs isolated from the BALB/c susceptible mouse strain, but not the C57BL/6 resistant mice

Besides strain A mice, there are several other strains of mice that are also susceptible to ECTV infection, such as BALB/c and DBA/2 mice (45). I next investigate whether p28 was essential for ECTV production in the PMs from other susceptible mice. PMs from BALB/c mice were purified as described previously and infected with ECTV, ECTV-Δp28, or ECTV-Δp28-Rev at a MOI of 0.03 for 48 h. ECTV-Δp28 replication was compromised in BALB/c PMs and restored with the revertant virus **(Figure 3.9A)**. Therefore, p28 is required for the ECTV production in PMs from more than one susceptible mouse strain. In addition to PMs from susceptible mice, I examined whether deletion of p28 inhibited ECTV production in the PMs isolated from resistant mice, C57BL/6 (45). PMs were infected with ECTV, ECTV-Δp28, or ECTV-Δp28-Rev at a MOI of 0.03 for 48 h before testing the virus titers. I found that ECTV, with or without p28, can replicate in the PMs from C57BL/6 mice **(Figure 3.9B)**. This result is consistent with previous work demonstrating that the replication of ECTV in PMs from resistant mice was not compromised by disruption of the RING domain of p28 (154). Taken together, these results indicate that p28 is critical for efficient ECTV production in PMs of two susceptible mice, strain A and BALB/c mice, but that p28 is not required in the PMs of resistant mice, C57BL/6.

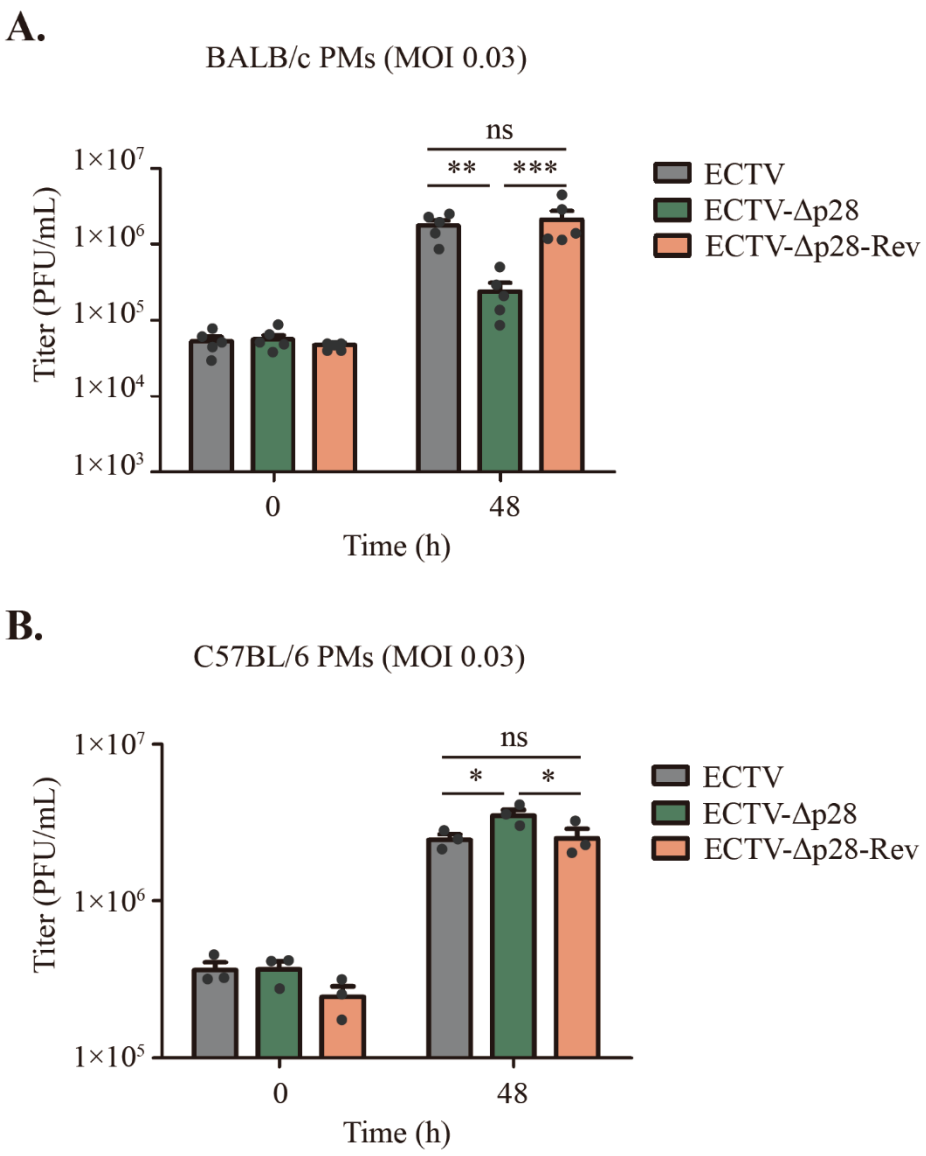

Figure 3.9 p28 deletion compromises virus production in PMs isolated from the susceptible mouse strain, BALB/c

Virus production in PMs isolated from BALB/c **(A)** and C57BL/6 **(B)** cells infected with ECTV, ECTV-Δp28, or ECTV-Δp28-Rev was examined at 48 hpi. Viral titers are presented as PFU/mL. Results presented represent the mean and standard deviation of 5 **(A)** or 3 **(B)** independent experiments with results from individual experiments indicated as points. A two-way ANOVA was used to calculate statistical significance. ns; not significant, *; $p \leq 0.05$, **; $p \leq 0.01$, ***; $p \leq 0.001$. This figure was adapted from Dong, J *et al*., 2022 (173).

3.2.6 Complete deletion of p28 impairs virus factory formation and late gene expression in strain A PMs infected at low MOI

Disruption of the ECTV p28 RING domain inhibited virus factory formation during ECTV replication in PMs at high MOI infection (154). To investigate whether this was true during ECTV-Δp28 infection, we infected strain A PMs with ECTV or ECTV-Δp28 at a MOI of 3 and examined virus factory formation and viral gene expression by IF. Cells were fixed and stained with anti-I3 Ab, which also recognizes its homolog in ECTV, EVM056, and was used to indicate viral infection. The anti-D13 Ab also recognizes its homolog in ECTV, EVM102, which served as an indicator of late protein expression. We used DAPI to stain the nuclei and virus factories (indicated by arrows in **Figure 3.10**). Regardless of whether infected with ECTV or ECTV-Δp28, all cells expressed the viral protein EVM056 under high MOI (MOI 3) infection, indicating that all cells were infected and the deletion of p28 did not affect virus entry. Intriguingly, virus factory formation was observed in both ECTV and ECTV-Δp28-infected PMs **(Figure 3.10A)**. In addition, the deletion of p28 did not block the expression of viral late protein **(Figure 3.10A)**. These data are consistent with our previous finding that the replication of ECTV in PMs from strain A mice was not dramatically impaired by p28 deletion at high MOI **(Figure 3.6A)**. I next examined factory formation and gene expression in PMs infected at low MOI (MOI 0.03). Virus factories were observed in cells infected with ECTV and the ECTV-Δp28-Rev virus at 12 hpi, but few factories were observed in cells infected with ECTV-Δp28 even at 48 hpi

A.

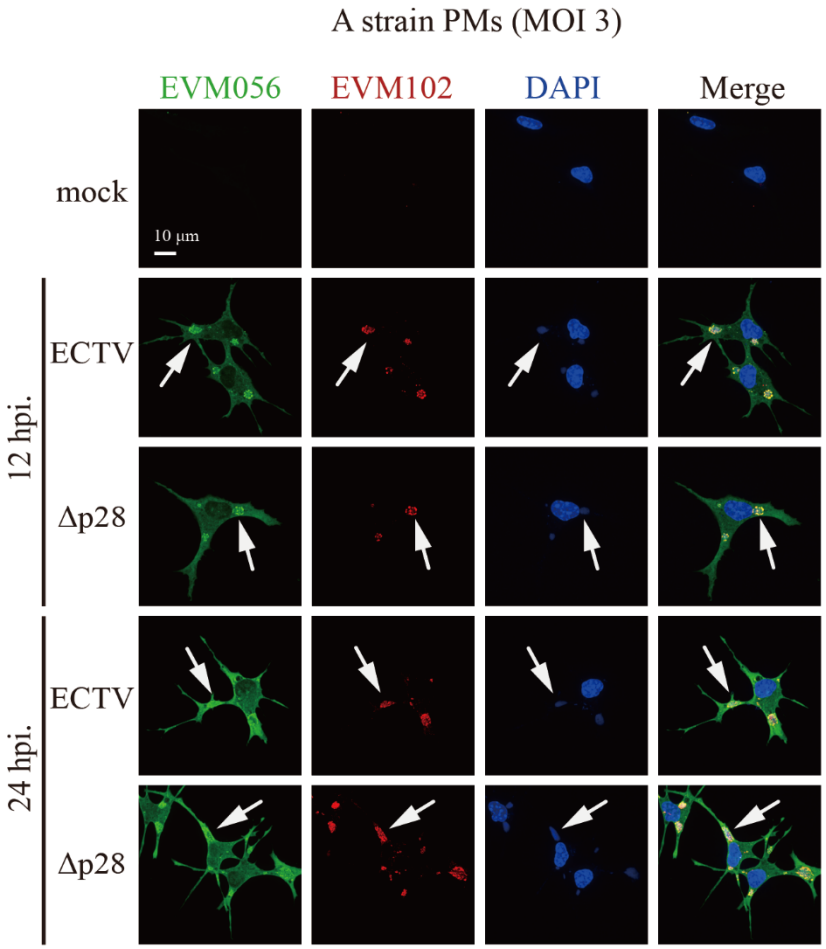
A strain PMs (MOI 3)
EVM056
EVM102
DAPI
Merge
mock
10 μm
12 hpi.
ECTV
Δp28
24 hpi.
ECTV
Δp28

B.

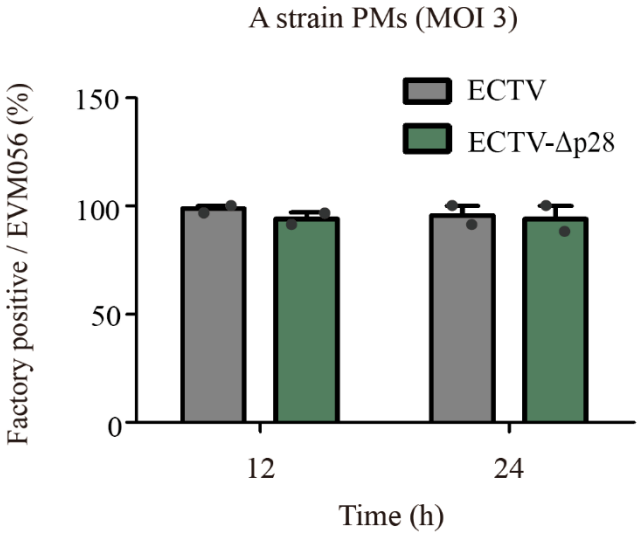
A strain PMs (MOI 3)
ECTV
ECTV-Δp28
Factory positive / EVM056 (%)
150
100
50
0
12
24
Time (h)

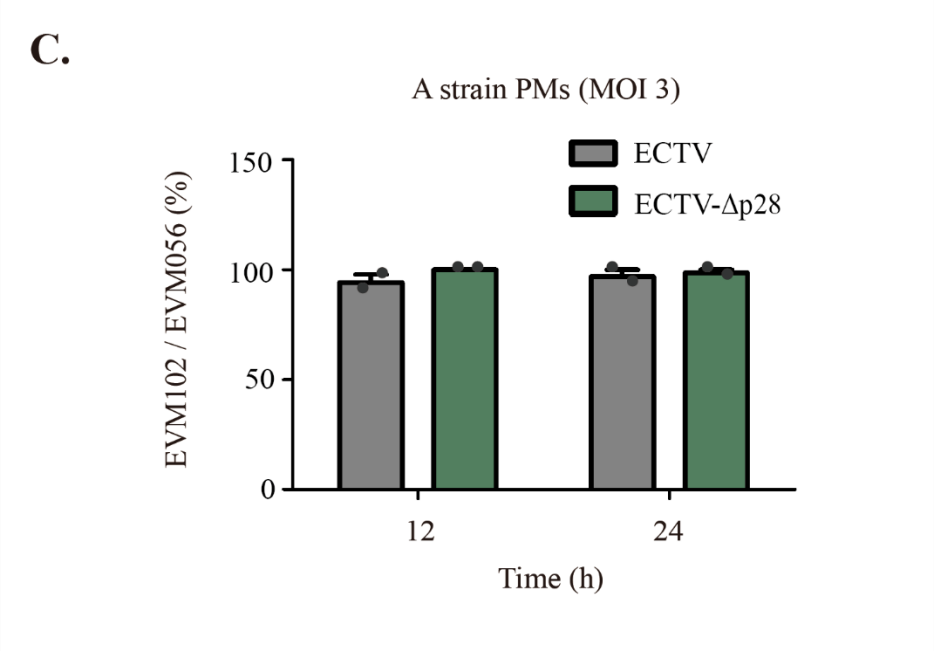

Figure 3.10 Complete deletion of p28 does not affect virus factory formation and late gene expression in strain A PMs infected at high MOI

A, Isolated PMs were seeded on glass slides and either left uninfected or infected with ECTV, ECTV-Δp28 at a MOI of 3. Cells were fixed and permeabilized 12, or 24 hpi and stained with anti-I3 and anti-D13 Abs, as well as DAPI. Virus factories are indicated by arrows. Scale bar, 10 μm. The results presented in the figure were replicated in 2 independent experiments, and the figure displays one of the 2 replicates. **B,** The percentage of infected cells (EVM056 positive) with an obvious virus factory was determined from images. In each experiment, 10 random fields were measured, and the experiment was repeated twice. **C,** The percentage of infected cells (EVM056 positive) with visible late gene expression (EVM102 positive) was determined from the images. In each experiment, 10 random fields were measured. This figure was adapted from Dong, J *et al*., 2022 (173).

(Figure 3.11A). I calculated the percentage of infected cells (EVM056 positive) with an obvious virus factory from 10 random fields **(Figure 3.11B)** and found that virus factories were found in more than 80% of the PMs infected with ECTV or ECTV-Δp28-Rev at 12 hpi. The percentage of the infected cells with a virus factory increased to nearly 100% at 48 h post ECTV or ECTV-Δp28-Rev infection **(Figure 3.11B)**. However, deletion of p28 inhibited the formation of detectable virus factories. Few infected cells formed visible virus factories at 12 hpi or 24 hpi **(Figure 3.11B)**. At 48 hpi, less than 10% of the infected cells had virus factories, which is significantly lower than the percentage of infected cells with virus factories in the PMs infected with the ECTV expressing p28 **(Figure 3.11B)**. Likewise, expression of the viral late protein, EVM102, was impaired in cells infected with the ECTV-Δp28 virus at low MOI **(Figure 3.11A and C)**. Furthermore, at low MOI infection (MOI 0.03), a small portion of cells were infected and are EVM056-positive **(Figure 3.11D)**. A comparable portion of PMs (<5%) expressed EVM056 at 12 hpi with ECTV, ECTV-Δp28 or ECTV-Δp28-Rev **(Figure 3.11D)**. This suggested that the PMs were infected with similar amounts of these viruses. A significant increase of the proportion of EVM056-positive cells in PMs infected with ECTV or ECTV-Δp28-Rev was observed at 24 and 48 hpi **(Figure 3.11D)**. In contrast, no increase in the percentage of EVM056-positive cells was observed in PMs infected with ECTV-Δp28 virus **(Figure 3.11D)**. Overall, our results show that p28 was important for virus factory formation and late gene expression when PMs were infected at low MOI. In addition, ECTV lacking p28 impaired

virus replication in PMs infected at low MOI.

3.2.7 p28 deletion inhibited virus DNA replication in strain A PMs

The observation that virus factory formation was impaired led us to investigate whether viral genome replication was compromised in strain A PMs infected with the ECTV-Δp28 virus at low MOI. To answer this question, I purified total DNA from infected PMs and examined viral genome copy number by qPCR using previously described method (53). The genome copy number of ECTV and revertant virus in strain A PMs increased with infection time **(Figure 3.12A)**. However, the viral genome copy number in ECTV-Δp28-infected cells did not increase over time **(Figure 3.12A)**. I also examined the changes in viral genome copy number of the three viruses in the PMs from resistant mice, C57BL/6. At low MOI infection, genome copy numbers of the three viruses increased to comparable levels **(Figure 3.12B)**. No significant difference in viral genome copy number was observed in the C57BL/6 mice PMs infected with ECTV with or without p28 gene **(Figure 3.12B)**. Next, to determine whether the ECTV-Δp28 genome replication was completely or partially impaired, I used cytosine analog, Ara-C, to block DNA synthesis (135), and examined the viral genome copy number of ECTV-Δp28 in infected PMs treated or untreated with Ara-C. Genome copy numbers of both ECTV and ECTV-Δp28-Rev dropped significantly in the Ara-C-treated PMs from strain A mice **(Figure 3.13)**. A trend towards reduced ECTV-Δp28 genome replication was also observed, however, this reduction was not statistically significant when compared with untreated cells

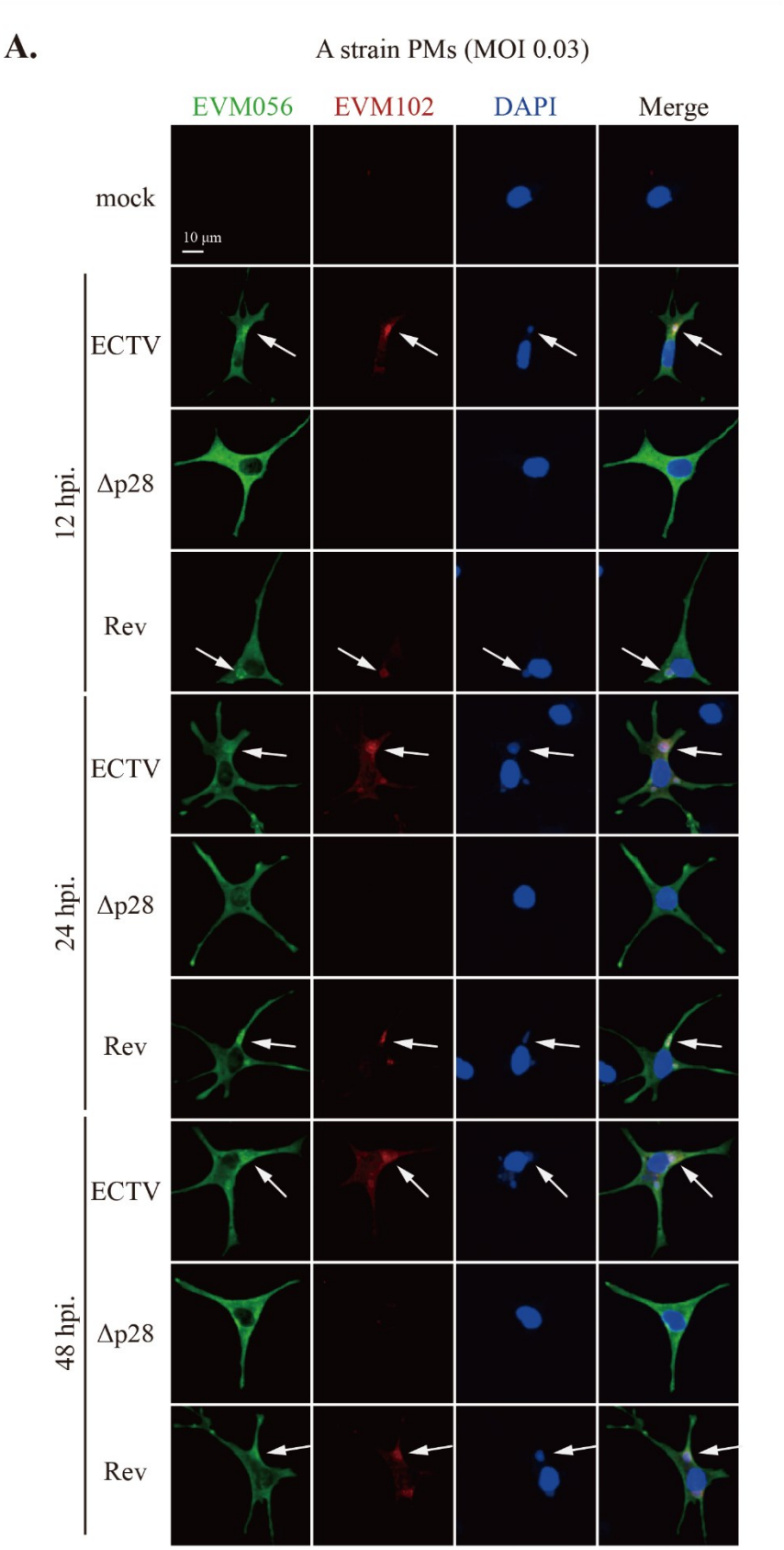
A.
A strain PMs (MOI 0.03)
EVM056
EVM102
DAPI
Merge
mock
10 μm
12 hpi.
ECTV
Δp28
Rev
24 hpi.
ECTV
Δp28
Rev
48 hpi.
ECTV
Δp28
Rev

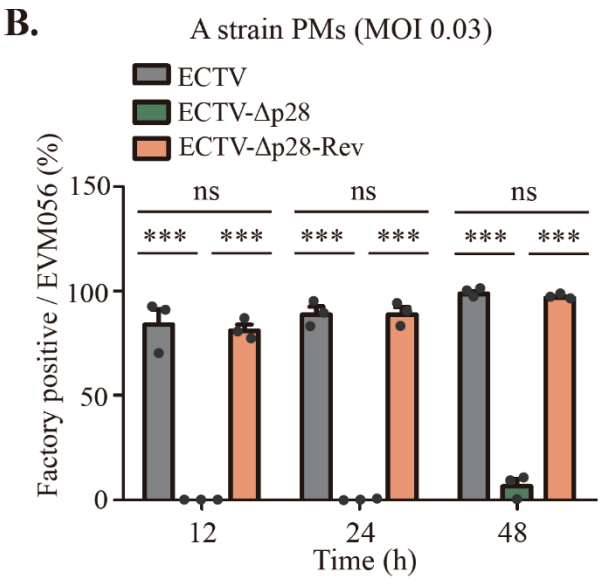
B.
A strain PMs (MOI 0.03)
ECTV
ECTV-Δp28
ECTV-Δp28-Rev
Factory positive / EVM056 (%)
150
100
50
0
ns
ns
ns
***
***
***
***
***
***
12
24
48
Time (h)

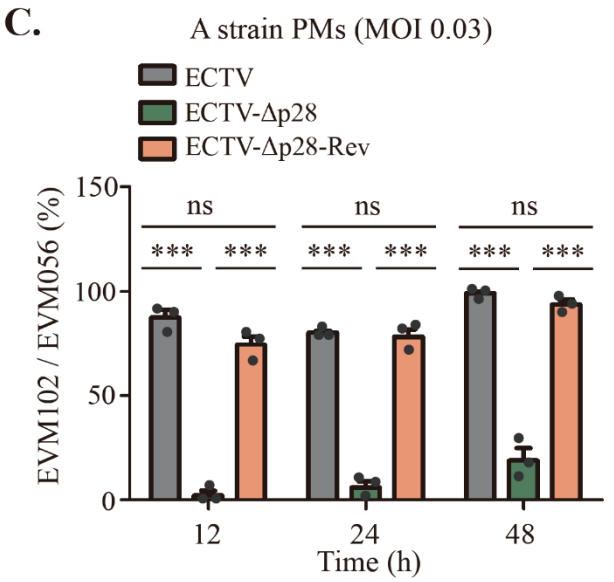
C.
A strain PMs (MOI 0.03)
ECTV
ECTV-Δp28
ECTV-Δp28-Rev
EVM102 / EVM056 (%)
150
100
50
0
ns
ns
ns
***
***
***
***
***
***
12
24
48
Time (h)

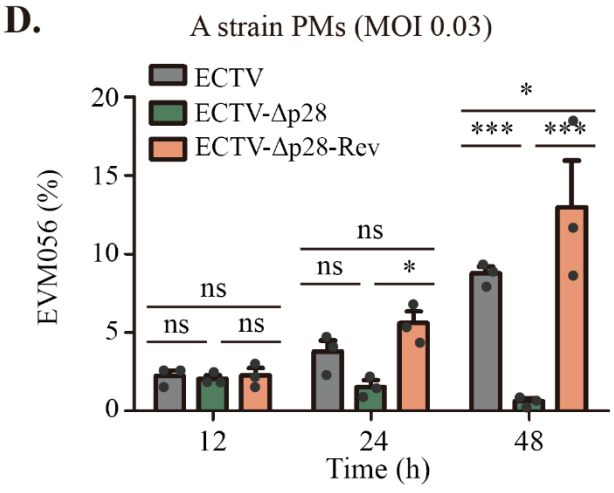
D.
A strain PMs (MOI 0.03)
ECTV
ECTV-Δp28
ECTV-Δp28-Rev
EVM056 (%)
20
15
10
5
0
*
***
***
ns
ns
*
ns
ns
ns
12
24
48
Time (h)

Figure 3.11. Complete deletion of p28 impairs virus factory formation and late gene expression in strain A PMs infected at low MOI

A, Isolated PMs were seeded on glass slides and either left uninfected or infected with ECTV, ECTV-Δp28, or the revertant virus at a MOI of 0.03. Cells were fixed and permeabilized 12, 24, or 48 hpi and stained with anti-I3 and anti-D13 Abs, as well as DAPI. Virus factories are indicated by arrows. Scale bar, 10 μm. The results presented in the figure were replicated in 3 independent experiments, and the figure displays one of the 3 replicates. **B,** The percentage of infected cells (EVM056 positive) with an obvious virus factory was determined from images. In each experiment, 10 random fields were measured, and the experiment was repeated 3 times. **C,** The percentage of infected cells (EVM056 positive) with visible late gene expression (EVM102 positive) was determined from the images. In each experiment, 10 random fields were measured. **D,** The number of infected cells (EVM056 positive) was determined at the indicated times post-infection. In each experiment, 10 random fields were measured. Results presented represent the mean and standard deviation of 3 independent experiments with results from individual experiments indicated as points. A two-way ANOVA was used to calculate statistical significance. ns; not significant, *; $p \leq 0.05$, ***; $p \leq 0.001$. This figure was adapted from Dong, J *et al*., 2022 (173).

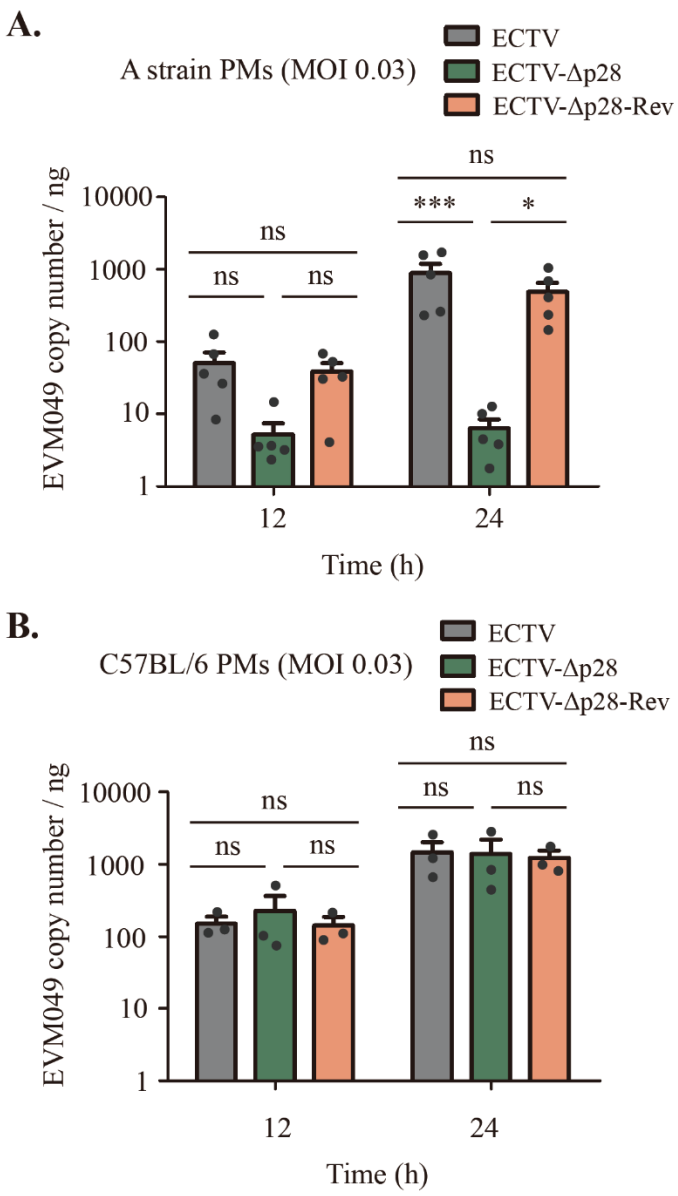

Figure 3.12 Viral genomic DNA replication in PMs from strain A and C57BL/6 mice

PMs isolated from strain A **(A)** or C57BL/6 **(B)** mice were infected with ECTV, ECTV-Δp28, or the revertant virus at a MOI of 0.03. Viral and cellular DNA was purified by phenol extraction 12 and 24 hpi, and virus genome copy number was determined by qPCR. Results presented represent the mean and standard deviation of 5 **(A)** or 3 **(B)** independent experiments with results from individual experiments indicated as points. A two-way ANOVA was used to calculate statistical significance. ns; not significant, *; $p \leq 0.05$, ***; $p \leq 0.001$. This figure was adapted from Dong, J *et al*., 2022 (173).

(Figure 3.13). Thus, complete deletion of p28 results in a defect in ECTV genome replication in susceptible strain A PMs at low MOI infection. The genome replication defect induced by p28 deletion is comparable to the inhibition of DNA synthesis by Ara-C treatment.

3.3 Summary and brief discussion

In this study, we show that the requirement for p28 for efficient virus replication is not only dependent on the infected cell type and mouse strain, but the MOI as well. Of note, unlike previous studies, the production of wild-type ECTV did not significantly increase in strain A PMs infected at a high MOI. This may be due to a low proliferation rate of PMs, which might limit the resources available for virus replication. Consequently, the low replication level of wild-type ECTV may obscure the effect of p28 deletion on virus production at high MOI.

Using a Poisson distribution [$P(n) = \frac{m^n \times e^{-m}}{n!}$, m is MOI, n is the number of virions per cell] (176), the probability that a cell will be infected with at least one virion at a MOI of 3 is greater than 95%. Cells infected with only one virion at a MOI of 3 is ~15% of the total. It is interesting to note that the inhibition of virus factory formation and late protein expression was rarely observed in the infected strain A PMs at a MOI of 3 (which is much less than 15% of the total cells). This contrasted with the observation in the infected cells at a MOI of 0.03, which were mostly infected with one virion. These results suggested that the overall proportion of infected cells affects the requirement of p28 during ECTV

replication in PMs from strain A mice.

We show that ECTV completely lacking p28 is viable **(Figure 3.4)**; however, there is a severe impairment in virus factory formation, genome replication, and late gene expression in strain A PMs infected at low MOI **(Figure 3.11)**. Consistent with previous findings for the RING domain-deleted ECTV p28, the requirement for p28 is cell type-specific (154), we found a minimal role for p28 for virus production in two cell lines derived from strain A mice as well as strain A BMDMs **(Figure 3.8)**. However, p28 deletion compromised virus production in PMs isolated from the susceptible BALB/c strain **(Figure 3.9A)**; albeit the defect was less pronounced than observed in strain A PMs **(Figure 3.7C)**. Our results indicated that p28 is an essential factor in virus replication in certain contexts. Moreover, p28 is important for virus genome replication in certain cells. It is unclear at what step of virus replication p28 is required. This will be the future direction we will focus on and discuss in the overall discussion section. In addition, Identification of p28 substrates will be critical to further elucidating the function of p28.

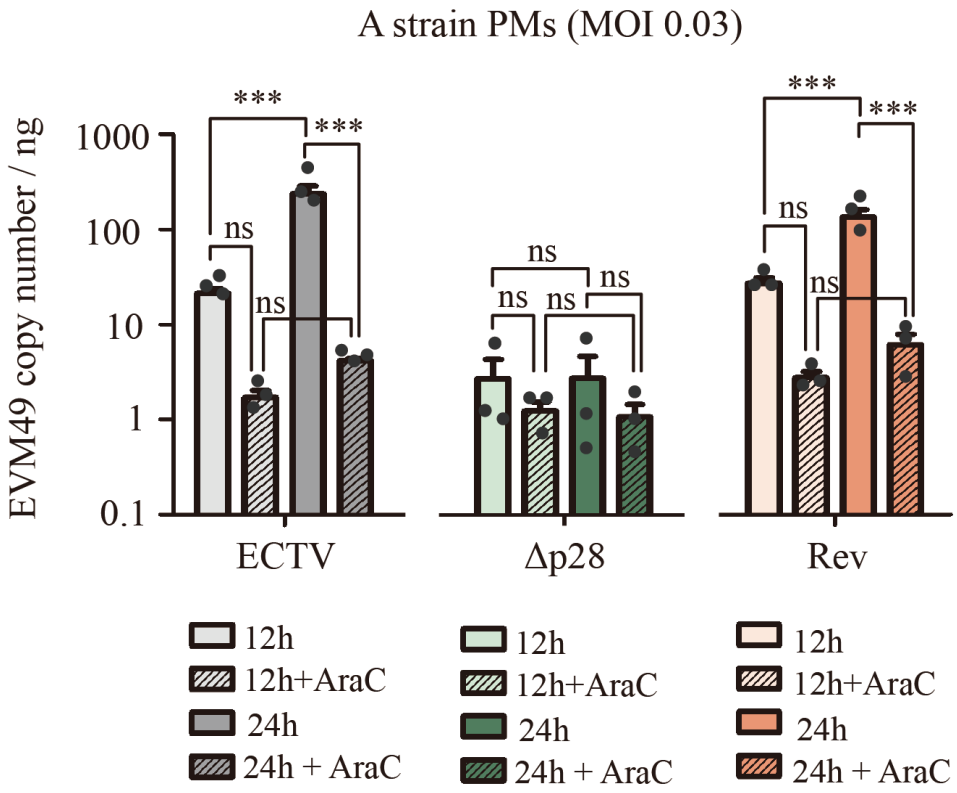

Figure 3.13 Viral genomic DNA replication in PMs with and without Ara-C

PMs isolated from strain A mice were treated with or without 40µg/mL Ara-C and infected with ECTV, ECTV-Δp28, or the revertant virus at a MOI of 0.03. Viral and cellular DNA was purified by phenol extraction 12 and 24 hpi, and virus genome copy number was determined by qPCR. Results presented represent the mean and standard deviation of 3 independent experiments with results from individual experiments indicated as points. A two-way ANOVA was used to calculate statistical significance. ns; not significant, ***; $p \leq 0.001$. This figure was adapted from Dong, J *et al*., 2022 (173).

Chapter 4: Developing tools to investigate substrates and binding properties of p28

Contributions to this chapter:

All experiments presented in this chapter were performed by me. The donor plasmids used to generate baculovirus expressing His-tagged p28 and its isolated domains were designed and ordered by Dr. Egor Tchesnokov.

4.1 Introduction

p28 is an E3 ligase which is expressed at both early and late stage of poxvirus infection (151). Previous studies have shown that p28 consists of two domains: an N-terminal KilA-N domain and a RING domain at the C-terminus (156, 158). The KilA-N domain of p28 shares a common structure with the DNA-binding APSES domain (156), and p28 encoded by SFV-N1R has been shown to bind DNA cellulose columns (155). A truncated p28 encoded by VACV-WR was detected in the complex of DNA cross-link to proteins by mass spectrometry analyzation (157). The KilA-N domain but not RING domain of p28 is required for p28 virus factory localization (151-155). Deletion of seven highly conserved amino acid residues (44-50; YINITKI) in the KilA-N domain results in the failure of p28 virus factory localization (153). The RING domain of p28 is crucial for virulence of ECTV *in vivo* (158). In addition, disruption of the RING domain impairs CPXV replication in human and mouse macrophages cell lines (160). As with other RING-finger domains, the RING domain of p28 has conserved cysteine and histidine residues (155). The first two conserved cysteines of the RING domain of p28, C173 and C176, are essential for the auto-ubiquitylation activity of p28 (151, 152). These results indicate that p28 has E3 Ub-ligase activity, however, the substrates of p28 have not yet been identified.

In this chapter, I used Ub-activated interaction traps (UBAITs) on a small scale to determine whether it could be a tool for capturing p28 substrates. UBAITs is a method to capture and identify E3 ligase substrates through E3 fusions with Ub (E3-Ub), whose Ub

moiety can trap proteins in close proximity to the E3 by forming a covalent bond (177). To capture substrates of p28, a FLAG-tagged p28 fusion with Ub (FLAG-p28-Ub) was expressed in the VACV-Cop-infected HeLa cells. In addition, to study the DNA binding properties of p28, I purified His-tagged p28 from baculovirus system. The E3 Ub-ligase activity and the DNA binding ability of the purified p28 were examined. Our purified p28 will be a valuable tool for us to study the functions of p28 at a molecular level.

4.2 Results

4.2.1 Characterization of FLAG-p28-Ub in infected cells

The UBAITs approach was validated with several RING Ub-ligases and trapped not only the substrates, but also proteins in close proximity to the E3 Ub-ligase (177). Therefore, I adopted the UBAITs approach to determine whether it can be used as a tool to capture proteins associated with p28. I designed a FLAG-tagged p28-Ub fusion protein **(Figure 4.1 ①)** and inserted its gene into a vector, pSC66, which was used to express the transgene from a poxvirus early/late promoter (178). The plasmid, pSC66-FLAG-p28-Ub, was transfected into cells infected with VACV-Cop which is a poxvirus strain without endogenous p28. Our rationale was that the FLAG-p28-Ub would covalently trap substrates of p28. **(Figure 4.1 ②③)**. The covalent bond between the Ub moiety and the associated proteins would allow us to purify these potential substrates of p28 by anti-FLAG Abs.

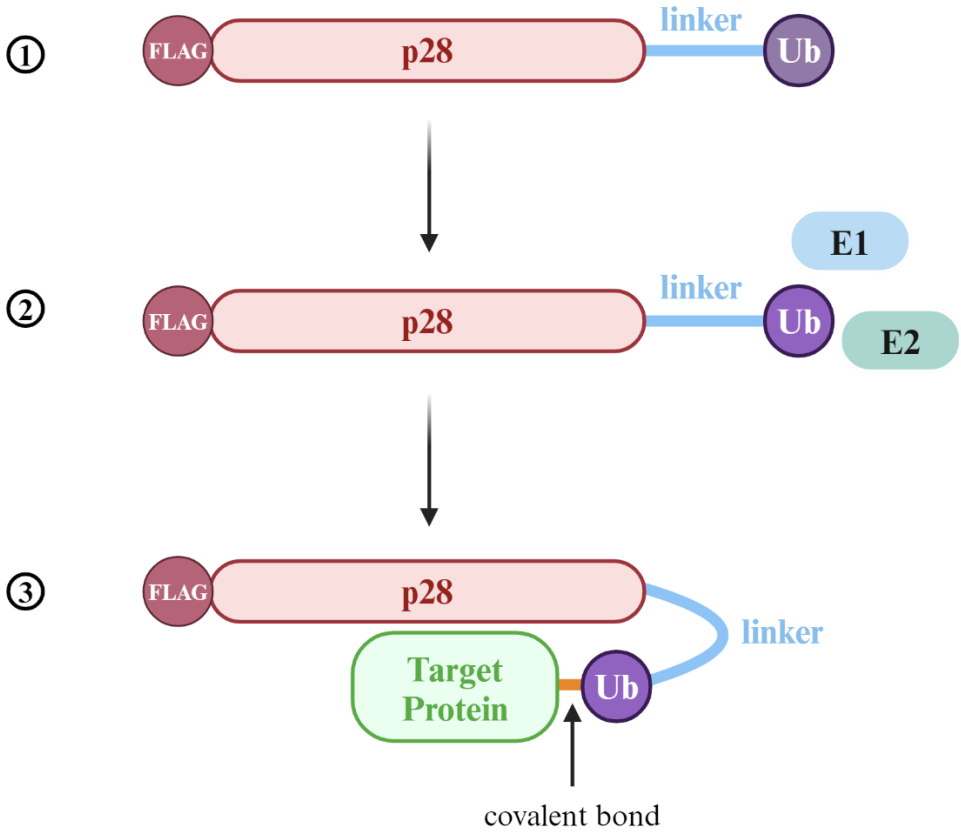

Figure 4.1 Diagram of FLAG-p28-Ub trapping potential substrates of p28

1) The schematic of FLAG-p28-Ub. The FLAG tag was added at the N terminus of p28. Ub was linked to the C terminus of p28 via a flexible linker, a 12-amino acid linker consisting of 3 GGSG peptide repeats. **2)** The Ub moiety is activated by E1 and transferred to E2. **3)** A covalent bond is formed between the Ub moiety, and the protein associated with the p28 moiety of the fusion protein.

To test the protein expression level of FLAG-p28-Ub in different cell lines, I transfected pSC66-FLAG-p28-Ub into BSC-40 and HeLa cells. Cells were then infected with VACV-Cop at a MOI of 3 for 18 h. I used pSC66-FLAG-p28 as a positive control for FLAG-tagged protein expression. Uninfected cells and VACV-Cop-infected cells transfected with pSC66 vector were included as negative controls. The expression level of FLAG-tagged proteins was examined by anti-FLAG western blotting **(Figure 4.2, top panel)**. Both FLAG-p28 and FLAG-p28-Ub were observed in VACV-Cop-infected BSC-40 and HeLa cells, and the size of FLAG-p28-Ub (~38 kDa) increased by ~10 kDa compared to FLAG-p28 (~29 kDa) as predicted **(Figure 4.2, top panel)**. However, these FLAG-tagged proteins were expressed at higher levels in HeLa cells than in BSC-40 cells **(Figure 4.2, top panel)**. The anti-p28 Ab was also used to examine the expression of FLAG-p28 and FLAG-p28-Ub. FLAG-p28 in BSC-40 cells and HeLa cells was observed in western blotting with anti-p28 Ab **(Figure 4.2, second panel from top)**. It is difficult to discern whether FLAG-p28-Ub was recognized by the anti-p28 Ab because the band of FLAG-p28-Ub merged with the non-specific band at ~34 kDa **(Figure 4.2, second panel from top)**. Nonetheless, a thicker band was observed in the pSC66-FLAG-p28-Ub-transfected HeLa cells, suggesting that FLAG-p28-Ub may be recognized by the anti-p28 Ab **(Figure 4.2, second panel from top)**. These results show that the expression of FLAG-p28 and FLAG-p28-Ub can be detected by the anti-FLAG Abs at the predicted sizes and the expression level of FLAG-p28-Ub in HeLa cells was higher than that in BSC-40 cells.

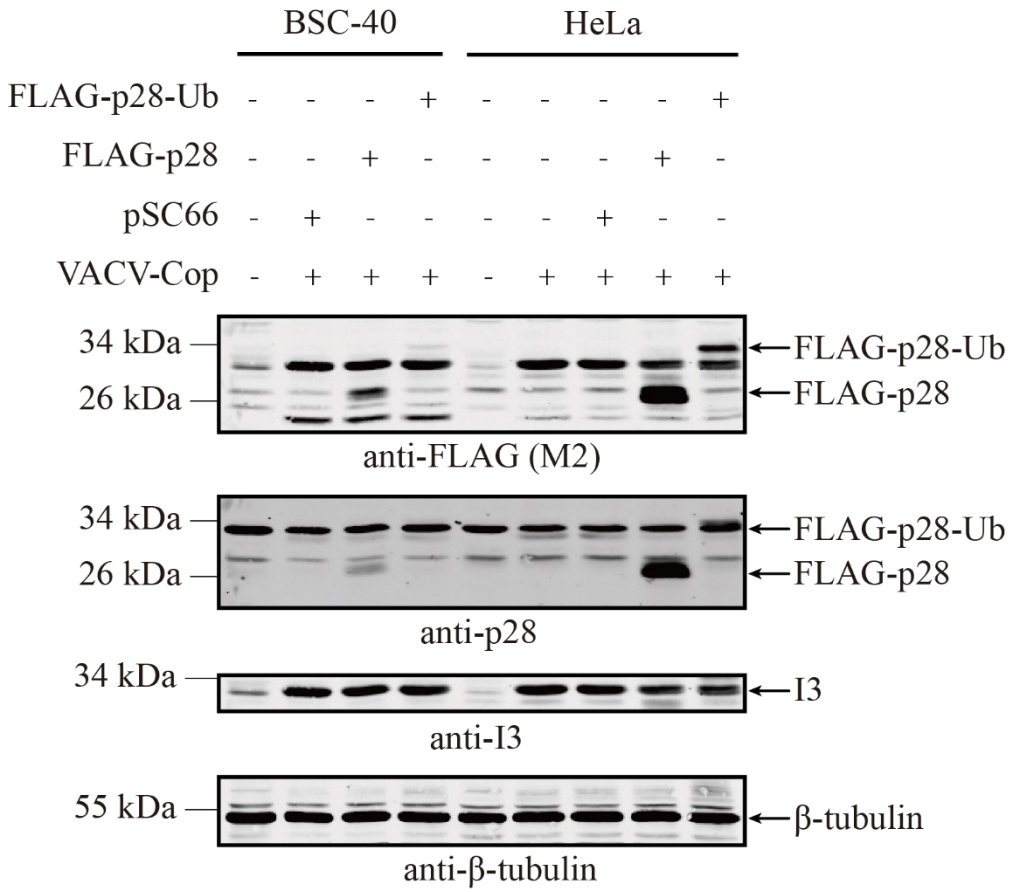

Figure 4.2 Expression of FLAG-p28-Ub in infected BSC-40 and HeLa cells

BSC-40 cells and HeLa cells were transfected with pSC66, or pSC66-FLAG-p28, or pSC66-FLAG-p28-Ub, and then infected with VACV-Cop at a MOI of 3 for 18 h. VACV I3 is used as an indicator of VACV-Cop infection. The anti-β-tublin blot was included to show protein loading. Molecular mass markers are indicated to the left of blots. The western blotting was performed by Patrick Paszkowski and me. The results presented in the figure were replicated in 3 independent experiments, and the figure displays one of the 3 replicates.

It is known that p28 localizes to virus factories during poxvirus infection (150-155). In addition, conjugated Ub co-localized to virus factories upon overexpression of FLAG-p28 in infected HeLa cells (152, 153). Confirming that the FLAG-p28-Ub maintains the same localization and effect on Ub as p28 is crucial for us to capture the appropriate proteins that associate with p28. To investigate the localization of FLAG-p28-Ub and conjugated Ub, HeLa cells were left untransfected or transfected with pSC66, pSC66-FLAG-p28, or pSC66-FLAG-p28-Ub and then infected with VACV-Cop at a MOI of 3. The localization of conjugated Ub and FLAG-tagged proteins were examined by IF microscopy using an anti-conjugated Ub Ab (FK2) or anti-FLAG Ab. DAPI was used to stain the nuclei and virus factories **(**indicated by arrows in **Figure 4.3**). Both FLAG-p28 and FLAG-p28-Ub were localized to virus factories, indicated by DAPI, at 4 and 8 hpi **(Figure 4.3, c2, d2, g2, and h2)**. Conjugated Ub was difficult to detect or diffuse in the cytoplasm in infected cells without p28 expression **(Figure 4.3, a3, b3, e3, and f3)**. In contract, conjugated Ub was enriched in the virus factory in cells expressing FLAG-p28 or FLAG-p28-Ub **(Figure 4.3, c3, d3, g3, and h3)**. These results demonstrate that adding Ub to the C terminus of p28 did not affect p28 localization or its ability to enrich conjugated Ub into virus factories.

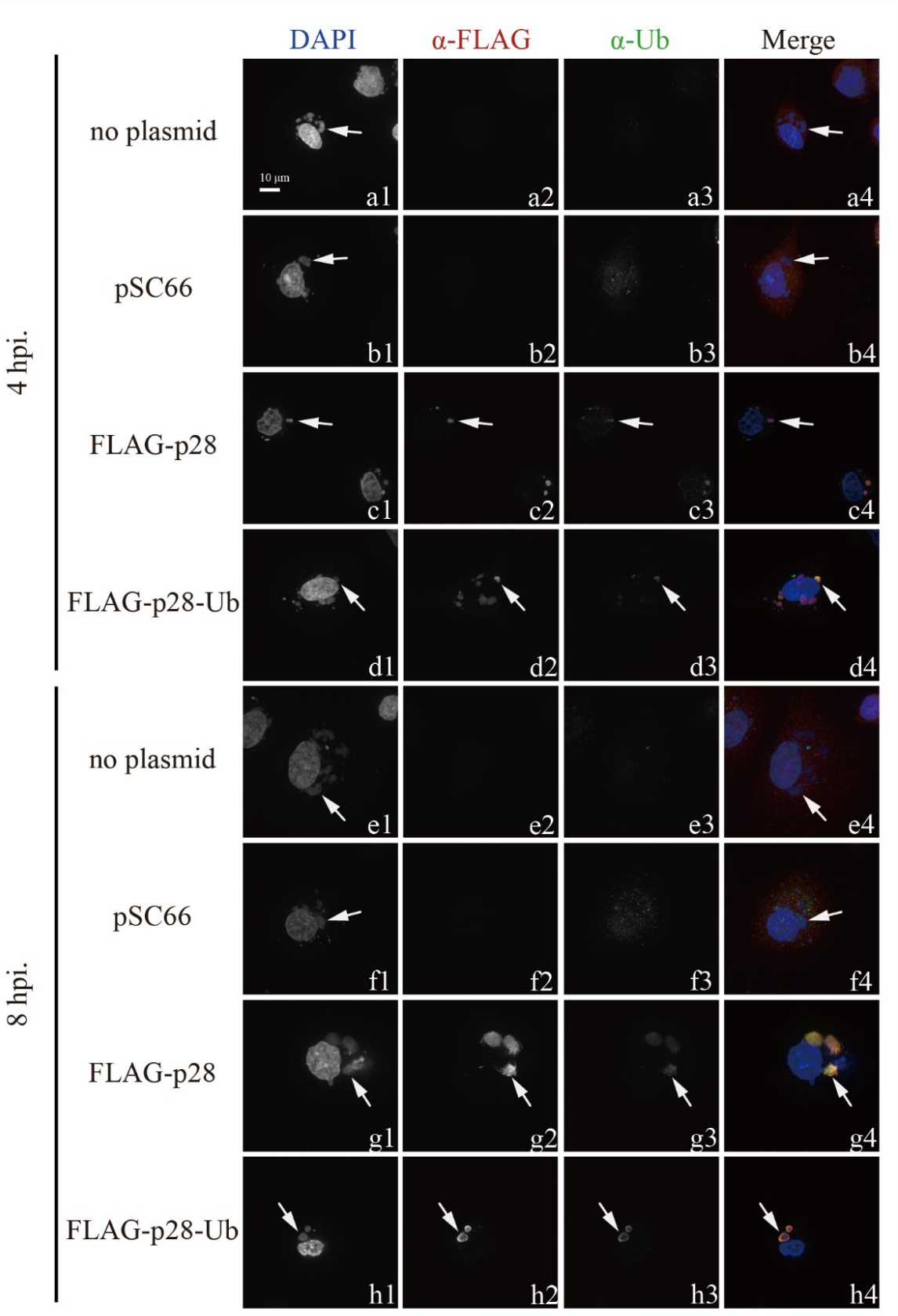
DAPI
α-FLAG
α-Ub
Merge
4 hpi.
8 hpi.
no plasmid
pSC66
FLAG-p28
FLAG-p28-Ub
no plasmid
pSC66
FLAG-p28
FLAG-p28-Ub
10 μm
a1
a2
a3
a4
b1
b2
b3
b4
c1
c2
c3
c4
d1
d2
d3
d4
e1
e2
e3
e4
f1
f2
f3
f4
g1
g2
g3
g4
h1
h2
h3
h4

Figure 4.3 Localization of FLAG-p28 and FLAG-p28-Ub in infected and HeLa cells

HeLa cells were seeded on glass slides and either left untransfected or transfected with pSC66, pSC66-FLAG-p28, or pSC66-FLAG-p28-Ub for 4 h. Cells were then infected with VACV-Cop at a MOI of 3. Cells were fixed and permeabilized at 4 or 8 hpi and stained with anti-FLAG and anti-conjugated Ub Abs, as well as DAPI. Virus factories are indicated by arrows. Scale bar, 10 μm. The results presented in the figure were replicated in 2 independent experiments, and the figure displays one of the 2 replicates.

4.2.2 Capturing p28-associated proteins in infected cells using UBAITs

Based on the previous results, I used UBAITs on a small scale to determine whether p28 substrates can be captured by FLAG-p28-Ub. I hypothesized that proteins in proximity to p28 would be covalently conjugated to FLAG-p28-Ub and formed high molecular weight (HMW) species in anti-FLAG IPs. I used FLAG-p28-Ub to trap the p28-associated proteins in HeLa cells infected with VACV-Cop. HeLa cells were left untransfected or transfected with pSC66, pSC66-FLAG-p28, or pSC66-FLAG-p28-Ub and then infected with VACV-Cop at a MOI of 3. HeLa cells infected with VACV-Cop with and without pSC66 transfection were negative controls in this experiment. I also have HeLa cells transfected with pSC66-FLAG-p28 to compare with the fusion p28 with Ub (FLAG-p28-Ub). The expression of the FLAG-tagged proteins was checked by western blotting with anti-FLAG Ab **(Figure 4.4A)**. Then, I used anti-FLAG (M2) to immunoprecipitate FLAG-tagged p28 and their associated proteins from the lysates of transfected and infected HeLa cells. To detect the FLAG-tagged p28 with Ub chains, I used 4-15% gradient gel to separate the proteins and then detected them by western blotting with an anti-FLAG rabbit Ab **(Figure 4.4B)**. Both FLAG-p28 and FLAG-p28-Ub could be immunoprecipitated from cell lysates using anti-FLAG Ab **(Figure 4.4B)**. Western blotting analysis of the FLAG-p28-Ub IP sample showed the appearance of HMW anti-FLAG immunoreactive smear, which was not observed in either our negative controls or FLAG-p28 IP sample **(Figure 4.4B, indicated by an asterisk)**. These results indicate that the FLAG-p28-Ub trapped proteins

associated with p28 during poxvirus infection.

4.2.3 Examining the interaction between FLAG-p28-Ub and Hsp70

A previous study by our group suggested Hsp70, a member of heat shock protein, is one of the potential proteins associated with p28 and co-localized with p28 in virus factories during poxvirus infection (179). However, no evidence was found that Hsp70 is ubiquitylated by p28. To determine whether Hsp70 is trapped by FLAG-p28-Ub, I immunoprecipitated FLAG-tagged proteins and their associated proteins with anti-FLAG (M2) Ab and then detected the proteins by western blotting with anti-FLAG Ab **(Figure 4.5A)** or anti-Hsp70 Ab **(Figure 4.5B)**. No FLAG-tagged protein was detected in the negative control (HeLa cells transfected with pSC66 and infected with VACV-Cop) **(Figure 4.5A, first lane)**. The high molecular weight (HMW) smear was still observed in the anti-FLAG-p28-Ub IP sample, but not in FLAG-p28 IP sample **(Figure 4.5A, indicated by an asterisk)**. A weak Hsp70 band was observed in both FLAG-p28 and FLAG-p28-Ub IPs **(Figure 4.5B)**. These results suggested that the FLAG-p28-Ub associated with Hsp70 which was previously identified as a potential p28-associated protein during poxvirus infection. The size of the Hsp70 recognized by its Ab was not changed which suggested that the Hsp70 interacted with FLAG-p28-Ub, but no covalent bond was formed between them.

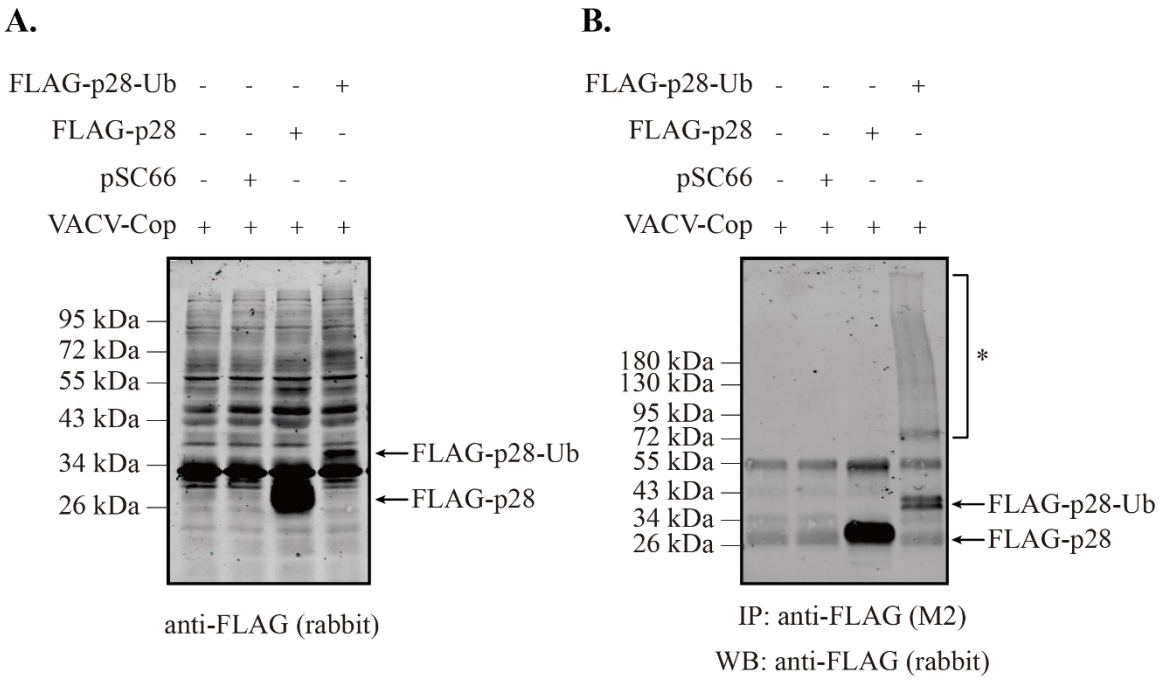

Figure 4.4 IP to trap p28-associated proteins by FLAG tag

A, HeLa cells were left untransfected or transfected with pSC66, or pSC66-FLAG-p28, or pSC66-FLAG-p28-Ub, and then infected with VACV-Cop at a MOI of 3 for 18 h. A small amount of the whole cell lysates was examined by western blotting with anti-FLAG rabbit Ab to check the expression of the FLAG-tagged proteins. **B,** Lysates of infected HeLa cells transfected with indicated plasmids were used to perform anti-FLAG (M2) IPs to capture the FLAG-tagged proteins and their associated proteins. IPs were then separated by SDS-PAGE gradient gel (4-15%) and western blotted with an anti-FLAG rabbit Ab. Molecular mass markers are indicated to the left of blots. The results presented in the figure were replicated in 3 independent experiments, and the figure displays one of the 3 replicates.

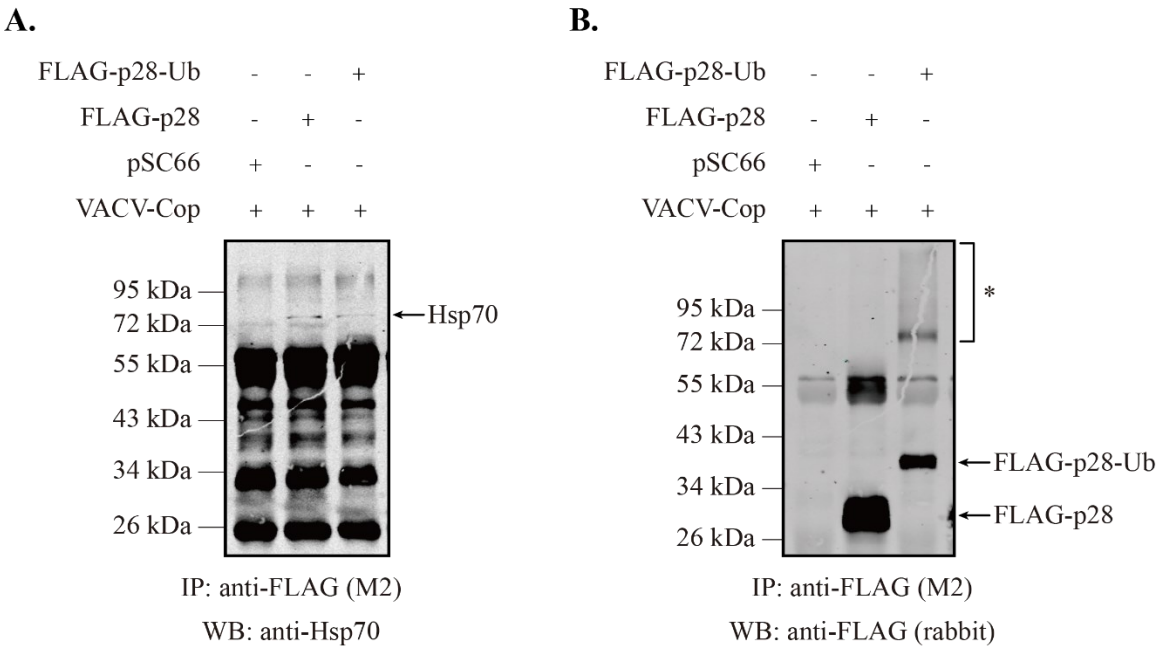

Figure 4.5 Interaction between p28 and Hsp70

Lysates of infected HeLa cells transfected with indicated plasmids were used to perform anti-FLAG (M2) IPs to capture the FLAG-tagged proteins and its associated proteins. IPs were then analyzed by western blotting with an anti-Hsp70 Ab **(A)** or anti-FLAG rabbit Ab **(B)**. The HMW bands in the anti-FLAG IPs were indicated by asterisk. Molecular mass markers are indicated to the left of blots. The results presented in the figure were replicated in 2 independent experiments, and the figure displays one of the 2 replicates.

4.2.4 Purification of p28 and its isolated domains from *E. coli*

To characterize the substrates of p28, how p28 binds DNA, and whether the KilA-N domain is important for the function of p28 *in vitro*, I tried to purify p28 and its isolated domains. I generated glutathione S-transferase (GST) constructs expressing p28 and the isolated, KilA-N and RING domains in *E. coli* **(Figure 4.6)**. The p28 gene or its isolated domains were inserted into pGEX-4T-1, which was used in previously studies to express GST fusion proteins under the regulation of the lactose operon (152, 180). The expressions of the GST fusion proteins in *E. coli* BL21 cells were induced by IPTG. Lysates were run on SDS-PAGE gels followed by Coomassie blue stain **(Figure 4.7)**. Total cellular protein levels were increased after IPTG induction **(Figure 4.7, lane I)** compared with the total cellular protein before IPTG induction in the GST, GST-RING, and GST-p28 samples which is consistent with growth of the bacteria over the induction period **(Figure 4.7, lane C)**. However, cells transformed with pGEX-4T-1-KilA-N consistently showed a very slight increase in the total protein after IPTG induction **(Figure 4.7B, lane I and C)**, suggesting these cells have a lower growth rate compared with the cells transformed with other plasmids under IPTG treatment. After cell disruption by sonication, most of the intracellular proteins remain in the pellet rather than in the soluble supernatant **(Figure 4.7, lane P and S)**. Proteins of the predicted size of the GST fusion proteins were indicated by arrows **(Figure 4.7)**. Thus, the *E. coli* expression system cannot express the GST fusion proteins as a soluble form in the supernatant. Then, I investigated another system to

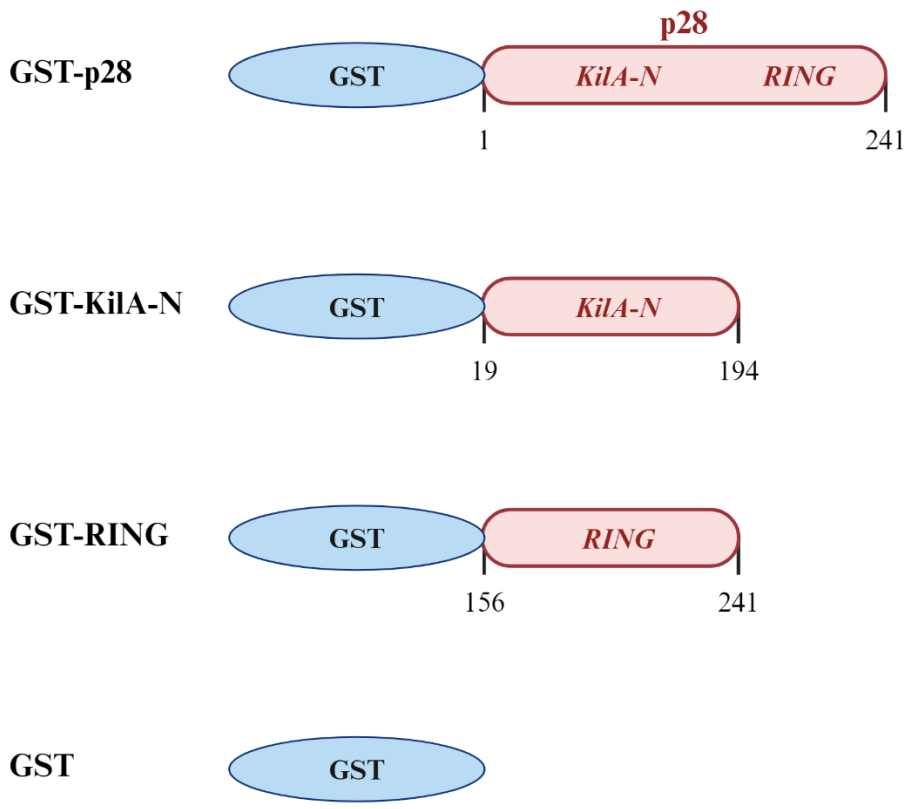

Figure 4.6 Schematic of GST-tagged p28 and its isolated domains

GST tag (shown in blue) was added at the N terminus of p28 or the isolated domains of p28 (shown in purple).

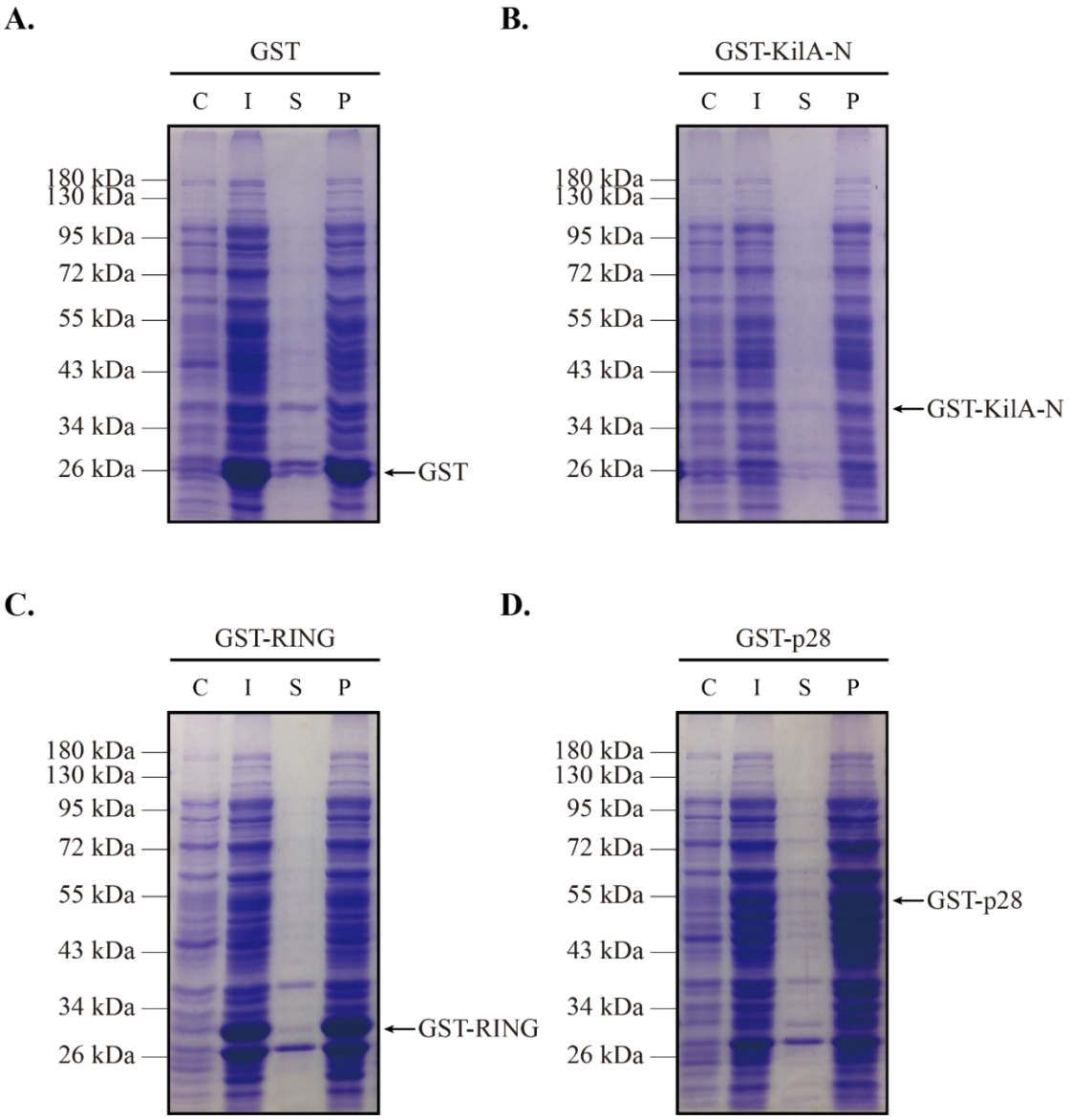

Figure 4.7 Expression of GST fusion proteins in *E. coli*

GST **(A)**, GST-KilA-N **(B)**, GST-RING **(C)**, and GST-p28 **(D)** expression were induced by IPTG. Cells in equal volume of media were harvest before (C) and after (I) IPTG treatment. The loading volume of the soluble (S) and insoluble pellet (P) was adjusted to ensure that it was obtained from the same number of cells. C; total cellular protein before IPTG induction (control), I; total cellular protein after IPTG induction, P; insoluble cell pellet, S; soluble supernatant after sonication. Molecular mass markers are indicated to the left of gels. The arrows show the predicted size of the indicated proteins. The results presented in the figure were replicated in 2 independent experiments, and the figure displays one of the 2 replicates.

express p28 and its isolated domains.

4.2.5 Purification of p28 and its isolated domains from Baculovirus-infected insect cells

Poxvirus p28 was purified by Huang *et al.* using a baculovirus expression vector system (BEVS) (149). BEVSs are widely used as a manufacturing platform for recombinant protein expression due to many advantages such as fast manufacturing speed and inherent safety (181). Compared with *E. coli* expression system, BEVS express proteins in insect cells and provides a eukaryotic environment for post-translational modifications of the recombinant proteins (182, 183). Thus, I used BEVS to express His-tagged p28 for purification **(Figure 4.8)**. The baculovirus expressing His-p28 was generated with the help of Dr. Egor Tchesnokov. Donor plasmids with the His-p28 gene were transformed into competent DH 10 Bac cells and recombination of the His-p28 gene into the Bacmid in DH 10 Bac cells was selected for. To construct baculovirus expressing His-p28, bacmid DNA was transfected into Sf9 insect cell line. The infected Sf9 cells were disrupted by sonication and soluble His-p28 protein in the supernatant was purified using a Ni-NTA column. Different concentrations of imidazole were used to elute the His-tagged p28 from the Ni-NTA column and the samples were then analyzed by SDS-PAGE and western blotting with an anti-His Ab **(Figure 4.9)**. Coomassie-stained SDS-PAGE gels showed that highly purified His-p28 was eluted from the column with 200 mM imidazole **(Figure 4.9A)**. The purified His-p28 eluted with 200 mM imidazole was recognized by

anti-His Ab by western blotting **(Figure 4.9B)**. These results show that soluble His-p28 was expressed using a BEVS and could be purified to high purity via the His tag.

To purify His-tagged p28 domains from insect cells, I generated baculovirus and expressed His-KilA-N or His-RING in Sf9 cells as described above. The infection of Sf9 cells with these baculoviruses inhibited the growth of cells **(Figure 4.10A, a1, b1 and c1 and B)**. Interestingly, a significantly weaker green fluorescent protein (GFP) signal was observed in Sf9 cells infected with baculovirus containing the His-KilA-N gene than cells infected with baculovirus with the His-RING gene **(Figure 4.10A, b2 and c2)**. Of note, the promoter of the GFP gene in the baculovirus is different from the promoter of the His-tagged protein gene. Therefore, the expression level of GFP is not necessarily correlated with the expression level of the His-tagged proteins. To examine the expression of His-tagged proteins, the proteins in the infected cells (whole cell lysate) and the soluble proteins in the supernatant after sonication were tested by western blotting with an anti-His Ab **(Figure 4.11A)**. The His-RING and His-KilA-N expression were tested on the same membrane in Figure 4.11 with non-relevant lanes removed from the middle. The result showed that the His-RING was observed in both whole cell lysate and soluble supernatant, while the His-KilA-N was not observed on the membrane strained with anti-His Ab **(Figure 4.11A,** the proteins predicted sizes were indicated by arrows**)**. Although the soluble His-RING was expressed in the supernatant **(Figure 4.11A)**, it did not bind with the Ni-NTA beads and could not be purified via its His tag **(Figure 4.11B).**

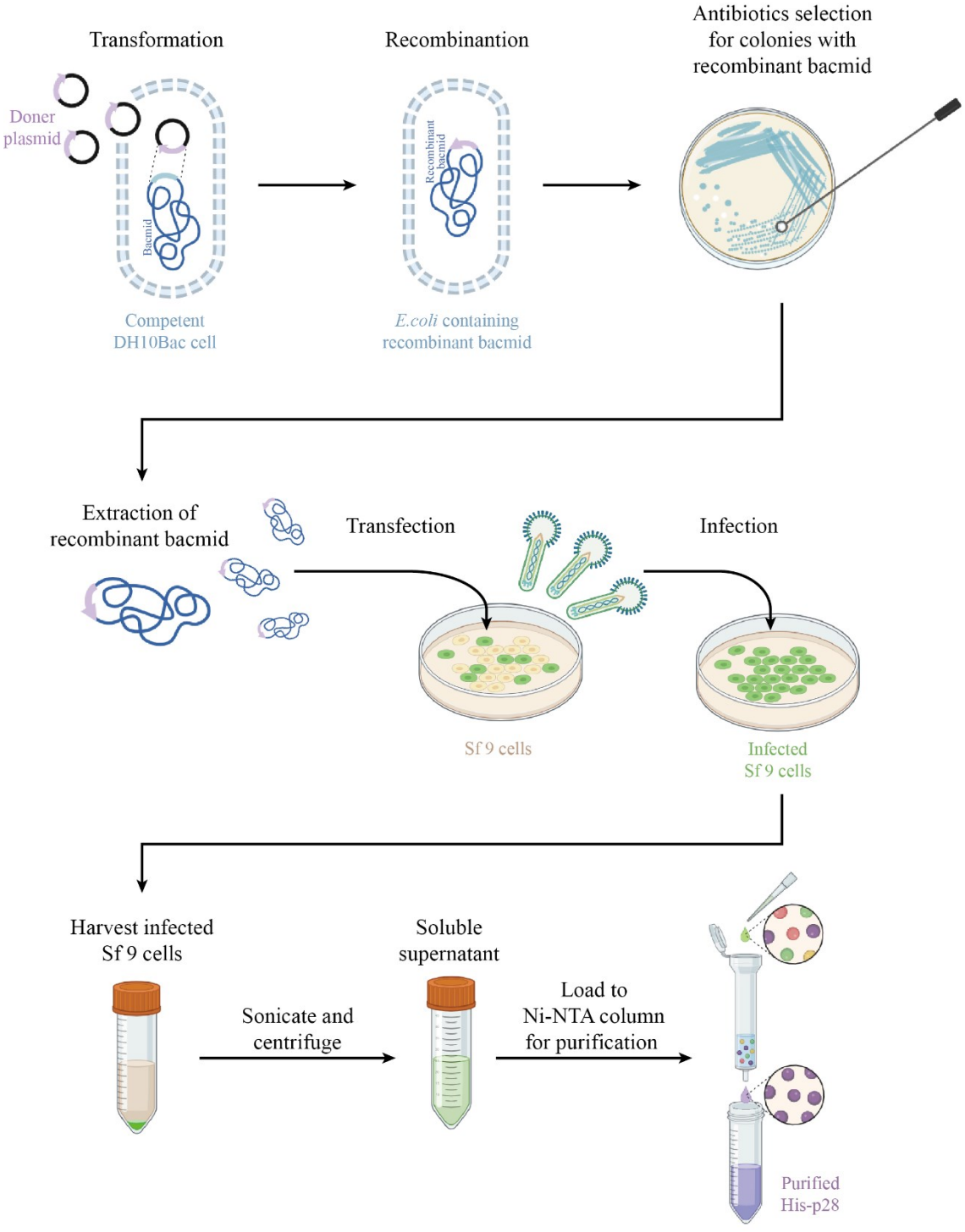
Transformation
Recombinantion
Antibiotics selection for colonies with recombinant bacmid
Doner plasmid
Bacmid
Recombinant bacmid
Competent DH10Bac cell
E.coli containing recombinant bacmid
Extraction of recombinant bacmid
Transfection
Infection
Sf 9 cells
Infected Sf 9 cells
Harvest infected Sf 9 cells
Soluble supernatant
Sonicate and centrifuge
Load to Ni-NTA column for purification
Purified His-p28

Figure 4.8 Schematic of His-p28 purification from Baculovirus-infected insect cells

Donor plasmids containing the His-p28 were transformed into competent DH 10 Bac cells. The gene of His-p28 was inserted into the Bacmid DNA via recombination. Bacteria with the inserted His-p28 gene were selected for and extracted from these cells. The bacmid DNA with His-p28 gene was transfected into Sf9 cells to generate baculoviruses. The baculoviruses expressed green fluorescent protein (GFP) and were secreted from the cells. The media containing baculoviruses were incubated with more Sf9 cells for His-p28 expression. The infected Sf9 cells with expressed His-p28 were harvested by centrifuge. These cells were then disrupted by sonication. Soluble proteins in the supernatant were flowed through a Ni-NTA column for purification.

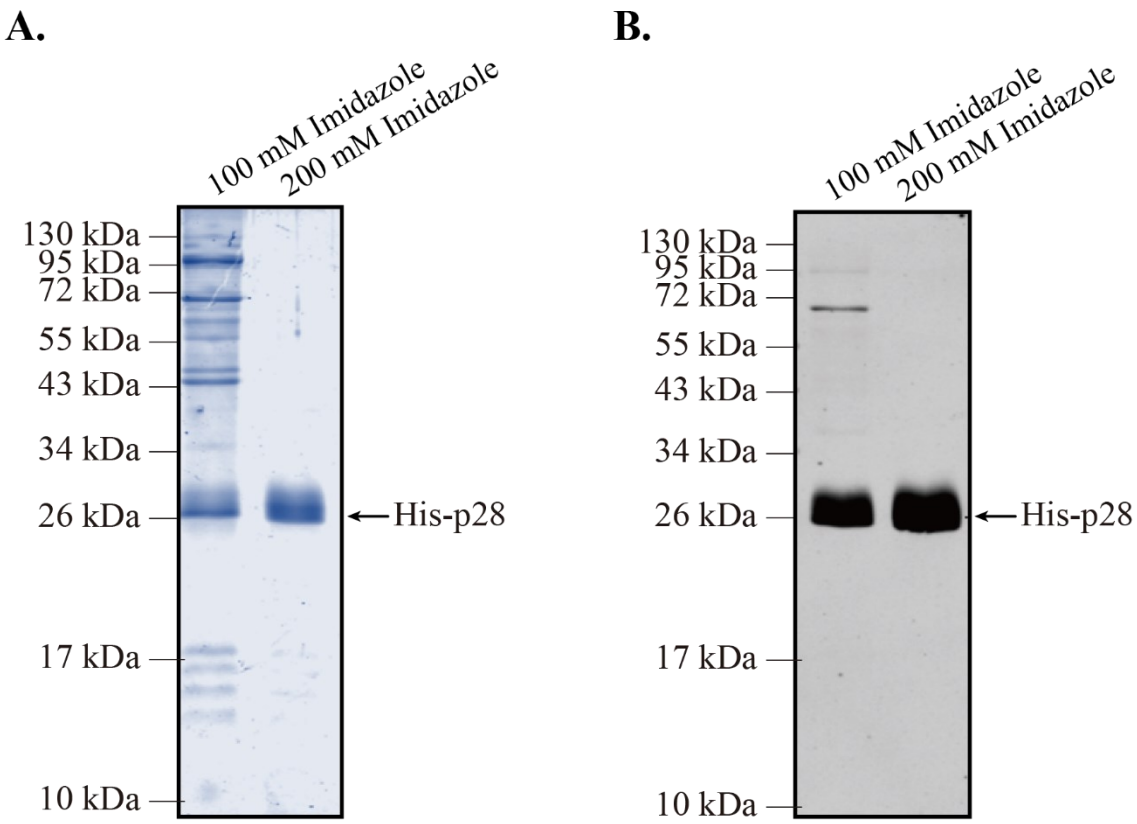

Figure 4.9 His-p28 purified from baculovirus system was recognized by an anti-His Ab

Proteins were eluted from the Ni-NTA column with 100 mM or 200 mM of imidazole were analyzed by Coomassie-stained SDS-PAGE gel **(A)** and western blotting with an anti-His Ab **(B)**. Molecular mass markers are indicated to the left of blots. The results presented in the figure were replicated in 2 independent experiments, and the figure displays one of the 2 replicates.

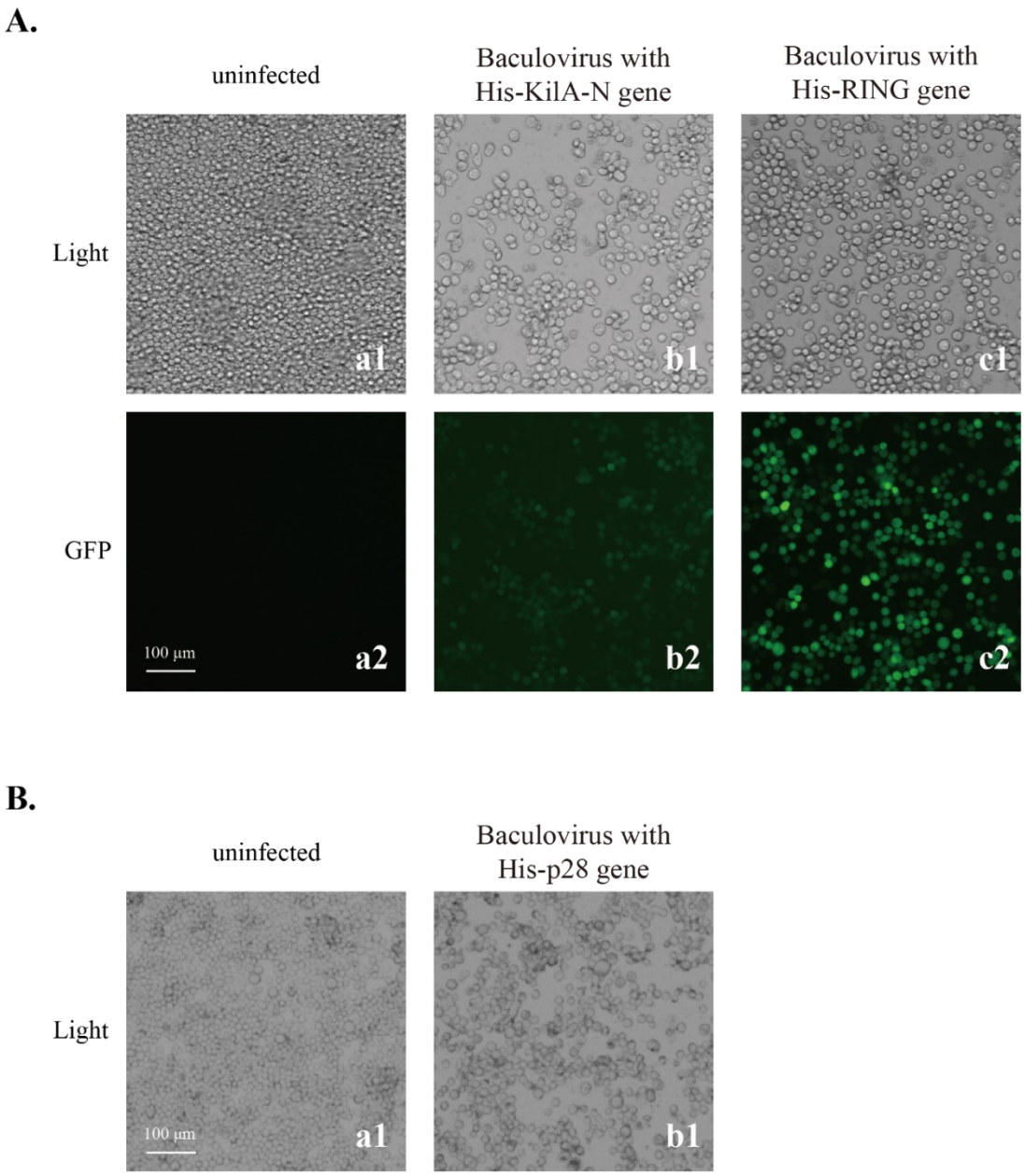

Figure 4.10 Sf9 insect cells infected with BEVS expressing His-tagged proteins

Sf9 cells were seeded in 6-well plate. Cells were then left uninfected (A; a1 and B; a1) or infected with baculovirus with His-KilA-N gene (**A**; b), His-RING gene (**A**; c), or His-p28 (**B**; b) for 48 h. The cell density was observed under bright field (**A**; a1, b1, c1, and **B**). The GFP level in cells infected with indicated baculoviruses were shown in **A**; a2, b2, c2. Scale bar, 100 µm. The results presented in the figure were replicated in 2 independent experiments, and the figure displays one of the 2 replicates.

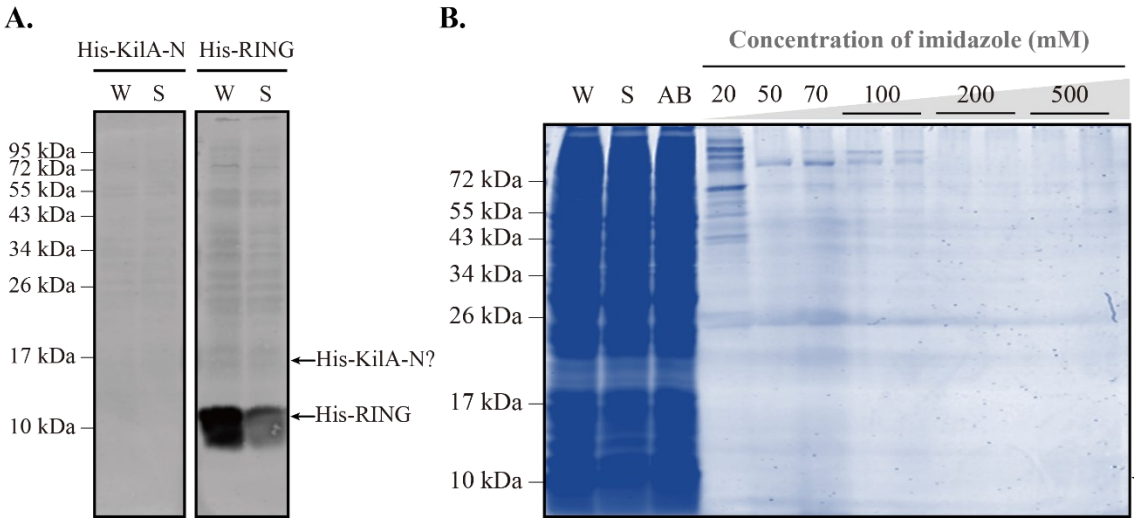

Figure 4.11 Purification of His-tagged p28 domains using BEVS

A, Proteins in whole cell lysate (W) and soluble proteins in the supernatant after sonication (S) were separated by SDS-PAGE gel followed by western blotting with an anti-His Ab. The four lanes were on the same membrane, with non-relevant lanes removed from the middle. The loading volume of each lane was adjusted to ensure that it was obtained from the same number of cells. **B,** Purification of His-RING. Proteins in whole cell lysate (W), soluble proteins in the supernatant after sonication (S), and soluble proteins after binding (AB) to the Ni-NTA beads were separated by SDS-PAGE gel. The loading volume of the first three lanes was adjusted to ensure that it was obtained from the same number of cells. Proteins were eluted from the Ni-NTA column with elution buffer with increasing concentration of imidazole (from 20 mM to 500 mM) were loaded and analyzed by SDS-PAGE and Coomassie staining. Molecular mass markers are indicated to the left of gels. The results presented in the figure were replicated in 2 independent experiments, and the figure displays one of the 2 replicates.

Taken together, I purified His-p28 via insect cells infected with recombinant baculovirus. However, purification of domains of p28 alone was not successful, either because of difficulties with expression (His-KilA-N domain) or a failure of interaction between protein and the beads (His-RING domain).

4.2.6 Purified His-p28 possesses auto-ubiquitylation activity

Previous studies have demonstrated that purified p28 can be auto-ubiquitylated when incubated with E1, E2, Ub, and ATP, confirming that p28 has E3 ligase activity (149, 151-153). To determine whether the purified His-p28 folds is active, I tested the auto-ubiquitylation of p28 *in vitro*. His-p28 protein was incubated with purified E1, E2, ATP, and Ub. In this experiment, five negative controls were used by removing each component individually. Anti-His western blotting showed that a small portion of His-p28 formed HMW bands, whereas most His-p28 was not ubiquitylated **(Figure 4.12A, lane 1)**. HMW bands formed in the reaction were also observed by western blotting with anti-conjugated Ub, but not observed in the negative controls, except lane 4 whose bands are possibly formed because of the Ub on E2 **(Figure 4.12B, lane 1, indicated by an asterisk)**. A large portion of His-p28 was not ubiquitylated **(Figure 4.12A)**, suggesting that 3 μM His-p28 might be too much in the reactions. To optimize the amount of His-p28 in the reactions, I decreased the amount of His-p28 by serial dilution **(Figure 4.12C)**. A reaction without ATP served as a negative control in this experiment. Although no HMW bands were observed in the western blots with the anti-His Ab **(Figure 4.12C)**, ubiquitylated bands were

recognized by an anti-conjugated Ub Ab and the concentration of these bands decreased as the amount of His-p28 protein was reduced **(Figure 4.12D, indicated by an asterisk)**. This data demonstrates that the purified His-p28 is functional and can auto-ubiquitylate itself, but the auto-ubiquitylated His-p28 cannot be recognized efficiently by the anti-His Ab. In addition, 0.3 μM of His-p28 was selected for our future ubiquitylation experiments.

4.2.7 Examining the binding of His-p28 with poxviral DNA

The N-terminal KilA-N domain of p28 is homologous to the DNA binding APSES domain, indicating that the KilA-N domain of p28 may have the ability to binds to DNA (156). In addition, the p28 have been shown to bind ssDNA and dsDNA columns (155), and identified in the DNA-protein complex during poxvirus infection (157). Furthermore, p28 localizes to virus factories during poxvirus infection (150-155). Thus, I tested whether the purified His-p28 could bind viral DNA *in vitro*. I obtained VACV hairpin DNA, the dsDNA with mismatched nucleotides at the ends of poxvirus genome, from Dr. Evans's lab. These mismatched nucleotides result in the hairpin DNA with both ssDNA and dsDNA structures. VACV labeled hairpin DNA was incubated with His-p28. Purified His-I1 protein (VACV encoded DNA binding protein, from Dr. Evans's lab) was used as a positive control (53). Electrophoretic mobility shift assay (EMSA), also known as band shift assay, showed that the hairpin DNA binds to His-I1 and His-p28, causing DNA band shifts **(Figure 4.13A, indicated by arrows)**. To rule out the non-specific binding between His-p28 and viral hairpin DNA, I incubated hairpin DNA with other purified His-tagged

proteins that, to our knowledge, do not bind DNA. These control proteins are tobacco etch virus protease (TEVp, ~27 kDa, Ctrl 1) (184), galectin 8 (~36 kDa, Ctrl 2) (185), and rhomboid protease from haemophilus influenzae (hiGlpG, ~22 kDa, Ctrl 3) (186) obtained from Dr. M. Joanne Lemieux's lab **(Figure 4.13B)**. No band shift was observed between hairpin DNA and TEVp (Ctrl 1) **(Figure 4.13B, lane 2)**. However, when the hairpin DNA was incubated with the other two negative controls, galectin 8 or hiGlpG, the EMSA showed a similar DNA band shift as the shift observed in p28-DNA reaction **(Figure 4.13B, lane 3** and **4)**. These results suggested that purified His-p28 bound DNA *in vitro*. However, we could not rule out the possibility that the interaction between His-p28 and DNA we examined was non-specific.

4.3 Summary and brief discussion

In this chapter, I tested whether UBAITs is an accessible approach to capture the potential substrates of p28 during poxvirus infection. pSC66-FLAG-p28-Ub was transfected into HeLa cells to express FLAG-p28-Ub during VACV-Cop infection. FLAG-p28-Ub localized to virus factories **(Figure 4.3)** and enriched conjugated Ub into poxvirus factories as FLAG-p28 (151, 153) **(Figure 4.3)**. I purified FLAG-p28-Ub and its associated proteins by anti-FLAG IP. The HMW species were observed in the western blotting with anti-FLAG Ab **(Figure 4.4B)**. However, this was not observed in the FLAG-p28 IP **(Figure 4.4B)**. These HMW species likely present substrates covalently linked to FLAG-p28-Ub.

UBAITs can be used to trap proteins associated with p28 and identify the potential

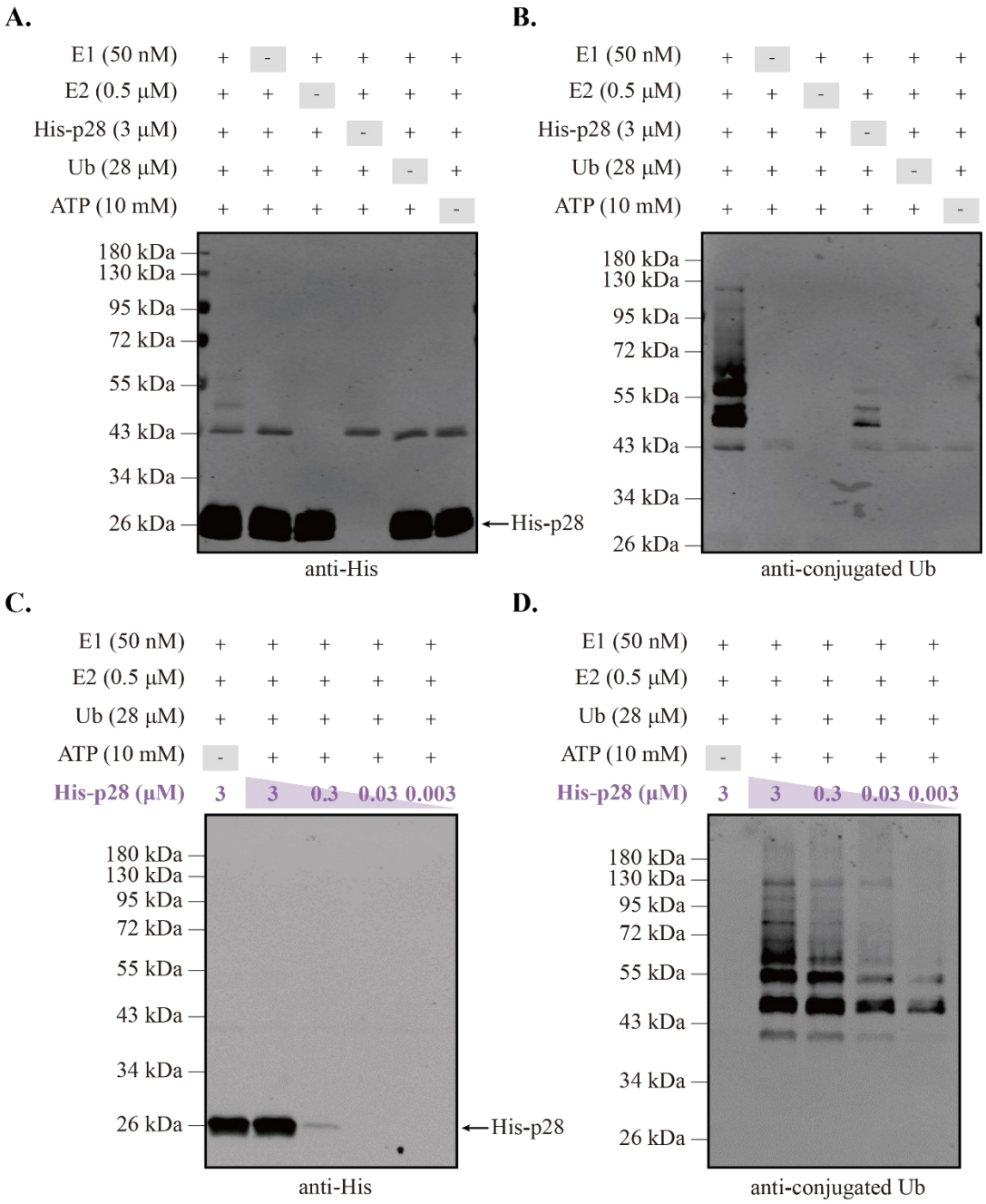

Figure 4.12 Auto-ubiquitylation activity of His-p28

Auto-ubiquitylation reactions with purified His-p28 and the indicated ubiquitylation components. The products of each reaction were analyzed by western blotting with anti-His **(A** and **C)** or anti-conjugated Ub **(B** and **D)**. Molecular mass markers are indicated to the left of gels. The results presented in the figure were replicated in 2 independent experiments, and the figure displays one of the 2 replicates.

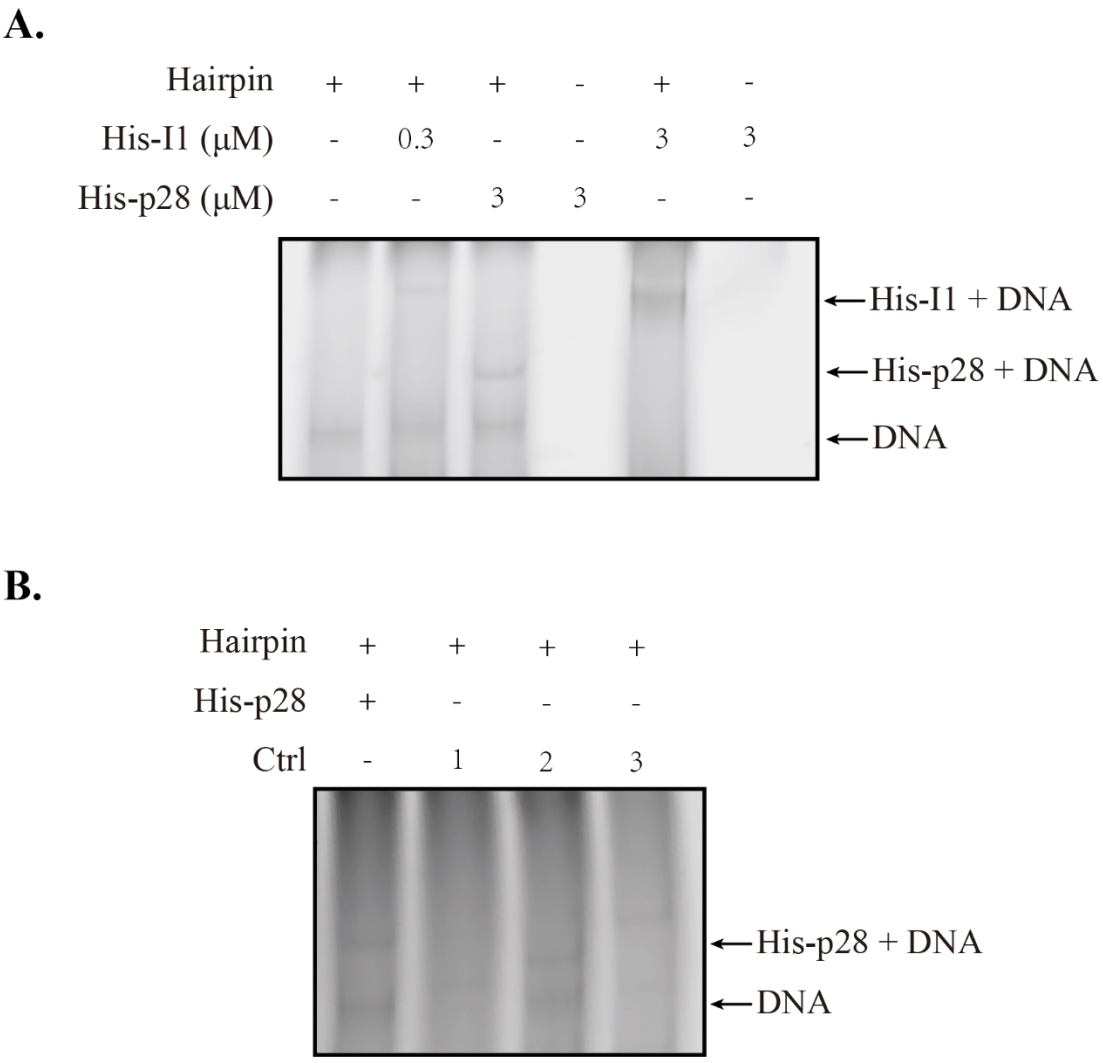

Figure 4.13 His-p28 binds to poxviral hairpin DNA

His-tagged proteins was incubated with labeled viral hairpin DNA at 37℃ for 30 min and then analyzed by EMSA. DNA and DNA with proteins were separated by non- denaturing polyacrylamide gel. His-I1 **(A)** was the positive control. **B,** Several His-tagged purified proteins were used as negative controls to compare with His-p28. Ctrl 1; tobacco etch virus nuclear-inclusion-a endopeptidase (or TEV protease, TEVp), Ctrl 2; galectin 8, Ctrl 3; hiGlpG. The results presented in the figure were replicated in 2 independent experiments, and the figure displays one of the 2 replicates.

substrates of p28. For example, I observed Hsp70 associated with FLAG-p28-Ub. However, the size was at the predicted protein size of Hsp70, suggesting Hsp70 was not covalently attached with FLAG-p28-Ub **(Figure 4.5)**. Hsp70 is a highly conserved heat shock protein and present in all major cellular compartments in eukaryotic cells (187). The substrate-binding domain of Hsp70 non-specifically binds to hydrophobic peptides, allowing Hsp70 to correct protein folding and prevent aggregation (188). Hsp70 is involved in various cellular processes, including proliferation, apoptosis, and immune response pathways (189). Additionally, it plays a role in virus entry, replication, or assembly for multiple viruses (190-193). During poxvirus infection, the mRNA level of Hsp70 increases (194). This suggests host cell Hsp70 may contribute to poxvirus replication. It is possible that p28 recruits Hsp70 to the virus factory to assist in p28 or other viral protein folding. Alternatively, p28 may not directly bind Hsp70. For example, both p28 and Hsp70 binds to DNA or other proteins during poxvirus infection. Further studies are needed to determine whether p28 recruits Hsp70 for the benefit of poxviruses.

Previous studies showed that p28 can bind DNA *in vitro* and during VACV infection (155-157). To further investigate the binding properties of p28, I tried to purify p28 and its isolated domains. Two protein expression systems, *E. coli* and BEVS, were utilized to express p28 and its isolated domains. Unfortunately, little soluble GST-tagged p28 protein or isolated domains were expressed by *E. coli* **(Figure 4.7)**. While, His-tagged p28 was expressed by and successfully purified from BEVS **(Figure 4.9 and 4.11)**. The auto-

ubiquitylation assay showed that the purified His-p28 has E3 Ub-ligase activity **(Figure 4.12)**. However, the HMW species of His-p28 auto-ubiquitylation were not observed in western blotting with anti-His Ab **(Figure 4.12C)**, but only observed in the western blotting with anti-conjugated Ub Ab **(Figure 4.12D)**. It is possible that the ubiquitylation of His-p28 blocks the recognization of the His tag on p28 by anti-His Ab. Another possibility was that the anti-His Ab was not sensitive enough to detect the small amounts of ubiquitylated His-p28 in the auto-ubiquitylation system.

To determine whether purified His-p28 interacts with viral DNA, I examined the interaction of p28 and viral hairpin DNA by EMSA assay **(Figure 4.13)**. In addition, three purified His-tagged proteins were incubated with the hairpin DNA to determine whether the interaction between p28 and viral hairpin DNA was specific. These control proteins included soluble proteins (TEVp and galectin 8) and a membrane protein (hiGlpG) that, to our knowledge, have not been shown to bind to DNA **(Figure 4.13B)**. As predicated, incubating viral hairpin DNA with TEVp, a protease that cleaves the peptide consensus sequence, ENLYFQG (195, 196), did not induced band shift, suggesting it did not bind viral DNA. However, both galectin 8 and hiGlpG induced a band-shift with viral hairpin DNA. Galectin 8 is a carbohydrate binding protein which senses viral spike glycoprotein during SARS-CoV-2 infection (197). It can be cleaved by viral protease, 3-chymotrypsin-like protease, which is critical for virus to escape from host defenses (197). The hiGlpG is a member of the rhomboid peptidases that localizes to cell membrane and cleaves

transmembrane proteins (186, 198). Neither galectin 8 nor hiGlpG has been shown to bind to DNA to our knowledge. Taken together, these results suggest that the purified His-p28 binds DNA *in vitro*. However, it is worth noting that this interaction appears weak, and there is a possibility of non-specific binding. The method requires improvement to reduce the effect of non-specific binding. The future directions will focus on improving this method and further examine how p28 binds DNA (see the overall discussion 6.2.4).

Chapter 5: Characterizing changes in protein ubiquitylation during poxvirus infection

Data present in this chapter is under review:

"Jianing Dong, Shu Luo, Summer Smyth, Grace Melvie, Olivier Julien, Robert J. Ingham. Characterizing changes in protein ubiquitylation during vaccinia virus infection." (manuscript # JVI00430-24)

Contributions to this chapter:

All the experiments presented in this chapter were performed by me, except for the LC-MS/MS (Figure 5.2), which was performed by Shu Luo in Dr. Olivier Julien's Lab. Grace Melvie and Summer Smyth (undergraduate students I supervised) contributed some of the western blotting experiments. Lysates of MPXV (Clade IIb)-infected HeLa cells were provided by Drs. James Lin and David Evans (University of Alberta).

The writing of this chapter is adapted from Dong *et al.* 2023, which was written by Dr. Ingham and me with input from the other authors.

5.1 Introduction

Poxviruses co-opt the UPS to facilitate virus replication (81-84), evade the immune response (135, 144, 145, 199, 200), and block programmed cell death of infected cells (140). Moreover, the UPS is an integral component of innate immune signalling pathways used by the host to respond to infection. For example, innate anti-viral signalling pathways, such as those involved in the activation of retinoic acid-inducible gene I (RIG-I) (201, 202), and NF-κB (203, 204), utilize degradative and non-degradative ubiquitylation. In addition, the UPS is an important part of the adaptive immune response by processing viral peptides for presentation in major histocompatibility complex (MHC) class I (205).

To further elucidate how the UPS is engaged early during poxvirus infection, we identified and quantified peptides with a Ub remnant motif (diGly peptides) purified from lysates of uninfected and VACV-Cop-infected HeLa cells. diGly peptides that significantly changed in infected cells were associated with proteins involved in anti-viral signalling, Ub and Ub-like protein signalling, and DNA replication/repair. Of note, several ubiquitylated peptides from TRIM25 were enriched for or exclusively found in VACV-Cop-infected cells. TRIM25 is an E3 ligase for Ub and the Ub-like protein, interferon stimulated gene 15 (ISG15), and performs several functions including activation of the type I interferon response. We found that TRIM25 HMW, likely ubiquitylated, species were evident as early as 1-hour post-infection and largely dependent on *de novo* protein synthesis and E1 Ub-activating enzyme activity at the time of infection. Moreover, total TRIM25

levels decreased over the course of infection. HMW TRIM25 species were also evident, to varying degrees, in HeLa cells infected with other VACV strains and OPVs. Finally, we determined that a gene(s) in either arm of the VACV-Cop genome was sufficient to induce TRIM25 HMW species. Taken together, this study has revealed novel information about how the UPS is altered during poxvirus infection.

5.2 Results

5.2.1 Identification of diGly peptides from uninfected and VACV-Cop-infected HeLa cells

To investigate changes in protein ubiquitylation during poxvirus infection, HeLa cells were pre-treated with the proteasome inhibitor, MG132, for 1 h and either left uninfected or infected with VACV-Cop at a MOI of 3 for 1 h followed by an additional 4 h incubation in the presence of MG132 **(Figure 5.1A)**. Lysates were then subjected to trypsin digestion and diGly peptides were enriched for before being analyzed by mass spectrometry. diGly enrichment utilizes an Ab that recognizes the diGly remnant present on ubiquitylated lysine residues after digestion with trypsin (206, 207). Three independent experiments identified 1753 (1494 cellular and 259 viral) distinct diGly peptides **(Figure 5.1B)**. The majority of peptides (≥78%) were identified in both uninfected and infected cells **(Figure 5.1C)**, albeit their abundance was not necessarily the same. Moreover, there was considerable overlap in diGly peptides identified between the independent experiments **(Table 5.1)**.

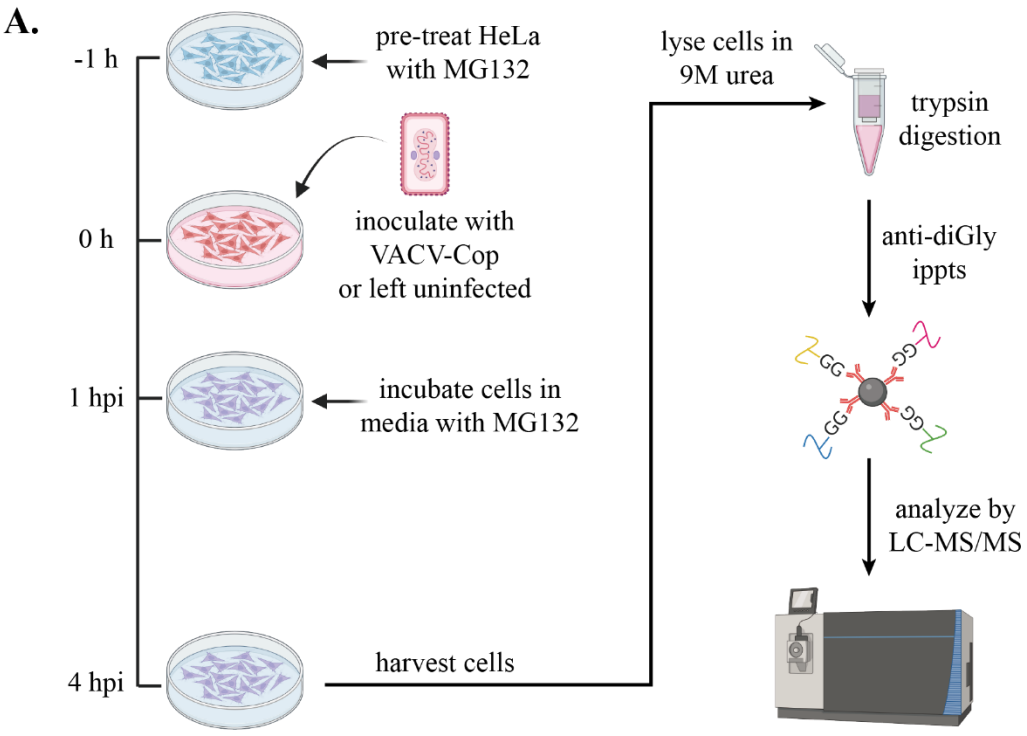
A.
-1 h
pre-treat HeLa
with MG132
0 h
inoculate with
VACV-Cop
or left uninfected
1 hpi
incubate cells in
media with MG132
4 hpi
harvest cells
lyse cells in
9M urea
trypsin
digestion
anti-diGly
ippts
analyze by
LC-MS/MS

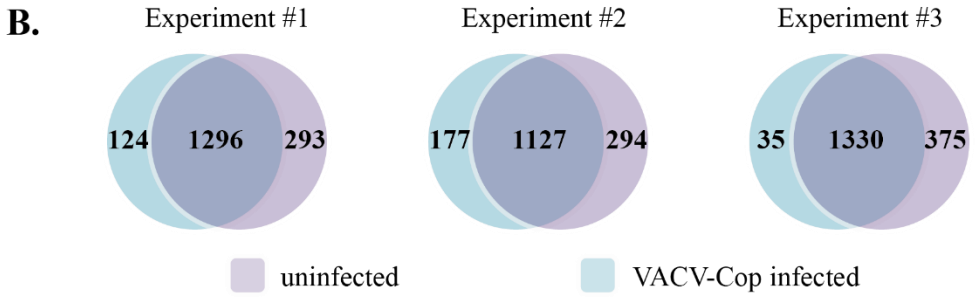
B.
Experiment #1
124
1296
293
Experiment #2
177
1127
294
Experiment #3
35
1330
375
uninfected
VACV-Cop infected

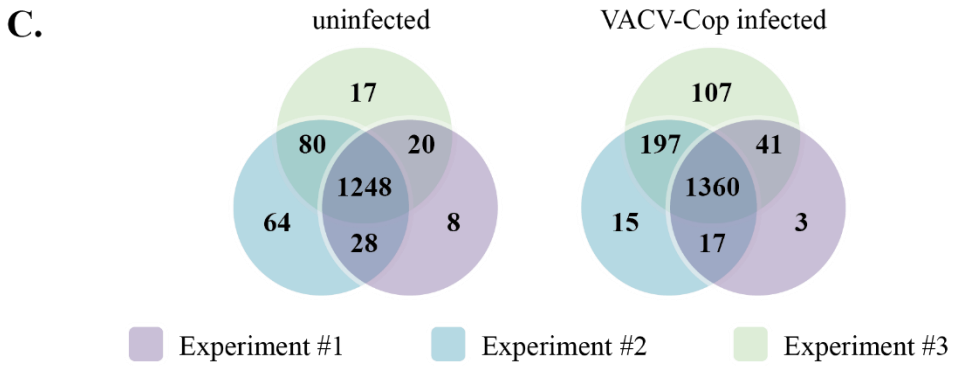
C.
uninfected
17
80
20
1248
64
8
28
VACV-Cop infected
107
197
41
1360
15
3
17
Experiment #1
Experiment #2
Experiment #3

Figure 5.1 Identification of diGly peptides by LC-MS/MS

A, Outline of the experimental workflow used for the purification and identification of diGly peptides. **B,** Venn diagrams illustrating the number of the peptides identified in uninfected cells, VACV-Cop-infected cells, or both in each independent experiment. **C,** Venn diagrams illustrating the number of the peptides identified in uninfected or infected cells in common between the 3 independent experiments. The generation of cell lysates was performed by me, and the enrichment of diGly peptides and LC-MS/MS were performed by Shu Luo.

Experiment	Uninfected	VACV-Cop-infected
1	1420	1589
2	1304	1421
3	1365	1705
Total	1753 (1494 cellular and 259 viral)	

Table 5.1 Summary of diGly peptides identified in the three independent experiments

List of the number of diGly peptides identified in HeLa cells uninfected or infected with VACV-Cop in each independent experiment and the total number of diGly peptides identified in the 3 experiments.

We focused our analysis on the 1720 diGly peptides found in at least 2 independent experiments. Quantifying average peptide abundance over the three independent experiments revealed 304 peptides enriched for (≥ 2-fold change and $p \leq 0.05$) in VACV-Cop-infected cells. The majority of these diGly peptides (247; 81%) were from viral proteins, and 57 peptides were associated with cellular proteins **(Figure 5.2)**. Furthermore, we identified 37 cellular diGly peptides enriched for (≥ 2-fold change and $p \leq 0.05$) in uninfected cells **(Figure 5.2)**.

5.2.2 Differentially enriched diGly peptides include those from proteins associated with anti-viral signalling

Pathway enrichment analysis by Metascape was performed to determine whether any cellular pathways or processes were overrepresented from proteins associated with diGly peptides preferentially found in uninfected or infected cells. Translation and the cell cycle were categories associated with proteins with peptides enriched in infected cells **(Figure 5.3A)**, whereas processes linked to proteins with peptides enriched in uninfected cells included deubiquitylation, viral infection pathways, DNA replication, and necroptosis **(Figure 5.3B)**. However, since these analyses may not include all known functions attributed to these proteins, we examined the literature to identify additional activities regulated by these proteins. We found that several of the peptides were from proteins associated with anti-viral signalling, Ub/Ub-like signalling, and DNA replication/repair

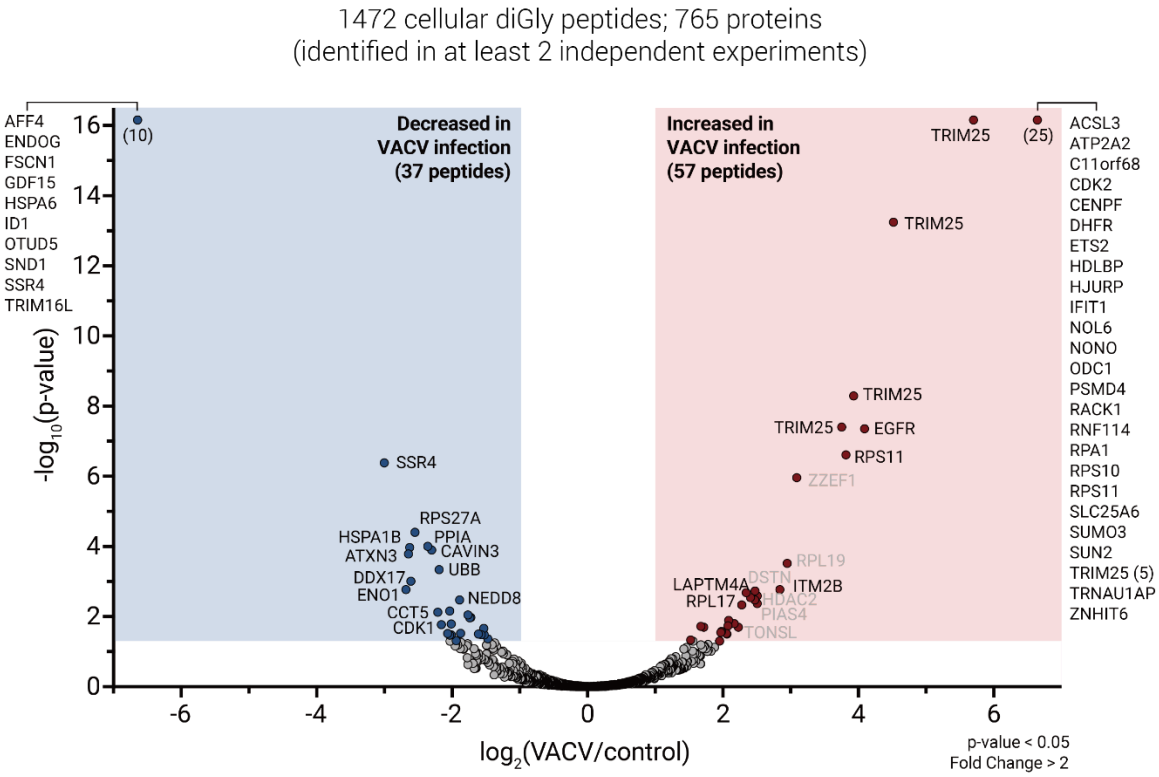

Figure 5.2 Volcano plot of cellular diGly peptides derived from host proteins found in at least two independent experiments

Peptides in blue were enriched ≥2-fold (p value ≤ 0.05) in uninfected cells, whereas peptides in pink were enriched ≥2-fold (p value ≤ 0.05) in VACV-Cop-infected cells. Peptides in grey were considered of lower confidence given their prominent enrichment in only one of the replicates. This figure was generated by Shu Luo.

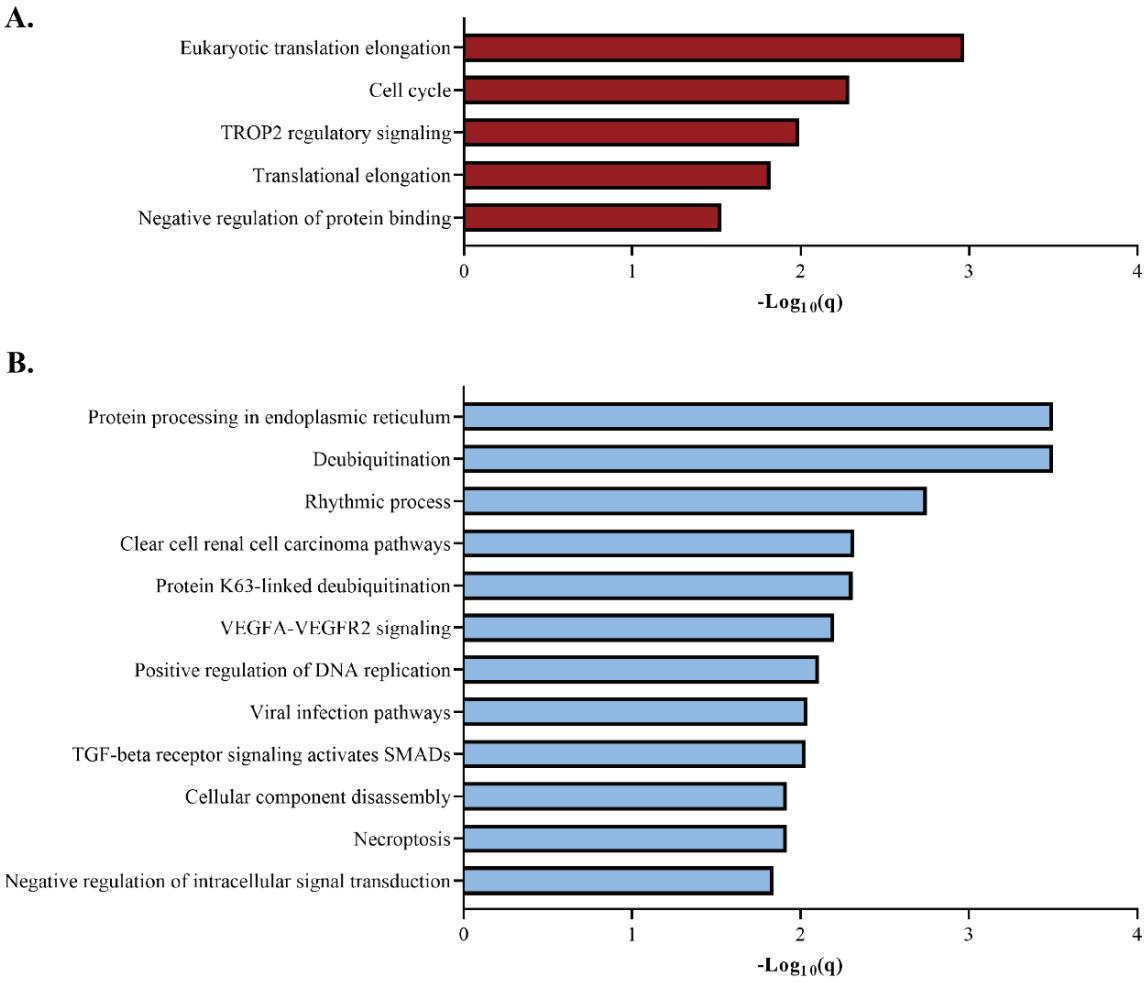

Figure 5.3 Analysis of cell signalling pathways and processes associated with proteins with diGly peptides enriched in infected or uninfected cells

Metascape analysis of proteins associated with diGly peptides enriched VACV-Cop-infected **(A)** or uninfected **(B)** HeLa cells. Categories with significant adjusted *p* value ($q \leq 0.05$) are shown.

(Figure 5.4). Moreover, several peptides were from proteins previously implicated in poxvirus infection including IFITs (135), WDR6 (208), RACK1 (209), DDX5 (210), and EGFR (211).

The identification of a diGly lysine residue on a peptide is indicative of the site being ubiquitylated. However, it does not provide any information about the consequence of this ubiquitylation. Therefore, I compared our data to published work that analyzed changes in protein levels in telomerase reverse transcriptase (TERT)-immortalized primary human fetal foreskin fibroblast (HFFF-TERT) cells infected with VACV-WR (171). Despite this study using a different cell line and VACV strain, several of the proteins with diGly peptides enriched in VACV-Cop-infected HeLa cells were decreased over the course of infection **(Figure 5.5)**. Furthermore, this study showed that protein levels for most of the down-regulated proteins could be partially rescued by treatment with MG132 **(Figure 5.5)**. This indicates these proteins are likely degraded in a proteasome-dependent manner in VACV-infected cells which has been shown for the IFIT proteins (135). Intriguingly, the levels of many proteins with diGly peptides enriched in infected cells did not decrease over the course of infection **(Figure 5.5)**. This suggests that ubiquitylation of these proteins may serve a non-degradative function.

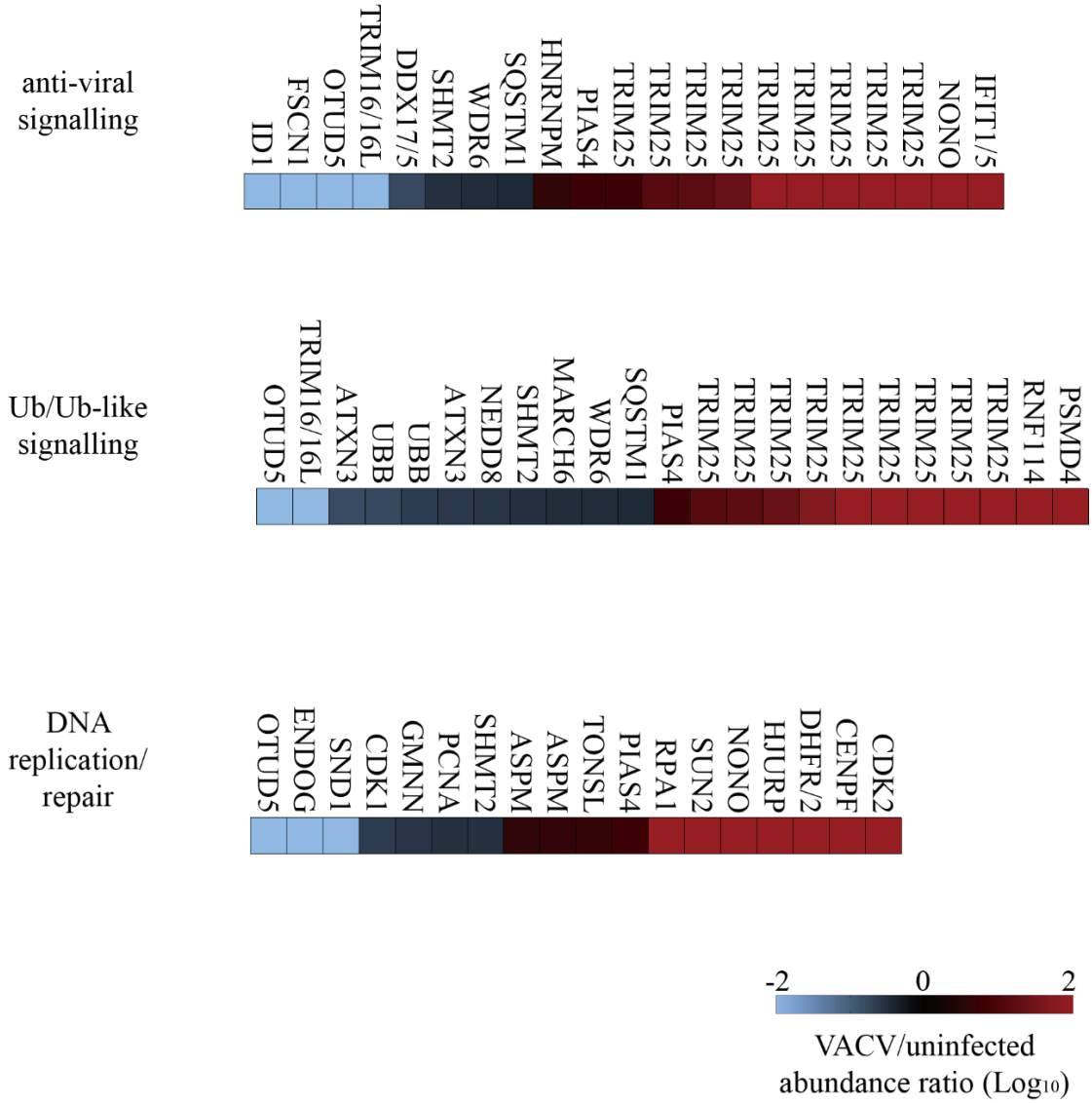

Figure 5.4 Heat map of identified diGly peptides from proteins associated with anti-viral signalling, Ub or Ub-like signalling, or DNA replication/repair

Heat map of identified diGly peptides from proteins associated with anti-viral signalling, Ub or Ub-like signalling, or DNA replication/repair was determined from the literature. The abundance ratio (VACV infected/uninfected; Log_{10} scale) is indicated. Peptides with an abundance ratio of -2 were exclusively found in uninfected cells, whereas those with an abundance ratio of 2 were found exclusively in infected cells.

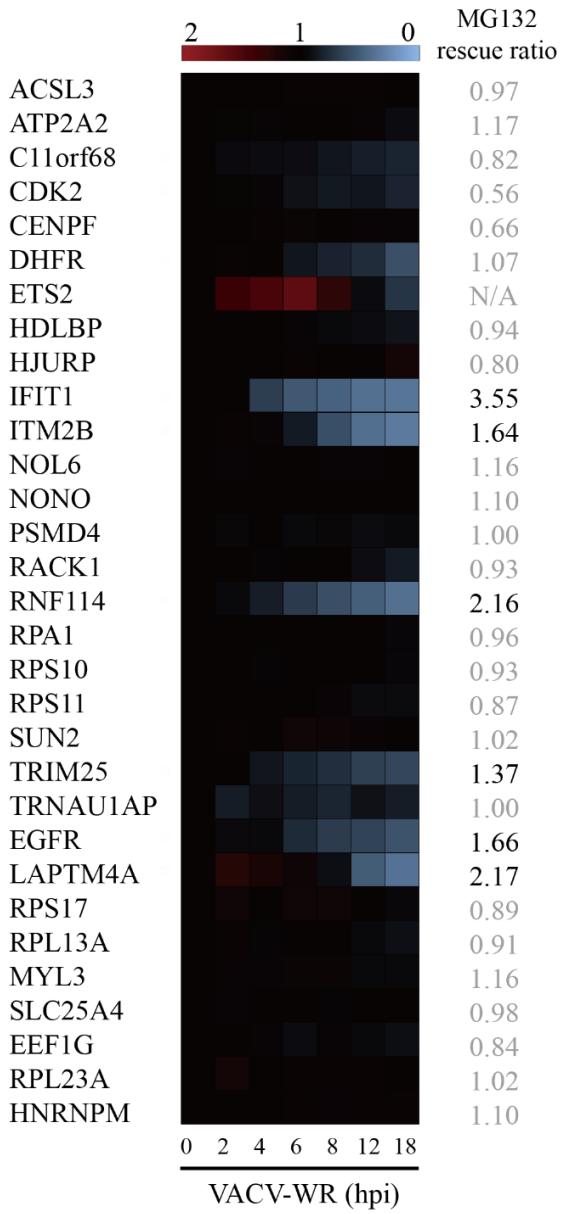

Figure 5.5 Examination of the levels of proteins with enriched diGly peptides in cells infected with VACV-WR

The abundance of proteins with diGly peptides enriched in VACV-Cop-infected HeLa cells were examined using the dataset generated by Soday *et al.* (171) which examined changes in protein levels over the course of VACV-WR infection of HFFF-TERT cells. The heat map shows the changes in protein levels during infection relative to the uninfected sample which was arbitrarily set at 1. MG132 rescue ratio, as determined by (171), is indicated. Those with a rescue ratio greater ≥1.25 are indicated in black.

The most striking observation from the diGly enrichment data was the identification of 9 diGly peptides, that could be definitively assigned to 6 lysine residues, from TRIM25 **(Figure 5.2)** that were enriched for or exclusively found in VACV-Cop-infected HeLa cells. Moreover, TRIM25 levels were found to decrease ~40% in a proteasome-dependent manner over the course of infection of HFFF-TERT cells with VACV-WR **(Figure 5.5)** (171). TRIM25 is a RING domain-containing E3 Ub-ligase (212) that also functions as an E3 ligase for the Ub-related molecule, ISG15 (213) **(Figure 5.6)**. TRIM25 performs many different functions (214), but is perhaps best known for introducing K63-linked Ub chains onto RIG-I (215, 216). RIG-I is a pattern recognition receptor that recognizes viral RNA and initiates signals that lead to the production of type I interferons (reviewed in (217)). Rather than promoting RIG-I degradation, ubiquitylation of RIG-I by TRIM25 promotes RIG-I activation (215). It is therefore not surprising that many viruses have acquired mechanisms to interfere with the ability of TRIM25 to ubiquitylate RIG-I ((218-220) as examples). However, no studies have examined whether poxviruses interfere with TRIM25 signalling. Therefore, we decided to further investigate the putative ubiquitylation of TRIM25 in VACV-infected cells.

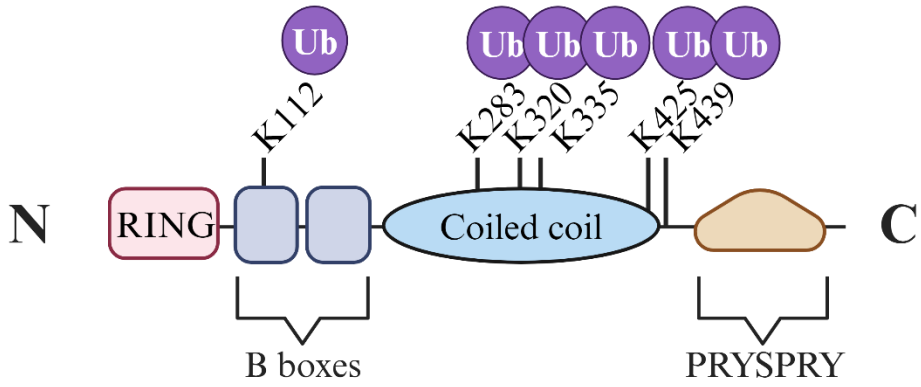

Figure 5.6 TRIM25 and the location of identified diGly peptides

Cartoon showing the location of identified TRIM25 diGly peptides. The relative position of domains was obtained from (221).

5.2.3 VACV-Cop infection results in the formation of HMW TRIM25 species and a decrease in TRIM25 levels

Our diGly enrichment experiments suggested that TRIM25 was ubiquitylated early after VACV infection. In support of this notion, western blotting experiments revealed the appearance of HMW, potentially ubiquitylated, TRIM25 species and a decrease in the lower molecular weight (LMW) TRIM25 band over the course infection **(Figure 5.7A)**. HMW TRIM25 proteins were evident as early as 1 hpi, persisted throughout infection, but were reduced at 24 hpi **(Figure 5.7A)**. Quantification of total anti-TRIM25 immunoreactive bands in uninfected and infected cells showed a decrease in anti-TRIM25 levels over the course of infection **(Figure 5.7B)**.

Proteomics data from Soday *et al*. (171) suggests that not all proteins we identified as being preferentially ubiquitylated in VACV-Cop-infected cells are degraded (**Figure 5.5**). For example, CDK2 levels were relatively unchanged over the course of VACV-WR infection of HFFF-TERT cells, but we identified a putative CDK2 ubiquitylated peptide exclusively in VACV-Cop-infected cells **(Figure 5.2)**. Therefore, we examined CDK2 levels in VACV-Cop-infected HeLa cells by western blotting and found that CDK2 levels did not decrease over the course of infection **(Figures 5.7C** and **D)**. Taken together, these observations are consistent with TRIM25 being ubiquitylated and targeted for degradation in VACV-infected cells. Moreover, these findings show that not all ubiquitylated proteins are significantly degraded.

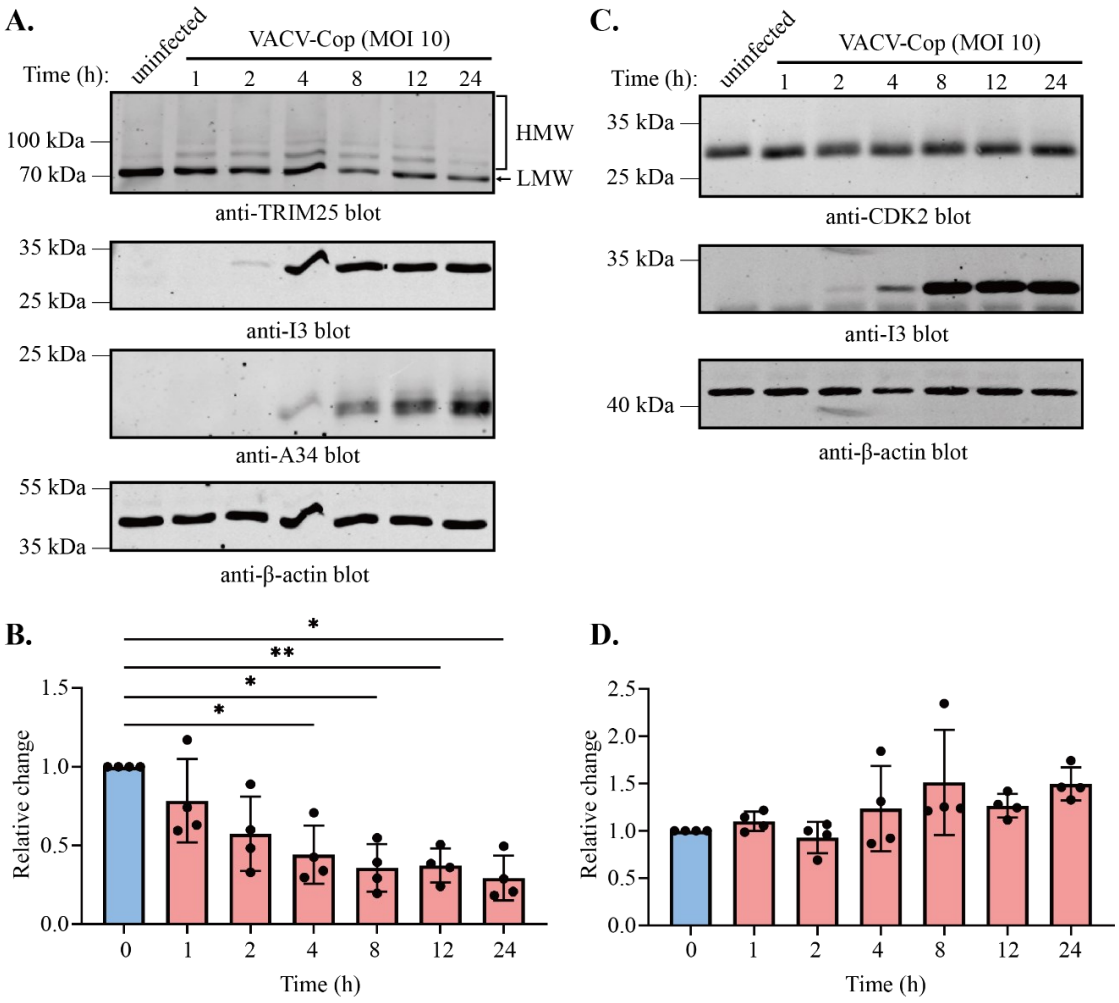

Figure 5.7 VACV-Cop infection results in the formation of TRIM25 HMW species and a decreased TRIM25 levels

Protein level of TRIM25 **(A** and **B)** and CDK2 **(C** and **D)** in HeLa cells infected with VACV-Cop. Lysates of uninfected HeLa cells or HeLa cells infected (MOI of 10) for the indicated times with VACV-Cop were immunoblotted with Abs against the indicated proteins. I3 and A34 are viral proteins that are indicators of virus infection and late protein expression, respectively. Western blots of these proteins were included to show the course of infection. The anti-β-actin blots were included to show protein loading. Molecular mass markers are indicated to the left of blots. Quantitative analysis of TRIM25 **(B)** and CDK2 **(D)** immunoreactive bands in VACV-Cop-infected cells (mean and standard deviation) relative to uninfected cells from 4 independent experiments. A one-way ANOVA was used to calculate statistical significance between uninfected cells (0 h time point) and the indicated time points post-infection. *; $p \leq 0.05$, **; $p \leq 0.01$. The western blot anti-CDK2 was obtained from Grace Melvie.

5.2.4 MG132 treatment modestly rescues TRIM25 levels in VACV-Cop-infected cells

Proteomics studies suggest that TRIM25 is degraded in a proteasome-dependent manner **(Figure 5.5)** (171). To directly test this, HeLa cells were treated before and after inoculation with the proteasome inhibitor, MG132, and TRIM25 levels were examined 4 and 8 hpi **(Figure 5.8A)**. Total TRIM25 levels were modestly increased in cells treated with MG132 **(Figure 5.8B)**, more so 8 hpi, but this difference was not statistically significant **(Figures 5.8C** and **D)**. Similar observations were made for the LMW TRIM25 species **(Figures 5.8B, E,** and **F)**. MG132 treatment blocked expression of the B5 viral late protein **(Figure 5.8B)** which is consistent with studies showing late gene expression requires proteasome activity (81, 82, 84). Thus, the reduction in TRIM25 protein levels is, at least in part, due to proteasomal degradation.

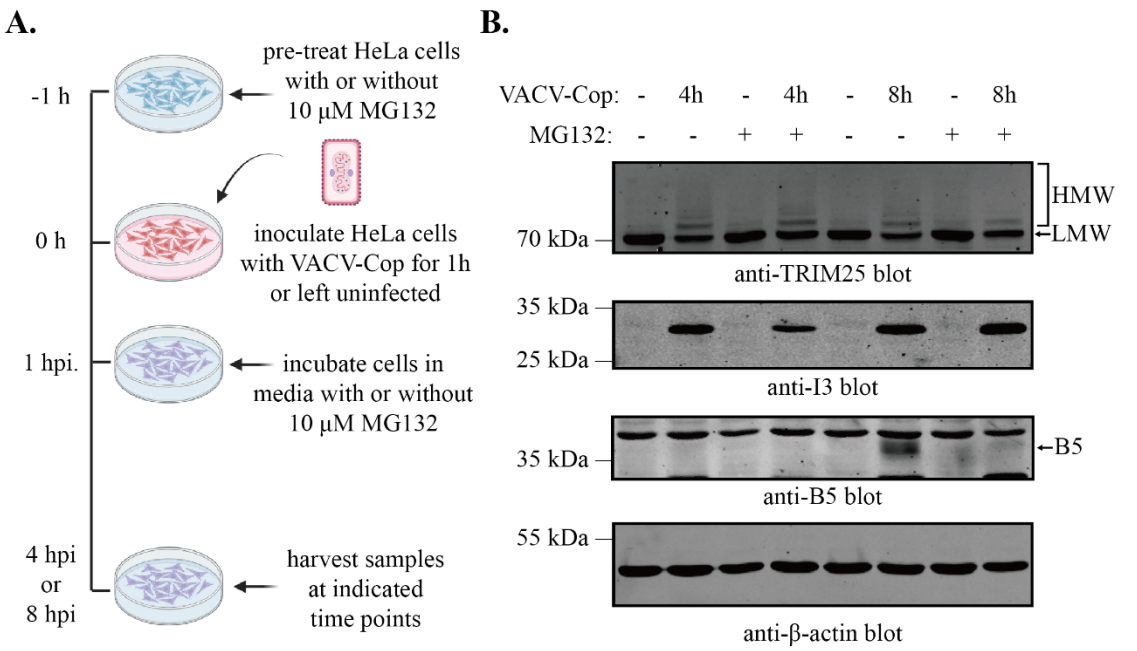
A.
-1 h
pre-treat HeLa cells with or without 10 μM MG132
0 h
inoculate HeLa cells with VACV-Cop for 1h or left uninfected
1 hpi.
incubate cells in media with or without 10 μM MG132
4 hpi or 8 hpi
harvest samples at indicated time points
B.
VACV-Cop: - 4h - 4h - 8h - 8h
MG132: - - + + - - + +
70 kDa
HMW
LMW
anti-TRIM25 blot
35 kDa
25 kDa
anti-I3 blot
35 kDa
B5
anti-B5 blot
55 kDa
anti-β-actin blot

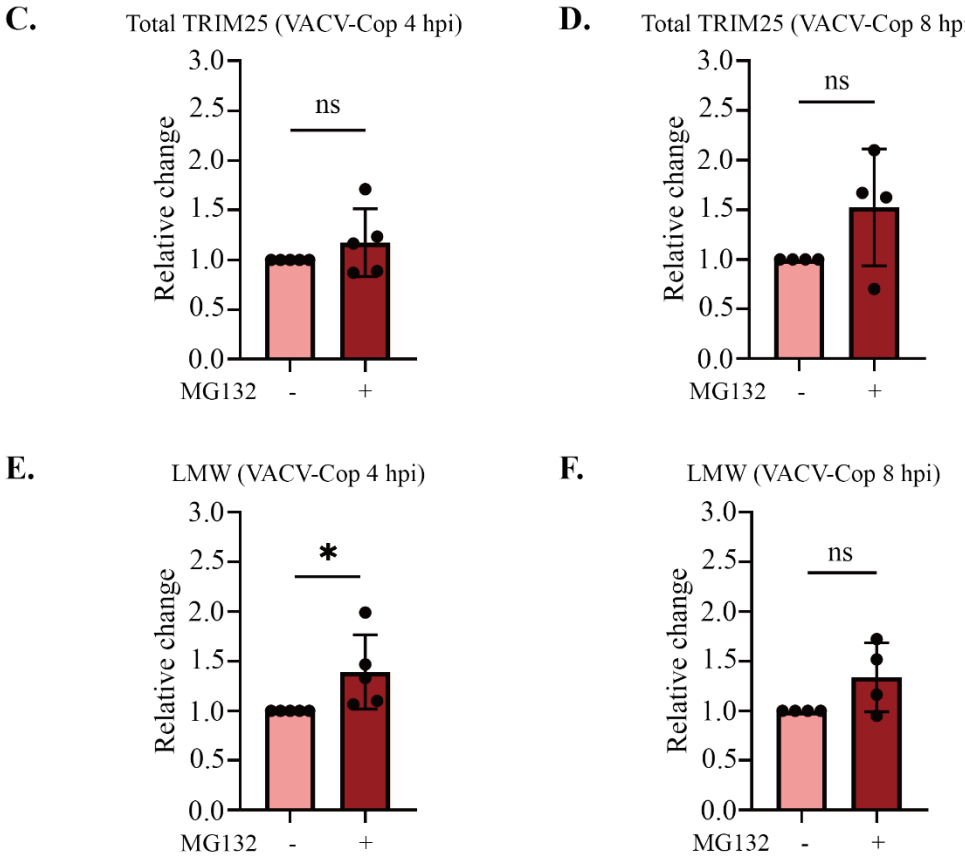
C.
Total TRIM25 (VACV-Cop 4 hpi)
Relative change
ns
MG132 - +
D.
Total TRIM25 (VACV-Cop 8 hpi)
Relative change
ns
MG132 - +
E.
LMW (VACV-Cop 4 hpi)
Relative change
*
MG132 - +
F.
LMW (VACV-Cop 8 hpi)
Relative change
ns
MG132 - +

Figure 5.8 MG132 treatment modestly rescues TRIM25 levels in VACV-Cop-infected HeLa cells

A, Outline of the experimental workflow used in this experiment. **B,** Lysates were immunoblotted for Abs against the indicated proteins. I3 and B5 were used to indicate viral infection and late protein expression, respectively. Western blots for these proteins were included to show the course of virus infection. The anti-β-actin blots were included to show protein loading. Molecular mass markers are indicated to the left of blots. Quantitative analysis of total anti-TRIM25 immuno-reactive bands 4 **(C)** or 8 **(D)** hpi in cells infected in the presence or absence of MG132 are shown. Quantification is from 5 **(C)** or 4 **(D)** independent experiments and expressed relative to the samples not treated (-) with MG132. The abundance of the LMW TRIM25 band 4 **(E)** or 8 **(F)** hpi are shown. Quantification represents the mean and standard deviation from 5 **(E)** or 4 **(F)** independent experiments and expressed relative to the samples not treated (-) with MG132. A paired, one-tailed Student t test was used to calculate statistical significance. ns; not significant, *; $p \leq 0.05$.

5.2.5 TRIM25 is ubiquitylated in VACV-Cop-infected HeLa cells and the formation of HMW species is dependent on E1 Ub-activating enzyme activity

To directly examine whether TRIM25 is ubiquitylated in VACV-Cop-infected cells, I immunoprecipitated TRIM25 from lysates of VACV-Cop-infected or uninfected HeLa cells and immunoblotted with an anti-Ub Ab **(Figure 5.9A)**. Anti-Ub immunoreactive bands (>100 kDa), were observed in larger abundance anti-TRIM25 IPs from infected cell lysates **(Figure 5.9A; upper panel** (indicated by an asterisk)**)** than anti-TRIM25 IPs from uninfected lysates or isotype control IPs from infected lysates. These bands were much larger than the HMW TRIM25 bands observed in anti-TRIM25 blots (see **Figure 5.7A**). When I reprobed the same blot for TRIM25, I also saw a weak smear of proteins **(Figure 5.9A; lower panel**, indicated by an asterisk) of the same size as the anti-Ub immunoreactive bands in the anti-Ub blot **(Figure 5.9A; upper panel)**. Moreover, this reprobe showed I could weakly immunoprecipitate at least one of the HMW TRIM25 bands **(Figure 5.9A; lower panel)** observed in anti-TRIM25 blots of cell lysates **(Figure 5.7A)**.

I next used an Ab that recognizes conjugated Ub to immunoprecipitate ubiquitylated proteins from cells and asked whether this enriched for HMW TRIM25 species. While some TRIM25 was observed in isotype control IPs from lysates of VACV-Cop-infected cells, more TRIM25, in particular HMW species were observed in the anti-conjugated Ub IPs **(Figure 5.9B; upper panel)**. This enrichment of HMW TRIM25 species is suggestive of these being ubiquitylated forms of the protein.

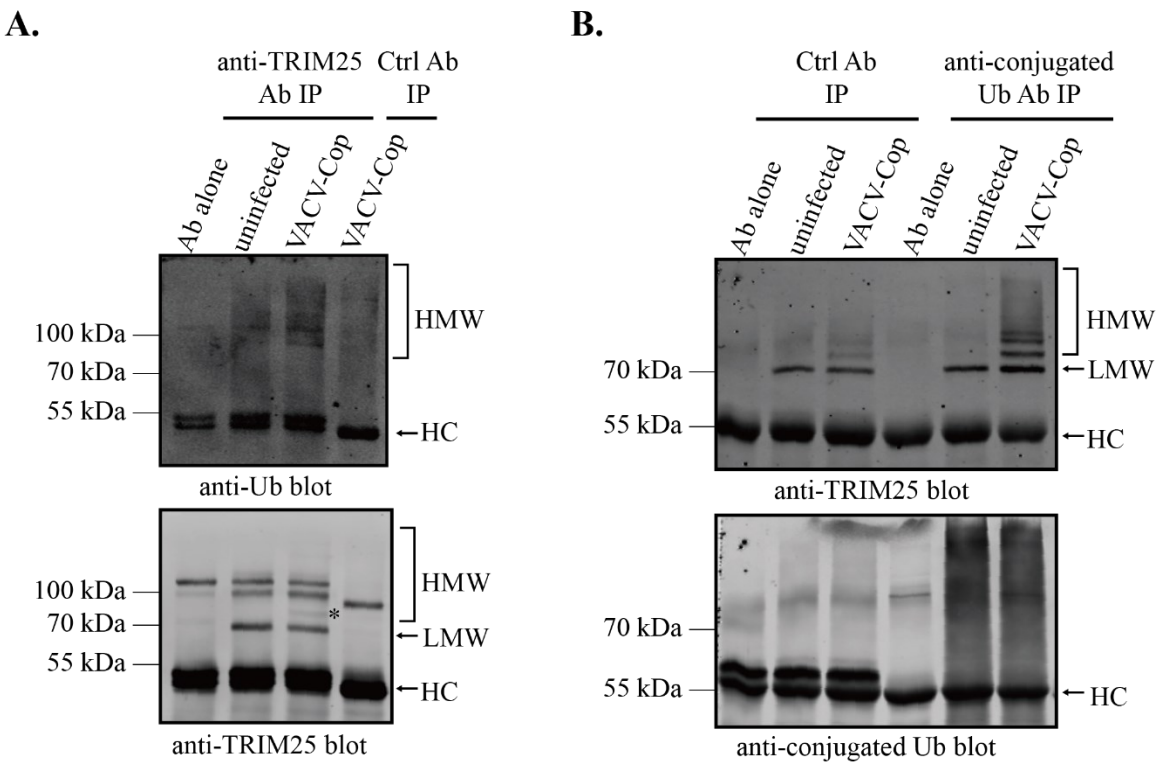

Figure 5.9 TRIM25 is ubiquitylated in VACV-Cop-infected cells

A, Cell lysates from uninfected or HeLa cells infected for 4 h with VACV-Cop (MOI of 10) used to perform anti-TRIM25 IPs with an isotype control IPs (ctrl Ab, anti-HJURP IP) from infected lysates was included to rule out non-specifically bound ubiquitylated proteins. anti-TRIM25 IPs with the lysate omitted (Ab alone) were performed to indicate bands derived from the anti-TRIM25 Ab. Non-specific bands were indicated by Δ. IPs were then western blotted with an anti-Ub Ab (upper panel) before being reprobed with the anti-TRIM25 Ab (lower panel). HC; heavy chain of the Ab used for IP. **B,** Lysates described in **A** were immunoprecipitated with an anti-conjugated Ub Ab or isotype control (anti-6xHis tag Ab) and immunoblotted from TRIM25 (upper panel) before being reprobed with the anti-conjugated Ub Ab. HC; heavy chain of the Ab used for IP. Molecular mass markers are indicated to the left of blots. The results presented in the figure were replicated in 2 independent experiments, and the figure displays one of the 2 replicates.

To further investigate whether the HMW TRIM25 species are ubiquitylated forms of the protein, we pre-treated HeLa cells with the E1 Ub-activating enzyme inhibitor, TAK-243 (222), and infected cells with VACV-Cop in the presence of the inhibitor **(Figure 5.10A)**. A dose-dependent decrease in TRIM25 HMW species was observed in infected cells treated with TAK-243 **(Figure 5.10B; upper panel)** and this was associated with a decrease in I3 protein expression **(Figure 5.10B; middle panel)**. An examination of ubiquitylated proteins in lysates from TAK-243-treated cells revealed the inhibitor was effective at reducing total cellular ubiquitylation **(Figure 5.10C)**. We further examined the effect of TAK-243 treatment on TRIM25 HMW species when added post-infection **(Figure 5.11A)**. In contrast to what was observed when cells were pre-treated prior to infection, TAK-243 treatment post-infection did not reduce the level of TRIM25 HMW species **(Figure 5.11B; upper panel)**. However, the levels of total ubiquitylated proteins did decrease in a dose-dependent manner **(Figure 5.11C)**. Taken together, these results show that E1 activity is required for the formation of HMW TRIM25 species at the time of infection but is dispensable post-infection.

Proteins modified on lysine residues with the Ub-like proteins, NEDD8 and ISG15, also generate diGly peptides after trypsin digestion (206, 223). However, the vast majority of diGly sites are derived from ubiquitylation (223). Nonetheless, we examined whether the formation of HMW TRIM25 species was affected by treatment with the neddylation E1 protein inhibitor, MLN4924 **(Figure 5.12A)**. No decrease in HMW TRIM25 species

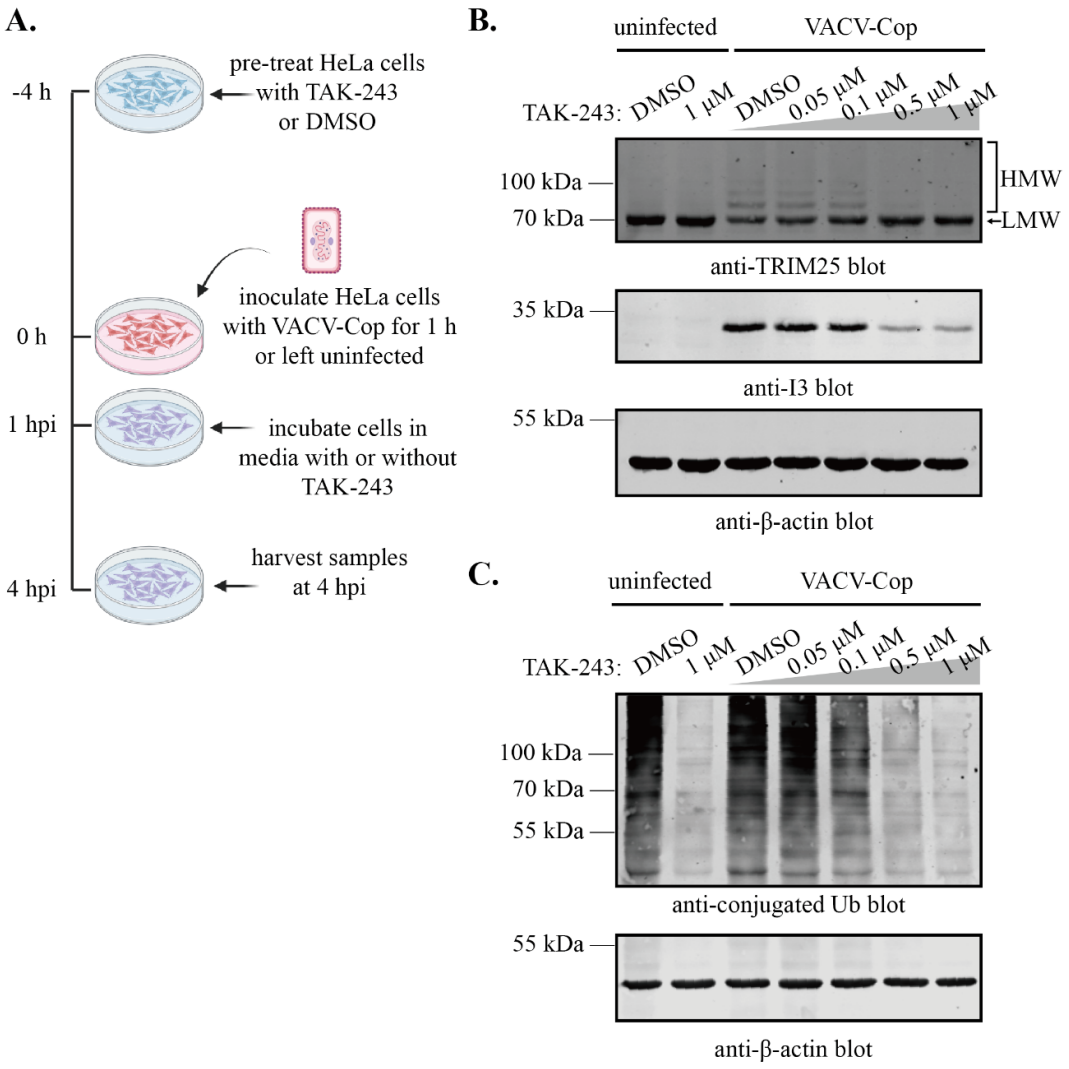

Figure 5.10 TRIM25 ubiquitylation in VACV-Cop-infected cells pre-treated with E1 inhibitor

A, Schematic of the experimental workflow used to examine the effect of the E1 inhibitor, TAK-243, pre-treatment on TRIM25 HMW species. **B** and **C**, Lysates from uninfected cells or cells with VACV-Cop for 4 h (MOI of 10) treated with TAK-243 were immunoblotted with Abs against the indicated proteins. The anti-I3 blot shows infection of the cells, and the anti-β-actin blots show protein loading. The conjugated Ub Ab recognizes mono- and poly-ubiquitylated proteins. The anti-β-actin blots were included to show protein loading. Molecular mass markers are indicated to the left of blots. The western blot shown was performed by Grace Melvie, while I prepared the cell lysates for the initial repeat experiment. The results presented in the figure were replicated in 3 independent experiments, and the figure displays one of the 3 replicates.

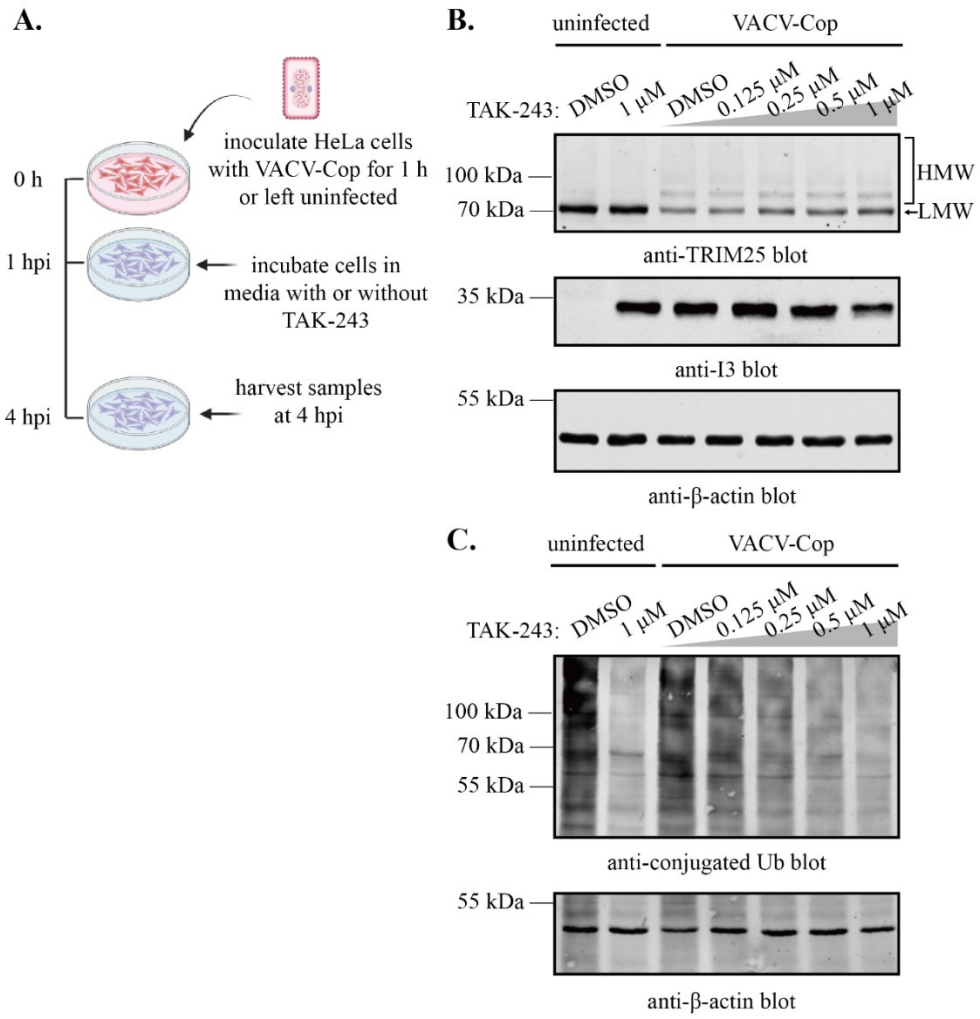

Figure 5.11 TRIM25 ubiquitylation in VACV-Cop-infected cells treated with E1 inhibitor

A, Schematic of the experimental workflow used to examine the effect of the E1 inhibitor, TAK-243, on TRIM25 HMW species. **B** and **C,** Lysates from uninfected cells or cells with VACV-Cop for 4 h (MOI of 10) treated with TAK-243 were immunoblotted with Abs against the indicated proteins. The anti-I3 blot shows infection of the cells, and the anti-β-actin blots show protein loading. The conjugated Ub Ab recognizes mono- and poly-ubiquitylated proteins. The anti-β-actin blots were included to show protein loading. Molecular mass markers are indicated to the left of blots. This western blot was performed by Grace Melvie. The results presented in the figure were replicated in 3 independent experiments, and the figure displays one of the 3 replicates.

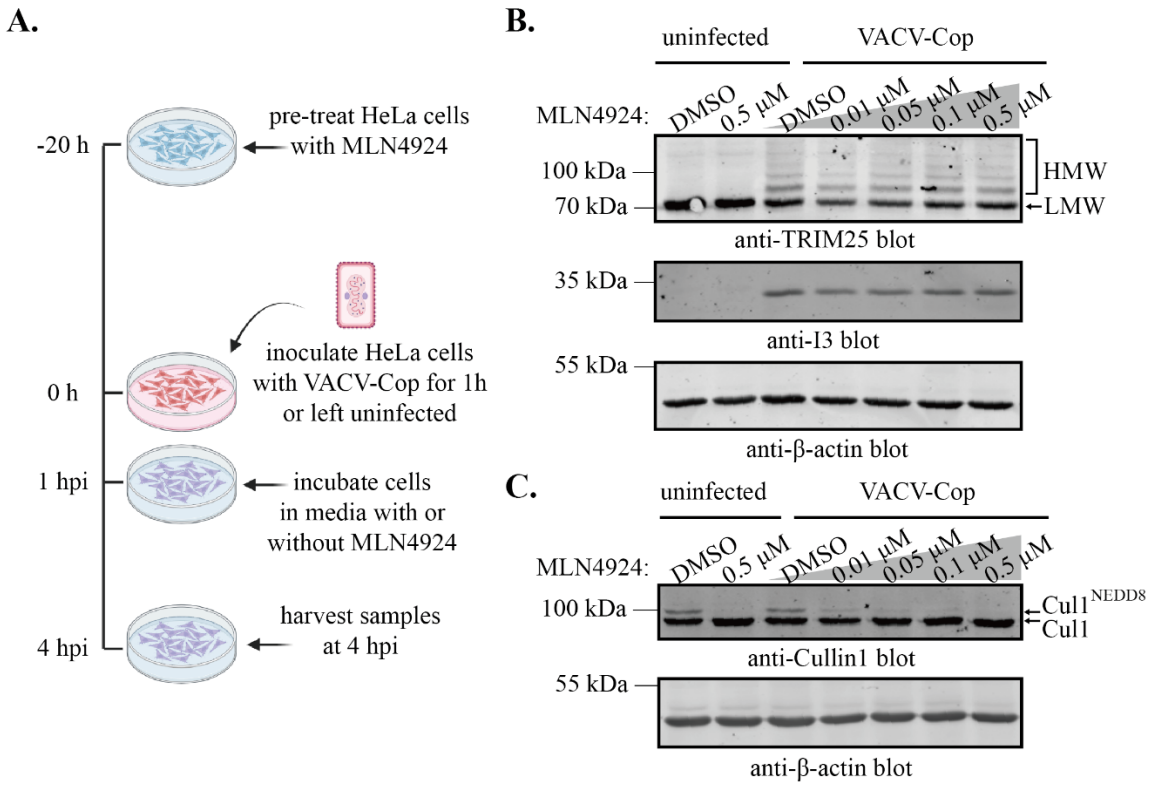

Figure 5.12 TRIM25 ubiquitylation in VACV-Cop-infected cells pretreated and treated with neddylation E1 inhibitor

A, Schematic of the experimental workflow used to examine the effect of neddylation E1 inhibitor, MLN4924 on TRIM25 HMW species. **B** and **C,** Lysates from uninfected cells or cells with VACV-Cop for 4 h (MOI of 10) treated with MLN4924 were immunoblotted with Abs against the indicated proteins. The anti-I3 blot shows infection of the cells, and the anti-β-actin blots show protein loading. The anti-Cul1 Ab recognizes both unmodified Cul1 and NEDD8-modified Cul1 (NEDD8-Cul1). The anti-β-actin blots were included to show protein loading. Molecular mass markers are indicated to the left of blots. The western blot was performed by Grace Melvie. The results presented in the figure were replicated in 3 independent experiments, and the figure displays one of the 3 replicates.

was observed in cells treated with MLN4924 **(Figure 5.12B; upper panel)**. However, neddylation of a known NEDD8 modified protein, Cul1 (224), was affected by MLN4924 treatment **(Figure 5.12C; upper panel)**. Taken together, these experiments support the notion that TRIM25 is ubiquitylated, but not neddylated, in VACV-Cop-infected cells.

5.2.6 TRIM25 ubiquitylation in VACV-Cop-infected HeLa cells is largely dependent on new protein synthesis and can be induced by UV-inactivated virus

The fact that ubiquitylation of TRIM25 occurred early after VACV-Cop infection led us to examine how infection induced this modification. I treated HeLa cells with the protein synthesis inhibitor, cycloheximide (CHX), prior to and after inoculation and examined TRIM25 protein levels **(Figure 5.13A)**. CHX treatment completely blocked I3 expression and impaired the appearance of HMW TRIM25 species in VACV-Cop-infected cells **(Figures 5.13B)**. Total TRIM25 levels and levels of the LMW TRIM25 band were not significantly different in cells treated with or without CHX **(Figure 5.13C** and **D)**. Thus, *de novo* protein synthesis is contributory, but not essential for the induction of TRIM25 HMW species in VACV-infected cells.

I also examined whether UV-inactivated VACV particles could induce TRIM25 ubiquitylation **(Figure 5.14A)**. VACV-Cop exposed to a dose of UV light (0.1 J/cm^2) that resulted in no detectable plaques on BSC-40 cells **(Figure 5.14B)** was still able to induce TRIM25 HMW species **(Figure 5.14C)**, despite no detectable VACV I3 protein expression

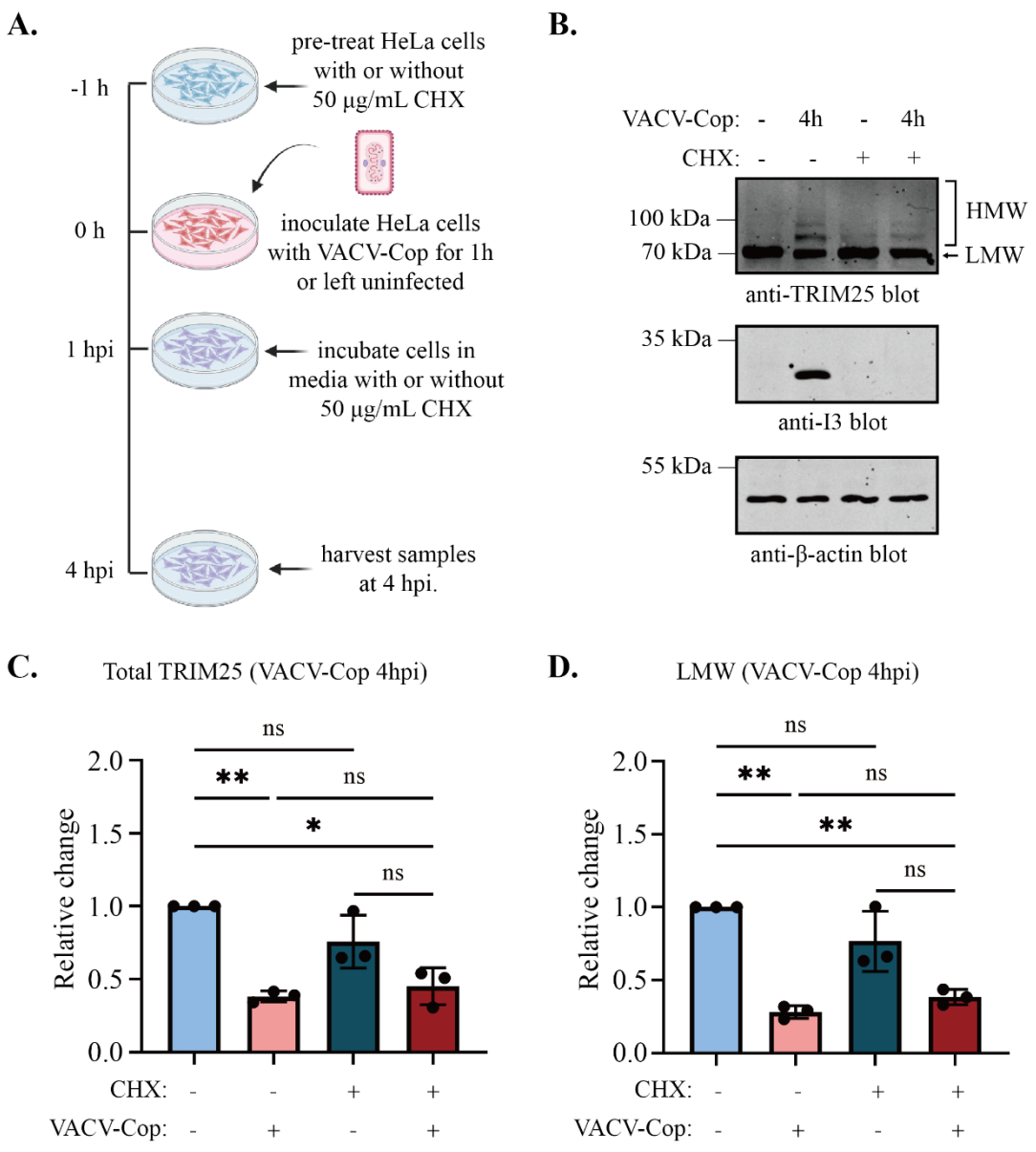

Figure 5.13 TRIM25 ubiquitylation in VACV-Cop-infected HeLa cells does not absolutely require new protein synthesis

A, Experimental approach used to evaluate the effect of inhibiting protein synthesis (cycloheximide; CHX) on HMW and LMW TRIM25 species. **B**, Lysates from samples described in **A** were immunoblotted with Abs against the indicated proteins. The anti-I3 blot was included to show the effect of CHX on poxviral-protein expression. The anti-β-actin blot was included to show protein loading. Molecular mass markers are indicated to

the left of blots. Total TRIM25 levels **(C)** and levels of the LMW TRIM25 band **(D)** were quantified in the indicated samples and expressed relative the uninfected cells not treated with CHX (uninfected). Molecular mass markers are indicated to the left of blots. Results presented represent the mean and standard deviation from 3 independent experiments. One-way ANOVA was used to calculate statistical significance between samples. ns; not significant, *; $p \leq 0.05$, **; $p \leq 0.01$.

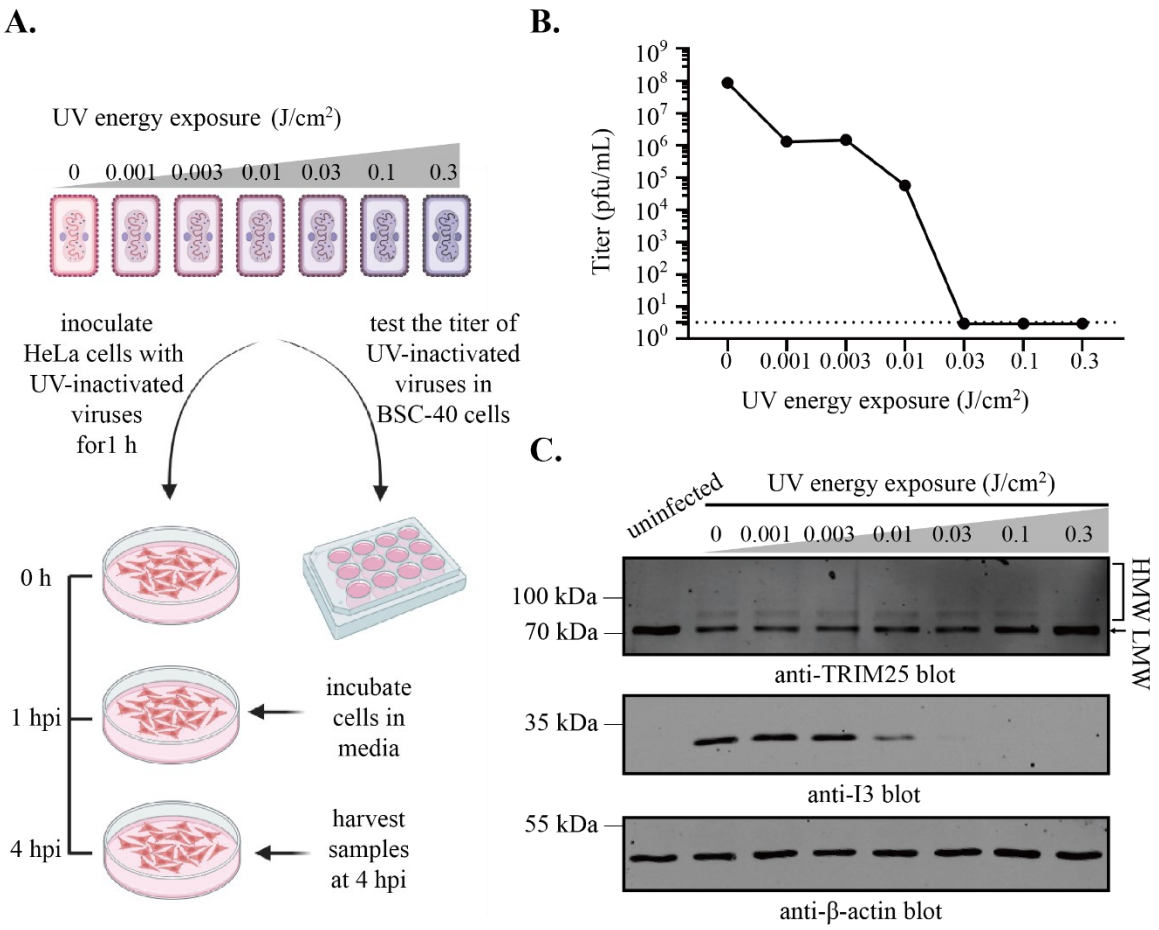

Figure 5.14 TRIM25 ubiquitylation in VACV-Cop-infected HeLa cells can be induced by UV-inactivated virus

A, VACV-Cop in media was exposed to the indicated doses of UV light before for being used to infect HeLa or BSC-40 cells (MOI of 10 equivalent) for western blot analysis or virus titer determinations, respectively. **B,** Titers of VACV-Cop in BSC-40 cells exposed to the indicated UV light energies. The dashed line presented the limit of detection. **C,** Western blot analyzing TRIM25 levels in HeLa cells inoculated with VACV-Cop treated with the indicated doses of UV light. The anti-I3 blot shows the effect of UV light on viral-protein expression and the anti-β-actin blot indicates protein loading. Molecular mass markers are indicated to the left of blots. Results presented represent the mean and standard deviation from 3 independent experiments. One-way ANOVA was used to calculate statistical significance between samples. ns; not significant, *; $p \leq 0.05$, **; $p \leq 0.01$. The results presented in B and C were replicated in 2 independent experiments, and the figure displays one of the 2 replicates.

being observed in cells infected at this UV dose **(Figure 5.14C)**. However, TRIM25 HMW species were not observed when cells were inoculated with virus exposed to 0.3 J/cm^2 **(Figure 5.14C)**. Thus, UV-inactivated VACV-Cop that is unable to replicate and express the viral protein can still induce TRIM25 HMW species.

5.2.7 TRIM25 is degraded in HeLa cells infected with other VACV strains and OPVs

We next investigated whether the modification of TRIM25 was observed in cells infected with other VACV strains. Western blotting analysis revealed HMW forms of TRIM25 were evident in HeLa cells infected with each of the VACV strains tested **(Figure 5.15)**. However, the formation of HMW TRIM25 species varied amongst the strains. For instance, cells infected with VACV-WR consistently resulted in fainter TRIM25 HMW bands and less decrease in the TRIM25 LMW band **(Figure 5.15)**.

We also examined whether infection of HeLa cells with other OPVs could modify TRIM25. HMW TRIM25 species and a decrease in anti-TRIM25 immunoreactive bands were observed in cells infected with CPXV-BR **(Figure 5.16A** and **B)** or MPXV-Clade IIb strain **(Figure 5.16C** and **D)**. Interestingly, we observed a significant decrease in TRIM25 levels **(Figure 5.16A** and **B)**, but no HMW TRIM25 species, in HeLa cells infected with ECTV-Mos **(Figure 5.16A)**. Thus, decreased TRIM25 levels appears to be a common feature of OPV infection, but the formation of HMW species is not.

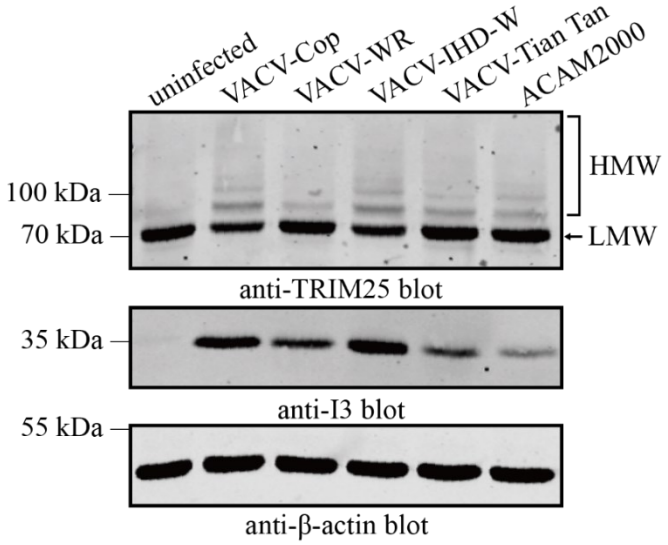

Figure 5.15 TRIM25 is degraded in HeLa cells infected with other VACV strains

HeLa cells were either left uninfected or infected with the indicated VACV strains for 4 h (MOI of 10). Lysates were immunoblotted with Abs against the indicated proteins. The anti-I3 blot was used to show viral infection. The anti-β-actin blot was included to show protein loading. Molecular mass markers are indicated to the left of blots. The western blot shown was performed by Grace Melvie, while I prepared these cell lysates and performed the initial repeat experiment. The results presented in the figure were replicated in 3 independent experiments, and the figure displays one of the 3 replicates.

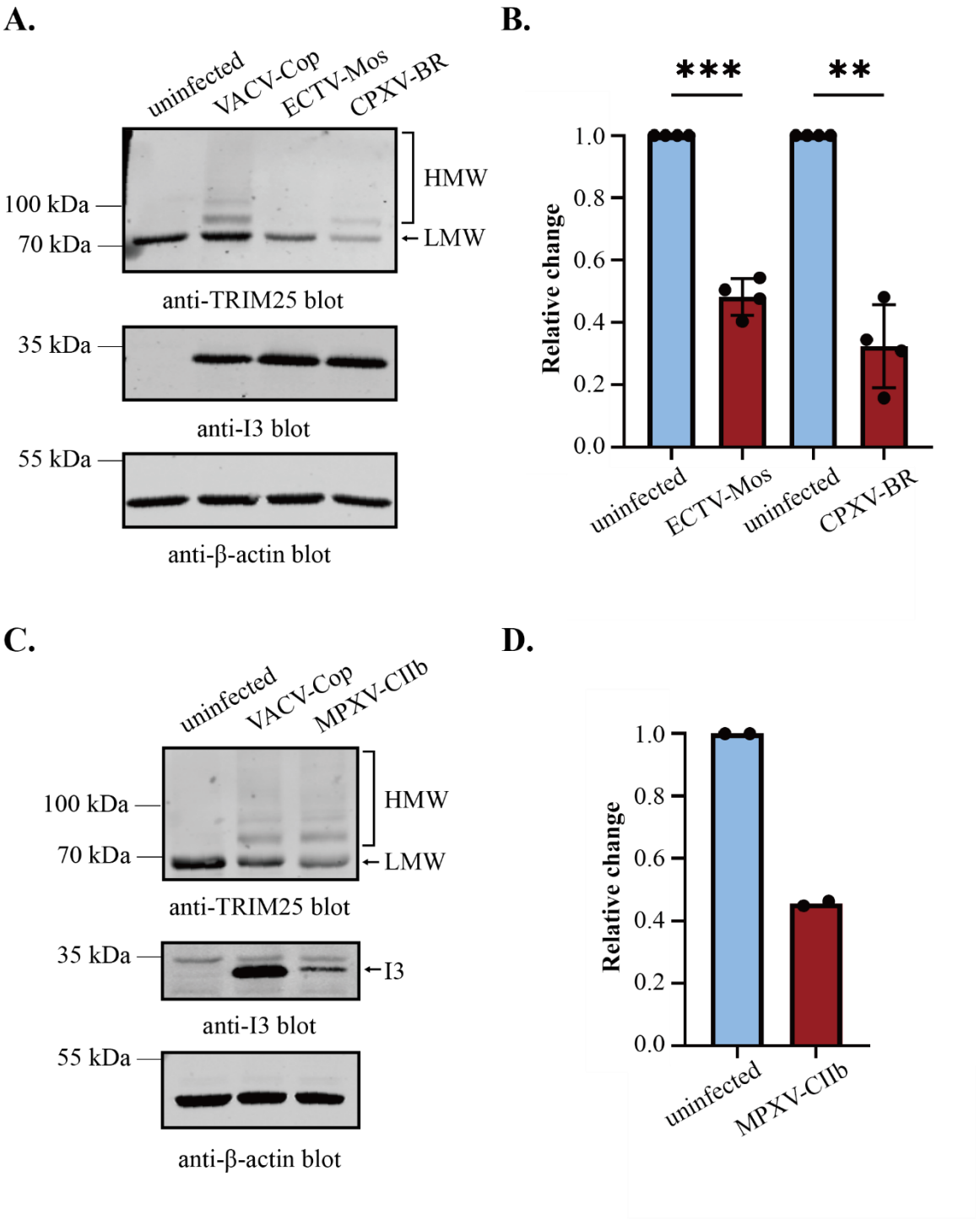
A.
uninfected
VACV-Cop
ECTV-Mos
CPXV-BR
100 kDa
70 kDa
HMW
LMW
anti-TRIM25 blot
35 kDa
anti-I3 blot
55 kDa
anti-β-actin blot
B.
***
**
Relative change
1.0
0.8
0.6
0.4
0.2
0.0
uninfected
ECTV-Mos
uninfected
CPXV-BR
C.
uninfected
VACV-Cop
MPXV-CIIb
100 kDa
70 kDa
HMW
LMW
anti-TRIM25 blot
35 kDa
I3
anti-I3 blot
55 kDa
anti-β-actin blot
D.
Relative change
1.0
0.8
0.6
0.4
0.2
0.0
uninfected
MPXV-CIIb

Figure 5.16 TRIM25 is degraded in HeLa cells infected with different OPVs

A, VACV-Cop, ECTV-Mos, and CPXV-BR were used to infect HeLa cells for 4 h (MOI of 10) or cells were left uninfected. Lysates were then immunoblotted with Abs against the indicated proteins. Total TRIM25 levels in HeLa cells infected with ECTV-Mos and CPXV-BR **(B)** were quantified and expressed relative to uninfected cells. Results presented represent the mean and standard deviation from 4 independent experiments. **C**, HeLa cells were either left uninfected or infected with MPXV (Clade IIb **(CIIb)** strain) for 4 h (MOI of 10). Lysates were immunoblotted with Abs against the indicated proteins. **D**, Total TRIM25 levels in HeLa cells infected with MPXV-CIIb was quantified and expressed relative the uninfected cells. Results presented are the mean from 2 independent experiments. A paired, one-tailed student *t* test was used to calculate statistical significance between samples. **; $p \leq 0.01$, ***; $p \leq 0.001$. The anti-I3 blot was included to show evidence of viral infection. The anti-β-actin blot was included to show protein loading. Molecular mass markers are indicated to the left of blots. One-way ANOVA. ns; not significant. The generation of cell lysates in A was performed by me, and cell lysates in C were provided by Drs. James Lin and David Evans (University of Alberta). The western blots were performed by Grace Melvie.

To determine whether modification of TRIM25 is observable in other cell types, 293T cells were infected with VACV-Cop or ECTV-Mos. Similar to what was observed in HeLa cells, HMW TRIM25 species and a reduction in the LMW species was observed in VACV-Cop-infected 293T cells **(Figure 5.17)**. Also consistent with our findings in HeLa cells, HMW TRIM25 species were not observed in 293T cells infected with ECTV-Mos, but a decrease in the LMW species was apparent **(Figure 5.17)**. Thus, TRIM25 ubiquitylation in response to VACV-Cop infection is not specific to HeLa cells.

5.2.8 A gene(s) located in either arm of the VACV genome is sufficient to induce TRIM25 ubiquitylation

To investigate whether a VACV gene(s) was required for the formation of TRIM25 HMW species, we infected HeLa cells with VACV-Cop strains with large deletions in either the left (vP796), right (vP759), or both (vP811) arms of the virus genome **(Figure 5.18A)** (164). Cells infected with either of the single arm deletion viruses resulted in the formation of HMW TRIM25 species band, but this was not observed in cells infected with the vP811 virus **(Figure 5.18B)**. Therefore, a gene(s) in either arm of the VACV-Cop genome is sufficient to induce TRIM25 ubiquitylation.

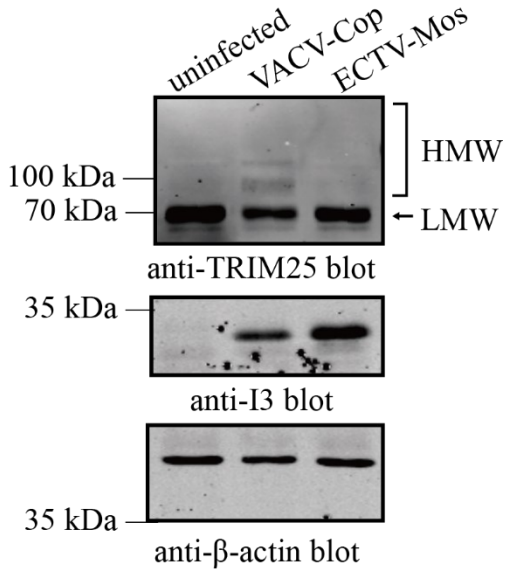

Figure 5.17 TRIM25 ubiquitylation in 293T cells infected with VACV-Cop or ECTV-Mos

293T cells were either left uninfected or infected with the VACV-Cop or ECTV-Mos for 4 h (MOI of 10). Lysates were immunoblotted with Abs against the indicated proteins. Anti-I3 blots were included to show evidence of viral infection. anti-β-actin blots were included to show protein loading. Molecular mass markers are indicated to the left of blots. The generation of cell lysates was performed by me, and the western blot was performed by Summer Smyth. The results presented in the figure were replicated in 3 independent experiments, and the figure displays one of the 3 replicates.

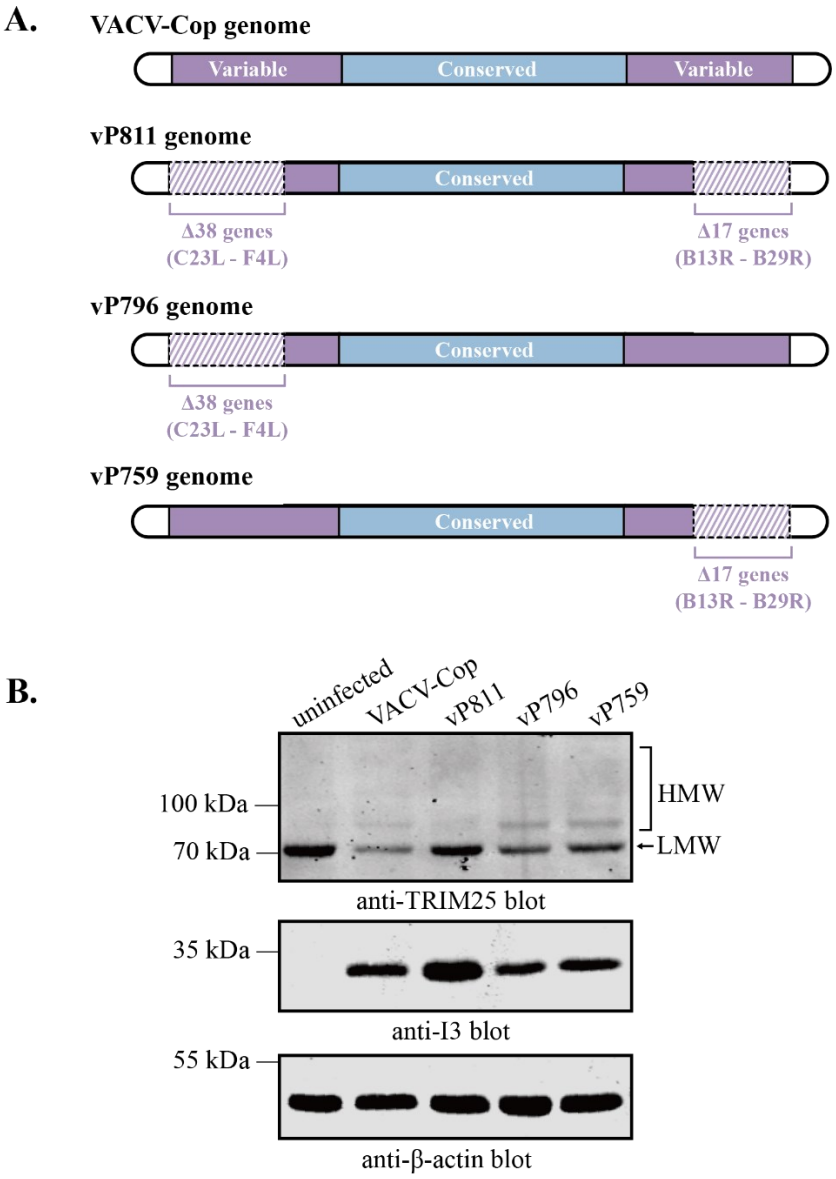

Figure 5.18 TRIM25 is degraded in cells infected with VACV with large deletions

A, Cartoons showing the genomes of VACV-Cop and the viruses (vP811, vP796 and vP759) with the indicated deletions in VACV-Cop genome. **B**, A gene(s) located in either arm of the VACV genome is sufficient to induce TRIM25 ubiquitylation. Lysates of HeLa cells uninfected or infected (MOI of 10) for 4 h with indicated viruses were immunoblotted with Abs against the indicated proteins. Molecular mass markers are indicated to the left of blots. The western blot shown was performed by Grace Melvie, while I prepared these cell lysates and performed the initial repeat experiment. The results presented in the figure were replicated in 3 independent experiments, and the figure displays one of the 3 replicates.

5.2.9 Loss of TRIM25 does not significantly alter the growth rate of VACV-Cop or vP811

Many members of the TRIM superfamily are associated with innate immune signaling and restricting virus infection (225). For example, TRIM5α was recently demonstrated to restrict OPV infection and VACV overcomes this restriction factor, in part, by promoting TRIM5α ubiquitylation and degradation (122). Therefore, degradation of TRIM family proteins is one strategy used by poxviruses to evade the host immune response in order to efficiently replicate in cells. We postulated that reduced TRIM25 levels, and/or the formation of HMW ubiquitylated species may be important for VACV-Cop to overcome the anti-viral activity of TRIM25. Because vP811 cannot induce TRIM25 HMW, likely ubiquitylated forms of TRIM25 **(Figure 5.18A)**, we hypothesized that TRIM25 may limit the replication of this virus. To test this hypothesis, we generated TRIM25 knock-out HeLa cell lines using clustered regularly interspaced short palindromic repeats (CRISPR)/Cas9-mediated gene editing **(Figure 5.19A)**. We then performed multi-step growth curves with VACV-Cop and vP811 in two control and two TRIM25 knock-out cell lines. Overall, there was no consistent difference in the growth rate of either of these viruses in control or TRIM25 knock-out HeLa cells **(Figure 5.19B**, **C** and **5.17)**. Thus, TRIM25 deletion in HeLa cells is not sufficient to confer a growth advantage for VACV-Cop or vP811.

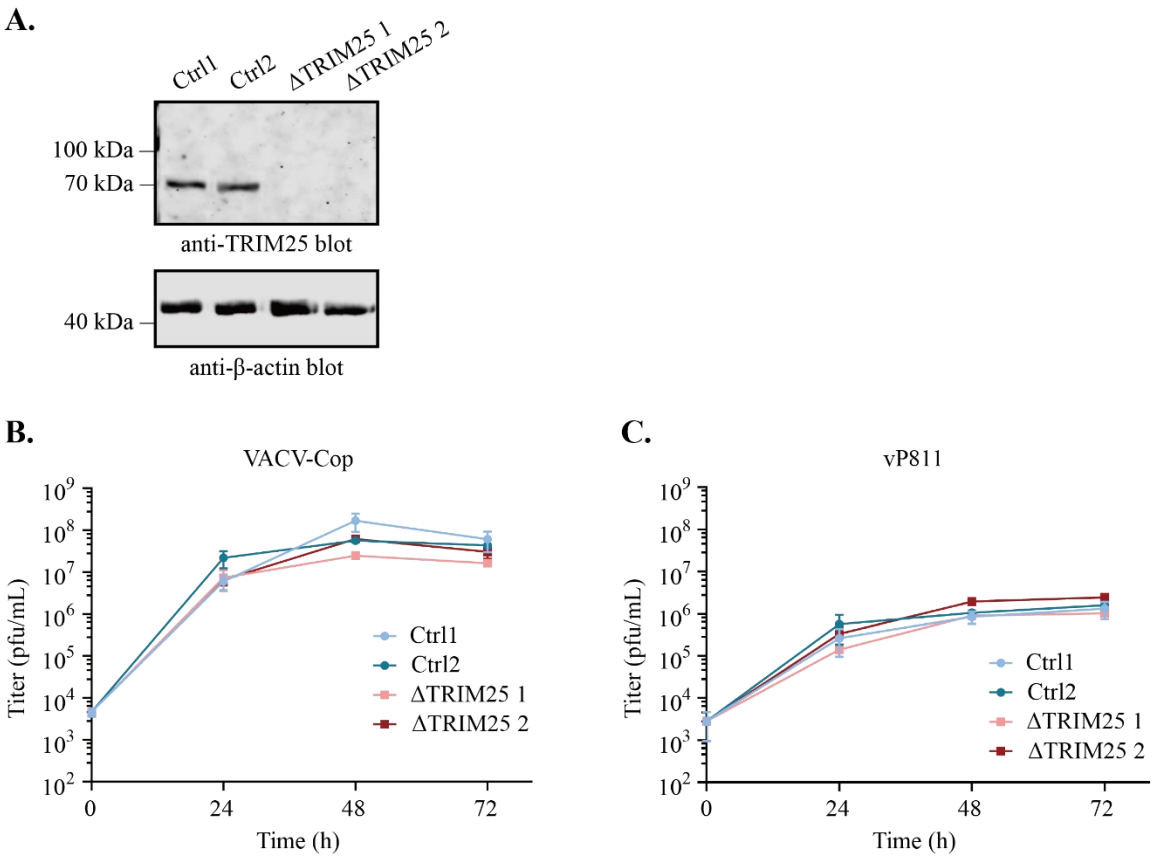

Figure 5.19 The absence of TRIM25 in HeLa cells does not affect viral replication of VACV-Cop or vP811

A, Immunoblot analysis showing the absence of TRIM25 in two knock-out HeLa cell clones, and the presence in clones from cells electroporated with a non-targeting (control) guide RNA. The anti-β-actin blot was included to show protein loading. Molecular mass markers are indicated to the left of blots. The results presented in the figure were replicated in 3 independent experiments, and the figure displays one of the 3 replicates. Viral titers from HeLa cells with or without TRIM25 were infected with VACV-Cop **(B)** or vP811 **(C)** at a MOI of 0.03 for the indicated times. The data represents the average and standard error of the mean of 4 independent experiments. A two-way ANOVA was used to calculate statistical significance between the titer of virus in ΔTRIM25 and control cells at the indicated time points post-infection. ns; not significant. The generation of TRIM25 knock-out HeLa cells was performed by me, and the growth curves were determined by Summer Smyth.

A.

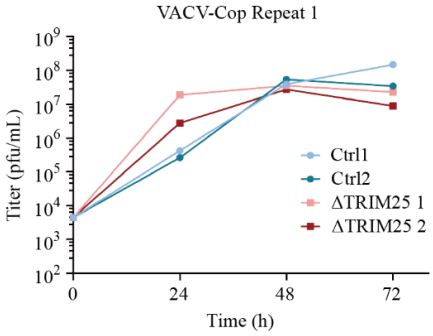
VACV-Cop Repeat 1
Titer (pfu/mL)
Time (h)
Ctrl1
Ctrl2
ΔTRIM25 1
ΔTRIM25 2

B.

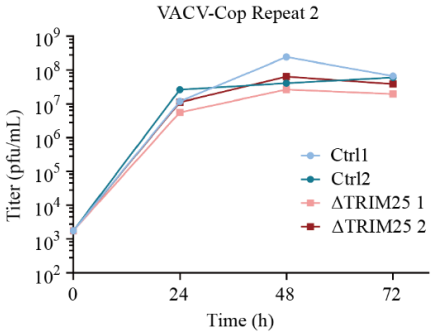
VACV-Cop Repeat 2
Titer (pfu/mL)
Time (h)
Ctrl1
Ctrl2
ΔTRIM25 1
ΔTRIM25 2

C.

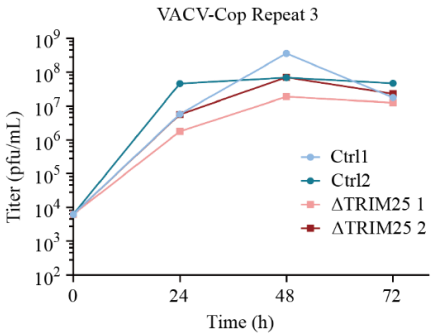
VACV-Cop Repeat 3
Titer (pfu/mL)
Time (h)
Ctrl1
Ctrl2
ΔTRIM25 1
ΔTRIM25 2

D.

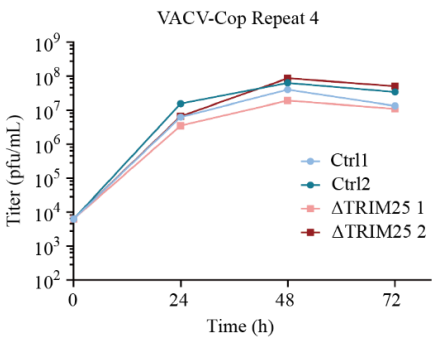
VACV-Cop Repeat 4
Titer (pfu/mL)
Time (h)
Ctrl1
Ctrl2
ΔTRIM25 1
ΔTRIM25 2

E.

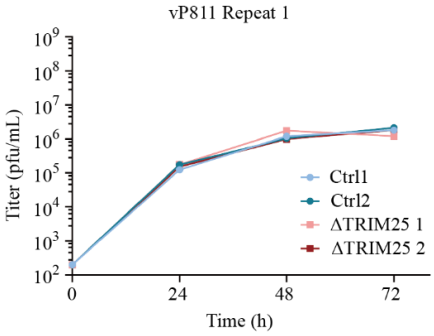
vP811 Repeat 1
Titer (pfu/mL)
Time (h)
Ctrl1
Ctrl2
ΔTRIM25 1
ΔTRIM25 2

F.

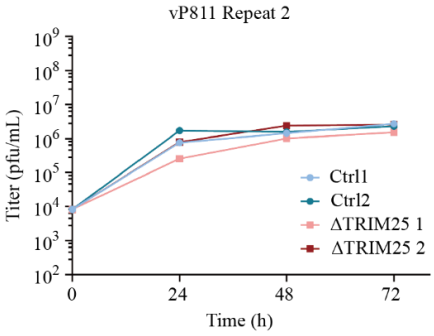
vP811 Repeat 2
Titer (pfu/mL)
Time (h)
Ctrl1
Ctrl2
ΔTRIM25 1
ΔTRIM25 2

G.

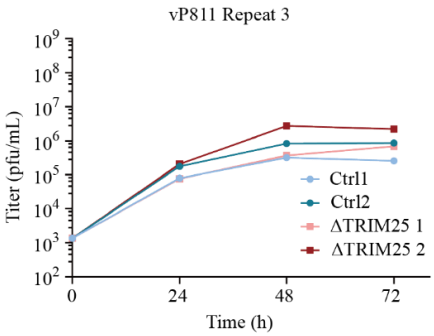
vP811 Repeat 3
Titer (pfu/mL)
Time (h)
Ctrl1
Ctrl2
ΔTRIM25 1
ΔTRIM25 2

H.

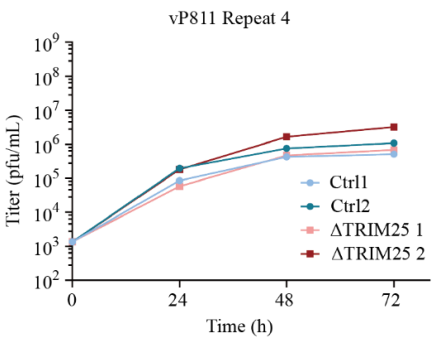
vP811 Repeat 4
Titer (pfu/mL)
Time (h)
Ctrl1
Ctrl2
ΔTRIM25 1
ΔTRIM25 2

Figure 5.20 The titers of VACV-Cop and vP811 in ΔTRIM25 and control cells

The raw data for the virus growth curves combined in Figure 5.19 B and C. Viral titers from HeLa cells with or without TRIM25 were infected with VACV-Cop **(A to D)** or vP811 **(E to H)** at a MOI of 0.03 for the indicated times in each repeat experiment. The generation of TRIM25 knock-out HeLa cells was performed by me, and the growth curves were performed by Summer Smyth.

5.3 Summary and discussion

In this chapter, we identified and quantified diGly peptides to study how the Ub system is involved in VACV infection at early time points (206, 207) **(Figure 5.1)**. There were 1753 distinct diGly peptides identified from the three independent experiments **(Table 5.1)**, of which 57 cellular diGly peptides were found enriched in VACV-infected HeLa cells **(Figure 5.2)**, 9 diGly peptides were identified from TRIM25 **(Figure 5.4)**. We further observed TRIM25 HMW species after VACV-Cop infection, and a decrease in anti-TRIM25 immunoreactive bands by western blotting **(Figure 5.7A** and **B)**. Additionally, an increase in the HMW species of TRIM25 was also observed in anti-conjugated Ub IPs from VACV-Cop infected cells **(Figure 5.9B)**. The decrease of TRIM25 was modestly rescued by proteasome inhibitor (MG132) treatment **(Figure 5.8)**. This suggests that some of the ubiquitylated TRIM25 was degraded through UPS, but it cannot be ruled out that ubiquitylated TRIM25 may have some non-degradative function. For example, many potential ubiquitylation sites localized in the B-box domain and the coiled-coil domain (Figure 5.6). Since these domains are critical for the oligomerization and activation of TRIM25 (214, 220, 225-227), these modifications may inhibit TRIM25 function by impairing its oligomerization.

The majority of diGly peptides are generated from trypsin digested ubiquitylated proteins, whereas a small fraction (< 6%) can be produced by proteins modified with other small Ub-like proteins, such as NEDD8 and ISG15 (206, 223). Thus, we used neddylation

E1 protein inhibitor (MLN4924) to treat cells and then found the VACV infection still induced HMW TRIM25 in HeLa cells **(Figure 5.12)**. In contrast, the E1 Ub-activating enzyme inhibitor (TAK-243) treatment significantly inhibited the HMW TRIM25 formation in VACV-infected cells **(Figure 5.10)**. These results indicated that TRIM25 HMW were not neddylated. However, we cannot rule out the possibility that it was ISGylation, and this would require further investigation in future studies.

To investigate what induced the TRIM25 ubiquitylation during VACV infection, we inhibited *de novo* protein synthesis by CHX treatment. A modest decrease in the immunoreactive bands of TRIM25 was observed in VACV-infected cells treated with CHX **(Figure 5.13)**. UV-inactivated virus also induced the formation of HMW TRIM25 **(Figure 5.14)**. The infection with VACV with large deletions (vP811, vP759, and vP798) showed that a gene(s) located in either arm of VACV genome is sufficient to induce TRIM25 HMW **(Figure 5.18)**.

Other strains of VACV and members of OPV also induced the HMW TRIM25 during infection **(Figure 5.16)**. The ubiquitylation of TRIM25 was not only observed in HeLa cells but also in 293T cells **(Figure 5.17)**. Therefore, ubiquitylation of TRIM25 could be a general response to multiple poxvirus infections. However, knocking-out TRIM25 did not affect virus replication **(Figure 5.19)**. This is not surprising, given that many poxviral proteins inhibit anti-viral signalling pathways downstream of TRIM25. Such possibilities will be further discussed in the general discussion section.

Chapter 6: Overall discussion and future directions

Parts of this chapter of this thesis have been published in:

"Jianing Dong, Patrick Paszkowski, Dana Kocincova, Robert J. Ingham. Complete deletion of Ectromelia virus p28 impairs virus genome replication in a mouse strain, cell type, and multiplicity of infection-dependent manner. *Virus Research.* 323 (2023) 198968, doi: 10.1016/j.virusres.2022.198968."

And the manuscript:

"Jianing Dong, Shu Luo, Summer Smyth, Grace Melvie, Olivier Julien, Robert J. Ingham. Characterizing changes in protein ubiquitylation during vaccinia virus infection." (Under review, manuscript # JVI00430-24)

6.1 General conclusions and thesis overview

In this thesis, I have studied how poxvirus encoded E3 Ub-ligases function during poxvirus infection and examined protein ubiquitylation early after poxvirus infection. In Chapter 3, I determined the role of p28, a poxvirus encoded E3 Ub-ligase, during ECTV replication. Our p28 knock-out ECTV (ECTV-Δp28) exhibited severely impaired virus production in a mouse strain, cell type, and MOI-dependent manner. Genome replication of ECTV-Δp28 was drastically inhibited in PMs from susceptible strain A mice infected at low MOI infection. I will further discuss the impact of the differences in MOI and cell type on virus replication, as well as the steps p28 is involved in poxvirus replication in the following sections. In Chapter 4, I expressed a FLAG-tagged p28 protein with a fusion Ub moiety (UBAITs) in VACV-infected cells to develop a tool to trap p28 substrate proteins. In addition, I purified recombinant His-p28 and examined the interaction between p28 and VACV hairpin DNA. I will further discuss the ways to utilize these tools in the future.

To further elucidate how poxviruses affect protein ubiquitylation early after VACV-Cop infection, in Chapter 5, we identified and quantified diGly peptides in cells with or without VACV-Cop infection at 4 hpi. These included 9 peptides associated with TRIM25, a cellular E3 Ub/ISG15-ligase. The HMW species of TRIM25, most likely ubiquitylated TRIM25, were observed in HeLa cells infected with VACV-Cop and their formation required a gene(s) in either arm of the VACV-Cop genome. In this chapter, I will discuss some other diGly peptides whose abundance was significantly changed after VACV-Cop

infection. Furthermore, I will discuss potential viral gene(s) that could induce TRIM25 ubiquitylation and the consequences of TRIM25 ubiquitylation on virus infection.

6.2 Investigating the role of p28 during ECTV replication

p28 is a poxviral E3 Ub-ligase and functions as a context-specific virulence factor. To further investigate the function of this enigmatic protein, in Chapter 3, we completely deleted p28 gene from ECTV and generated ECTV-Δp28 **(Figure 3.1)**. The replication of ECTV-Δp28 was not significantly inhibited in many cell lines, including African green monkey kidney cell line, BSC-40 cells **(Figure 3.4),** and cell lines from susceptible strain A mice, YAC-1 cells **(Figure 3.8A)** and Neuro-2a cells **(Figure 3.8B)**. In addition, the replication of ECTV-Δp28 was not severely impaired in BMDM from susceptible strain A mice **(Figure 3.8C)**. However, in PMs from susceptible strain A mice, deletion of p28 resulted in a severe impairment in virus production at low MOI (MOI 0.03) infection **(Figure 3.5B)**, but not at high MOI (MOI 3) infection **(Figure 3.5A)**. A similar phenotype was also observed in PMs from another susceptible mouse strain, BALB/c mice, at low MOI infection **(Figure 3.9A)**. Interestingly, virus production was not impaired by p28 deletion in PMs from C57BL/6 mice **(Figure 3.9B)**, a resistant mouse strain. Further experiments indicated that deletion of p28 impaired virus genome replication and late gene expression in strain A PMs infected at low MOI **(Figure 3.11** and **6.1)**.

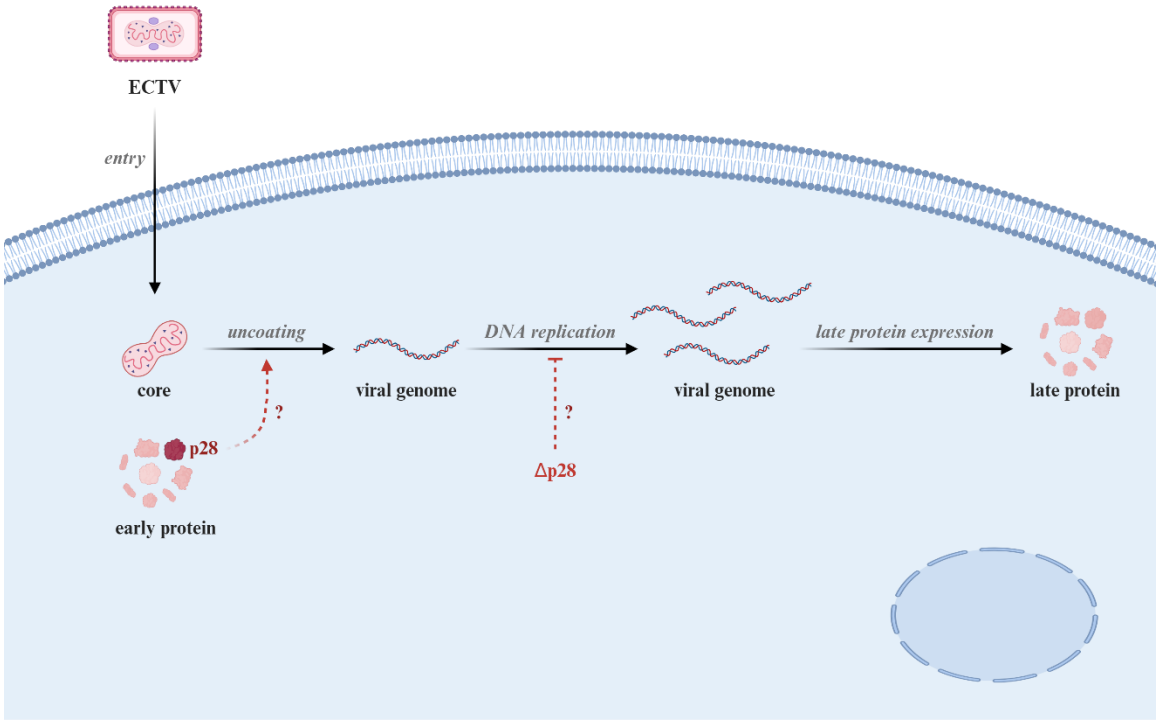

Figure 6.1 Model for the role of p28 during ECTV infection in PMs from strain A mice at low MOI infection

Following entry into PMs from strain A mice, the ECTV virus core is released into the cytoplasm. Cells infected with both ECTV and ECTV-Δp28 showed expression of viral protein, EVM056 (VACV I3), suggesting that p28 deletion does not inhibit virus entry. However, the absence of p28 significantly impaired viral genome replication and late protein expression. Therefore, p28 is essential either during viral genome replication or virus genome uncoating.

6.2.1 MOI dependence

An intriguing difference between our findings and those of the Buller group was a difference in the requirement for p28 in virus production at high MOI. The RING domain-deleted p28 virus was compromised in virus production, factory formation, and genome replication in strain A PMs infected at high MOI (MOI 5) (154). In contrast, we found very little defect at high MOI (MOI 3), but a severe impairment when cells were infected at low MOI (MOI 0.03) **(Figure 3.6 and 3.7C)**. We postulate that two reasons could account for this difference. Whereas we generated a complete p28 knock-out, the Buller group disrupted the p28 RING domain by exchanging it with a *gpt* cassette. Whether this disrupted gene resulted in a truncated protein consisting of the N-terminal KilA-N domain was not investigated (154). This putative truncated protein may retain some activity which could explain the observed differences. However, in CPXV, a complete deletion of p28 and a truncated mutant lacking the p28 RING domain exhibited a comparable growth defect (160). This suggests that, at least in J774A.1 macrophages infected with CPXV, a RING deletion mutant is comparable to a complete knock-out. Alternatively, the differences could be related to differences in calculated titers. We were unable to obtain the Buller lab's virus or determine how to accurately generate their virus to test which of these possibilities is correct. Nonetheless, it is important to note that both studies demonstrate p28 is important for virus factory formation and genome replication in strain A PMs.

It is unclear why the requirement for p28 is MOI-dependent, but a similar phenomenon

has been observed in human cytomegalovirus (HCMV). Deletion of HCMV genes that encode for the regulatory viral tegument proteins, ppUL35 (228) or ppUL69 (229), resulted in a defect in virus production that was dependent on MOI. These proteins are involved in immediate early gene transcription, and it was argued that redundancy amongst tegument proteins may compensate for the loss of a single protein (230). While p28 is not present in the virion (154), we hypothesize that at high MOI, a protein(s) present in virus particles and/or a product of an early gene(s) may be able to compensate for loss of p28. In support of this notion, functional redundancy has been described for the 68 kDa ANKR/F-box protein (68-ank) (OPG203) VACV E3 Ub-ligase substrate adapter. Liu *et al*. showed that deletion of 68-ank in modified VACV Ankara resulted in a virus uncoating and DNA replication defect (80). Intriguingly, the deletion could be rescued by either the BTB/Kelch substrate adapter, C5 (OPG30), or the poxviral immune evasion (PIE) superfamily member, M2 (OPG38), both of which are structurally unrelated to 68-ank. Thus, there may be a similar redundancy with respect to the function of p28 where another ECTV protein(s) compensates for loss of p28 during high MOI infection.

6.2.2 Cell-type specificity

We also further investigated the apparent cell-type specificity requirement for p28. Similar to previous reports (154), we found that loss of p28 minimally affected ECTV replication in cell lines derived from strain A mice **(Figure 3.8 A and B)**. Moreover, we found that deletion of p28 did not significantly compromise virus production in BMDMs

derived from this mouse strain **(Figure 3.8C)**. This suggests that there is a particular requirement for p28 to infect PMs at low MOI, which is supported by our findings that the loss of p28 also impaired virus production in PMs isolated from the BALB/c susceptible mouse strain **(Figure 3.9A)**. We did not see this effect in PMs isolated from the resistant C57BL/6 mouse strain **(Figure 3.9B)**, further demonstrating that p28 is required in strain A-specific manner. More recently, deletion of p28 from CPXV also resulted in a strong genome replication defect in rat PMs infected at a MOI of 0.1 (160). However, contrasting with the data of the Buller group (154), deletion of p28 from CPXV impaired virus genome replication in the RAW 264.7 macrophage cell line (160). Thus, the function of p28 may also differ between poxviruses. An alignment of p28 protein sequences from several OPVs demonstrated a high degree of sequence similarity between homologues **(Figure 1.10)**. Nonetheless, several amino acids differ between the ECTV and CPXV p28 sequences, particularly within the KilA-N domains, which could impart functional differences on these proteins.

Although we observed the greatest effect of loss of p28 in PMs, it is not clear how relevant PMs are to the natural infection of mice with ECTV. ECTV infection is thought to occur primarily through microabrasions in the skin, particularly on the footpad (45). It was suggested that infection of macrophages at the site of infection are required to disseminate the virus to the spleen and liver, where ECTV further replicates and ultimately results in the death of susceptible mouse strains (154). Consistent with this idea, ECTV p28 was not

required for virus replication at the site of infection in strain A mice, but it was important for dissemination to the spleen and liver (158). CPXV p28 was also argued to facilitate CPXV spread via infection of macrophages (160).

6.2.3 Future directions: Is p28 involved in virus uncoating?

The most important unaddressed question with respect to p28 is its function during infection. Our data is consistent with previous suggestions that p28 functions before or at the time of genome replication (154). Since EVM056 (VACV I3) was expressed in strain A PMs infected with the p28 knock-out virus at low MOI **(Figure 3.11A)**, the processes of virion binding and entry do not appear to be inhibited by p28 deletion. At about 2 hpi, virus uncoating occurs which releases viral genomic DNA for replication and allows transcription of intermediate/late genes (231). Moreover, virus intermediate/late gene expression is dependent on genome replication (232). Given that we observe a defect in both genome replication and late gene expression, it is likely that p28 plays a role in enabling virus uncoating or DNA replication. Therefore, our future work will be focused on determining whether ECTV-Δp28 virus is deficient in virus uncoating in PMs from susceptible mice **(Figure 6.1)**. Of note, the VACV ANKR/F-box substrate adapter, C9, regulates virus uncoating and DNA replication by targeting IFIT proteins for proteasomal degradation (134, 135). In addition, cellular Cul3 is required for virus uncoating, arguing that viral and/or cellular BTB/Kelch proteins are involved in this process (84). Thus, other than p28, there are multiple examples of poxviral E3 Ub-ligases involved in the early steps

of virus infection.

6.3 Developing tools to investigate substrates and DNA binding properties of p28

p28 is a critical virulence factor during poxvirus infection in susceptible mice (158). The RING domain of p28 is essential for virus replication in macrophages from susceptible mice (160) suggesting the E3 Ub-ligase activity may be crucial for poxvirus infection. Thus, identify the substrates of p28 is essential to understand the role of p28 during poxvirus infection. I showed that expressing FLAG-p28-Ub in poxvirus infected cells allowed me to capture potential substrates of p28 **(Figure 4.4)**. In addition, previous studies suggest p28, including full length p28 and a truncated p28 with a KilA-N domain, binds DNA (155-157). To further investigate the interactions between p28 and viral DNA, I purified His-p28 from BEVS **(Figure 4.9)**. The E3 Ub-ligase activity of the purified protein was examined by auto-ubiquitylation assay **(Figure 4.12)**. EMSA assays showed that purified His-p28 was associated with viral hairpin DNA **(Figure 4.13)**. However, we did observe binding between hairpin DNA and proteins that we would not be predicted to bind DNA **(Figure 4.13)**. These results indicate that the binding of His-p28 to DNA requires further investigation to determine whether the interaction between His-p28 and viral hairpin DNA is specific in this assay.

6.3.1 UBAITs

To trap potential substrate proteins of p28, I constructed a plasmid, pSC66-FLAG-p28-Ub, to express FLAG-p28-Ub during poxvirus infection. Fusion expression with Ub

did not affect the properties and functions of p28. Like p28, FLAG-p28-Ub was expressed in VACV-Cop-infected HeLa cells and localized to virus factories **(Figure 4.2 and 4.3)**. Furthermore, FLAG-p28-Ub enriched conjugated Ub into poxvirus factories similar to FLAG-p28 (151, 153) **(Figure 4.3)**. To capture the potential substrate proteins of p28, I purified them by anti-FLAG IP. The HMW species, likely formed by the proteins covalently bonded with FLAG-p28-Ub, were observed in the western blotting with anti-FLAG Ab **(Figure 4.4B)**. It is worth noting that UBAITs can also trap proteins that do not form a covalent bond but are only associate with them (177). In this study, I also observed Hsp70 associated with FLAG-p28-Ub without an increase in Hsp70 molecular weight, suggesting Hsp70 interacted with FLAG-p28-Ub without forming a covalent bond **(Figure 4.5)**. It should also be noted that proteins captured by UBAITs are not necessarily substrates. For instance, Psh1 is an E3 Ub-ligase which has a RING domain at the N terminus (233). The Psh1 UBAITs trapped the substrate of Psh1, Cse4 (233), as well as other proteins including Spt16, which are not substrates but associated with Psh1 (177). Thus, proteins trapped by p28 UBAITs can be substrates also proteins that associated with p28. In the future, a larger scale UBAITs experiment will be performed to identify these FLAG-p28-Ub captured proteins by mass spectrometry.

6.3.2 *E. coli* and BEVS

I tried to purify recombinant p28 and its isolated domains, which would help us to investigate how p28 binds DNA and characterize substrates of p28. Two protein expression

systems, *E. coli* and BEVS, were utilized to express p28 and its isolated domains. Unfortunately, little soluble GST-tagged p28 protein or isolated domains were expressed by *E. coli* **(Figure 4.7)**. While, His-tagged p28 was expressed by and successfully purified from BEVS **(Figure 4.9 and 4.11)**. This difference may be due to advantages of the eukaryotic cell expression system. For example, expressing His-p28 in baculovirus infected insect cells, Sf9 cells, allows eukaryotic post-translational modifications of the His-tagged proteins (182, 183). Furthermore, given the DNA-binding properties of p28 (155-157), the protective nuclear membrane in eukaryotic cells may reduce the possibility of target proteins binding to cellular DNA compared with prokaryotic bacteria. This may also be the reason why the growth of insect cells was inhibited when they were infected with baculoviruses expressing the smaller protein, His-KilA-N, whose smaller molecular weight may translocate in the nucleus passively through the nucleus membrane (234) and bind to the cellular DNA **(Figure 4.10A)**. A similar result was also observed when GST-KilA-N expression was induced in *E. coli* **(Figure 4.7B)**. Since the isolated domains of p28 were not successfully purified from both *E. coli* and BEVS, purification of full length His-p28 with mutations in the KilA-N domain will be an alternative strategy to study p28 KilA-N domain functions.

6.3.3 Future directions: how does p28 bind DNA?

It was reported that p28 has the ability to bind DNA (155-157). I examined the interaction of purified His-p28 and viral hairpin DNA by EMSA assay. The results showed

His-p28 binds to poxviral hairpin DNA, which has both ssDNA and dsDNA structure (53) **(Figure 4.13)**. However, the experiment requires improvement to avoid non-specific binding between protein and DNA. It is still unclear whether p28 binds a specific DNA structure, such as ssDNA and dsDNA. Given that OPV genomes are AT-rich (46, 54), it is also worth investigating whether p28 specifically binds to viral DNA. In addition, the KilA-N homologues, APSES in *S. cerevisiae* and *C. albicans* binds 5'-ATGCAT-3', whereas other fungal APSES prefer 5'-ACGCGT-3' (235), suggesting the KilA-N domain of p28 may specifically recognize a DNA sequence. Future work will also focus on examining whether p28 binds these DNA sequences specifically.

It is most likely that p28 binds to DNA through the KilA-N domain. However, more experiments are needed to determine the DNA binding motif of p28. Since I cannot purify the isolated domains of p28 from both *E. coli* and BEVS **(Figure 4.7** and **4.11)**, purified His-p28 with mutations in p28 KilA-N domain will be useful to answer this question and identify the residues on the KilA-N domain, which are responsible for DNA binding. Additionally, determining whether mutant p28 can rescue the replication defects of ECTV-Δp28 in PMs from strain A mice can help us understand if DNA-binding properties are critical for p28 function. Furthermore, these purified p28 proteins can be used to test the interactions with potential substrates identified by UBAITs.

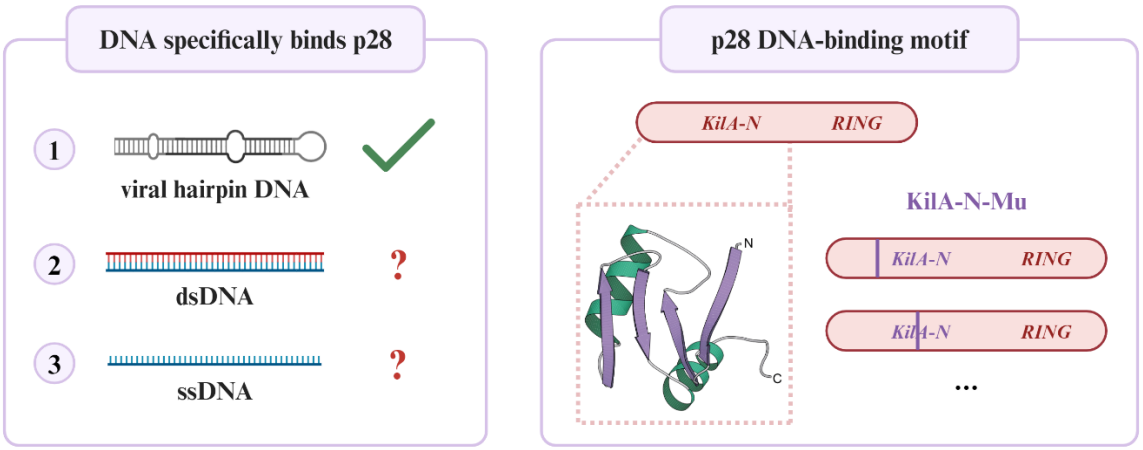

Figure 6.2 Model for the interactions between p28 and DNA

To further investigate how His-p28 binds to the hairpin DNA of VACV, whether p28 preferentially binds to a specific DNA structure will be examined. Due to nucleic acid mismatches, the hairpin DNA exhibits both ssDNA and dsDNA structures. Future experiments will investigate whether p28 preferentially binds to either of these DNA structures. As well, the DNA binding interface of p28 will be determined. The KilA-N domain and its homologue, APSES, bind DNA, but the DNA binding interface remains unclear. Therefore, variants of p28 with mutations in the KilA-N domain will be purified using BEVS, and their DNA binding ability will be examined using EMSA. The structure shown in this figure represents APSES domain, adapted from Iyer, L *et al.* (2002) (156).

6.4 TRIM25 and poxvirus infection

Ubiquitylation is a versatile post-translational modification that is required for poxviruses to replicate viral genomes and evade the host immune response (82, 106, 236). At the same time, both degradative and non-degradative protein ubiquitylation are critical components of the innate immune responses to infection (236). In this chapter, we took a proteomics approach to examine changes in protein ubiquitylation early after VACV infection **(Figure 5.1)**. Our results showed that, in addition to viral proteins, the ubiquitylation of many host proteins was altered during infection **(Figure 5.2)**. We found that ubiquitylation **(Figure 5.9)**, and probable degradation **(Figure 5.7A** and **5.7B)**, of the cellular E3 Ub/ISG15-ligase, TRIM25, was induced by infection with VACV and other OPVs early after infection **(Figure 5.16)**. We observed that TRIM25 is ubiquitylated in an E1 Ub-activating enzyme-dependent manner early after infection **(Figure 5.10** and **6.3)** The ubiquitylation of TRIM25 was highly dependent on *de novo* protein synthesis **(Figure 5.13** and **6.3)**. Moreover, a gene(s) in either arm of the VACV-Cop genome is sufficient to promote the formation of these species **(Figure 5.18** and **6.3)**. Taken together, this study has revealed novel information about how the UPS is altered during poxvirus infection.

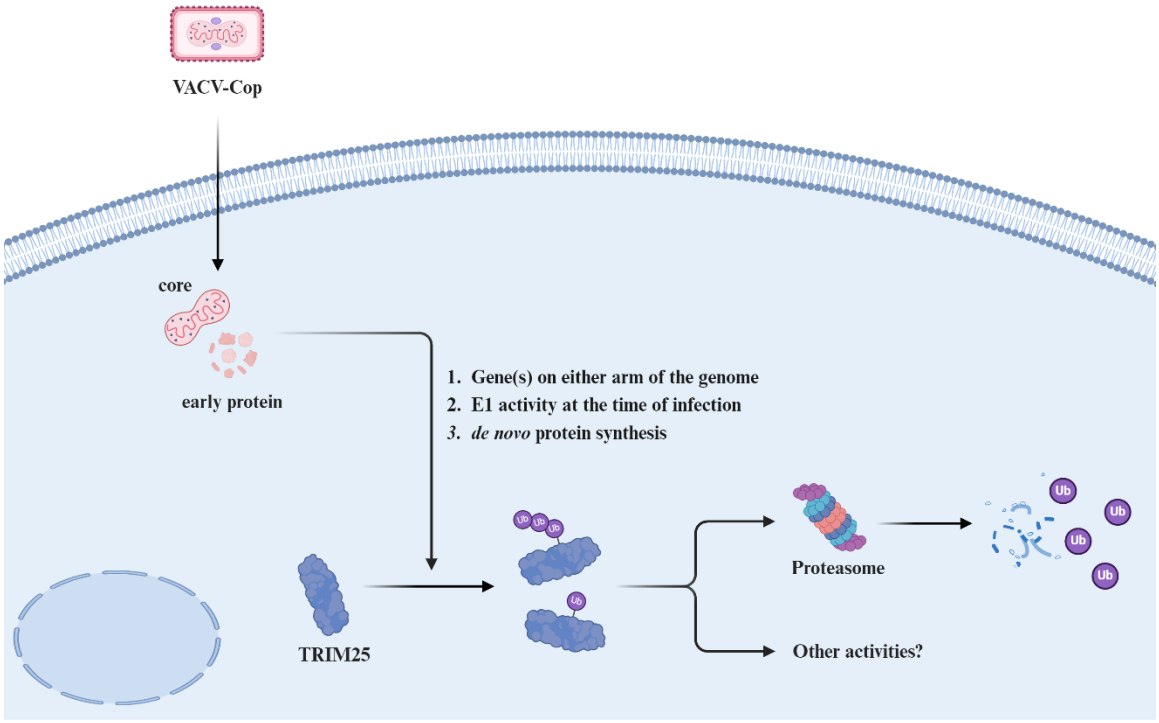

Figure 6.3 Model for TRIM25 ubiquitylation in poxviral infected cells

VACV-Cop infection induces TRIM25 ubiquitylation and degradation in infected HeLa cells. This is largely dependent on *de novo* protein synthesis and E1 activity at the time of infection. Moreover, a gene(s) located on either arm of the VACV-Cop genome is required for the formation of HMW TRIM25 species.

6.4.1 Proteins associated with the identified diGly peptides

To further investigate how the UPS is engaged early during poxvirus infection, we purified and identified diGly peptides using the diGly enrichment approach (206, 207). We were most interested in cellular diGly peptides that change in abundance during infection and were particularly struck by the number of diGly peptides from proteins previously implicated in poxvirus infection. For example, an IFIT1 and/or 5 diGly peptide was found exclusively in VACV-Cop-infected cells **(Figure 5.2)**. The IFITs are a family of anti-viral factors that are induced by interferon and can inhibit the transcription of viral RNAs via a number of mechanisms (237). IFITs are recognized by the VACV C9 E3 Ub-ligase ANKR/F-box substrate adapter, and Ub-mediated degradation of these proteins is important for poxvirus infection (135). Intriguingly, several of the enriched diGly peptides were from proteins shown to play a role in poxvirus infection. For example, we identified 5 diGly peptides for the RACK1 scaffolding protein, of which one (K175), was exclusively found in VACV-Cop-infected cells **(Figure 5.2)**. RACK1 performs many functions one of which is to regulate translation as a component of ribosomes (209, 238). RACK1 is phosphorylated by the VACV-encoded B1 kinase to selectively increase translation of viral RNAs (239). Of note, RACK1 protein levels did not decrease in VACV-WR-infected HFFF-TERT cells **(Figure 5.5)** (171) suggesting that modification of RACK1 on K175 may perform a regulatory rather than a degradatory function. Likewise, our results suggest that ubiquitylation of CDK2 in VACV-Cop-infected cells could also serve a non-

degradative function **(Figure 5.7C** and **D)**.

6.4.2 OPVs induce TRIM25 ubiquitylation

The most intriguing observation from our diGly enrichment experiments was the number of TRIM25 diGly peptides either enriched for or exclusively found in VACV-Cop-infected HeLa cells **(Figure 5.2)**. Of note, a study using diGly enrichment to identify ubiquitylated proteins in mature CPXV virions with a limited examination of cellular protein ubiquitylation during CPXV infection of HeLa cells identified diGly peptides from TRIM25 and several other proteins identified in our study (83). We observed HMW TRIM25 species as early as 1 h after VACV-Cop infection **(Figure 5.6)**, and HMW species were observed in cells infected with other VACV strains **(Figure 5.15)** and all other OPVs examined, except for ECTV **(Figure 5.16)**. These HMW TRIM25 species persisted throughout infection and likely represent mono- and di-ubiquitylated forms of TRIM25 that are likely not degraded. Moreover, we observed a decrease in total TRIM25 levels in HeLa cells infected with all poxviruses examined, even as early as 4 hpi. In addition, we found that MG132 treatment modestly enhanced TRIM25 levels **(Figure 5.8)** consistent with data suggesting that some TRIM25 is degraded via the proteasome during VACV infection **(Figure 5.5)** (171). However, we cannot rule out that the decrease in anti-TRIM25 immunoreactive bands in infected cells may be due to the anti-TRIM25 Ab having reduced affinity for the modified protein. Moreover, since poxvirus infection leads to a shut-down of host translation (240), reduced TRIM25 levels is also likely due to decreased TRIM25

translation, especially at the later stages of infection.

The trypsin digestion of proteins modified by the Ub-like proteins, ISG15 and NEDD8, also generates diGly motifs (223). Since the formation of HMW TRIM25 species was not inhibited in cells treated with neddylation E1 inhibitor **(Figure 5.12B)**, this argues these HMW species are not neddylated forms of the protein. In addition, specific ISGylation inhibitors are not available to our knowledge. Thus, we cannot rule out that HMW TRIM25 species may also represent ISGylated forms of TRIM25.

Using large deletion strains of VACV-Cop we were able to determine that a gene(s) in either end of the genome is sufficient to induce TRIM25 HMW species **(Figure 5.16A)**. This observation is perhaps not surprising given that poxviruses have many duplicated genes at the ends of their genomes (241). Examining the genome of VACV-Cop we found 9 duplicated genes in common between the two arms that are deleted in vP811. However, it may not be a duplicated gene that is responsible as completely unrelated proteins have been shown to have redundant functions in VACV (134). Intriguingly, there are two ANKR/F-box substrate adapters missing in the deletions in the left (C9L) and right (B18R) arms of vP811 which could be mediating TRIM25 ubiquitylation.

6.4.3 Future directions: Does TRIM25 ubiquitylation affect virus infection?

An unaddressed question in this study is the consequence of TRIM25 ubiquitylation in poxvirus infected cells. The most likely scenario is that TRIM25 ubiquitylation targets the protein for degradation which inhibits activation of RIG-I and other innate immune

signalling events mediated by TRIM25. Many viruses interfere with TRIM25 activation of RIG-I. For example, the influenza A virus NS1 protein binds to the TRIM25 coiled coil domain (218). This blocks TRIM25 from multimerizing and ubiquitylating RIG-I thereby blocking RIG-I signalling (218). Similarly, the SARS-CoV nucleocapsid protein binds the TRIM25 PRY/SPRY domain and inhibits TRIM25 from interacting with and ubiquitylating RIG-I (219). Other viruses use alternative strategies to interfere with TRIM25-mediated activation of RIG-I. For example, the Epstein-Barr virus protein, BPLF1, forms a complex with TRIM25 and 14-3-3 proteins (220). This induces the auto-ubiquitylation of TRIM25 and sequesters TRIM25 away from RIG-I (220). Regardless of whether and how ubiquitylation impacts TRIM25 function, our findings show that knocking out TRIM25 in HeLa was not sufficient to enhance the growth rate of VACV-Cop or vP811 **(Figure 5.19)**. We think this result is not surprising given that poxviruses have several strategies to suppress anti-viral signaling pathways downstream of TRIM25. For example, VACV C6 inhibits IFN expression by blocking IRF3 activation and nuclear translocation during poxvirus infection (242). IRF3 activation is also inhibited by the VACV N1 protein interacting with the IKK complex and suppressing NF-κB signalling (243). NF-κB signalling is also inhibited by VACV A49 mimicking cellular IκBα and preventing IκBα degradation, thereby blocking the nuclear translocation of p65 NF-κB (34, 244). Thus, additional mechanisms possessed by poxviruses to inhibit signalling events downstream of TRIM25 are very likely compensating for the loss of TRIM25.

Future work will focus on identifying the gene(s) responsible for inducing TRIM25 ubiquitylation and determining the consequence of this ubiquitylation on TRIM25 function. Finally, we plan to investigate other proteins with enriched diGly peptides to examine whether and how ubiquitylation of these proteins benefit poxviruses.

References

1. Hughes AL, Irausquin S, Friedman R. The evolutionary biology of poxviruses. Infection, Genetics and Evolution. 2010;10(1):50-9.
2. Lefkowitz EJ, Wang C, Upton C. Poxviruses: past, present and future. Virus Res. 2006;117(1):105-18.
3. Wang Q, Burles K, Couturier B, Randall CM, Shisler J, Barry M. Ectromelia virus encodes a BTB/kelch protein, EVM150, that inhibits NF-kappaB signaling. J Virol. 2014;88(9):4853-65.
4. van Buuren N, Burles K, Schriewer J, Mehta N, Parker S, Buller RM, et al. EVM005: an ectromelia-encoded protein with dual roles in NF-kappaB inhibition and virulence. PLoS Pathog. 2014;10(8):e1004326.
5. Sperling KM, Schwantes A, Staib C, Schnierle BS, Sutter G. The orthopoxvirus 68-kilodalton ankyrin-like protein is essential for DNA replication and complete gene expression of modified vaccinia virus Ankara in nonpermissive human and murine cells. J Virol. 2009;83(12):6029-38.
6. Blanie S, Mortier J, Delverdier M, Bertagnoli S, Camus-Bouclainville C. M148R and M149R are two virulence factors for myxoma virus pathogenesis in the European rabbit. Vet Res. 2009;40(1):11.
7. Sanchez-Sampedro L, Perdiguero B, Mejias-Perez E, Garcia-Arriaza J, Di Pilato M, Esteban M. The evolution of poxvirus vaccines. Viruses. 2015;7(4):1726-803.
8. Nagy E, Krell PJ, Heckert RA, Derbyshire JB. Vaccination of chickens with a recombinant fowlpox virus containing the hemagglutinin-neuraminidase gene of Newcastle disease virus under the control of the fowlpox virus thymidine kinase promoter. Canadian Journal of Veterinary Research. 1994;58(4):306.
9. Iritani Y, Aoyama S, Takigami S, Hayashi Y, Ogawa R, Yanagida N, et al. Antibody response to Newcastle disease virus (NDV) of recombinant fowlpox virus (FPV) expressing a hemagglutinin-neuraminidase of NDV into chickens in the presence of antibody to NDV or FPV. Avian Diseases. 1991:659-61.
10. Vagnozzi A, Zavala G, Riblet SM, Mundt A, García M. Protection induced by commercially available live-attenuated and recombinant viral vector vaccines against infectious laryngotracheitis virus in broiler chickens. Avian pathology. 2012;41(1):21-31.
11. Davison S, Gingerich EN, Casavant S, Eckroade RJ. Evaluation of the efficacy of a live fowlpox-vectored infectious laryngotracheitis/avian encephalomyelitis vaccine against ILT viral challenge. Avian diseases. 2006;50(1):50-4.
12. Mehendale S, Thakar M, Sahay S, Kumar M, Shete A, Sathyamurthi P, et al. Safety and immunogenicity of DNA and MVA HIV-1 subtype C vaccine prime-boost regimens: a phase I randomised Trial in HIV-uninfected Indian volunteers. PLoS One.

2013;8(2):e55831.
13. Vasan S, Schlesinger SJ, Chen Z, Hurley A, Lombardo A, Than S, et al. Phase 1 safety and immunogenicity evaluation of ADMVA, a multigenic, modified vaccinia Ankara-HIV-1 B'/C candidate vaccine. PLoS One. 2010;5(1):e8816.
14. Kreijtz JH, Goeijenbier M, Moesker FM, van den Dries L, Goeijenbier S, De Gruyter HL, et al. Safety and immunogenicity of a modified-vaccinia-virus-Ankara-based influenza A H5N1 vaccine: a randomised, double-blind phase 1/2a clinical trial. Lancet Infect Dis. 2014;14(12):1196-207.
15. Cavenaugh JS, Awi D, Mendy M, Hill AV, Whittle H, McConkey SJ. Partially randomized, non-blinded trial of DNA and MVA therapeutic vaccines based on hepatitis B virus surface protein for chronic HBV infection. PLoS One. 2011;6(2):e14626.
16. Hodgson SH, Choudhary P, Elias SC, Milne KH, Rampling TW, Biswas S, et al. Combining viral vectored and protein-in-adjuvant vaccines against the blood-stage malaria antigen AMA1: report on a phase 1a clinical trial. Mol Ther. 2014;22(12):2142-54.
17. Sheehy SH, Duncan CJ, Elias SC, Biswas S, Collins KA, O'Hara GA, et al. Phase Ia clinical evaluation of the safety and immunogenicity of the Plasmodium falciparum blood-stage antigen AMA1 in ChAd63 and MVA vaccine vectors. PLoS One. 2012;7(2):e31208.
18. ICTV. Current ICTV Taxonomy Release. Available online: https://ictv.global/taxonomy/ (2022 release).
19. Poxviridae. In: Maclachlan NJ, and Edward J. Dubovi, editor. Fenner's Veterinary Virology2017. p. 157-74.
20. Meyer H, Ehmann R, Smith GL. Smallpox in the Post-Eradication Era. Viruses. 2020;12(2).
21. Oliveira GP, Rodrigues RAL, Lima MT, Drumond BP, Abrahao JS. Poxvirus Host Range Genes and Virus-Host Spectrum: A Critical Review. Viruses. 2017;9(11).
22. Theves C, Biagini P, Crubezy E. The rediscovery of smallpox. Clin Microbiol Infect. 2014;20(3):210-8.
23. Henderson DA. The eradication of smallpox. Scientific American. 1976;235(4):25-33.
24. Li P, Li J, Ayada I, Avan A, Zheng Q, Peppelenbosch MP, et al. Clinical Features, Antiviral Treatment, and Patient Outcomes: A Systematic Review and Comparative Analysis of the Previous and the 2022 Mpox Outbreaks. J Infect Dis. 2023;228(4):391-401.
25. Jezek Z, Grab B, Dixon H. Stochastic model for interhuman spread of monkeypox. American journal of epidemiology. 1987;126(6):1082-92.
26. Weinstein RA, Weber DJ, Rutala WA. Risks and prevention of nosocomial transmission of rare zoonotic diseases. Clinical Infectious Diseases. 2001;32(3):446-56.
27. Riedel S. Smallpox and biological warfare: a disease revisited. Proceedings (Baylor University Medical Center). 2005;18(1):13.
28. Arita I, Gispen R, Kalter SS, Wah LT, Marennikova SS, Netter R, et al. Outbreaks of monkeypox and serological surveys in nonhuman primates. Bulletin of the World Health

Organization. 1972;46(5):625.
29. Zaucha GM, Jahrling PB, Geisbert TW, Swearengen JR, Hensley L. The pathology of experimental aerosolized monkeypox virus infection in cynomolgus monkeys (Macaca fascicularis). Laboratory investigation. 2001;81(12):1581-600.
30. Magnus Pv, Andersen EK, Petersen KB, Birch-Andersen A. A pox-like disease in cynomolgus monkeys. Acta Pathologica Microbiologica Scandinavica. 1959;46(2):156-76.
31. CIC. Available online: https://www.cdc.gov/poxvirus/mpox/response/2022/index.html (Data as of October 26 2023 at 2:00 pm EDT).
32. Henderson DA, Inglesby TV, Bartlett JG, Ascher MS, Eitzen E, Jahrling PB, et al. Smallpox as a biological weapon: medical and public health management. Jama. 1999;281(22):2127-37.
33. Shah S. New threat from poxviruses. JSTOR; 2013.
34. Mansur DS, Maluquer de Motes C, Unterholzner L, Sumner RP, Ferguson BJ, Ren H, et al. Poxvirus targeting of E3 ligase beta-TrCP by molecular mimicry: a mechanism to inhibit NF-kappaB activation and promote immune evasion and virulence. PLoS Pathog. 2013;9(2):e1003183.
35. Barrett JW, McFadden G. Origin and evolution of poxviruses. Origin and Evolution of Viruses: Elsevier; 2008. p. 431-46.
36. Jenner E. An inquiry into the causes and effects of the variolae vaccinae: a disease discovered in some of the western counties of England, particularly Gloucestershire, and known by the name of the cow pox. Scientific and Medical Knowledge Production, 1796-1918: Routledge; 1945. p. 40-50.
37. Geddes AM. The history of smallpox. Clin Dermatol. 2006;24(3):152-7.
38. Henderson DA. Edward Jenner's vaccine. Public Health Reports. 1997;112(2):116.
39. Tulman ER, Delhon G, Afonso CL, Lu Z, Zsak L, Sandybaev NT, et al. Genome of horsepox virus. J Virol. 2006;80(18):9244-58.
40. Jacobs BL, Langland JO, Kibler KV, Denzler KL, White SD, Holechek SA, et al. Vaccinia virus vaccines: past, present and future. Antiviral Res. 2009;84(1):1-13.
41. Monath TP, Caldwell JR, Mundt W, Fusco J, Johnson CS, Buller M, et al. ACAM2000 clonal Vero cell culture vaccinia virus (New York City Board of Health strain)--a second-generation smallpox vaccine for biological defense. Int J Infect Dis. 2004;8 Suppl 2:S31-44.
42. Carroll MW, Moss B. Host range and cytopathogenicity of the highly attenuated MVA strain of vaccinia virus: propagation and generation of recombinant viruses in a nonhuman mammalian cell line. Virology. 1997;238(2):198-211.
43. McCurdy LH, Larkin BD, Martin JE, Graham BS. Modified vaccinia Ankara: potential as an alternative smallpox vaccine. Clinical infectious diseases. 2004;38(12):1749-53.

44. Buller RM, Palumbo GJ. Poxvirus pathogenesis. Microbiological reviews. 1991;55(1):80-122.
45. Sigal LJ. The Pathogenesis and Immunobiology of Mousepox. Adv Immunol. 2016;129:251-76.
46. Chen N, Danila MI, Feng Z, Buller RML, Wang C, Han X, et al. The genomic sequence of ectromelia virus, the causative agent of mousepox. Virology. 2003;317(1):165-86.
47. Esteban DJ, Buller RM. Ectromelia virus: the causative agent of mousepox. J Gen Virol. 2005;86(Pt 10):2645-59.
48. Esteban D, Parker S, Schriewer J, Hartzler H, Buller RM. Mousepox, a small animal model of smallpox. Vaccinia Virus and Poxvirology: Methods and Protocols. 2012:177-98.
49. Schriewer J, Buller RML, Owens G. Mouse models for studying orthopoxvirus respiratory infections. Vaccinia Virus and Poxvirology: Methods and Protocols. 2004:289-307.
50. Gubser C, Hue S, Kellam P, Smith GL. Poxvirus genomes: a phylogenetic analysis. J Gen Virol. 2004;85(Pt 1):105-17.
51. Goebel SJ, Johnson GP, Perkus ME, Davis SW, Winslow JP, Paoletti E. The complete DNA sequence of vaccinia virus. Virology. 1990;179(1):247-66.
52. Baroudy BM, Venkatesan S, Moss B. Incompletely base-paired flip-flop terminal loops link the two DNA strands of the vaccinia virus genome into one uninterrupted polynucleotide chain. Cell. 1982;28(2):315-24.
53. Shenouda MM, Noyce RS, Lee SZ, Wang JL, Lin YC, Favis NA, et al. The mismatched nucleotides encoded in vaccinia virus flip-and-flop hairpin telomeres serve an essential role in virion maturation. PLoS Pathog. 2022;18(3):e1010392.
54. Senkevich TG, Yutin N, Wolf YI, Koonin EV, Moss B. Ancient gene capture and recent gene loss shape the evolution of orthopoxvirus-host interaction genes. MBio. 2021;12(4):10.1128/mbio. 01495-21.
55. Cyrklaff M, Risco C, Fernández JJ, Jiménez MV, Estéban M, Baumeister W, et al. Cryo-electron tomography of vaccinia virus. Proceedings of the National Academy of Sciences. 2005;102(8):2772-7.
56. Chlanda P, Carbajal MA, Cyrklaff M, Griffiths G, Krijnse-Locker J. Membrane rupture generates single open membrane sheets during vaccinia virus assembly. Cell Host Microbe. 2009;6(1):81-90.
57. Chichon FJ, Rodriguez MJ, Risco C, Fraile-Ramos A, Fernandez JJ, Esteban M, et al. Membrane remodelling during vaccinia virus morphogenesis. Biol Cell. 2009;101(7):401-14.
58. Hsiao J-C, Chung C-S, Chang W. Vaccinia virus envelope D8L protein binds to cell surface chondroitin sulfate and mediates the adsorption of intracellular mature virions to cells. Journal of virology. 1999;73(10):8750-61.
59. Foo CH, Lou H, Whitbeck JC, Ponce-de-Leon M, Atanasiu D, Eisenberg RJ, et al.

Vaccinia virus L1 binds to cell surfaces and blocks virus entry independently of glycosaminoglycans. Virology. 2009;385(2):368-82.
60. Chiu WL, Lin CL, Yang MH, Tzou DL, Chang W. Vaccinia virus 4c (A26L) protein on intracellular mature virus binds to the extracellular cellular matrix laminin. J Virol. 2007;81(5):2149-57.
61. Smith GL, Vanderplasschen A, Law M. The formation and function of extracellular enveloped vaccinia virus. Journal of General Virology. 2002;83(12):2915-31.
62. Blasco R, Moss B. Extracellular vaccinia virus formation and cell-to-cell virus transmission are prevented by deletion of the gene encoding the 37,000-Dalton outer envelope protein. Journal of virology. 1991;65(11):5910-20.
63. Moss B. Poxvirus cell entry: how many proteins does it take? Viruses. 2012;4(5):688-707.
64. Evans E, Klemperer N, Ghosh R, Traktman P. The vaccinia virus D5 protein, which is required for DNA replication, is a nucleic acid-independent nucleoside triphosphatase. Journal of virology. 1995;69(9):5353-61.
65. Vanderplasschen A, Hollinshead M, Smith GL. Antibodies against vaccinia virus do not neutralize extracellular enveloped virus but prevent virus release from infected cells and comet formation. J Gen Virol. 1997;78 (Pt 8):2041-8.
66. Schmidt FI, Bleck CK, Mercer J. Poxvirus host cell entry. Curr Opin Virol. 2012;2(1):20-7.
67. Schmidt FI, Bleck CK, Helenius A, Mercer J. Vaccinia extracellular virions enter cells by macropinocytosis and acid-activated membrane rupture. EMBO J. 2011;30(17):3647-61.
68. Law M, Carter GC, Roberts KL, Hollinshead M, Smith GL. Ligand-induced and nonfusogenic dissolution of a viral membrane. Proceedings of the National Academy of Sciences. 2006;103(15):5989-94.
69. Moss B. Membrane fusion during poxvirus entry. Semin Cell Dev Biol. 2016;60:89-96.
70. Nelson GE, Sisler JR, Chandran D, Moss B. Vaccinia virus entry/fusion complex subunit A28 is a target of neutralizing and protective antibodies. Virology. 2008;380(2):394-401.
71. Wolffe EJ, Vijaya S, Moss B. A myristylated membrane protein encoded by the vaccinia virus L1R open reading frame is the target of potent neutralizing monoclonal antibodies. Virology. 1995;211(1):53-63.
72. Wagenaar TR, Moss B. Expression of the A56 and K2 proteins is sufficient to inhibit vaccinia virus entry and cell fusion. J Virol. 2009;83(4):1546-54.
73. Laliberte JP, Moss B. A novel mode of poxvirus superinfection exclusion that prevents fusion of the lipid bilayers of viral and cellular membranes. J Virol. 2014;88(17):9751-68.
74. Meade N, King M, Munger J, Walsh D. mTOR Dysregulation by Vaccinia Virus F17

Controls Multiple Processes with Varying Roles in Infection. J Virol. 2019;93(15).
75. Najarro P, Traktman P, Lewis JA. Vaccinia virus blocks gamma interferon signal transduction: viral VH1 phosphatase reverses Stat1 activation. J Virol. 2001;75(7):3185-96.
76. Greseth MD, Traktman P. The Life Cycle of the Vaccinia Virus Genome. Annu Rev Virol. 2022;9(1):239-59.
77. Mallardo M, Leithe E, Schleich S, Roos N, Doglio L, Krijnse Locker J. Relationship between vaccinia virus intracellular cores, early mRNAs, and DNA replication sites. J Virol. 2002;76(10):5167-83.
78. Kovacs GR, Vasilakis N, Moss B. Regulation of viral intermediate gene expression by the vaccinia virus B1 protein kinase. J Virol. 2001;75(9):4048-55.
79. Kilcher S, Schmidt FI, Schneider C, Kopf M, Helenius A, Mercer J. siRNA screen of early poxvirus genes identifies the AAA+ ATPase D5 as the virus genome-uncoating factor. Cell Host Microbe. 2014;15(1):103-12.
80. Liu B, Panda D, Mendez-Rios JD, Ganesan S, Wyatt LS, Moss B. Identification of Poxvirus Genome Uncoating and DNA Replication Factors with Mutually Redundant Roles. J Virol. 2018;92(7):e02152-17.
81. Satheshkumar PS, Anton LC, Sanz P, Moss B. Inhibition of the ubiquitin-proteasome system prevents vaccinia virus DNA replication and expression of intermediate and late genes. J Virol. 2009;83(6):2469-79.
82. Teale A, Campbell S, Van Buuren N, Magee WC, Watmough K, Couturier B, et al. Orthopoxviruses require a functional ubiquitin-proteasome system for productive replication. J Virol. 2009;83(5):2099-108.
83. Grossegesse M, Doellinger J, Fritsch A, Laue M, Piesker J, Schaade L, et al. Global ubiquitination analysis reveals extensive modification and proteasomal degradation of cowpox virus proteins, but preservation of viral cores. Sci Rep. 2018;8(1):1807.
84. Mercer J, Snijder B, Sacher R, Burkard C, Bleck CK, Stahlberg H, et al. RNAi screening reveals proteasome- and Cullin3-dependent stages in vaccinia virus infection. Cell Rep. 2012;2(4):1036-47.
85. Katsafanas GC, Moss B. Colocalization of transcription and translation within cytoplasmic poxvirus factories coordinates viral expression and subjugates host functions. Cell host & microbe. 2007;2(4):221-8.
86. Tolonen N, Doglio L, Schleich S, Locker JK. Vaccinia virus DNA replication occurs in endoplasmic reticulum-enclosed cytoplasmic mini-nuclei. Molecular biology of the cell. 2001;12(7):2031-46.
87. Lin YCJ, Evans DH. Vaccinia virus particles mix inefficiently, and in a way that would restrict viral recombination, in coinfected cells. Journal of virology. 2010;84(5):2432-43.
88. Paszkowski P, Noyce RS, Evans DH. Live-Cell Imaging of Vaccinia Virus Recombination. PLoS Pathog. 2016;12(8):e1005824.

89. Kaverin NV, Varich NL, Surgay VV, Chernos VI. A quantitative estimation of poxvirus genome fraction transcribed as “early” and “late” mRNA. Virology. 1975;65(1):112-9.
90. Roberts KL, Smith GL. Vaccinia virus morphogenesis and dissemination. Trends Microbiol. 2008;16(10):472-9.
91. Szajner P, Weisberg AS, Lebowitz J, Heuser J, Moss B. External scaffold of spherical immature poxvirus particles is made of protein trimers, forming a honeycomb lattice. J Cell Biol. 2005;170(6):971-81.
92. Bisht H, Weisberg AS, Szajner P, Moss B. Assembly and disassembly of the capsid-like external scaffold of immature virions during vaccinia virus morphogenesis. J Virol. 2009;83(18):9140-50.
93. Williams O, Wolffe EJ, Weisberg AS, Merchlinsky M. Vaccinia virus WR gene A5L is required for morphogenesis of mature virions. Journal of virology. 1999;73(6):4590-9.
94. Hiller G, Weber K. Golgi-derived membranes that contain an acylated viral polypeptide are used for vaccinia virus envelopment. Journal of Virology. 1985;55(3):651-9.
95. Schmelz M, Sodeik B, Ericsson M, Wolffe EJ, Shida H, Hiller G, et al. Assembly of vaccinia virus: the second wrapping cisterna is derived from the trans Golgi network. Journal of virology. 1994;68(1):130-47.
96. Tooze J, Hollinshead M, Reis B, Radsak K, Kern H. Progeny vaccinia and human cytomegalovirus particles utilize early endosomal cisternae for their envelopes. European journal of cell biology. 1993;60(1):163-78.
97. Erlandson KJ, Bisht H, Weisberg AS, Hyun SI, Hansen BT, Fischer ER, et al. Poxviruses Encode a Reticulon-Like Protein that Promotes Membrane Curvature. Cell Rep. 2016;14(9):2084-91.
98. Gao WND, Carpentier DCJ, Ewles HA, Lee SA, Smith GL. Vaccinia virus proteins A36 and F12/E2 show strong preferences for different kinesin light chain isoforms. Traffic. 2017;18(8):505-18.
99. Xu A, Basant A, Schleich S, Newsome TP, Way M. Kinesin-1 transports morphologically distinct intracellular virions during vaccinia infection. Journal of Cell Science. 2023;136(5).
100. Ward BM, Moss B. Vaccinia Virus Intracellular Movement Is Associated with Microtubules and Independent of Actin Tails. Journal of Virology. 2001;75(23):11651-63.
101. Rietdorf J, Ploubidou A, Reckmann I, Holmström A, Frischknecht F, Zettl M, et al. Kinesin-dependent movement on microtubules precedes actin-based motility of vaccinia virus. Nature cell biology. 2001;3(11):992-1000.
102. Hollinshead M, Rodger G, Van Eijl H, Law M, Hollinshead R, Vaux DJT, et al. Vaccinia virus utilizes microtubules for movement to the cell surface. The Journal of Cell Biology. 2001;154(2):389-402.
103. Dikic I, Schulman BA. An expanded lexicon for the ubiquitin code. Nat Rev Mol

Cell Biol. 2023;24(4):273-87.
104. Kolla S, Ye M, Mark KG, Rape M. Assembly and function of branched ubiquitin chains. Trends Biochem Sci. 2022;47(9):759-71.
105. Gu H, Jan Fada B. Specificity in Ubiquitination Triggered by Virus Infection. Int J Mol Sci. 2020;21(11).
106. Barry M, van Buuren N, Burles K, Mottet K, Wang Q, Teale A. Poxvirus exploitation of the ubiquitin-proteasome system. Viruses. 2010;2(10):2356-80.
107. Swatek KN, Komander D. Ubiquitin modifications. Cell Res. 2016;26(4):399-422.
108. Song L, Luo ZQ. Post-translational regulation of ubiquitin signaling. J Cell Biol. 2019;218(6):1776-86.
109. Zheng N, Shabek N. Ubiquitin Ligases: Structure, Function, and Regulation. Annu Rev Biochem. 2017;86:129-57.
110. Jeong Y, Oh AR, Jung YH, Gi H, Kim YU, Kim K. Targeting E3 ubiquitin ligases and their adaptors as a therapeutic strategy for metabolic diseases. Exp Mol Med. 2023;55(10):2097-104.
111. Chen Z, Sui J, Zhang F, Zhang C. Cullin family proteins and tumorigenesis: genetic association and molecular mechanisms. J Cancer. 2015;6(3):233-42.
112. Sarikas A, Hartmann T, Pan Z-Q. The cullin protein family. Genome biology. 2011;12:1-12.
113. Skaar JR, Pagan JK, Pagano M. Mechanisms and function of substrate recruitment by F-box proteins. Nat Rev Mol Cell Biol. 2013;14(6):369-81.
114. Zhou C, Seibert V, Geyer R, Rhee E, Lyapina S, Cope G, et al. The fission yeast COP9/signalosome is involved in cullin modification by ubiquitin-related Ned8p. BMC biochemistry. 2001;2(1):1-11.
115. Saha A, Deshaies RJ. Multimodal activation of the ubiquitin ligase SCF by Nedd8 conjugation. Molecular cell. 2008;32(1):21-31.
116. Duda DM, Borg LA, Scott DC, Hunt HW, Hammel M, Schulman BA. Structural insights into NEDD8 activation of cullin-RING ligases: conformational control of conjugation. Cell. 2008;134(6):995-1006.
117. Goldenberg SJ, Cascio TC, Shumway SD, Garbutt KC, Liu J, Xiong Y, et al. Structure of the Cand1-Cul1-Roc1 complex reveals regulatory mechanisms for the assembly of the multisubunit cullin-dependent ubiquitin ligases. Cell. 2004;119(4):517-28.
118. Pintard L, Willems A, Peter M. Cullin-based ubiquitin ligases: Cul3-BTB complexes join the family. EMBO J. 2004;23(8):1681-7.
119. Yau R, Rape M. The increasing complexity of the ubiquitin code. Nat Cell Biol. 2016;18(6):579-86.
120. Nakagawa T, Nakayama K. Protein monoubiquitylation: targets and diverse functions. Genes Cells. 2015;20(7):543-62.
121. Xu P, Duong DM, Seyfried NT, Cheng D, Xie Y, Robert J, et al. Quantitative

proteomics reveals the function of unconventional ubiquitin chains in proteasomal degradation. Cell. 2009;137(1):133-45.
122. Zhao Y, Lu Y, Richardson S, Sreekumar M, Albarnaz JD, Smith GL. TRIM5alpha restricts poxviruses and is antagonized by CypA and the viral protein C6. Nature. 2023;620(7975):873-80.
123. Hershko A, Ciechanover A. The ubiquitin system. Annual review of biochemistry. 1998;67(1):425-79.
124. Chen ZJ, Sun LJ. Nonproteolytic functions of ubiquitin in cell signaling. Mol Cell. 2009;33(3):275-86.
125. McManus FP, Lamoliatte F, Thibault P. Identification of cross talk between SUMOylation and ubiquitylation using a sequential peptide immunopurification approach. Nat Protoc. 2017;12(11):2342-58.
126. Gibbs-Seymour I, Oka Y, Rajendra E, Weinert BT, Passmore LA, Patel KJ, et al. Ubiquitin-SUMO circuitry controls activated fanconi anemia ID complex dosage in response to DNA damage. Mol Cell. 2015;57(1):150-64.
127. Swaney DL, Rodriguez-Mias RA, Villen J. Phosphorylation of ubiquitin at Ser65 affects its polymerization, targets, and proteome-wide turnover. EMBO Rep. 2015;16(9):1131-44.
128. Ohtake F, Saeki Y, Sakamoto K, Ohtake K, Nishikawa H, Tsuchiya H, et al. Ubiquitin acetylation inhibits polyubiquitin chain elongation. EMBO Rep. 2015;16(2):192-201.
129. Wauer T, Swatek KN, Wagstaff JL, Gladkova C, Pruneda JN, Michel MA, et al. Ubiquitin Ser65 phosphorylation affects ubiquitin structure, chain assembly and hydrolysis. EMBO J. 2015;34(3):307-25.
130. Lant S, Maluquer de Motes C. Poxvirus Interactions with the Host Ubiquitin System. Pathogens. 2021;10(8).
131. Ingham RJ, Loubich Facundo F, Dong J. Poxviral ANKR/F-box proteins: substrate adapters for ubiquitylation and more. Pathogens. 2022;11(8):875.
132. Herbert MH, Squire CJ, Mercer AA. Poxviral ankyrin proteins. Viruses. 2015;7(2):709-38.
133. Sonnberg S, Fleming SB, Mercer AA. Phylogenetic analysis of the large family of poxvirus ankyrin-repeat proteins reveals orthologue groups within and across chordopoxvirus genera. J Gen Virol. 2011;92(Pt 11):2596-607.
134. Liu R, Moss B. Vaccinia Virus C9 Ankyrin Repeat/F-Box Protein Is a Newly Identified Antagonist of the Type I Interferon-Induced Antiviral State. J Virol. 2018b;92(9):e00053-18.
135. Liu R, Olano LR, Mirzakhanyan Y, Gershon PD, Moss B. Vaccinia Virus Ankyrin-Repeat/F-Box Protein Targets Interferon-Induced IFITs for Proteasomal Degradation. Cell Rep. 2019;29(4):816-28.

136. Mears HV, Sweeney TR. Better together: the role of IFIT protein-protein interactions in the antiviral response. J Gen Virol. 2018;99(11):1463-77.
137. Daffis S, Szretter KJ, Schriewer J, Li J, Youn S, Errett J, et al. 2'-O methylation of the viral mRNA cap evades host restriction by IFIT family members. Nature. 2010;468(7322):452-6.
138. Mohamed MR, Rahman MM, Lanchbury JS, Shattuck D, Neff C, Dufford M, et al. Proteomic screening of variola virus reveals a unique NF-κB inhibitor that is highly conserved among pathogenic orthopoxviruses. Proceedings of the National Academy of Sciences. 2009;106(22):9045-50.
139. Mohamed MR, Rahman MM, Rice A, Moyer RW, Werden SJ, McFadden G. Cowpox virus expresses a novel ankyrin repeat NF-kappaB inhibitor that controls inflammatory cell influx into virus-infected tissues and is critical for virus pathogenesis. J Virol. 2009;83(18):9223-36.
140. Liu Z, Nailwal H, Rector J, Rahman MM, Sam R, McFadden G, et al. A class of viral inducer of degradation of the necroptosis adaptor RIPK3 regulates virus-induced inflammation. Immunity. 2021;54(2):247-58.
141. Cho YS, Challa S, Moquin D, Genga R, Ray TD, Guildford M, et al. Phosphorylation-driven assembly of the RIP1-RIP3 complex regulates programmed necrosis and virus-induced inflammation. Cell. 2009;137(6):1112-23.
142. Ramsey-Ewing AL, Moss B. Complementation of a vaccinia virus host-range K1L gene deletion by the nonhomologous CP77 gene. Virology. 1996;222(1):75-86.
143. Odon V, Georgana I, Holley J, Morata J, Maluquer de Motes C. Novel Class of Viral Ankyrin Proteins Targeting the Host E3 Ubiquitin Ligase Cullin-2. J Virol. 2018;92(23).
144. Pires de Miranda M, Reading PC, Tscharke DC, Murphy BJ, Smith GL. The vaccinia virus kelch-like protein C2L affects calcium-independent adhesion to the extracellular matrix and inflammation in a murine intradermal model. J Gen Virol. 2003;84(Pt 9):2459-71.
145. Froggatt GC, Smith GL, Beard PM. Vaccinia virus gene F3L encodes an intracellular protein that affects the innate immune response. J Gen Virol. 2007;88(Pt 7):1917-21.
146. Pallett MA, Ren H, Zhang RY, Scutts SR, Gonzalez L, Zhu Z, et al. Vaccinia virus BBK E3 ligase adaptor A55 targets importin-dependent NF-kappaB activation and inhibits CD8(+) T-cell memory. J Virol. 2019:e00051-19.
147. Burles K, Irwin CR, Burton RL, Schriewer J, Evans DH, Buller RM, et al. Initial characterization of vaccinia virus B4 suggests a role in virus spread. Virology. 2014;456-457:108-20.
148. Esposito JJ, Sammons SA, Frace AM, Osborne JD, Olsen-Rasmussen M, Zhang M, et al. Genome sequence diversity and clues to the evolution of variola (smallpox) virus.

Science. 2006;313(5788):807-12.
149. Huang J, Huang Q, Zhou X, Shen MM, Yen A, Yu SX, et al. The poxvirus p28 virulence factor is an E3 ubiquitin ligase. J Biol Chem. 2004;279(52):54110-6.
150. Upton C, Schiff L, Rice S, Dowdeswell T, Yang X, McFadden G. A poxvirus protein with a RING finger motif binds zinc and localizes in virus factories. Journal of virology. 1994;68(7):4186-95.
151. Bareiss B, Barry M. Fowlpox virus encodes two p28-like ubiquitin ligases that are expressed early and late during infection. Virology. 2014;462-463:60-70.
152. Nerenberg BT, Taylor J, Bartee E, Gouveia K, Barry M, Fruh K. The poxviral RING protein p28 is a ubiquitin ligase that targets ubiquitin to viral replication factories. J Virol. 2005;79(1):597-601.
153. Mottet K, Bareiss B, Milne CD, Barry M. The poxvirus encoded ubiquitin ligase, p28, is regulated by proteasomal degradation and autoubiquitination. Virology. 2014;468-470:363-78.
154. Senkevich TG, Wolffe EJ, Buller RML. Ectromelia Virus Ring Finger Protein Is Localized in Virus Factories and Is Required for Virus-Replication in Macrophages. Journal of Virology. 1995;69(7):4103-11.
155. Brick DJ, Burke RD, Schiff L, Upton C. Shope fibroma virus RING finger protein N1R binds DNA and inhibits apoptosis. Virology. 1998;249(1):42-51.
156. Iyer LM, Koonin EV, Aravind L. Extensive domain shuffling in transcription regulators of DNA viruses and implications for the origin of fungal APSES transcription factors. Genome biology. 2002;3(3):research0012. 1.
157. Senkevich TG, Katsafanas GC, Weisberg A, Olano LR, Moss B. Identification of Vaccinia Virus Replisome and Transcriptome Proteins by Isolation of Proteins on Nascent DNA Coupled with Mass Spectrometry. J Virol. 2017;91(19).
158. Senkevich TG, Koonin EV, Buller RML. A poxvirus protein with a RING zinc finger motif is of crucial importance for virulence. Virology. 1994;198(1):118-28.
159. Brick DJ, Burke RD, Minkley AA, Upton C. Ectromelia virus virulence factor p28 acts upstream of caspase-3 in response to UV light-induced apoptosis. Journal of General Virology. 2000;81:1087-97.
160. Bourquain D, Schrick L, Tischer BK, Osterrieder K, Schaade L, Nitsche A. Replication of cowpox virus in macrophages is dependent on the host range factor p28/N1R. Virol J. 2021;18(1):173.
161. Ray A, Dittel BN. Isolation of mouse peritoneal cavity cells. J Vis Exp. 2010;35:e1488.
162. Zhang X, Goncalves R, Mosser DM. The isolation and characterization of murine macrophages. Curr Protoc Immunol. 2008;Chapter 14:Unit 14 1.
163. Trouplin V, Boucherit N, Gorvel L, Conti F, Mottola G, Ghigo E. Bone marrow-derived macrophage production. J Vis Exp. 2013(81):e50966.

164. Perkus., Goebel SJ, Davis SW, Johnson GP, Norton EK, Paoletti E. Deletion of 55 open reading frames from the termini of vaccinia virus. Virology. 1991;180(1):406-10.
165. Rintoul JL, Wang J, Gammon DB, van Buuren NJ, Garson K, Jardine K, et al. A selectable and excisable marker system for the rapid creation of recombinant poxviruses. PLoS One. 2011;6(9):e24643.
166. Baker JL, Ward BM. Development and comparison of a quantitative TaqMan-MGB real-time PCR assay to three other methods of quantifying vaccinia virions. J Virol Methods. 2014;196:126-32.
167. Noyce RS, Lederman S, Evans DH. Construction of an infectious horsepox virus vaccine from chemically synthesized DNA fragments. PLoS One. 2018;13(1):e0188453.
168. Bhatwa A, Wang W, Hassan YI, Abraham N, Li XZ, Zhou T. Challenges Associated With the Formation of Recombinant Protein Inclusion Bodies in Escherichia coli and Strategies to Address Them for Industrial Applications. Front Bioeng Biotechnol. 2021;9:630551.
169. Garzoni F, Bieniossek C, Berger I. The MultiBac BEVS for producing proteins and their complexes (Prot54). Epigenesys Eu Protoc. 2012.
170. Zhou Y, Zhou B, Pache L, Chang M, Khodabakhshi AH, Tanaseichuk O, et al. Metascape provides a biologist-oriented resource for the analysis of systems-level datasets. Nat Commun. 2019;10(1):1523.
171. Soday L, Lu Y, Albarnaz JD, Davies CTR, Antrobus R, Smith GL, et al. Quantitative Temporal Proteomic Analysis of Vaccinia Virus Infection Reveals Regulation of Histone Deacetylases by an Interferon Antagonist. Cell Rep. 2019;27(6):1920-33 e7.
172. Evans TG, Bussey L, Eagling-Vose E, Rutkowski K, Ellis C, Argent C, et al. Efficacy and safety of a universal influenza A vaccine (MVA-NP+M1) in adults when given after seasonal quadrivalent influenza vaccine immunisation (FLU009): a phase 2b, randomised, double-blind trial. Lancet Infect Dis. 2022;22(6):857-66.
173. Dong J, Paszkowski P, Kocincova D, Ingham RJ. Complete deletion of Ectromelia virus p28 impairs virus genome replication in a mouse strain, cell type, and multiplicity of infection-dependent manner. Virus Res. 2022;323:198968.
174. Rochester SC, Traktman P. Characterization of the single-stranded DNA binding protein encoded by the vaccinia virus I3 gene. Journal of virology. 1998;72(4):2917-26.
175. Hirschmann P, Vos JC, Stunnenberg HG. Mutational analysis of a vaccinia virus intermediate promoter in vivo and in vitro. Journal of virology. 1990;64(12):6063-9.
176. Gueret V, Negrete-Virgen JA, Lyddiatt A, Al-Rubeai M. Rapid titration of adenoviral infectivity by flow cytometry in batch culture of infected HEK293 cells. Cytotechnology. 2002;38:87-97.
177. O'Connor HF, Lyon N, Leung JW, Agarwal P, Swaim CD, Miller KM, et al. Ubiquitin-Activated Interaction Traps (UBAITs) identify E3 ligase binding partners. EMBO Rep. 2015;16(12):1699-712.

178. Chakrabarti S, Sisler JR, Moss B. Compact, synthetic, vaccinia virus early/late promoter for protein expression. Biotechniques. 1997;23(6):1094-7.
179. Lehman BJ. Characterization of the Poxviral Encoded Ubiquitin Ligase p28 [Doctoral dissertation]: University of Alberta; 2015.
180. Mansouri M, Bartee E, Gouveia K, Hovey Nerenberg BT, Barrett J, Thomas L, et al. The PHD/LAP-Domain Protein M153R of Myxomavirus Is a Ubiquitin Ligase That Induces the Rapid Internalization and Lysosomal Destruction of CD4. Journal of Virology. 2003;77(2):1427-40.
181. Felberbaum RS. The baculovirus expression vector system: A commercial manufacturing platform for viral vaccines and gene therapy vectors. Biotechnol J. 2015;10(5):702-14.
182. Klenk H-D. Post-translational modifications in insect cells. Insect Cell Culture: Fundamental and Applied Aspects. 2002:139-44.
183. Chen N, Kong X, Zhao S, Xiaofeng W. Post-translational modification of baculovirus-encoded proteins. Virus Res. 2020;279:197865.
184. Arutyunova E, Panwar P, Skiba PM, Gale N, Mak MW, Lemieux MJ. Allosteric regulation of rhomboid intramembrane proteolysis. EMBO J. 2014;33(17):1869-81.
185. Chen SA, Arutyunova E, Lu J, Khan MB, Rut W, Zmudzinski M, et al. SARS-CoV-2 M(pro) Protease Variants of Concern Display Altered Viral Substrate and Cell Host Target Galectin-8 Processing but Retain Sensitivity toward Antivirals. ACS Cent Sci. 2023;9(4):696-708.
186. Lemieux MJ, Fischer SJ, Cherney MM, Bateman KS, James MNG. The crystal structure of the rhomboid peptidase from Haemophilus influenzae provides insight into intramembrane proteolysis. Proceedings of the National Academy of Sciences. 2007;104(3):750-4.
187. Sharma D, Masison DC. Hsp70 structure, function, regulation and influence on yeast prions. Protein and peptide letters. 2009;16(6):571-81.
188. Zhu X, Zhao X, Burkholder WF, Gragerov A, Ogata CM, Gottesman ME, et al. Structural analysis of substrate binding by the molecular chaperone DnaK. Science. 1996;272(5268):1606-14.
189. Mayer MP, Bukau B. Hsp70 chaperones: cellular functions and molecular mechanism. Cell Mol Life Sci. 2005;62(6):670-84.
190. Pujhari S, Brustolin M, Macias VM, Nissly RH, Nomura M, Kuchipudi SV, et al. Heat shock protein 70 (Hsp70) mediates Zika virus entry, replication, and egress from host cells. Emerging microbes & infections. 2019;8(1):8-16.
191. Das S, Laxminarayana SV, Chandra N, Ravi V, Desai A. Heat shock protein 70 on Neuro2a cells is a putative receptor for Japanese encephalitis virus. Virology. 2009;385(1):47-57.
192. Niewiarowska J, D'Halluin J-C, Belin M-T. Adenovirus capsid proteins interact

with HSP70 proteins after penetration in human or rodent cells. Experimental cell research. 1992;201(2):408-16.
193. Khachatoorian R, Ganapathy E, Ahmadieh Y, Wheatley N, Sundberg C, Jung C-L, et al. The NS5A-binding heat shock proteins HSC70 and HSP70 play distinct roles in the hepatitis C viral life cycle. Virology. 2014;454:118-27.
194. Jindal S, Young RA. Vaccinia virus infection induces a stress response that leads to association of Hsp70 with viral proteins. Journal of Virology. 1992;66(9):5357-62.
195. Carrington JC, Dougherty WG. A viral cleavage site cassette: identification of amino acid sequences required for tobacco etch virus polyprotein processing. Proceedings of the National Academy of Sciences. 1988;85(10):3391-5.
196. Kostallas G, Lofdahl PA, Samuelson P. Substrate profiling of tobacco etch virus protease using a novel fluorescence-assisted whole-cell assay. PLoS One. 2011;6(1):e16136.
197. Pablos I, Machado Y, de Jesus HCR, Mohamud Y, Kappelhoff R, Lindskog C, et al. Mechanistic insights into COVID-19 by global analysis of the SARS-CoV-2 3CL(pro) substrate degradome. Cell Rep. 2021;37(4):109892.
198. Ha Y, Akiyama Y, Xue Y. Structure and mechanism of rhomboid protease. J Biol Chem. 2013;288(22):15430-6.
199. Pallett MA, Ren H, Zhang RY, Scutts SR, Gonzalez L, Zhu Z, et al. Vaccinia Virus BBK E3 Ligase Adaptor A55 Targets Importin-Dependent NF-kappaB Activation and Inhibits CD8(+) T-Cell Memory. J Virol. 2019;93(10).
200. Liu R, Moss B. Vaccinia Virus C9 Ankyrin Repeat/F-Box Protein Is a Newly Identified Antagonist of the Type I Interferon-Induced Antiviral State. J Virol. 2018;92(9).
201. Chen W, Han C, Xie B, Hu X, Yu Q, Shi L, et al. Induction of Siglec-G by RNA viruses inhibits the innate immune response by promoting RIG-I degradation. Cell. 2013;152(3):467-78.
202. Manivannan P, Siddiqui MA, Malathi K. RNase L Amplifies Interferon Signaling by Inducing Protein Kinase R-Mediated Antiviral Stress Granules. J Virol. 2020;94(13).
203. Platanitis E, Decker T. Regulatory Networks Involving STATs, IRFs, and NFkappaB in Inflammation. Front Immunol. 2018;9:2542.
204. Ivashkiv LB, Donlin LT. Regulation of type I interferon responses. Nat Rev Immunol. 2014;14(1):36-49.
205. Nathan JA, Lehner PJ. The trafficking and regulation of membrane receptors by the RING-CH ubiquitin E3 ligases. Exp Cell Res. 2009;315(9):1593-600.
206. Kim W, Bennett EJ, Huttlin EL, Guo A, Li J, Possemato A, et al. Systematic and quantitative assessment of the ubiquitin-modified proteome. Mol Cell. 2011;44(2):325-40.
207. Xu G, Paige JS, Jaffrey SR. Global analysis of lysine ubiquitination by ubiquitin remnant immunoaffinity profiling. Nat Biotechnol. 2010;28(8):868-73.
208. Sivan G, Ormanoglu P, Buehler EC, Martin SE, Moss B. Identification of

Restriction Factors by Human Genome-Wide RNA Interference Screening of Viral Host Range Mutants Exemplified by Discovery of SAMD9 and WDR6 as Inhibitors of the Vaccinia Virus K1L-C7L- Mutant. mBio. 2015;6(4):e01122.
209. Park C, Walsh D. RACK1 Regulates Poxvirus Protein Synthesis Independently of Its Role in Ribosome-Based Stress Signaling. J Virol. 2022;96(18):e0109322.
210. Rahman MM, Bagdassarian E, Ali MAM, McFadden G. Identification of host DEAD-box RNA helicases that regulate cellular tropism of oncolytic Myxoma virus in human cancer cells. Sci Rep. 2017;7(1):15710.
211.Beerli C, Yakimovich A, Kilcher S, Reynoso GV, Flaschner G, Muller DJ, et al. Vaccinia virus hijacks EGFR signalling to enhance virus spread through rapid and directed infected cell motility. Nat Microbiol. 2019;4(2):216-25.
212. Urano T, Saito T, Tsukui T, Fujita M, Hosoi T, Muramatsu M, et al. Efp targets 14-3-3σ for proteolysis and promotes breast tumour growth. Nature. 2002;417(6891):871-5.
213. Zou W, Zhang DE. The interferon-inducible ubiquitin-protein isopeptide ligase (E3) EFP also functions as an ISG15 E3 ligase. J Biol Chem. 2006;281(7):3989-94.
214. Martin-Vicente M, Medrano LM, Resino S, Garcia-Sastre A, Martinez I. TRIM25 in the Regulation of the Antiviral Innate Immunity. Front Immunol. 2017;8:1187.
215. Gack MU, Shin YC, Joo CH, Urano T, Liang C, Sun L, et al. TRIM25 RING-finger E3 ubiquitin ligase is essential for RIG-I-mediated antiviral activity. Nature. 2007;446(7138):916-20.
216. Gack MU, Kirchhofer A, Shin YC, Inn K-S, Liang C, Cui S, et al. Roles of RIG-I N-terminal tandem CARD and splice variant in TRIM25-mediated antiviral signal transduction. Proceedings of the National Academy of Sciences. 2008;105(43):16743-8.
217. Thoresen D, Wang W, Galls D, Guo R, Xu L, Pyle AM. The molecular mechanism of RIG-I activation and signaling. Immunological Reviews. 2021;304(1):154-68.
218. Gack MU, Albrecht RA, Urano T, Inn KS, Huang IC, Carnero E, et al. Influenza A virus NS1 targets the ubiquitin ligase TRIM25 to evade recognition by the host viral RNA sensor RIG-I. Cell Host Microbe. 2009;5(5):439-49.
219. Hu Y, Li W, Gao T, Cui Y, Jin Y, Li P, et al. The Severe Acute Respiratory Syndrome Coronavirus Nucleocapsid Inhibits Type I Interferon Production by Interfering with TRIM25-Mediated RIG-I Ubiquitination. J Virol. 2017;91(8).
220. Gupta S, Yla-Anttila P, Sandalova T, Sun R, Achour A, Masucci MG. 14-3-3 scaffold proteins mediate the inactivation of trim25 and inhibition of the type I interferon response by herpesvirus deconjugases. PLoS Pathog. 2019;15(11):e1008146.
221. Koliopoulos MG, Esposito D, Christodoulou E, Taylor IA, Rittinger K. Functional role of TRIM E3 ligase oligomerization and regulation of catalytic activity. EMBO J. 2016;35(11):1204-18.
222. Hyer ML, Milhollen MA, Ciavarri J, Fleming P, Traore T, Sappal D, et al. A small-

molecule inhibitor of the ubiquitin activating enzyme for cancer treatment. Nat Med. 2018;24(2):186-93.
223. Udeshi ND, Mertins P, Svinkina T, Carr SA. Large-scale identification of ubiquitination sites by mass spectrometry. Nat Protoc. 2013;8(10):1950-60.
224. Morimoto M, Nishida T, Nagayama Y, Yasuda H. Nedd8-modification of Cul1 is promoted by Roc1 as a Nedd8-E3 ligase and regulates its stability. Biochem Biophys Res Commun. 2003;301(2):392-8.
225. Koepke L, Gack MU, Sparrer KM. The antiviral activities of TRIM proteins. Curr Opin Microbiol. 2021;59:50-7.
226. Tecalco-Cruz AC, Abraham-Juarez MJ, Solleiro-Villavicencio H, Ramirez-Jarquin JO. TRIM25: A central factor in breast cancer. World J Clin Oncol. 2021;12(8):646-55.
227. Choudhury NR, Heikel G, Michlewski G. TRIM25 and its emerging RNA - binding roles in antiviral defense. Wiley Interdisciplinary Reviews: RNA. 2020;11(4):e1588.
228. Schierling K, Buser C, Mertens T, Winkler M. Human cytomegalovirus tegument protein ppUL35 is important for viral replication and particle formation. J Virol. 2005;79(5):3084-96.
229. Hayashi ML, Blankenship C, Shenk T. Human cytomegalovirus UL69 protein is required for efficient accumulation of infected cells in the G1 phase of the cell cycle. Proceedings of the National Academy of Sciences. 2000;97(6):2692-6.
230. Meier JL, Keller MJ, McCoy JJ. Requirement of multiple cis-acting elements in the human cytomegalovirus major immediate-early distal enhancer for viral gene expression and replication. J Virol. 2002;76(1):313-26.
231. Boyle K, Traktman P. Poxviruses. Viral genome replication: Springer; 2009. p. 225-47.
232. Moss B. Poxvirus DNA replication. Cold Spring Harb Perspect Biol. 2013;5(9).
233. Hewawasam G, Shivaraju M, Mattingly M, Venkatesh S, Martin-Brown S, Florens L, et al. Psh1 is an E3 ubiquitin ligase that targets the centromeric histone variant Cse4. Molecular cell. 2010;40(3):444-54.
234. Timney BL, Raveh B, Mironska R, Trivedi JM, Kim SJ, Russel D, et al. Simple rules for passive diffusion through the nuclear pore complex. J Cell Biol. 2016;215(1):57-76.
235. Medina EM, Walsh E, Buchler NE. Evolutionary innovation, fungal cell biology, and the lateral gene transfer of a viral KilA-N domain. Curr Opin Genet Dev. 2019;58-59:103-10.
236. Yu H, Bruneau RC, Brennan G, Rothenburg S. Battle Royale: Innate Recognition of Poxviruses and Viral Immune Evasion. Biomedicines. 2021;9(7).

237. Fensterl V, Sen GC. Interferon-induced Ifit proteins: their role in viral pathogenesis. J Virol. 2015;89(5):2462-8.
238. Adams DR, Ron D, Kiely PA. RACK1, A multifaceted scaffolding protein: Structure and function. Cell communication and signaling. 2011;9(1):1-24.
239. Jha S, Rollins MG, Fuchs G, Procter DJ, Hall EA, Cozzolino K, et al. Trans-kingdom mimicry underlies ribosome customization by a poxvirus kinase. Nature. 2017;546(7660):651-5.
240. Meade N, DiGiuseppe S, Walsh D. Translational control during poxvirus infection. Wiley Interdiscip Rev RNA. 2019;10(2):e1515.
241. Brennan G, Stoian AMM, Yu H, Rahman MJ, Banerjee S, Stroup JN, et al. Molecular mechanisms of poxvirus evolution. MBio. 2023;14(1):e01526-22.
242. Unterholzner L, Sumner RP, Baran M, Ren H, Mansur DS, Bourke NM, et al. Vaccinia virus protein C6 is a virulence factor that binds TBK-1 adaptor proteins and inhibits activation of IRF3 and IRF7. PLoS Pathog. 2011;7(9):e1002247.
243. DiPerna G, Stack J, Bowie AG, Boyd A, Kotwal G, Zhang Z, et al. Poxvirus protein N1L targets the I-kappaB kinase complex, inhibits signaling to NF-kappaB by the tumor necrosis factor superfamily of receptors, and inhibits NF-kappaB and IRF3 signaling by toll-like receptors. J Biol Chem. 2004;279(35):36570-8.
244. Schroder M, Baran M, Bowie AG. Viral targeting of DEAD box protein 3 reveals its role in TBK1/IKKepsilon-mediated IRF activation. EMBO J. 2008;27(15):2147-57.